Reaction Engineering Implications of Using Water for the Conversion of Lignocellulosic Biomass

by

Maksim Vasilev Tyufekchiev

A Dissertation

Submitted to the Faculty of

Worcester Polytechnic Institute

In partial fulfillment of the requirements for the

Degree of Doctor of Philosophy

in

Chemical Engineering

December 2019

Dr. Michael Timko, Academic Advisor
Chemical Engineering Department, WPI,

Dr. Aaron Deskins, Committee Member
Chemical Engineering Department, WPI

Dr. Ronald Grimm, Committee Member
Chemistry and Biochemistry Department, WPI

Dr. Christopher Lambert, Committee Member,
Chemistry and Biochemistry Department, WPI

Dr. Susan Roberts, Head of Chemical Engineering Department, WPI

Executive Summary

Utilization of renewable lignocellulosic plant biomass feedstocks to fuels and chemicals is gaining ever increasing attention as a sustainable and carbon neutral alternative to fossil fuels. However, conversion strategies are not economically competitive preventing adoption and commercialization of commodity products. Cellulose hydrolysis is a potential route for the utilization of lignocellulosic biomass and its conversion to renewable fuels and chemicals. During that process, the chemical bonds in the cellulose polymer structure are broken via the action of water and a catalyst to produce glucose or other soluble products. However, substrate reactivity and lack catalyst recyclability contribute to the high cost of biomass processing. We addressed the use of solid acids as recyclable catalysts for cellulose hydrolysis and the effect of water on interpreting the activity and on the recyclability of the materials. Further, we studied the effects of water on the reactivity of the cellulose substrate and proposed an alternative to hydrolysis.

Solid acid catalysts have emerged as a recyclable alternative to liquid homogeneous acids and enzymes for the depolymerization of cellulose and selective production of glucose. However, still in the developmental stage, there is little mechanistic understanding of how such materials catalyze cellulose hydrolysis. A challenge to developing structure-reactivity relationships is the incomplete structural characterization of solid acids. To elucidate, we focused on a chloromethyl polystyrene based polymeric solid acid catalyst CMP-SO_3H-0.3 that had exhibited remarkable activity towards depolymerizing cellulose. In CMP-SO_3H-0.3 benzyl chloride groups are hypothesized to interact with cellulose via a hydrogen bonding and sulfonic acid groups catalyze the split of the glycosidic bond. However, nuclear magnetic resonance spectroscopy analysis revealed the presence of hydroxyl groups in the catalyst structure. Detailed radial analysis of polymer beads with Raman

microscopy showed that the external catalyst surface, which would hypothetically interact with cellulose, lacks chlorine groups. In conjunction with the catalytic activity, which was greater than the activity of catalysts without binding-capable groups, suggested contribution from the hydroxyl groups. However, analysis of CMP-SO_3H-0.3 post hydrolysis revealed further increase of the content of hydroxyl groups. This indicated benzyl chloride group hydrolysis by water to hydroxyl moieties with hydrochloric acid as the other product, implying catalytic effects of the leached acid. Indeed, we quantified the content of the leached hydrochloric acid and confirmed that it was mostly responsible for the observed catalytic activity of CMP-SO_3H-0.3.

We addressed the implications of homogenous acid leaching due to hydrothermal degradation of solid acid catalysts by testing selected catalysts representative of different structural classes used for cellulose hydrolysis. Treatment of the catalysts at 150 °C for identical periods of time applied in cellulose hydrolysis generated leachates, whose activity was compared to the apparent cellulose hydrolysis activity of the solid acid catalysts. The leachates resulted in greater cellulose hydrolysis, implying there are no solid-solid interactions between solid acid catalysts and the cellulose substrate. We developed an analytical framework for facile testing of solid acid catalysts and determining whether there are solid-solid interactions with cellulose. The catalysts tested did not provide conclusive evidence of such interactions. We used kinetic modeling to quantify the contribution of the homogeneous acid and compare them to experimental results. However, this analysis revealed that homogenous acid catalyzed cellulose hydrolysis; further, we discovered that the soluble products interact with the solid acid catalyst resulting in further leaching of homogenous acid. The overall conclusion for solid acid catalyzed cellulose hydrolysis in water is summarized in the following cartoon:

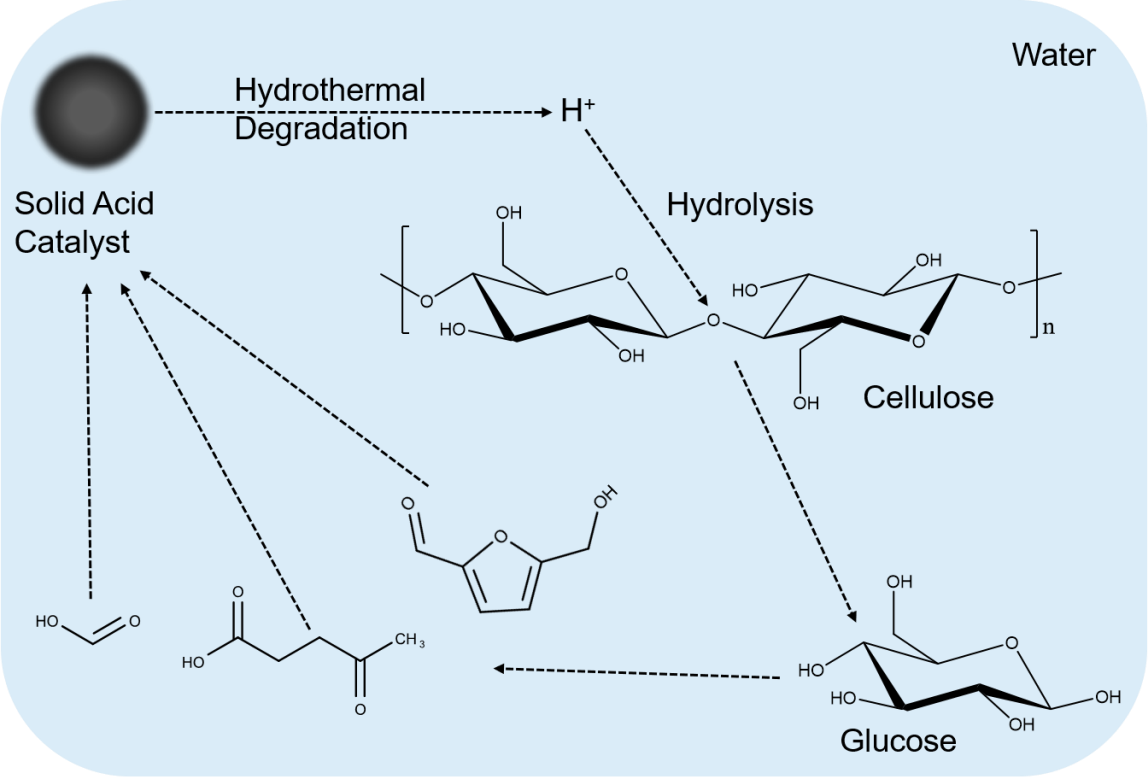

Cellulose crystallinity has been implicated a structural parameter determining the reactivity of cellulose. This has motivated decrystallization pretreatment methods to enhance cellulose hydrolysis. However, it has been known for quite a while that amorphous cellulose recrystallizes in liquid water, which calls into question current theoretical understanding of cellulose reactivity. We decrystallized cellulose via ball milling, measured the crystallinity, and subjected the substrate to hydrolysis with hydrochloric acid in water. Initial correlation between crystallinity and reactivity yielded a direct proportionality. To further examine the effect of water-induced recrystallization we treated ball-milled cellulose in hydrothermal conditions at which cellulose hydrolysis doesn't occur and observed an increase of substrate crystallinity. We then subjected the recrystallized cellulose to acid hydrolysis and compared the reactivity to the ball-milled-only substrate. The hydrolysis results of the two substrates did not differ, implying that crystallinity was not responsible for determining the reactivity of cellulose. However, we treated the ball-milled

substrate in the acid hydrolysis conditions for 5 minutes, time interval not enough to result in release of soluble sugars and discovered that within this timeframe the crystallinity had already reached its final value. The recrystallized substrate was still more reactive than highly crystalline cellulose. Nuclear magnetic resonance analysis revealed that the recrystallized cellulose consists of allomorphs type I and II with greater crystal surface. Rapid water-induced recrystallization prevented determining the intrinsic reactivity of amorphous cellulose. For this purpose, we used ethanolysis as a probe reaction, since ethanol does not promote recrystallization. Indeed, ball-milled cellulose was more reactive than either recrystallized or highly crystalline substrates. The conclusions from that study were used to update the mechanism of cellulose hydrolysis:

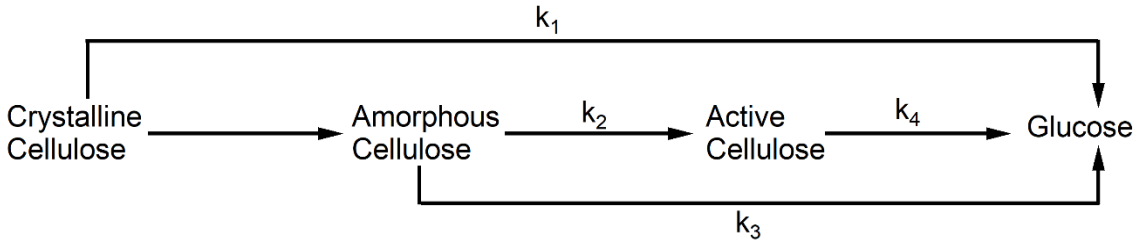

Cellulose conversion was studied in ethanol as a means to avoid limitations imposed by water-induced recrystallization and increase depolymerization rates. Crystalline cellulose resulted in only 3% conversion after 60 minutes, while ball-milled substrate in 38% and 24% yield of ethyl glucopyranoside at 140 °C and 0.1M HCl as catalyst. Hydrolysis at the same conditions afforded only 21% conversion. Increasing ethanolysis reaction time to 90 minutes did not result in a commensurate increase of conversion and yield, indicating either exhaustion of amorphous cellulose regions or solubility and equilibrium limits. Further treatment of already ethanoyzed substrate with fresh solvent provided support of the solubility-equilibrium hypothesis as additional conversion was observed. Treatment of ethanolyzed ball-milled cellulose with hot liquid water resulted in release of soluble oligomeric species. X-ray diffraction and nuclear magnetic resonance

of ethanolyzed ball-milled cellulose revealed increase of crystallinity post reaction. These results suggested that soluble oligomers are trapped in the cellulose structure due to recrystallization during ethanolysis. The recrystallization was attributed to the scission relaxation phenomenon. To suppress this effect, we used co-solvents capable of swelling cellulose. Interestingly, water was the only solvent capable of increasing cellulose conversion and ethyl glucopyranoside yield to 48% and 26%, respectively. Alternatively, additional ball milling and ethanolysis of ethanolyzed cellulose increased the values to 62% and 42%, respectively. Using ethanolysis as a process to depolymerize cellulose to constituent monomers provides the opportunity to lower costs by circumventing the stabilizing effects of water and by decreasing energy requirements due to the lower heat capacity of ethanol compared to water. Therefore, it merits further investigation. The ethanolysis mechanism is summarized in the following scheme:

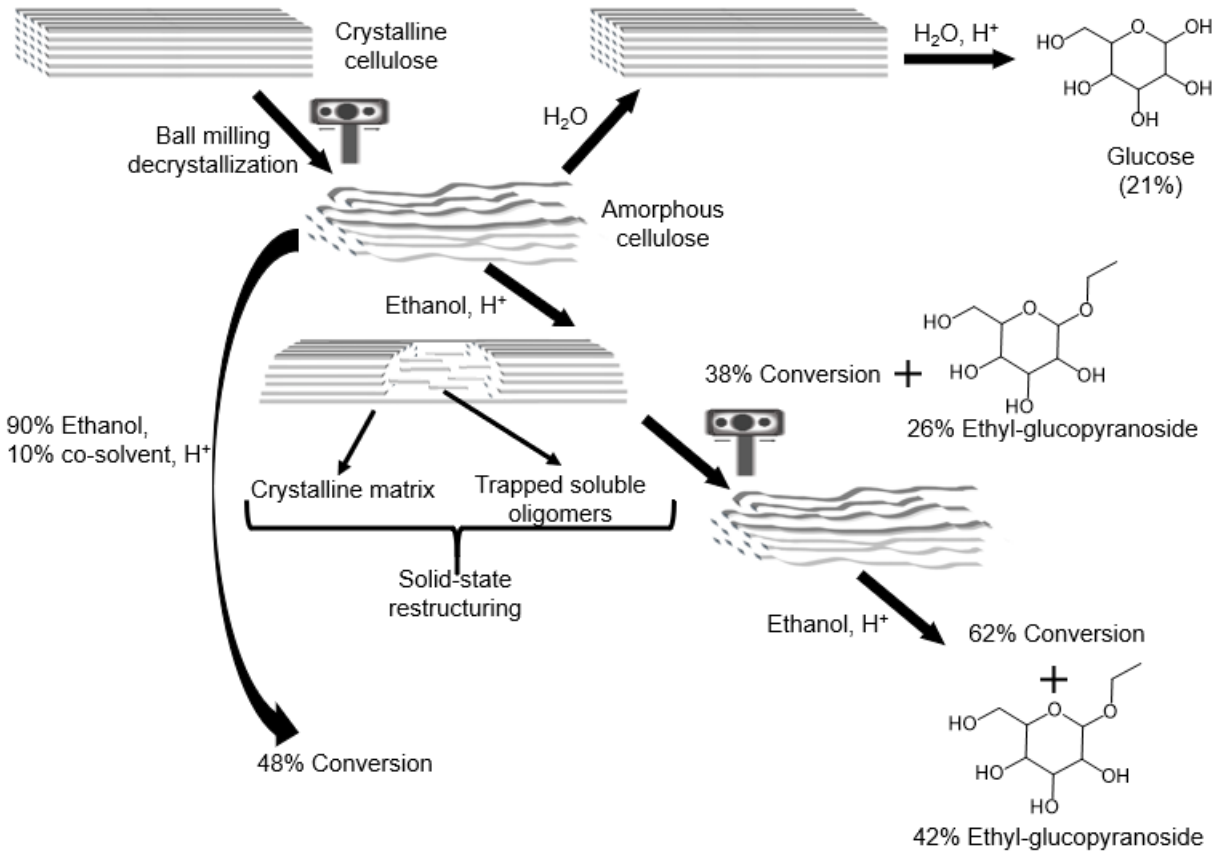

Acknowledgements

No words can describe my great appreciation for the people who contributed to my development during my Ph.D. studies! I can only attempt to express my gratitude.

I am grateful for having Prof. Michael Timko as an academic advisor. He was a positive force in my life, constantly providing me with the support I needed, pushing me forward, motivating me, and inspiring me. Countless discussions and valuable feedback from Mike made me not only a better researcher, but also a better person. It was a pleasure to discuss ideas with him. Although, quite often I disregarded his directions, and to my benefit sometimes it worked in my favor, I wish I had listened to Mike more often. I owe him a big thank you for his patience and unshakable belief in me and for being such a great mentor.

I would also like acknowledge and thank my committee members Prof. Marion Emmert, Prof. Aaron Deskins, Prof. Ronald Grimm, and Prof. Christopher Lambert. Although I was intimidated by their critical examination of my work, their hard questions made me a thoughtful researcher. I owe a significant portion of my accomplishments to the high standards they nurtured in me. I would like to thank Prof. Emmert for her assistances on an experimental and analytical level as well as connecting us to amazing collaborators. Prof. Deskins advised me and my students on modeling interactions between molecules that we were interested and provided valuable feedback. Prof. Grimm (or Ron, as he always asked me to refer to him) was a source of ideas and points of views that I had not considered and that broadened my horizon. In addition, he was very helpful and patiently taught me how to use X-ray Photoelectron Spectroscopy. Prof. Lambert was always available in Goddard Hall to assist me with chemicals, to answer questions regarding organic chemistry, and to chat about football.

I would like to acknowledge and thank our collaborators. I was very happy to work with Prof. Klaus Schmidt-Rohr, Pu Duan (Ph.D. Student), and Shichen Yuan (Post-doctoral researcher) from Brandeis University, who carried out Nuclear Magnetic Resonance analysis of our samples. Their integrity, work ethics, and level of expertise are exemplary and inspiring! I would also like to thank Prof. Kristalla Prather and her team Jason Boock (Post-doctoral researcher), Lisa Guay (Ph.D. student), Stephanie Doong (Ph.D. student), Kevin Fox (Ph.D. student) from Massachusetts Institute of Technology. For two years they provided me with access to their equipment which was instrumental to my research. Unaware, Jason became my mentor as he was happy to share his experience, answer my eager questions, and listen to my incessant complaints; he was a great company to have beer with at AICHE conferences. Prof. Marcus Foston and his student James Meyer (Ph.D. student) from Washington University at St. Louis assisted us with analyzing cellulose samples; Prof. Foston was also very happy to share his immense experience and knowledge he had of biomass deconstruction. I was happy to work with Prof. Sergio Granados-Focil from Clark University who was a constant companion during our studies of polymer catalysts and cellulose; his expertise was instrumental in understanding the behavior of polymers. Also from Clark University Dr. Frederick Greenaway taught us Electron Paramagnetic Resonance analysis and eagerly characterized our samples.

I should also recognize the colleagues from WPI. I want to mention Prof. Geoffrey Tompsett, Douglas White, and Tom Partington. Prof. Tompsett was always making sure we were safe in the lab. He was also constantly available to give advice and provide help and supported me and my colleagues during our studies. Doug maintained a high standard of organization and usage of the X-ray diffractometer and was always there fix the mistakes we made. Tom always surpassed my expectation in engineering of custom parts necessary for my experiments. Longkuan Xiang was very helpful in providing me access to the Bioprocessing Center so that I can use the equipment there. Wenwen Yao carried out ion chromatography analysis of our samples, for which I am very thankful.

I need to acknowledge all the undergraduate volunteers, REU, and MQP students that worked with me. Their work contributed so much: Andrew Wood, Luke Habib, Zachary Burgess, Jordan Finzel, Zachary Weiland, Stephanie Sontgerath, Christopher Skangos, Katherine Gomes, Caroline Murphy, and Katherine Ralph. I hope I have not missed anyone.

My fellow Timko lab mates Azadeh Zaker (good morning hug-buddy), Avery Brown (fellow Caribbean), Alex Maag (the best pizza-baking roommate), and Ziyang Zang (another poor soul studying solid acid and cellulose) were a great companionship for all those years. It will take me a whole book to share all the good stories I had with them, I am happy for all the support, fun, and difficult times we had. They were the best fellow Ph.D. colleagues I could ask for. I should mention also Zijian Ma, Tongie Zhang, Joseph Zheng, Yuanpu Wang, Brendon McKeogh, Patricia Guerra, and John Hobson made the lab a great place to work, full of wonderful people.

Throughout the years I became good friends with Behnam Partopour with whom we discussed the difficulties international students face. Behnam was an indispensable part of my support system for which I am very grateful. Also, I should acknowledge all the people with whom I had the pleasure to work and start an organization (CEGO): Lindsay Lozeau, Satish Iyemperumal, Lida Farsi, Ivan Ding, and Cameron Armstrong. The list of people goes on so I will briefly mention a few other colleagues who I am happy to have befriended: Todd Alexander (another WPI fossil like me and gym-guru), Cyrus Kian (crypto-buddy), Heather Leclerc (coffee-mate), Leslie Brodeur, and Tiffany Royal.

I need to express my utmost gratitude to the people who made my studies possible. My family always stressed the importance of education. My parents, Vasil and Veselina, and my brother, Vladimir, sacrificed so much so that I can get an education in the USA. My sister-in-law, Magdalena, and my two gorgeous nephews, Deyan and Alex, provided the warmth that I needed even from across the ocean. No accomplishment or recognition can ever outweigh the time spent with my family. Courtnae-Symone Currie was the reason I undertook graduate studies. She inspired me, motivated me, and persuaded me to follow my dreams. She sacrificed her own time to provide me with much needed support in difficult moments and her family, Matthieu and Marjorie, made me feel as one of their own, for which I will be forever grateful.

Last, but not the least, I need to thank all my friends who patiently waited me for months to leave the lab and to spend time with them. I will not be able to list them all, but they made my graduate student experience more bearable, knowing they were always there for me.

Table of Contents

Table of Figures

Table of Schemes

Table of Tables

CHAPTER 1

Introduction and Motivation

Despite global inaction, the scientific evidences are conclusive that global warming is taking place.[1] Several of the warmest years ever to be recorded have occurred since the 1980's which directly correlates with the ever-increasing atmospheric CO_2 concentration.[2, 3] The majority of anthropogenic CO_2 emissions are attributed to the burning of fossil fuels.[3] Climate change mitigation strategies involve CO_2 emission reduction, which ultimately requires divestment from fossil fuels and a transition to renewable and carbon neutral or negative energy sources and technologies.[4-6] Currently, however, fossil resources account for approximately 80% of the total energy consumed in the United States (see Figure 1.1.).

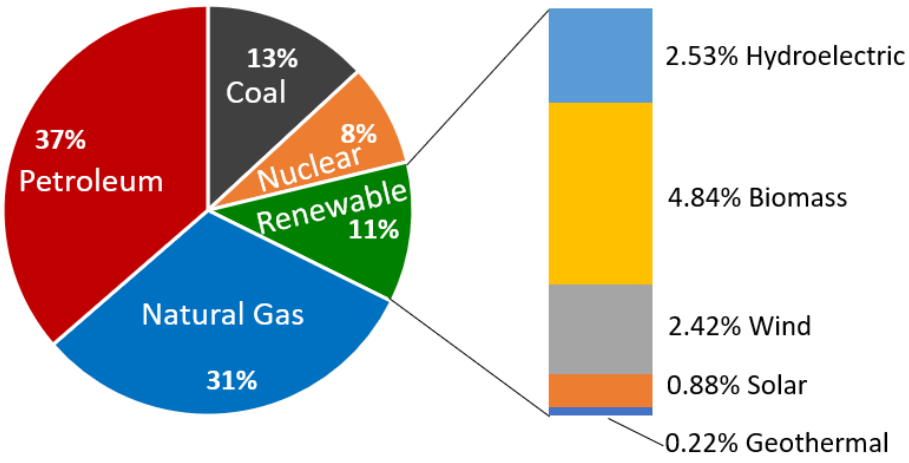

Figure 1.1. U.S. energy consumption by source in 2018. Data was obtained from Energy Information Administration (eia.gov).

Energy generated by combustion of fossil fuels powers virtually every sector of the modern economy, from electricity, transportation, and industry, to residential and commercial needs. Considering the enormity of their utility and penetration, a widespread replacement would require both technological advances as well as resource diversification.[6] Future industrial and energy needs will be satisfied by rationally integrated net zero emission systems including solar, wind, and nuclear power, carbon dioxide capture and conversion, and biomass utilization.[7] However, carbon intensive sectors such as steelmaking, aviation, shipping, and long-distance transport will continue to rely on energy generated by fossil fuels.[7] Accordingly, liquid fuels will have to satisfy a significant portion of the energy demands in the coming decades, which cannot be provided by wind, solar, or hydrothermal power generation.[8] In addition, petroleum, natural gas, and coal are main feedstocks in the chemical industry, solidifying their dominant role which imposes additional requirements on renewable sources.[9] Emerging energy and industrial approaches will have to meet the challenges that replacement of fossil fuels posits.

Biomass a renewable plant-based resource that can be utilized to produce both fuels and chemicals.[10] Through photosynthesis, biomass absorbs CO_2 and stores it in its structure, later to be emitted back in the atmosphere after a conversion process, such as combustion, a cycle that does not result in atmospheric accumulation of CO_2. In fact, proper land management and rational utilization practices can result in CO_2 negative overall process.[11] Therefore, biomass utilization represents an opportunity for net zero greenhouse gas emissions alternative to fossil fuels and the technological role they play in human civilization. Undoubtedly, biomass will play a central role in the transition from fossil fuels.[12]

Currently, biomass constitutes approximately 5% of the US energy mix (see Figure 1.1.). Department of Energy projects sustainable production of 1.3 billion tons per year by 2030 of non-

edible plant matter, enough to replace 30% of current US fossil fuel usage.[13] Non-edible plant structures have an advantage over starch-based feedstocks as they do not serve as a source for food production.[14] The huge potential is exemplified by the passing of the Renewable Fuel Standard (RFS) by the US Congress in 2005.[15] The projections introduced in the RFS posed an increasing role of lignocellulosic (non-edible) biomass as a source of fuels.[16]

Ultimately, economic competitiveness determines the adoption of lignocellulosic and displacement of fossil-based fuels.[17] However, the price of the renewable lignocellulosic fuels is greater than its gasoline energy equivalence.[18] The main reason stems in the fact that lignocellulosic biomass conversion requires substantial capital investments which hinders large scale production.[19] As a corollary, the volume of lignocellulosic based fuels produced was an order of magnitude lower than the RFS targets.[20] Despite its potential, widespread utilization and commercialization of lignocellulosic biomass remains an elusive goal.

The studies presented here are guided by the overarching theme of cost reduction of lignocellulosic biomass conversion. The approach is bottom-up: generating a theoretical framework of promising deconstruction technologies and addressing a fundamental aspect of the susceptibility of lignocellulosic biomass to chemical breakdown.

1.1. References

1.J. Cook, N. Oreskes, P. T. Doran, W. R. L. Anderegg, B. Verheggen, E. W. Maibach, J. S. Carlton, S. Lewandowsky, A. G. Skuce, S. A. Green, D. Nuccitelli, P. Jacobs, M. Richardson, B. Winkler, R. Painting and K. Rice, *Environmental Research Letters*, 2016, **11**, 048002.

2.J. Yin, J. Overpeck, C. Peyser and R. Stouffer, *Geophysical Research Letters*, 2018, **45**, 1069-1078.

3.B. Ekwurzel, J. Boneham, M. W. Dalton, R. Heede, R. J. Mera, M. R. Allen and P. C. Frumhoff, *Climatic Change*, 2017, **144**, 579-590.

4.N. Bauer, V. Bosetti, M. Hamdi-Cherif, A. Kitous, D. McCollum, A. Méjean, S. Rao, H. Turton, L. Paroussos, S. Ashina, K. Calvin, K. Wada and D. van Vuuren, *Technological Forecasting and Social Change*, 2015, **90**, 243-256.

5.M. Bui, C. S. Adjiman, A. Bardow, E. J. Anthony, A. Boston, S. Brown, P. S. Fennell, S. Fuss, A. Galindo and L. A. Hackett, *Energy & Environmental Science*, 2018, **11**, 1062-1176.

6.P. A. Owusu and S. Asumadu-Sarkodie, *Cogent Engineering*, 2016, **3**, 1167990.

7.S. J. Davis, N. S. Lewis, M. Shaner, S. Aggarwal, D. Arent, I. L. Azevedo, S. M. Benson, T. Bradley, J. Brouwer and Y.-M. Chiang, *Science*, 2018, **360**, eaas9793.

8.L. M. Fulton, L. R. Lynd, A. Körner, N. Greene and L. R. Tonachel, *Biofuels, Bioproducts and Biorefining*, 2015, **9**, 476-483.

9.J. J. Bozell, *Science*, 2010, **329**, 522-523.

10.F. H. Isikgor and C. R. Becer, *Polymer Chemistry*, 2015, **6**, 4497-4559.

11.G. P. Robertson, S. K. Hamilton, B. L. Barham, B. E. Dale, R. C. Izaurralde, R. D. Jackson, D. A. Landis, S. M. Swinton, K. D. Thelen and J. M. Tiedje, *Science*, 2017, **356**.

12.V. Balan, D. Chiaramonti and S. Kumar, *Biofuels, Bioproducts and Biorefining*, 2013, **7**, 732-759.

13.M. Langholtz, B. Stokes and L. Eaton, *Oak Ridge National Laboratory, Oak Ridge, Tennessee, managed by UT-Battelle, LLC for the US Department of Energy*, 2016, **2016**, 1-411.

14.H. B. Aditiya, T. M. I. Mahlia, W. T. Chong, H. Nur and A. H. Sebayang, *Renewable and Sustainable Energy Reviews*, 2016, **66**, 631-653.

15.J. Hill, L. Tajibaeva and S. Polasky, *Energy Policy*, 2016, **97**, 351-353.

16.K. Bracmort and T. Cowan, *The Renewable Fuel Standard (RFS): waiver authority and modification of volumes*, Congressional Research Service, 2016.

17. Chen and P. M. Smith, *Biomass and bioenergy*, 2017, **102**, 52-61.

18.T. R. Brown, *Bioresource Technology*, 2015, **178**, 166-176.

19.L. R. Lynd, X. Liang, M. J. Biddy, A. Allee, H. Cai, T. Foust, M. E. Himmel, M. S. Laser, M. Wang and C. E. Wyman, *Curr Opin Biotechnol*, 2017, **45**, 202-211.

20.L. R. Lynd, *Nat Biotechnol*, 2017, **35**, 912-915.

CHAPTER 2

Background and Objectives

The renewability of lignocellulosic biomass and its technological potential for displacement of fossil feedstock has attracted significant research interest in its conversion to commercially relevant products.[1] Furthermore, the utilization of biomass represents an economic opportunity for revitalizing rural communities by providing employment and source of income.[2] Considering its environmental and socioeconomic benefits it is important to address the technological barriers that prevent competitive conversion of lignocellulosic biomass and commercialization of lignocellulosic fuels and chemicals.[3, 4]

This section will provide a brief overview of certain technological aspects of lignocellulosic biomass conversion to low molecular weight products and will focus on two main aspects of cellulose depolymerization.

2.1. Structure and Composition of Lignocellulosic Biomass

The difficulties of converting lignocellulose to commercial products are routed in its chemical structure. Lignocellulosic biomass is composed mainly of three polymers – hemicellulose, cellulose, and lignin (see Figure 2.1.).[5] In plants, the three polymers are linked and form a complex composite structure, called cell wall, that encapsulates the inner contents of the cell.[5] The structure of the cell wall and specifically the organization of the polymer complex has evolved to provide structural support and protection against biological and chemical agents and deconstruction.[5]

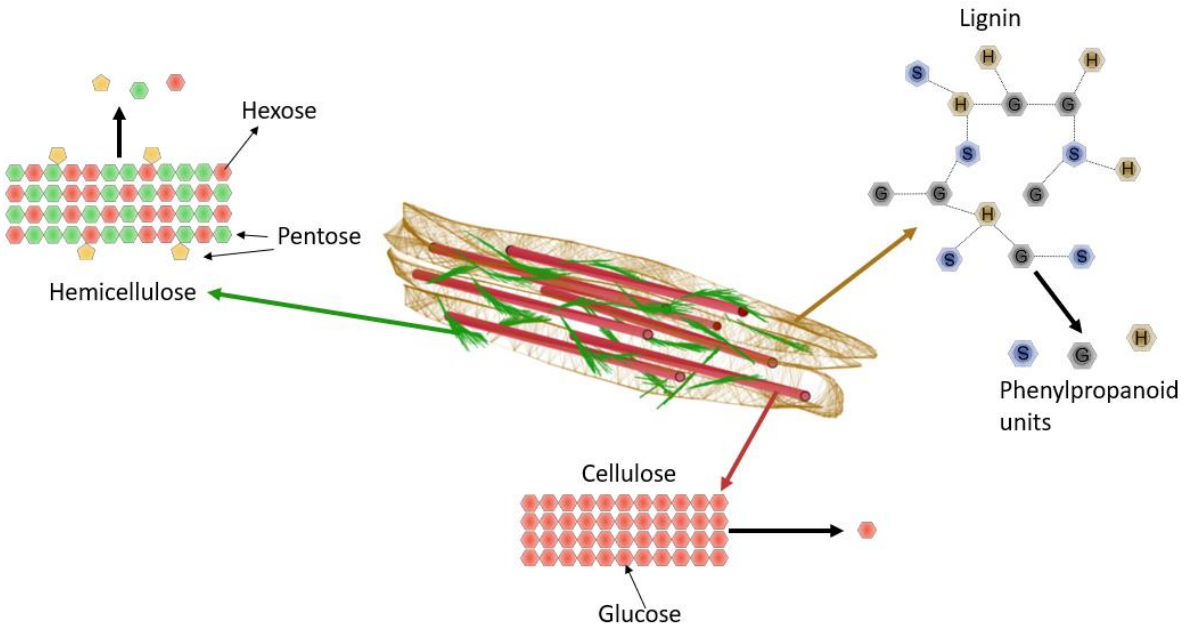

Figure 2.2. Artistic representation of the composite structure of lignocellulosic biomass forming the plant cell walls. The individual polymer components and their monomers are identified.[5]

2.2. Cellulose

Cellulose accounts for 35-55% of lignocellulose by mass, making it the most abundant polymer on earth.[6] It is a homopolymer composed of glucose units connected by β-1,4 glycosidic bonds.[7] Cellulose polymer chains interact with one another via hydrogen bonding and van der Vaal forces which results in highly organized crystalline structure.[7] The arraignment of the hydrogen bonding between the hydroxyl groups of the polymers determines the crystalline allomorph of cellulose crystals.[8] While several crystalline organizations are known, crystalline allomorph I (α and β) are present in lignocellulosic plant biomass.[7] The details of the crystalline structure of cellulose and its implications on conversion processes will be addressed later in this section. In the cell wall, cellulose chains are organized in microfibrils that are embedded in a lignin-hemicellulose matrix, which limits accessibility to depolymerization agents.[9]

2.3. Hemicellulose

Hemicellulose, composing 25-35% of lignocellulose, is a heteropolymer composed of five-carbon (pentoses) and six-carbon (hexoses) monomer carbohydrates, and acetylated sugar monomers connected by different glycosidic linkages.[10] Due the heterogeneity of its structure, hemicellulose does not form crystalline organization like cellulose.[1] In the plant cell wall it binds to both cellulose and lignin via hydrogen bonding and covalent linkages, resulting in a lignin-carbohydrate complex.[9]

2.4. Lignin

Lignin contributes between 20% and 30% to the mass of lignocellulose, depending on the plant species.[1] Lignin is a three-dimensional amorphous heteropolymer composed of phenylpropanoid units.[11] The constituting monomers can be characterized by the aromatic residues in their structure. p-hydroxyphenyl (H) monomer exhibits a hydroxyl group in para position to the propanoid chain. Guaiacyl (G) features two hydroxyl groups in meta and para positions. In addition to a hydroxyl group in para position, synapyl (S) monomer contains two methoxy groups in meta position.[11] Unlike the carbohydrate monomers, which are linked mainly by glycosidic bonds, lignin monomers are connected by a various C-O and C-C linkages which complicates its depolymerization.[11]

2.5. Depolymerization of Lignocellulosic Biomass

Synthesis of lignocellulosic fuels and chemicals relies on the deconstruction of cellulose, hemicellulose, and lignin to its monomeric structural components.[1, 12-14] The overall goal is depolymerizaiton of lignocellulosic biomass to low-molecular weight species that either are commodity chemicals or fuels or can serve as platform molecules for further upgrading.[15] Several engineering approaches exist for deconstruction of biomass; conversion can be classified based on

the process parameters such as temperature, residence time, solvent use, and targeted product.[16, 17] While the aim here is not to focus on the details of each process, a brief description is provided.

Gasification is an energy intensive process carried out at temperatures greater than 600 °C in the presence of water and aims to break the carbon-oxygen, carbon-carbon, even carbon-hydrogen bonds present in the biomass polymers producing syngas, a mixture of CO_2, CO, H_2, and CH_4,.[16-19] In addition to the gaseous products, heavier hydrocarbons classified as *tar* can be formed.[20] The chemical nature of tars depends on the process parameters used for gasification; low temperature result in oxygenated species, while higher temperatures favor heavier hydrocarbons.[20] The syngas can be upgraded to wide range of hydrocarbon products similar to those produces by fossil fuels.[21] While tars are an undesirable product from gasification, they can be valorized by cracking and converted to diesel-like molecules.[22]

Pyrolysis is a thermal approach for depolymerization of lignocellulose that typically takes place at temperatures below 800 °C and in inert environment employing various reactor configurations and residence times.[18] As a slightly less severe process than gasification, pyrolysis can retain some of the chemical bonds present in the polymeric molecules resulting in the formation of low molecular weight volatile species, liquid products, CO_2, and solid residue of carbonized material.[23] Retaining some of the bonds during this depolymerization approach offers for direct yield of desired products, potentially reducing the necessity further upgrading processes. The engineering challenges that currently are the focus of intense research include increasing yields and selectivities of desired products.[24] Significant efforts attempt to fundamentally understand the underlying reactions and minimize side pathways, ensuring optimum selectivity.[23, 25, 26]

Significant reduction of temperature can be achieved by using water as a reaction medium in a thermochemical processes termed hydrothermal liquefaction where reaction takes place between 200° C and 400 °C.[19, 27] Such conditions favor scission of carbon-oxygen bonds, but breaking as well as reformation of carbon-carbon bonds also occurs. Typically, this approach targets a complex bio-oil mixture as a product, whereas side products are gaseous, aqueous soluble, and solid species.[27, 28] The bio-oil is composed of large number of oxygenated species and finds several uses. Its heating value is similar to fossil oil which makes it suitable for use as a combustion fuel. While the bio-oil can also serve for the production of specialty chemicals the high number of species necessitates separation processes that result in additional increase of the cost of an already expensive process.[29] The lower yields of bio-oil compared to pyrolysis, but better quality, has motivated strategies for increasing the product.[29] Maximizing the oil yield is typically achieved by the use of catalysts that assist the deoxygenation of species or by upgrading the aqueous soluble species.[30, 31]

The abovementioned processes require significant energy inputs to achieve the reaction temperatures employed in the depolymerization of lignocellulosic biomass. In addition, at those severe conditions the depolymerization products are highly reactive and can further decompose. This leads to large number of reactions involving complex mechanisms that complicate or completely prevent selective control of desired pathways. As a result, a mixture of products is obtained, and carbon can be lost to CO_2. Further upgrading to specific products requires additional separation and purification units, which increases the overall cost of conversion.

On the other hand, the polymers can be selectively deconstructed to their monomeric units by rational reaction engineering design. For example, hydrolysis of the carbohydrate fraction of lignocellulosic biomass is a selective process that depolymerizes and solubilizes the hemicellulose

and cellulose components in water.[10, 32, 33] From a process perspective, since lignocellulosic biomass characteristically contains certain amount of moisture, hydrolysis is an appropriate approach as it doesn't require energy intensive feedstock drying.[34] In addition, water is a non-toxic solvent which renders the process inherently environmentally friendly.[35] The main goal of hydrolysis is selective scission of the glycosidic carbon-oxygen bonds linking the sugar monomers; these linkages are typically the most reactive bonds in the carbohydrate fractions. At the conditions at which hydrolysis is typically carried out (below 300 °C and dilute or no acid) the cellulose is in solid state and does not undergo phase changes, inherent for gasification, pyrolysis, and liquefaction, which reduces complexity and offers greater control of the deconstruction reaction.[36] Therefore, the process is inherently heterogeneous, occurring on the surface of the solid substrate, progressing by polymer chain length reduction and release of soluble molecules in the reaction medium.[37-40] The sugar monomers can then be upgraded via fermentation or via chemocatalytic processes to targeted products.[1, 41] Upgrading, especially fermentation, can be carried out in the same aqueous sugar solutions resultant from hydrolysis which reduces the necessity for additional purification steps.

Even greater control of the depolymerization reactions of lignocelluosic biomass can be achieved due to differences in reactivity of the hemicellulosic and cellulosic fractions. The two biopolymers can be depolymerized separately by adjusting the process conditions, despite the structural nature of the lignocellulosic complex (see Figure 2.1.).[10] Due to its heterogeneous and amorphous structure, hemicellulose is more reactive and can be solubilized at conditions at which cellulose remains relatively intact.[10] For example, Nitsos et al treated lignocel (a type of wood feedstock) in hot liquid water at temperatures between 100 °C and 220 °C and reported progressive removal of hemicellulose from the biomass substrate and a corresponding production of sugar

monomers.[42] At the same time virtually no conversion of cellulose to glucose monomers was observed. Similarly, Kumar et al. reported that treatment of switchgrass at temperature up to 190 °C resulted in nearly 80% of hemicellulose removal, with minimal losses of cellulose.[43] Dilute acid treatment can achieve similar results. Li et al treated switchgrass with 1.2 wt% H_2SO_4 at 160 C for 20 minutes and removed the majority of xylan, arabinan, and galactan, components of hemicellulosic fractions, while cellulosic glucan was only partially solubilized.[44] In contrast, cellulose requires significantly harsher conditions for depolymerization and solubilization.[45-47]

Therefore, hydrolysis offers a selective and highly controllable approach for the depolymerization of the carbohydrate fractions of lignocellulosic biomass. In fact, one of the main biorefinery concepts employs hydrolysis of cellulose and upgrading of the produced monomeric sugar to ethanol via fermentation. However, this strategy for converting biomass has failed to materialize on a commercial scale.

2.6. Cellulose Hydrolysis

The success of a hydrolysis-based biorefinery depends on the efficient depolymerization of cellulose.[48] Considering that cellulose composes the majority of the lignocellulosic complex, extracting its carbohydrates followed by subsequent upgrade to commodity products such as fuels and chemicals has to be economically competitive to conventional routes based on utilization of fossil-based resources.[49, 50] The main focus of cellulose hydrolysis is the targeted scission of the glycosidic bond by the addition of a water molecule and solubilization of its glucose monomer unit, thereby, achieving near quantitative product selectivity (see Scheme 2.1.). Generating a relatively pure glucose product solution, with minimum byproducts such as oligomeric cellulosic molecules or degradation compounds eliminates downstream purification units and thus reduces process costs.[51]

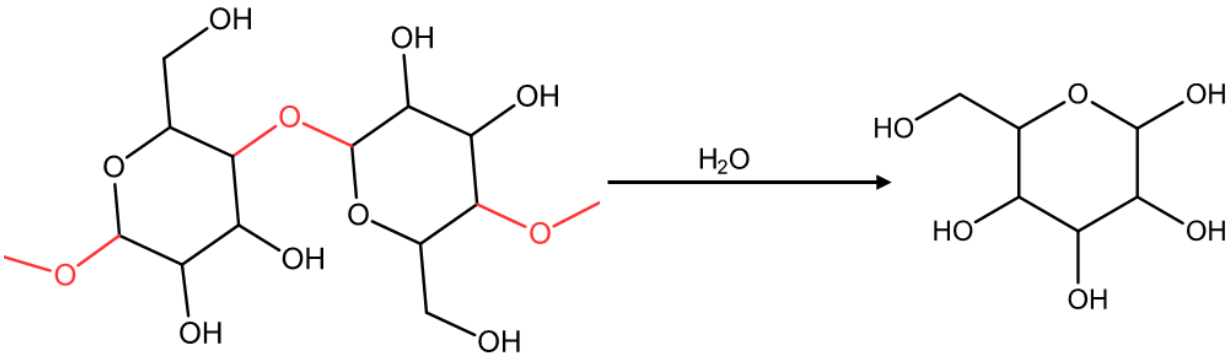

Scheme 2.1. Hydrolysis of cellulose polymer chains to glucose by addition of a water molecule. The glycosidic bond that is broken during the reaction is colored in red.

2.7. Utilization of Glucose

The glucose released from hydrolysis of cellulose can be converted to wide range of platform molecules and end products. For example, the hydrolysate solution can be directly inoculated, and glucose can be fermented to various acids or alcohols which find application as fuels or platform chemicals.[15] In addition, glucose can be converted via chemocatalytic routes.[1, 15, 52] Dehydration produces hydroxymethyl furfural, a fuel and polymer precursor.[53] Oxidation yields glucaric acid, which according to US Department of Energy report, is a building block for the production of industrially relevant chemicals.[54, 55] Glucose hydrogenation produces sorbitol, which finds applications in wide range of industries.[41] Conveniently, glucose conversion reactions are carried out in the presence of water which allows for the design of an integrated process from hydrolysis to value added product synthesis reducing the necessity for additional solvents.[41] Clearly, selective cellulose hydrolysis to glucose is a technologically relevant route for the utilization of lignocellulosic biomass.

Despite the benefits of greater reaction control, selectivity, and downstream processing, cellulose hydrolysis has remained economically uncompetitive process. Cellulose hydrolysis can

be carried out at various conditions employing the use of different catalysts. Efforts to decrease conversion costs merit from detailed understanding of the hydrolysis reaction that would allow identifying and selecting pathways resulting in minimizing costs.

2.8. Enzymatic Hydrolysis

Cellulose can be depolymerized to glucose via the action of biological catalysts called enzymes, collectively termed cellulases.[33] Three types of enzymes act synergistically to break down the glucan polymer. Endoglucanases randomly cleave glycosidic bonds in the interior of a polymer chain, cellobiohydrolases act on the polymer chain ends releasing cellobiose, and β-glucosidase hydrolyzes cellobiose to glucose.[33, 40] Endoglucanases generate new chain ends which are attacked by the cellobiohydrolases; β-glucosidase, on the other hand, reduce the concentration of cellobiose which has a poisoning effect on cellobiohydrolases.[33, 40]

The enzymes from the cellobiohydrolazes family are typically composed of 3 structural domains: a catalytic domain is connected to a cellulose (or carbohydrate) binding domain (CBD) via a peptide linker.[33] The enzyme first adsorbs on the cellulose surface, diffuses until a chain end is located and complexation with the catalytic domain occurs, followed by scission of a glycosidic bond and release of cellobiose decomplexation and desorption of the enzyme.[33]

Enzyme adsorption plays a significant role in the activity of the enzymes as cellobiohyrolases whose structure has been modified and their CBD structurally altered or completely removed exhibit lower activity.[56] Structural studies have elucidated the nature of the enzyme-cellulose recognition and complexation. For example, binding modules interact with crystalline cellulose surface via aromatic residues via non-specific CH-π interactions entropically displacing water.[57] Hydrogen bonding contributes to CBD-carbohydrate complexation by stabilizing the CH-π conformation and interacting with the hydroxyl groups of cellulose.[58]

Enzyme-catalyzed depolymerization occurs at relatively low temperatures – typical optimal temperature is 50 °C and reaction times are on the order of tens of hours to a few days.[33, 59] Increasing reaction rates cannot be achieved by raising temperature because the enzymes will undergo structural transformation and lose their activity, a processes termed denaturation.[60] Alternatively, increasing cellulose hydrolysis rates can be achieved by altering the reactivity of the lignocellulosic substrate as conceptually shown in Scheme 2.2. Considering that hydrolysis of solid cellulose substrate is a heterogeneous reaction it is likely limited by the accessible cellulose surface area.[61] Indeed, hydrolysis rates correlate with the accessibility of the lignocellulosic substrate to a molecule the size of enzymes.[62] Pretreatments that remove hemicellulose or lignin, such as hydrothermal, dilute acid, solvolysis and chlorite delignification, increase the access of enzymes and result in shorter reaction times and greater glucose yields.[63] In addition, unproductive binding of cellulase to lignin is reduced after delignification pretreatments, allowing further benefits for enzyme processivity.[64] Further, studies on pure cellulosic substrates further reveal that enzymes are more active at hydrolyzing cellulose with lower degree of crystalline organization.[65]

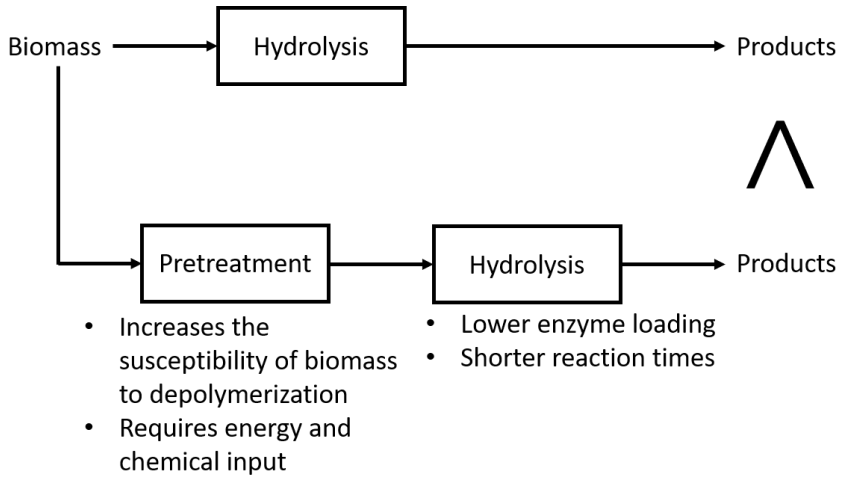

Scheme 2.2. Hydrolysis of biomass is enhanced by pretreatment that renders the lignocellulosic substrate more amenable to depolymerization. Hydrolysis of pretreated biomass has lower process requirements and results in greater product yields. Pretreatment requires energy and/or chemical inputs.

Therefore, achieving greater glucose yields in shorter reaction times, which ultimately results in lower conversion costs and greater process profitability, by enzyme-catalyzed hydrolysis of cellulose in a lignocellulosic matrix is heavily dependent on pretreatment methods that render the biomass more amenable to deconstruction. In addition, reducing the cost of producing enzymes is also an approach to make hydrolysis more economically competitive; however, there are still challenges in this area.[66]

2.9. Hydrothermal and Acid-catalyzed Cellulose Hydrolysis to Glucose

The rate of cellulose hydrolysis to glucose can be increased by elevating the temperature in a simple hydrothermal treatment (no catalyst) or with the use of homogeneous acids as catalysts.[67, 68] Such processes are a case of hydrothermal liquefaction, however, where the conditions favor production of cellulose depolymerization species instead of bio-oil. Hydrothermal hydrolysis of cellulose can be carried out at relatively mild temperatures (150 °C), where the reaction time is in the range of tens of minutes, or at more severe conditions such as near critical or supercritical water, at which the reaction time is in the order of a few seconds.[69, 70] To further increase the rate, homogeneous acid catalysts at various concentrations are employed;[32, 67] however, typically dilute acid conditions (concentrations of up to 2 wt% acid) are favored to reduce reactor corrosion issues and product degradation.[46, 71, 72]

Increasing temperature and/or acid concentration reduces reaction times by an order of magnitude compared to cellulose hydrolysis by enzymes. However, since the glucose product can react further at those condition, parallel increase of the glucose decomposition reactions also occurs (see Scheme 2.3).[72, 73] Specifically, glucose can dehydrate to hydroxymethylfurural (HMF); the activation energy of glucose dehydration to hydroxymethyl furfural is lower than the activation energy of cellulose hydrolysis to glucose, which imposes a balance between cellulose conversion

and glucose yields by means of increasing reaction temperature.[46, 72] Moreover, the acid catalyst used for cellulose hydrolysis also catalyzes glucose decompositon.[72] In addition, hydroxymethyl furfural is a highly reactive intermediate which can be decomposed to levulinic and formic acids or polymerize to form insoluble humin species.[74, 75] Effectively the increase of the cellulose hydrolysis rate by means of increasing temperature and acid catalysts is accompanied by product degradation and loss of selectivity.

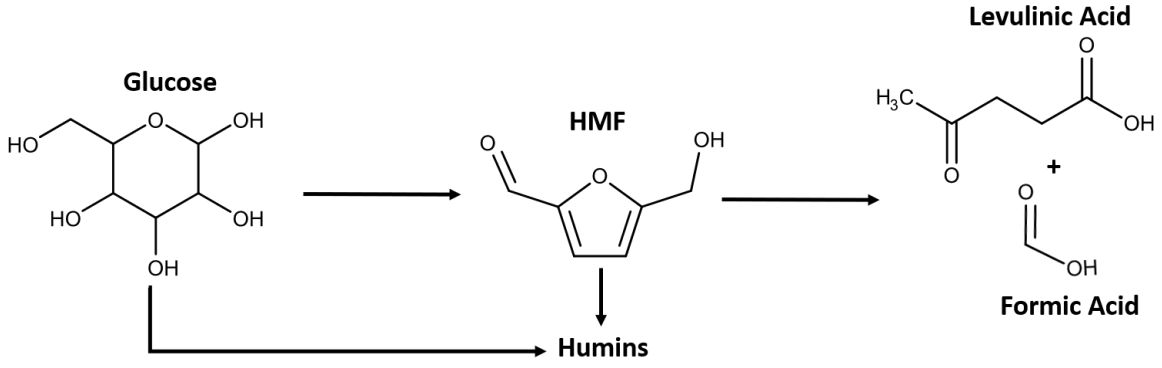

Scheme 2.3. Glucose degradation in hydrothermal environment. Glucose initially dehydrates to hydroxymethylfurfural (HMF). Further decomposition of HMF produces Levulinic acid and Formic acid. In addition, glucose and HMF can degrade to form insoluble humin species. These reactions are typically Brønsted acid catalyzed.

To mitigate the effects of glucose degradation, two strategies can be employed. First, reactor design can accommodate the necessity to limit glucose exposure to the severe reaction environment. For example, replacing batch reactors with semi continuous packed bed reactors, where the solid biomass substrate is packed in the reaction zone of the reactor, while the glucose is removed by continuous flow, offer greater yields and selectivities.[76] Despite that, the solid substrate can undergo reactions that result in char formation on the surface and trap the carbohydrates in the interior.[77] This can be circumvented by continuous flow reactors where biomass slurry is fed, hydrolyzed, and the products are rapidly evacuated from the reactor zone.[78]

Such an approach requires sophisticated reactor design and biomass slurry delivery system.[78] However, slurries are limited to around 5 to 10% mass loading due to the high pressure required for pumping limiting the concentration of glucose that can be achieved, necessitating additional downstream separation units.

Analogously to enzymatic hydrolysis, pretreatment of cellulose by means reducing its crystalline organization increases its conversion and product yields, allowing for reduction of process severity.[79, 80] For instance, cellulose pretreatment via ball milling increases the rate of conversion and glucose release.[81] The relationship between cellulose structure and its reactivity will be addressed later in the text.

Alternatively, cellulose hydrolysis can be used to produce hydroxymethyl furfural selectively.[41, 82] Since it is more reactive than glucose an approach to prevent it from reacting further is to employ two phase systems, where a solvent with greater hydroxymethyl furfural partition coefficient than water extracts the product as soon as it is formed.[41]

2.10. Engineering Considerations of Enzyme, Hydrothermal, and Acid Hydrolysis of Cellulose

Despite the promise that cellulose hydrolysis can be successfully applied for selective production of highly concentrated sugar solutions that can serve as a feedstock for synthesis of fuels and chemicals, it has not been commercially successful. In fact, ethanol produced from cellulosic sugars is more expensive than its gasoline equivalence, preventing competition with conventional fossil fuels.[48, 51]

It is important to address the technological challenges that contribute to the high costs of cellulose hydrolysis.[49, 83] Enzyme hydrolysis occurs at a relatively low rate. This limits the production capacity of a biorefinery and, thus, the revenues it can generate. As already mentioned,

pretreatment approaches can render lignocellulosic biomass more susceptible to degradation.[84] Indeed, pretreatment is typically included in technoeconomic models for ethanol production; despite that, the cost is still not competitive.[48, 51] The reaction rate of cellulose hydrolysis can be increased by higher enzyme loading.[85] However, not only enzymes expensive, but they also cannot be recycled, which imposes a balance between enzyme loading and overall process costs.[66, 86] As a result, enzyme hydrolysis and pretreatment are estimated to contribute 21% and 19%, respectively, to the price of cellulosic ethanol.[87]

The use of acid hydrolysis, on the other hand, suffers from loss of sugar selectivity. In addition, homogeneous acids promote corrosion damage to reactors, which necessitates the use expensive corrosion-resistant materials.[88] As mentioned, acid use can be reduced by cellulose decrystallization pretreatments. Interestingly, dilute acid hydrolysis pretreatment, aiming at selectively removing hemicellulose, has already been accounted for in calculating the cost of enzyme catalyzed conversion.[51] In such biorefinery concepts, the homogeneous acids are neutralized generating waste and are, thus, not recyclable.[51] While this analysis is applied specifically for pretreatment, a homogeneous acid cellulose hydrolysis process would necessitate identical treatment.

In contrast, hydrothermal hydrolysis does not employ the use of catalyst and is a promising approach.[69] However, in order to achieve high enough hydrolysis rates the temperature of the reaction has to be raised. Considering the heat capacity of water, this would require a significant amount of energy inputs.[51] From a process perspective, the heat generation for a biorefinery concept already represents a large portion of the operational costs for conversion; further increase of operating temperature would raise the energy requirements of the process, which will result in cost increase.

The analysis of the current engineering approaches for hydrolysis of lignocellulosic biomass identifies key parameters that contribute to the cost of depolymerization and biofuel production. First, the catalysts used to hydrolyze cellulose are not recyclable. Acid neutralization and purchasing fresh enzyme are two corollaries of that issue. Second, increasing the rate of cellulose hydrolysis to glucose without sacrificing product yields and selectivity requires reducing severity of conditions and pretreatment of the biomass substrate to increases its reactivity. A pretreatment step implies additional operational units and process costs.[48] Addressing those challenges requires fundamental understanding of the underlying chemical processes all in the context of water as a reaction medium.

2.11. Solid Acids as Recyclable Catalysts for Cellulose Hydrolysis

To overcome some of the limitations imposed by the use of enzymes or liquid acids, solid acid catalysts have emerged as a recyclable alternative.[89] Hypothetically, following hydrolysis solid acids can be recovered and reused; further, pretreatment and hydrolysis can be combined into one step, promising cost reduction. Compared to their liquid counterpart, solid acids have lower corrosion potential which allows for use of conventional materials for reactor construction.

Applying solid acid catalyst for cellulose hydrolysis is physically distinct from liquid-acid-catalyzed hydrolysis and from typical solid-acid-catalyzed gas or liquid phase reactions. Catalyst design and process development, from material synthesis to elucidation of reaction mechanism, must address the heterogeneous nature of the reaction. At the typical hydrothermal conditions used for hydrolysis, cellulose is a solid. Therefore, depolymerization catalyzed by a solid acid will occur on the contact surface between cellulose and the catalyst as shown in Figure 2.2. This imposes inherent mass transfer limitations; in contrast, homogeneous acid catalysis would occur on all accessible surfaces.

The current state of the solid acid catalyst for cellulose hydrolysis field is at the stage of material synthesis, characterization, and performance evaluation. Unlike hydrolysis by enzymes, the mechanism of solid-acid catalyzed hydrolysis is not elucidated, which prevents rational design of solid acid catalysts. Comparison of the cellulose hydrolysis catalyzed by different solid acid catalysts has been used as means to correlate the structure to the observed activity of the catalyst. For instance, conventional catalysts such as H-ZSM5 and H-mordenite do not exhibit activity greater than that of water at the same conditions.[90] On the other hand, materials such as sulfated zirconia, sulfonated polystyrene ion exchange resin (Amberlyst-15), and sulfonated activated carbon materials are able to hydrolyze cellulose and produce glucose, suggesting that strong Brønsted acids are necessary.[90-92] These observations raise the question – what are the structure-activity relationships of solid acid catalysts capable of hydrolyzing cellulose?

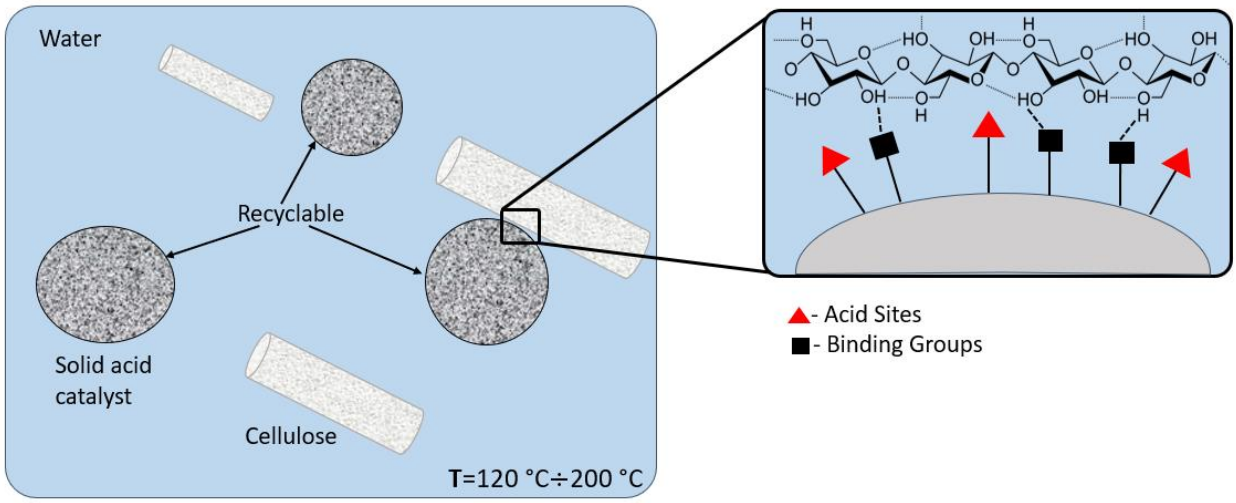

Figure 2.3. Application of solid acid catalysts for cellulose hydrolysis. Both the catalyst and the cellulose substrate are solids at the reaction conditions, which limits the depolymerization reaction to the contact surface area. The zoomed area depicts a hypothesized interaction between the solid acid catalyst and cellulose in which specific binding groups are thought to participate in non-covalent bonding to cellulose.

Binding is implied in increasing the time of contact of the two solids, thereby, increasing the probability for an acid group to hydrolyze the glycosidic bonds of cellulose.

Interestingly, catalysts that show good activity towards hydrolyzing cellulose and selectivity to glucose have multiple functional groups on their surface.[89, 91, 93-96] Most often such catalysts are decorated with catalytic strong acid groups such as sulfonic acid (-SO_3H) and with non-reactive groups such as carboxyl (-OH) or chlorine (-Cl) groups, or, as is the case of carbonaceous materials, exhibit delocalized π systems. It is hypothesized that the non-reactive groups increase the catalyst's affinity to cellulose by forming hydrogen bonds with the hydroxyl groups of cellulose (see Figure 2.2.).[91, 93] The binding hypothesis is supported by adsorption of soluble cellulosic molecules onto the solid acid catalyst at temperatures well below those used for cellulose hydrolysis.[93, 96-98] These non-reactive groups can serve as binding sites to the glucan chain; this supramolecular interaction can bring the β-1,4 glycosidic bonds and acidic sites to spatial proximity and conformation that is favorable for scission of the glycosidic bond as shown in Figure 2.2. The interactions between the solid cellulose substrate and the solid acid catalyst cannot be directly measured at the reaction conditions and, thus, the nature of the forces behind such binding cannot be elucidated.

Unfortunately, the plethora of proposed catalytic structures and the different conditions precludes a comparative and systemic analysis of different catalysts. Zuo et al addressed this by carrying out a systematic sulfonation of chloromethyl polystyrene, where chlorine is hypothesized to act as a binding group via hydrogen bonding to hydroxyl groups of cellulose and found an optimum composition that exhibited the highest cellulose hydrolysis activity, reminiscent of the Sabatier's principle.[99] Similar observations were made by Parveen et al who copolymerized 4-chloromethyl vinyl benzene and sulfonic acid-based ionic liquid and varied the amount of catalytic

and binding groups by changing the reactants ratio during the catalyst synthesis.[100] Qian synthesized a bifunctional catalyst with sulfonic acid groups and imidazolium chloride as a binding group by immobilizing and polymerizing 4-styrenesulfonate and imidazolium chloride on a ceramic or glass support and reported that varying the amount of functional groups affected the sugar yield after cellulose hydrolysis.[94] Such attempts only establish that presence of certain moieties that enhance the activity of the solid acid catalyst, but does not provide a direct evidence for interpreting the hydrolysis mechanism.

Development of structure-activity relationships depend on accurate catalyst characterization. Typically, catalysts are characterized by a bulk analysis method such as X-ray diffraction, X-ray photoelectron spectroscopy, elemental analysis, nuclear magnetic resonance, vibrational spectroscopy, and surface area analysis.[91, 93, 98-102] However, while the presence of functional groups is established by such techniques, only the external surfaces of the solid acid catalyst and solid cellulose substrate would interact, since the two are of relatively similar size and too large to diffuse of each other's porous structure. But bulk characterization does not provide the detailed structural representation of the external surface of the catalyst. Clearly, there is a gap in correlating the catalyst structure to its activity in hydrolyzing cellulose. This prevents identifying the catalytic site and implies that the mechanism that invokes binding between the catalyst and cellulose is just an unsupported hypothesis. Therefore, it is necessary to address this knowledge gap in order to elucidate the mechanism of cellulose depolymerization of solid acid catalysts.

In addition to the structure-activity inconsistencies, the interactions of the solid acid catalysts and the cellulose with the water solvent have also been overlooked in understanding the catalytic mechanism. Importantly, water can also form hydrogen bonds, which calls into question the conclusions deduced from adsorption analysis. Yabushita et al studied the adsorption of soluble

cellulosic oligomers on activated carbons and found that the interactions are dominated by entropically favored expulsion of water of the surface of the catalyst.[103] While increasing the chain length of the soluble cellulosic molecule resulted in greater adsorption on the activated carbons, raising the temperature reduced the equilibrium constant of the adsorption process.[103] Furthermore, Foo found that the adsorption decreased as the amount of oxygen containing hydrophylic groups of the activated carbon materials increased, suggesting competitive interactions with water.[96] Qi et al showed that varying the composition of the solvent, by introducing γ-valerolactone into the aqueous phase, affected the co-adsorption of glucose and water on zeolites.[104] However, no direct evidence of binding is presented for catalysts used for cellulose hydrolysis at reaction conditions with insoluble substrates nor have interactions with water been considered in the hypothetical mechanism.

Further development of solid acid catalysts for cellulose hydrolysis and elucidation of the catalytic mechanism require more detailed structural description of the catalysts and experimental approaches that can directly test the hypothesized mechanism. Specifically, external surface characterization should provide information on the catalytic site and additional performance tests will eliminate alternative possibility for activity interpretation.

2.12. Structure-Reactivity Relationship of Cellulose

Reduction of biomass conversion costs can be achieved by decreasing the reaction time and condition severity while maximizing product yields. Pretreatment of lignocellulosic biomass increases its susceptibility to deconstruction.[84] Different treatments aim at removing components and altering the structure to enhance cellulose hydrolysis.[63] For example, some pretreatments such as dilute acid or hydrothermal remove predominantly hemicellulose and parts of the lignin.[63] Other, solubilize the mainly the lignin fractions.[44, 105] Pretreatments like milling do not remove

individual components but impart structural changes that provide access to the solvent and the catalysts.[106, 107] Yet, since cellulose is more difficult to depolymerize then hemicellulose, understanding its reactivity and relating it to the structural characteristics of the polymer will allow for optimized pretreatment and depolymerization approaches that favor timely conversion and greater and more selective yields of small molecular weight products. As already mentioned, at typical hydrolysis reaction conditions cellulose is not soluble in water. Therefore, the reactivity is dependent on the supramolecular structural parameter.

Several characteristics describe the structural organization of solid cellulose substrates such as degree of polymerization, surface area, pore structure, and accessibility, particle size, and degree of crystallinity as shown in Figure 2.3.[7, 62, 108-110] Degree of polymerization (DP) of cellulose chains refers to the average chain length expressed as number of glucose units.[7, 111] Particle size, surface area, pore structure, and accessibility describe the geometric characteristic of cellulose substrates.[59, 62, 108] Crystallinity refers to the relative content of crystalline (organized repeating arrangement of the glucose units) and non-crystalline or amorphous regions in the structural organization of cellulose.[112] The crystal structure of cellulose is characterized by its extensive intra and interchain hydrogen bonding and chain stacking.[113, 114]

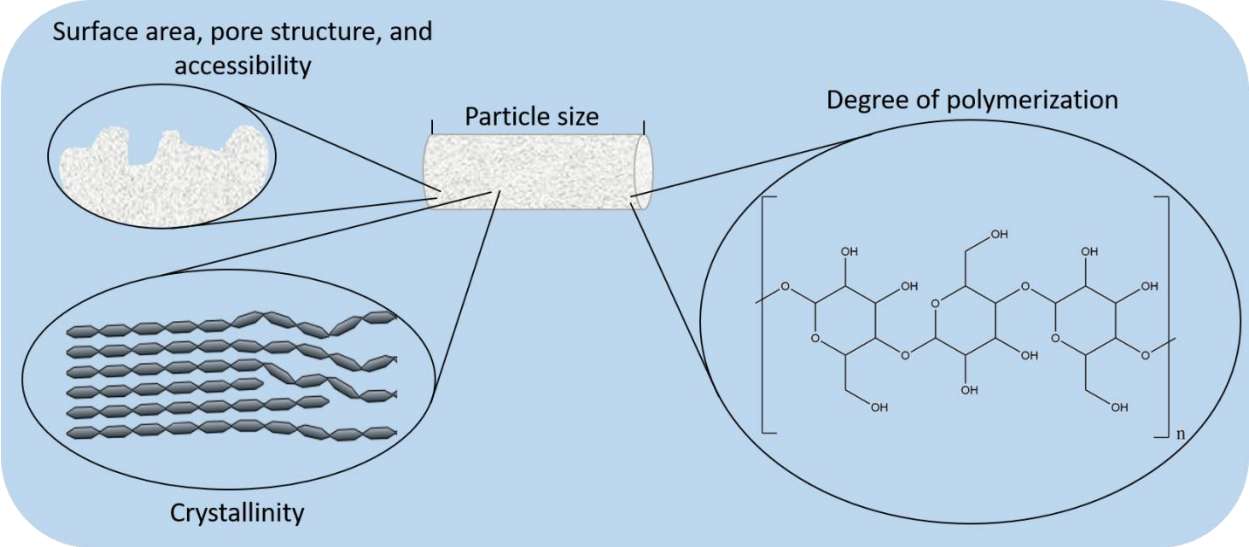

Figure 2.4. Physicochemical characteristics of solid cellulose substrates.

Cellulose reactivity in the context of hydrolysis has been widely studied. A typical analytical approach is to observe the changes of a structural parameter that occur during hydrolysis and to relate them to the substrate conversion and to the yield of soluble products.[59, 65, 79, 115, 116] Similarly, the cellulose substrate can be pretreated to alter its structure prior to hydrolysis.[80, 81, 117] However, during hydrolysis multiple structural parameters change at the same time, complicating the analysis.[79, 118-120] Therefore, directly attributing reactivity observations to a specific parameter may be incomplete or inaccurate. Furthermore, pretreatment to affect one structural characteristic prior to hydrolysis results in changes in other parameters.[121]

For instance, the degree of polymerization rapidly decreases during both acid and enzymatic hydrolysis; after high initial rate, the DP levels off and the reaction rate for conversion and release of soluble products significantly slows down.[37, 122, 123] This has been explained by hydrolysis of highly reactive amorphous regions; after their depletion the mode of hydrolysis is explained by chain-end attack.[116] Sinitsyn et al reported that the enzyme catalyzed hydrolysis rate was directly proportional to the accessibility of a molecule the size of an enzyme.[62] Additionally, progressive

deconstruction and solubilization of the solid cellulose substrate can change the pore structure, effectively increasing accessibility even further.[59] Similarly, an inverse relationship between crystallinity and reactivity has been reported as well as increases of crystallinity have been observed as the reaction progresses.[79, 120] Since pretreatment and hydrolysis result in changes of multiple structural characteristics, it is difficult to unravel the effects of each individual parameter to the reactivity of cellulose. As a result, both pretreatments and hydrolysis may not be optimized for greatest yield and selectivity of glucose.

Cellulose crystallinity represents an interesting case when analyzing the reactivity of cellulose towards hydrolysis. As already mentioned, rapid decrease of DP during hydrolysis is attributed to scission of highly reactive glycosidic bonds in the amorphous and non-crystalline regions of cellulose.[116, 119] Furthermore, pretreatments that decrease cellulose crystallinity such as ball milling, ionic liquid and concentrated acid dissolution and reprecipitation and swelling, result in an increase of the rate of hydrolysis.[69, 79, 115, 123] Interestingly, after hydrolysis the crystallinity of the residual cellulose substrate increases.[69, 79, 120] Along with changes in DP, these observations suggest that amorphous and non-crystalline regions of cellulose are more reactive than crystalline regions. Observations of lower thermal stability of decrystallized cellulose substrates provide further support of such arguments.[124, 125]

Decrystallizing cellulose to increase its reactivity, therefore, is a sensible preatreatment method. Thus, it is necessary to elucidate the structural characteristics of amorphous and non-crystalline cellulose that determine its susceptibility to depolymerization. Decrystallized cellulose exhibits lower density, greater water sorption capacity, greater surface area, and, as determined by nuclear magnetic resonance, greater content of surface chains.[39, 79, 124, 126] However, it is molecular-scale detail have not been fully understood. Mazeau and Heux used molecular dynamics simulation

to model amorphous cellulose and showed that it exhibits lower average number of hydrogen bonds, when compared to crystalline cellulose.[127] Chen et al modeled fibril bending and reported that at the point of the applied load the arrangement of the glucose units does not follow crystalline organization and the bonds are significantly strained.[128]

Kinetically, hydrolysis of the amorphous and crystalline fractions of cellulose cannot be explicitly described. The difficulty stems from the fact that unambiguous quantification of the relative fractions cannot be made. Since separation of the various fractions is physically impossible, various spectroscopic methods have been used to quantify crystallinity (the relative content of amorphous and crystalline regions) of cellulose substrates.[129, 130] However, the values are relative and heavily dependent on the technique of analysis.[129] On the other hand, crystallinity can be inferred from reactivity analysis.[131] Kinetic analysis of cellulose hydrolysis by assuming pseudo first order reaction of two species, crystalline and amorphous, reveals that the reaction rate for amorphous cellulose is an order of magnitude greater than for crystalline cellulose.[116, 131] Therefore, cellulose hydrolysis processes that aim at maximizing conversion and selective product yields while simultaneously minimizing the severity of the reaction conditions benefit from cellulose amorphization.

However, a phase transformation of amorphous cellulose to crystalline cellulose has been overlooked and not been accounted for in both the structural and kinetic analysis of decrystallized cellulose.[124, 126, 132-134] For instance, amorphized cellulose has been reported to recrystallize when exposed to humid air.[126] Similarly, exposure of ball-milled cellulose to water at room temperature results in reorganization and increase of the of the structural order.[124, 135] Recrystallization has been confirmed by various analytical techniques such as X-ray diffraction, nuclear magnetic resonance, thermal and sorption analysis.[124, 133, 135] This recrystallization is occurring at conditions where there

is no hydrolysis and has been attributed to the interactions with water.[124, 126, 135] However, all hydrolysis reactions are carried out in water. This raises questions regarding the interpretation of cellulose reactivity: what is the rate of water-induced recrystallization compared to hydrolysis, does recrystallization affect cellulose reactivity, and if not, is amorphous cellulose indeed more reactive than crystalline cellulose. Interestingly, despite decades of cellulose research the effects of recrystallization have not been addressed. In fact, crystallinity is typically measured prior to wetting with water indicating that correlations to reactivity are not representing the actual crystallinity of the cellulose substrate that undergoes hydrolysis, calling into question the structure-activity relationship altogether.

Provided that amorphous cellulose is more reactive than crystalline, water-induced recrystallization would reduce cellulose reactivity and thus the effectiveness of decrystallization methods. Accordingly, addressing water-induced recrystallization could provide alternative solvents or depolymerization strategies.

2.13. Concluding Remarks

Utilization of lignocellulosic biomass as a feedstock for the production of fuels and chemicals is dependent on economically competitive deconstruction and conversion processes. Currently, cellulose depolymerization is one of the bottlenecks that prevents commercialization of lignocellulosic biofuels. Cellulose hydrolysis for the selective production of concentrated sugar solutions is a promising route for the synthesis of renewable chemicals and fuels. However, the enzymes used to catalyze the reaction suffer from low reaction rates and inability to be recycled. Liquid acids on the other hand promote corrosion and product degradation and similarly are not recyclable. Thus, enzymes and liquid acids are consumables.

On the other hand, solid acid catalysts can be a recyclable alternative to enzymes and homogeneous acid for the catalytic depolymerization of cellulose and, if successful, promise cost reductions. However, the heterogeneous nature of solid acid catalyzed cellulose hydrolysis suggests a complex mechanism is at play. Current efforts at elucidating the mechanism of the reaction are limited to material synthesis, characterization, and performance analysis. Activity observations are correlated to structural characteristics and a hypothesized mechanism of solid acid catalyst action is forwarded which suggests binding interactions between solid acid and the solid cellulose substrate. However, direct measurements of such binding at reaction conditions is experimentally challenging and the hypothesis has not been directly tested.

One of the main knowledge gaps preventing elucidating the mechanism of solid acid catalyzed cellulose hydrolysis is the incomplete catalyst characterization. Specifically, while bulk structural analysis is carried out, there is little information on the external surface which would interact with the cellulose particles. As a result, the sites active at hydrolyzing the glycosidic bond in cellulose have not been identified but have only been hypothesized. Accordingly, the catalytic mechanism cannot be elucidated, despite the large amount of catalytic structures proposed and tested, which prevents rational catalyst design and process development. Therefore, one of the main problems to be tackled involves identifying the chemical moieties responsible for cellulose hydrolysis, which can be achieved by detailed characterization of the solid acid catalysts and specifically their external surfaces.

Approaching cellulose hydrolysis from a different perspective, namely reducing its resistance to depolymerization, also promises lowering conversion costs. The current theory differentiates the reactivity of amorphous and crystalline cellulose. This has motivated pretreatments that reduce the crystalline organization of the polymer since amorphous and non-crystalline cellulose is

depolymerized at a greater rate. Indeed, decrystallized cellulose exhibits greater reactivity towards hydrolysis than highly crystalline substrates. However, it was established that amorphous and decrystallized cellulose recrystallizes when contacted with gaseous or liquid water. In hydrolysis-based processes water is not only a reactant, but also a reaction medium, which provides ample environment for cellulose to interact with it. The recrystallization transformation has not been accounted for when interpreting hydrolysis results and developing structure-reactivity relationships.

Decrystallization pretreatments, while reducing the structural order, result in changes of other structural parameters. However, the real crystallinity (relative amount of amorphous and crystalline regions in the cellulose structure) of the substrate that undergoes hydrolysis is not clear since the rate of water-induced recrystallization has not been determined. Therefore, there is ambiguity surrounding the interpretation of greater reactivity of amorphous and noncrystalline cellulose. Provided that amorphous regions are indeed hydrolyzed at a greater rate, water-induced recrystallization would reduce the effectiveness of decrystallization pretreatments. On the other hand, if shown that there is no difference of reactivity of amorphous and crystalline cellulose, a new structure-reactivity correlation is necessary to explain the increased reactivity of cellulose substrates that have undergone decrystallization pretreatments. Hence, determining the effects of water-induced recrystallization can provide further details on the mechanism of cellulose hydrolysis and its structure-reactivity relationships. In addition, such a knowledge will serve as a fundamental guide for rational pretreatment and depolymerization processes that results in lower conversion costs.

2.14. Research Objectives

To address the knowledge gaps identified above, we designed our studies around the following objectives:

1. Development of structure-activity relationships for solid acid catalyzed cellulose hydrolysis

a. Detailed structural characterization focusing on the spatial distribution of chemical functionalities and the external surfaces of model solid acid catalysts and correlation to cellulose hydrolysis activity

b. Development of solid acid catalyzed cellulose hydrolysis model as a step towards elucidating the detailed mechanism of the reaction

2. Determining the effects of water-induced recrystallization on the reactivity of cellulose in water

a. Detailed structural characterization of decrystallized cellulose and elucidation of structural changes after interaction with water. Testing reactivity of decrystallized and recrystallized cellulose and incorporating water-induced recrystallization into cellulose hydrolysis models

b. Addressing the implications of water-induced cellulose recrystallization by depolymerizing decrystallized in non-aqueous solvents.

2.15. References:

1.F. H. Isikgor and C. R. Becer, *Polymer Chemistry*, 2015, **6**, 4497-4559.

2.A. P. Ingle, P. Ingle, I. Gupta and M. Rai, in *Sustainable Bioenergy*, eds. M. Rai and A. P. Ingle, Elsevier, 2019, DOI: https://doi.org/10.1016/B978-0-12-817654-2.00013-7, pp. 347-366.

3.G. M. Souza, M. V. R. Ballester, C. H. de Brito Cruz, H. Chum, B. Dale, V. H. Dale, E. C. M. Fernandes, T. Foust, A. Karp, L. Lynd, R. Maciel Filho, A. Milanez, F. Nigro, P. Osseweijer, L. M. Verdade, R. L. Victoria and L. Van der Wielen, *Environmental Development*, 2017, **23**, 57-64.

4.D. Yue, F. You and S. W. Snyder, *Computers & Chemical Engineering*, 2014, **66**, 36-56.

5.E. M. Rubin, *Nature*, 2008, **454**, 841-845.

6.M. J. Climent, A. Corma and S. Iborra, *Green Chemistry*, 2014, **16**.

7.A. C. O'sullivan, *Cellulose*, 1997, **4**, 173-207.

8.C. M. Lee, A. Mittal, A. L. Barnette, K. Kafle, Y. B. Park, H. Shin, D. K. Johnson, S. Park and S. H. Kim, *Cellulose*, 2013, **20**, 991-1000.

9.S. P. Chundawat, G. T. Beckham, M. E. Himmel and B. E. Dale, *Annu Rev Chem Biomol Eng*, 2011, **2**, 121-145.

10.P. Maki-Arvela, T. Salmi, B. Holmbom, S. Willfor and D. Y. Murzin, *Chem Rev*, 2011, **111**, 5638-5666.

11.F. G. Calvo-Flores and J. A. Dobado, *ChemSusChem*, 2010, **3**, 1227-1235.

12.D. M. Alonso, J. Q. Bond and J. A. Dumesic, *Green Chemistry*, 2010, **12**.

13.A. J. Ragauskas, G. T. Beckham, M. J. Biddy, R. Chandra, F. Chen, M. F. Davis, B. H. Davison, R. A. Dixon, P. Gilna, M. Keller, P. Langan, A. K. Naskar, J. N. Saddler, T. J. Tschaplinski, G. A. Tuskan and C. E. Wyman, *Science*, 2014, **344**, 1246843.

14.T. Salmi, D. Y. Murzin, P. Mäki-Arvela, B. Kusema, B. Holmbom, S. Willför and J. Wärnå, *AIChE Journal*, 2014, **60**, 1066-1077.

15.R. A. Sheldon, *Green Chem.*, 2014, **16**, 950-963.

16.T. R. Brown, *Bioresource Technology*, 2015, **178**, 166-176.

17.R. P. Anex, A. Aden, F. K. Kazi, J. Fortman, R. M. Swanson, M. M. Wright, J. A. Satrio, R. C. Brown, D. E. Daugaard, A. Platon, G. Kothandaraman, D. D. Hsu and A. Dutta, *Fuel*, 2010, **89**, S29-S35.

18.M. Patel, X. Zhang and A. Kumar, *Renewable and Sustainable Energy Reviews*, 2016, **53**, 1486-1499.

19.A. A. Peterson, F. Vogel, R. P. Lachance, M. Fröling, J. M. J. Antal and J. W. Tester, *Energy & Environmental Science*, 2008, **1**.

20.A. Molino, S. Chianese and D. Musmarra, *Journal of Energy Chemistry*, 2016, **25**, 10-25.

21.R. G. d. Santos and A. C. Alencar, *International Journal of Hydrogen Energy*, 2019, DOI: https://doi.org/10.1016/j.ijhydene.2019.07.133.

22.N. Laksmono, M. Paraschiv, K. Loubar and M. Tazerout, *Fuel Processing Technology*, 2013, **106**, 776-783.

23.F.-X. Collard and J. Blin, *Renewable and Sustainable Energy Reviews*, 2014, **38**, 594-608.

24.M. S. Mettler, D. G. Vlachos and P. J. Dauenhauer, *Energy & Environmental Science*, 2012, **5**.

25.G. SriBala, H.-H. Carstensen, K. M. Van Geem and G. B. Marin, *Wiley Interdisciplinary Reviews: Energy and Environment*, 2019, **8**, e326.

26.C. Quan, N. Gao and Q. Song, *Journal of Analytical and Applied Pyrolysis*, 2016, **121**, 84-92.

27.A. R. K. Gollakota, N. Kishore and S. Gu, *Renewable and Sustainable Energy Reviews*, 2018, **81**, 1378-1392.

28.T. H. Pedersen and L. A. Rosendahl, *Biomass and Bioenergy*, 2015, **83**, 206-215.

29.S. Xiu and A. Shahbazi, *Renewable and Sustainable Energy Reviews*, 2012, **16**, 4406-4414.

30.K. Alper, K. Tekin and S. Karagöz, *Energy & Fuels*, 2019, **33**, 3248-3256.

31.S. D. Davidson, J. A. Lopez-Ruiz, Y. Zhu, A. R. Cooper, K. O. Albrecht and R. A. Dagle, *ACS Sustainable Chemistry & Engineering*, 2019.

32.R. Rinaldi and F. Schuth, *ChemSusChem*, 2009, **2**, 1096-1107.

33.U. Bornscheuer, K. Buchholz and J. Seibel, *Angew Chem Int Ed Engl*, 2014, **53**, 10876-10893.

34.R. Samuelsson, J. Burvall and R. Jirjis, *Biomass and Bioenergy*, 2006, **30**, 929-934.

35.A. Kruse and N. Dahmen, *The Journal of Supercritical Fluids*, 2015, **96**, 36-45.

36.S. Deguchi, K. Tsujii and K. Horikoshi, *Green Chem.*, 2008, **10**, 191-196.

37.A. Sharples, *Transactions of the Faraday Society*, 1957, **53**, 1003-1013.

38.L. Vaquerizo, N. Abad-Fernández, R. B. Mato and M. J. Cocero, *Chemical Engineering Journal*, 2018, **350**, 463-473.

39.M. Lu, J. Li, L. Han and W. Xiao, *Bioresource Technology*, 2019, **273**, 1-7.

40.Y. H. Zhang and L. R. Lynd, *Biotechnol Bioeng*, 2004, **88**, 797-824.

41.P. C. Torres-Mayanga, D. Lachos-Perez, A. Mudhoo, S. Kumar, A. B. Brown, M. Tyufekchiev, G. Dragone, S. I. Mussatto, M. A. Rostagno, M. Timko and T. Forster-Carneiro, *Biomass and Bioenergy*, 2019, **130**, 105397.

42.C. K. Nitsos, K. A. Matis and K. S. Triantafyllidis, *ChemSusChem*, 2013, **6**, 110-122.

43.R. Kumar, G. Mago, V. Balan and C. E. Wyman, *Bioresour Technol*, 2009, **100**, 3948-3962.

44.C. Li, B. Knierim, C. Manisseri, R. Arora, H. V. Scheller, M. Auer, K. P. Vogel, B. A. Simmons and S. Singh, *Bioresource Technology*, 2010, **101**, 4900-4906.

45.N. Sweygers, N. Alewaters, R. Dewil and L. Appels, *Sci Rep*, 2018, **8**, 7719.

46.G. SriBala and R. Vinu, *Industrial & Engineering Chemistry Research*, 2014, **53**, 8714-8725.

47.M. Mohan, R. Timung, N. N. Deshavath, T. Banerjee, V. V. Goud and V. V. Dasu, *RSC Advances*, 2015, **5**, 103265-103275.

48.L. R. Lynd, X. Liang, M. J. Biddy, A. Allee, H. Cai, T. Foust, M. E. Himmel, M. S. Laser, M. Wang and C. E. Wyman, *Curr Opin Biotechnol*, 2017, **45**, 202-211.

49.L. R. Lynd, *Nat Biotechnol*, 2017, **35**, 912-915.

50.J. Han, J. S. Luterbacher, D. M. Alonso, J. A. Dumesic and C. T. Maravelias, *Bioresour Technol*, 2015, **182**, 258-266.

51.L. Tao, D. Schell, R. Davis, E. Tan, R. Elander and A. Bratis, *NREL 2012 achievement of ethanol cost targets: biochemical ethanol fermentation via dilute-acid pretreatment and enzymatic hydrolysis of corn stover*, National Renewable Energy Lab.(NREL), Golden, CO (United States), 2014.

52.S. Brethauer and M. H. Studer, *CHIMIA International Journal for Chemistry*, 2015, **69**, 572-581.

53.M. Nahavandi, T. Kasanneni, Z. S. Yuan, C. C. Xu and S. Rohani, *ACS Sustainable Chemistry & Engineering*, 2019, DOI: 10.1021/acssuschemeng.9b00250.

54.I. M. B. Reizman, A. R. Stenger, C. R. Reisch, A. Gupta, N. C. Connors and K. L. Prather, *Metabolic engineering communications*, 2015, **2**, 109-116.

55.T. Werpy and G. Petersen, *Top value added chemicals from biomass: volume I--results of screening for potential candidates from sugars and synthesis gas*, National Renewable Energy Lab., Golden, CO (US), 2004.

56.O. Shoseyov, Z. Shani and I. Levy, *Microbiology and Molecular Biology Reviews*, 2006, **70**, 283.

57.N. Georgelis, N. H. Yennawar and D. J. Cosgrove, *Proceedings of the National Academy of Sciences*, 2012, **109**, 14830-14835.

58.M. N. A. Mohamed, H. D. Watts, J. Guo, J. M. Catchmark and J. D. Kubicki, *Carbohydrate Research*, 2010, **345**, 1741-1751.

59.J. S. Luterbacher, J. Y. Parlange and L. P. Walker, *Biotechnol Bioeng*, 2013, **110**, 127-136.

60.J. Baker, K. Tatsumoto, K. Grohmann, J. Woodward, J. Wichert, S. Shoemaker and M. Himmel, *Applied biochemistry and biotechnology*, 1992, **34**, 217-231.

61.T. Jeoh, C. I. Ishizawa, M. F. Davis, M. E. Himmel, W. S. Adney and D. K. Johnson, *Biotechnol Bioeng*, 2007, **98**, 112-122.

62.A. Sinitsyn, A. Gusakov and E. Y. Vlasenko, *Applied Biochemistry and Biotechnology*, 1991, **30**, 43-59.

63.S. Sun, S. Sun, X. Cao and R. Sun, *Bioresour Technol*, 2016, **199**, 49-58.

64.J. V. Vermaas, L. Petridis, X. Qi, R. Schulz, B. Lindner and J. C. Smith, *Biotechnology for biofuels*, 2015, **8**, 217.

65.M. Hall, P. Bansal, J. H. Lee, M. J. Realff and A. S. Bommarius, *FEBS J*, 2010, **277**, 1571-1582.

66.E. Johnson, *Biofuels, Bioproducts and Biorefining*, 2016, **10**, 164-174.

67.H. Zhao, J. Kwak, Z. Conradzhang, H. Brown, B. Arey and J. Holladay, *Carbohydrate Polymers*, 2007, **68**, 235-241.

68.Y. Yu and H. Wu, *Energy & Fuels*, 2010, **24**, 1963-1971.

69.M. Möller, F. Harnisch and U. Schröder, *RSC Advances*, 2013, **3**.

70.D. A. Cantero Sposetti, DOI: 10.35376/10324/5374info:eu-repo/semantics/doctoralThesis, 2014.

71.B. Girisuta, L. Janssen and H. Heeres, *Industrial & engineering chemistry research*, 2007, **46**, 1696-1708.

72.R. Weingarten, J. Cho, R. Xing, W. C. Conner, Jr. and G. W. Huber, *ChemSusChem*, 2012, **5**, 1280-1290.

73.B. Girisuta, L. Janssen and H. Heeres, *Chemical Engineering Research and Design*, 2006, **84**, 339-349.

74.B. Girisuta, L. Janssen and H. Heeres, *Green Chemistry*, 2006, **8**, 701-709.

75.A. Chuntanapum, T. Shii and Y. Matsumura, *Journal of chemical engineering of Japan*, 2011, 1103010151-1103010151.

76.R. W. Torget, J. S. Kim and Y. Y. Lee, *Industrial & Engineering Chemistry Research*, 2000, **39**, 2817-2825.

77.Z. Ma, P. Guerra, M. Tyufekchiev, A. Zaker, G. A. Tompsett, P. C. T. Mayanga, T. Forster-Carneiro, P. Wang and M. T. Timko, *Sustainable Energy & Fuels*, 2017, **1**, 1950-1959.

78.D. A. Cantero, M. D. Bermejo and M. J. Cocero, *The Journal of Supercritical Fluids*, 2013, **75**, 48-57.

79.H. Zhao, J. H. Kwak, Y. Wang, J. A. Franz, J. M. White and J. E. Holladay, *Energy & Fuels*, 2006, **20**, 807-811.

80.K. Wu, G. Feng, Y. Liu, C. Liu, X. Zhang, S. Liu, B. Liang and H. Lu, *Bioresour Technol*, 2018, **261**, 28-35.

81.Y. Yu and H. Wu, *AIChE Journal*, 2011, **57**, 793-800.

82.Y. Yang, C.-w. Hu and M. M. Abu-Omar, *Green Chemistry*, 2012, **14**, 509-513.

83.D. Klein-Marcuschamer, P. Oleskowicz-Popiel, B. A. Simmons and H. W. Blanch, *Biotechnology and bioengineering*, 2012, **109**, 1083-1087.

84.P. Alvira, E. Tomas-Pejo, M. Ballesteros and M. J. Negro, *Bioresour Technol*, 2010, **101**, 4851-4861.

85.C. Tengborg, M. Galbe and G. Zacchi, *Biotechnology Progress*, 2001, **17**, 110-117.

86.D. Gomes, A. C. Rodrigues, L. Domingues and M. Gama, *Applied Microbiology and Biotechnology*, 2015, **99**, 4131-4143.

87.S. Chovau, D. Degrauwe and B. Van der Bruggen, *Renewable and Sustainable Energy Reviews*, 2013, **26**, 307-321.

88.P. Kritzer, *The Journal of Supercritical Fluids*, 2004, **29**, 1-29.

89.Y.-B. Huang and Y. Fu, *Green Chemistry*, 2013, **15**.

90.A. Onda, T. Ochi and K. Yanagisawa, *Green Chemistry*, 2008, **10**, 1033-1037.

91.A. Onda, T. Ochi and K. Yanagisawa, *Topics in Catalysis*, 2009, **52**, 801-807.

92.R. Rinaldi, N. Meine, J. vom Stein, R. Palkovits and F. Schuth, *ChemSusChem*, 2010, **3**, 266-276.

93.L. Shuai and X. Pan, *Energy & Environmental Science*, 2012, **5**.

94.X. Qian, J. Lei and S. R. Wickramasinghe, *RSC Advances*, 2013, **3**.

95.S. Li, Z. Gu, B. E. Bjornson and A. Muthukumarappan, *Journal of Environmental Chemical Engineering*, 2013, **1**, 1174-1181.

96.G. S. Foo and C. Sievers, *ChemSusChem*, 2015, **8**, 534-543.

97.S. Yuan, T. Li, Y. Wang, B. Cai, X. Wen, S. Shen, X. Peng and Y. Li, *Fuel*, 2019, **237**, 895-902.

98.S. Hu, T. J. Smith, W. Lou and M. Zong, *J Agric Food Chem*, 2014, **62**, 1905-1911.

99.Y. Zuo, Y. Zhang and Y. Fu, *ChemCatChem*, 2014, **6**, 753-757.

100.F. Parveen, K. Gupta and S. Upadhyayula, *Carbohydr Polym*, 2017, **159**, 146-151.

101.H.-X. Li, W.-J. Shi, X. Zhang, P. Liu, Q. Cao and L. e. Jin, *Journal of Chemical Technology & Biotechnology*, 2019, **n/a**.

102.R. Gong, Z. Ma, X. Wang, Y. Han, Y. Guo, G. Sun, Y. Li and J. Zhou, *RSC Advances*, 2019, **9**, 28902-28907.

103.M. Yabushita, H. Kobayashi, J. Y. Hasegawa, K. Hara and A. Fukuoka, *ChemSusChem*, 2014, **7**, 1443-1450.

104.L. Qi, R. Alamillo, W. A. Elliott, A. Andersen, D. W. Hoyt, E. D. Walter, K. S. Han, N. M. Washton, R. M. Rioux, J. A. Dumesic and S. L. Scott, *ACS Catalysis*, 2017, **7**, 3489-3500.

105.L. Matsakas, V. Raghavendran, O. Yakimenko, G. Persson, E. Olsson, U. Rova, L. Olsson and P. Christakopoulos, *Bioresour Technol*, 2019, **273**, 521-528.

106.Z. Lin, H. Huang, H. Zhang, L. Zhang, L. Yan and J. Chen, *Applied biochemistry and biotechnology*, 2010, **162**, 1872-1880.

107.A. S. A. da Silva, H. Inoue, T. Endo, S. Yano and E. P. Bon, *Bioresource technology*, 2010, **101**, 7402-7409.

108.A.-I. Yeh, Y.-C. Huang and S. H. Chen, *Carbohydrate Polymers*, 2010, **79**, 192-199.

109.A. Peciulyte, K. Karlstrom, P. T. Larsson and L. Olsson, *Biotechnol Biofuels*, 2015, **8**, 56.

110.S. D. Mansfield, C. Mooney and J. N. Saddler, *Biotechnology progress*, 1999, **15**, 804-816.

111.B. B. Hallac and A. J. Ragauskas, *Biofuels, Bioproducts and Biorefining*, 2011, **5**, 215-225.

112.C. Driemeier and G. A. Calligaris, *Journal of Applied Crystallography*, 2011, **44**, 184-192.

113.Y. Nishiyama, P. Langan and H. Chanzy, *Journal of the American Chemical Society*, 2002, **124**, 9074-9082.

114.D. Klemm, B. Heublein, H. P. Fink and A. Bohn, *Angew Chem Int Ed Engl*, 2005, **44**, 3358-3393.

115.T. Endo, E. M. Aung, S. Fujii, S. Hosomi, M. Kimizu, K. Ninomiya and K. Takahashi, *Carbohydr Polym*, 2017, **176**, 365-373.

116.P. Calvini, A. Gorassini and A. L. Merlani, *Cellulose*, 2007, **15**, 193-203.

117.N. Andersen, K. S. Johansen, M. Michelsen, E. H. Stenby, K. B. R. M. Krogh and L. Olsson, *Enzyme and Microbial Technology*, 2008, **42**, 362-370.

118.J. S. Luterbacher, J. M. Moran-Mirabal, E. W. Burkholder and L. P. Walker, *Biotechnol Bioeng*, 2015, **112**, 32-42.

119. C. H. Stephens, P. M. Whitmore, H. R. Morris and M. E. Bier, *Biomacromolecules*, 2008, **9**, 1093-1099.

120.K. Kafle, H. Shin, C. M. Lee, S. Park and S. H. Kim, *Sci Rep*, 2015, **5**, 15102.

121.Z. Ling, T. Wang, M. Makarem, M. Santiago Cintrón, H. N. Cheng, X. Kang, M. Bacher, A. Potthast, T. Rosenau, H. King, C. D. Delhom, S. Nam, J. Vincent Edwards, S. H. Kim, F. Xu and A. D. French, *Cellulose*, 2019, **26**, 305-328.

122.H. Håkansson, P. Ahlgren and U. Germgård, *Cellulose*, 2005, **12**, 327-335.

123.Y. H. P. Zhang and L. R. Lynd, *Biomacromolecules*, 2005, **6**, 1510-1515.

124.S. Ouajai and R. A. Shanks, *Cellulose*, 2006, **13**, 31-44.

125.Z. Wang, A. G. McDonald, R. J. M. Westerhof, S. R. A. Kersten, C. M. Cuba-Torres, S. Ha, B. Pecha and M. Garcia-Perez, *Journal of Analytical and Applied Pyrolysis*, 2013, **100**, 56-66.

126.D. F. Caulfield and R. Steffes, *Tappi Tech Ass Pulp Pap Indus*, 1969.

127.K. Mazeau and L. Heux, *The Journal of Physical Chemistry B*, 2003, **107**, 2394-2403.

128.P. Chen, Y. Ogawa, Y. Nishiyama, A. E. Ismail and K. Mazeau, *Cellulose*, 2018, **25**, 4345-4355.

129.S. Park, J. O. Baker, M. E. Himmel, P. A. Parilla and D. K. Johnson, *Biotechnology for biofuels*, 2010, **3**, 10.

130.P. Bansal, M. Hall, M. J. Realff, J. H. Lee and A. S. Bommarius, *Bioresour Technol*, 2010, **101**, 4461-4471.

131.H. J. Philipp, M. L. Nelson and H. M. Ziifle, *Textile research journal*, 1947, **17**, 585-596.

132.P. H. Hermans and A. Weidinger, *Journal of the American Chemical Society*, 1946, **68**, 1138-1138.

133.M. Kimura, T. Hatakeyama and J. Nakano, *Journal of Applied Polymer Science*, 1974, **18**, 3069-3076.

134.H. Hatakeyama and T. Hatakeyama, *Die Makromolekulare Chemie*, 1981, **182**, 1655-1668.

135.P. Wormald, K. Wickholm, P. T. Larsson and T. Iversen, *Cellulose*, 1996, **3**, 141-152.

CHAPTER 3

Cellulase-Inspired Solid Acids for Cellulose Hydrolysis: Structural Explanations for High Catalytic Activity

3.1. Introduction

The controlled and selective hydrolysis of cellulose has the potential to provide abundant access to carbon-based building blocks such as ethanol, glucose, hydroxymethylfurfural (HMF), and levulinic acid (LA) from renewable, underutilized resources.[1, 2] However, cellulose recalcitrance leads to slow conversion into more desirable small molecules.[3-8] Cellulose can be hydrolyzed by enzymes at low temperatures (50 °C) or by liquid acids at elevated temperatures.[7, 9] However, enzyme hydrolysis is occurs at very low rates that require tens of hours of reaction time, while acid-catalyzed hydrolysis requires high acid loadings or high temperatures, leading to side reactions that limit the yields of useful products.[10-15] Furthermore, both types of treatment are costly, as acids and enzymes employed are typically not recoverable.[16-18] This is one of the reasons why industrial-scale production of glucose from cellulose (on the pathway toward second generation bio-ethanol) is often challenging.[19]

Alternatives that have been discussed widely in recent years include solid acid catalysts for cellulose hydrolysis, as these acids might be recyclable after cellulose conversion and have shown promise for direct conversion of cellulose to glucose in high yields and with good selectivity.[20, 21] So-called “cellulase-mimetic” solid acids have provided especially remarkable results.[22-27] The hypothesized mechanism of action of these acids has been formulated in analogy to the design principles of cellulases (cellulose-cleaving enzymes), which exhibit a cellulose-binding domain

and a catalytic domain for cellulose hydrolysis.[7, 22] In enzymatic hydrolysis, these structural features allow cellulases to catalyze glycosidic bond hydrolysis more efficiently through binding to the cellulose surface.[7] Interestingly, aqueous glucan hydrolysis in the case of carbonaceous solid catalysts profits from association of glucans to the graphitic domains (binding), which is likely driven by entropically favored, hydrophobic effects and enthalpically favored C−H-π interactions.[28, 29] Similarly, glucan adsorption to mesoporous and microporous carbon materials has been documented.[30-33] In contrast, for polymeric solid acids, similar physicochemical principles for glucan adsorption are not as clearly established. The polymer-based solid acids with the highest activity for cellulose hydrolysis to date have been reported by Shuai and Pan and produce up to 93% glucose from cellulose under relatively mild conditions (H_2O, 120 °C, 10 h).[22] Pan's catalyst consists of an aromatic-rich, styrenic polymer decorated with C−Cl moieties (originally referred to as "binding groups") that are believed to enable hydrogen bonding to cellulose while the sulfonic acid moieties catalyze the glycosidic bond hydrolysis (see Scheme 3.1.). Unfortunately, no information on the quantitative composition or functional group distribution has been provided for Pan's catalyst, thus weakening the arguments for catalyst cellulose interactions.[22]

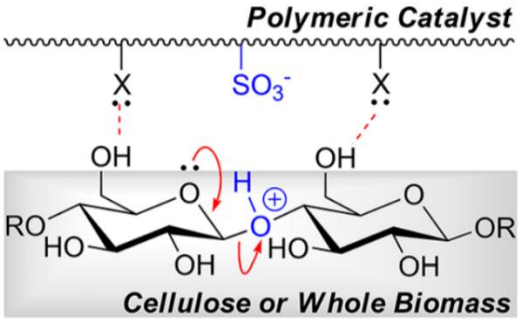

Scheme 3.4. Solid acid design based on Pan's catalyst: pre-coordination of sugar polymer through "binding sites" X acting as hydrogen bond acceptors.[22]

The development of structure-activity relationships relies on bulk characterization of solid acid material. Typical methods of analysis of the catalyst structures involve vibrational spectroscopy, solid-state nuclear magnetic resonance, elemental analysis, X-ray diffraction, X-ray electron spectroscopy, surface area, and solid-state titration of acid sites.[22-26, 31, 34-37] However, this approach overlooks the fact that cellulose is insoluble at the conditions applied for hydrolysis and the reaction between cellulose and the solid catalyst would occur on the interface of the two solids. Since cellulose substrates usually used for hydrolysis studies are microns in size, the depolymerization reaction will be limited to the external surfaces of the solid catalyst and the carbohydrate polymer, which is exemplified by the high substrate to catalyst loadings.[22, 23, 37] Thus, bulk measurements, which can measure sites within porous interior of the catalyst, would result in inaccurate correlations between structure and activity. However, there is lack of detailed structural characterization of solid acid catalysts that can be appropriately correlated to activity towards cellulose depolymerization.

Despite these issues, follow-up work by several different investigators has described similar design principles for polymer-based solid acids; designs incorporate hydrogen bonding functionalities (e.g., C−Cl, C−CO_2H) in addition to strongly acidic moieties.[23, 38, 39] Evidently, catalysts with such structural characteristics exhibit greater cellulose hydrolysis performance, which is used as a justification of the hypothesized mechanism of action. However, none of these catalysts match the reported activity of Pan's catalyst. Furthermore, the forwarded hypothesis of hydrogen bonding between binding groups solid acid catalyst and hydroxyl groups of cellulose does not seem to address the fact that water, used as a reaction medium, can also form hydrogen bonds and, in addition, is a lot more mobile than cellulose. As such, the question of whether the

presence of “binding groups” indeed leads to an increase in hydrolysis activity has not been unambiguously answered.

In this study we focused on elucidating the role of such binding groups in glycosidic bond hydrolysis through detailed structural and catalytic characterization of a representative solid acid catalyst. For this purpose, we synthesized a bifunctional polymer solid acid catalyst that had been reported by Zuo et al to exhibit high catalytic activity towards cellulose hydrolysis, reported after the initial description of Pan’s catalyst had appeared in the literature.[23] The catalyst contained -Cl and -SO_3H groups, where the former was hypothesized to participate in hydrogen bonding to the hydroxyl groups of cellulose and the latter as the acid site. The specific catalyst was selected due to its reproducible synthesis chemistry. Working with a well-established chemistry avoided laborious characterization and identification of chemical groups. Accordingly, we focused on elucidating the spatial distribution of chemical groups that are hypothesized to participate in the scission of the glycosidic bond. We attempted to describe the external surface of polymer catalyst beads to the best extent possible as the chemical moieties located on the external surface would potentially interact with cellulose particles. Finally, we correlated the catalyst activity towards hydrolyzing cellulose to the presence of the chemical groups present in the catalyst structure. Control experiments with catalyst that bear only -Cl groups or only -SO_3H groups were also carried out. For the purpose of distinguishing the material studied here from the one reported here the catalyst was labeled CMP-SO_3H-0.3 in this work.

3.2. Methodology

3.2.1. Materials

Chloromethyl polystyrene with 5.5 mmol/g Cl loading (0.3mm to 1.3 mm in diameter), thiourea, N,N-dimethylformamide (DMF), sufuric acid (95-98%), sodium hydroxide, methanol,

cellobiose, hydroxymethyl polystyrene (0.21 mm to 0.19 mm in diameter, functional loading of 2.0–3.0 mmol/g) and Avicel PH-101 microcrystalline cellulose were purchased from Sigma Aldrich.

3.2.2. Catalyst Synthesis

To prepare the bifunctional solid acid catalyst chloromethyl polystyrene (CMP) was functionalized to introduce sulfonic acid functionalities by a modified procedure reported by Zuo et al.[23] Chloromethyl polystyrene beads (12 g; corresponding to 66 mmol Cl, 1.00 equiv.) and DMF (120 mL) were heated to 120° C for 4 hours with constant stirring (150 rpm). The beads were filtered and washed with methanol (150 mL). Thiourea (1.5 g, 20 mmol, 0.30 equiv.; or 6.0 g, 79 mmol, 1.20 equiv.) was dissolved in methanol (120 mL). The resulting thiourea solution was reacted with the previously washed and swelled CMP beads without drying the beads; the resulting mixture was heated in an oil bath preheated to 65° C in a round-bottom flask capped with a rubber septum (1 h and 15 minutes reaction time with 0.3 equiv. thiourea; 7 h reaction time with 1.20 equiv. thiourea). The first step of modification is shown in Scheme 3.2.

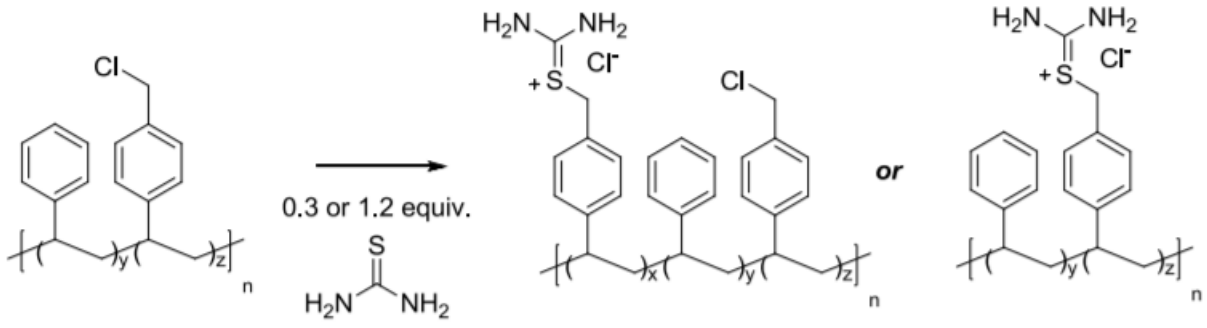

Scheme 3.5. Functionalization of chloromethyl polystyrene polymer with thiouronium salt after attachment of thiourea.

After the respective reaction times, the polymer beads were isolated by filtration and washed with DI water (500 mL). The resulting polymer beads were then reacted with NaOH (120 mL of a

1 M solution; 120 mmol; 1.8 equiv.) in a round-bottom flask, capped with a rubber septum; the flask was placed into an oil-bath at 100 °C for 45 min (for 0.3 equiv. to produce CMP-SO_3H-0.3) or 1 h (for 1.2 equiv. to produce CMP-SO_3H-1.2). The beads were isolated by filtration and washed with DI water (1000 mL). The washed beads were then reacted with 180 mL of 1 M H_2SO_4 for 5 h in oil bath at 40° C. The resultant thiol functionality is shown in Scheme 3.3.

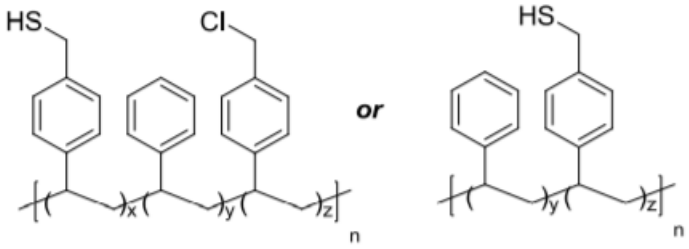

Scheme 3.6. Functionalization of the polymer with thiol groups by hydrolysis of thiouronium salt by NaOH and exchange by H_2SO_4.

The beads were isolated by filtration and washed with copious amounts of DI water until the filtrate showed a pH of 6 upon testing with a pH meter. The beads were then mixed with 180 mL of 30% H_2O_2 solution in water; the mixture was stirred at room temperature for 12 h. After this time, the polymer beads were filtered off and washed with copious amounts of DI water until the filtrate showed a pH of 6 upon testing with a pH meter. The washed beads were dried overnight at 65° C in an oven. The final product of the synthesis procedure is summarized in Scheme 3.4.

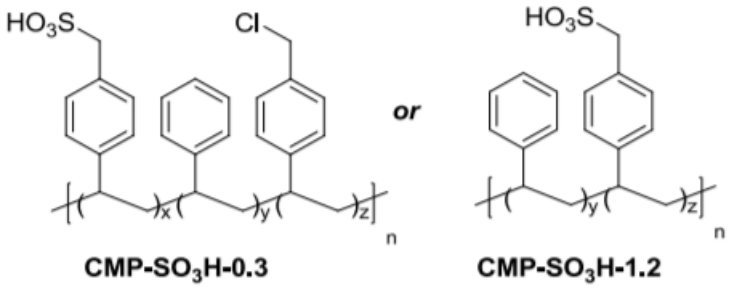

Scheme 3.7. Final product of catalyst synthesis. Bifunctional catalyst bearing chloromethyl and benzylic sulfonic acid groups and completely sulfonated catalyst. The numerical value in the naming of the catalyst indicates the chlorine to thiourea equivalence used in the first step of functionalization.

This specific catalyst was selected for the reproducibility of its synthesis. The functionalization of chloromethyl polystyrene with thiourea followed by hydrolysis and oxidation to sulfonic acid has been widely used for the preparation of chelating resins and polymer membranes.[40, 41]

3.2.3. Attenuated Total Reflectance Fourier Transform Infrared Spectroscopy (ATR-FTIR)

For the purpose of bulk spectroscopic analysis verifying successful modification of precursor polymers to desired catalyst functionality we used ATR infrared spectroscopy analysis. Spectra polymer beads at different stages of catalyst synthesis procedure were obtained on a Bruker Vertex 70 in the range from 600 to 4000 cm^{-1}. Each spectrum was averaged from 1024 scans with a resolution of 4 cm^{-1}.

3.2.4. Cross-sectional Analysis of Polymer Beads using Raman Microscopy

The detailed spatial structural characterization of the catalyst required dissecting the polymer beads and an analytical technique with enough spatial resolution to distinguish chemical spatial distribution of chemical groups from bulk composition. For this purpose, we employed Raman microscopy analysis. Horiba Xplora Raman Microscope with an excitation laser operating at 785 nm and an Olympus 100x magnification lens were used. The resulting laser spot was

approximately 1-5 μm in diameter, which was significantly smaller than the diameter of the polymer beads, which varied between 300 μm to 1200 μm, ensuring sufficient spatial resolution. Cross-sectional analysis of solid acid catalyst was carried out by cutting a bead with a razor blade in half; the bead was fixed on a glass slide with a double-side tape; the radial position of the excitation laser spot on the bead cross-section was varied by moving the microscope stage the desired distance.

3.2.5. Solid-state Nuclear Magnetic Resonance (ss-NMR)

An additional bulk characterization technique supplementing ATR-FTIR, we used solid-state NMR analyses were performed on a Bruker Avance 400 spectrometer at a 100 MHz ^{13}C resonance frequency with high-power ^{1}H decoupling, with magic-angle spinning (MAS) of 4-mm zirconia rotors in a double-resonance probe head at ambient temperature. The multiCP pulse sequence[42] was used at 14 kHz MAS to obtain quantitative ^{13}C NMR spectra, with a 4-s recycle delay, ten 1.1-ms cross polarization periods and a final 0.55-ms CP time, each separated by a ^{1}H repolarization time of 1.5 s; a rotation-synchronized Hahn echo was applied before detection to avoid baseline distortions.[43, 44] Corresponding spectra of nonprotonated C and mobile segments were obtained after 68 μs recoupled ^{1}H-^{13}C dipolar dephasing before detection.[45] Standard 4.2-μs ^{1}H and ^{13}C 90° pulses were used in the experiments described above. CH-only spectra were obtained for CMP and CMP-SO_3H-0.3 based on dipolar DEPT[46] at 5787 Hz MAS, with 3.7-μs ^{1}H 90° pulses.

3.2.6. Elemental Analysis

Elemental analysis was carried out to confirm successful polymer modification by observing the changes of the elemental composition post synthesis reactions. Specifically, in addition to the

typical C, O, and H analysis, quantification of Cl and S was also carried out. The analysis was performed by Galbraith Laboratories Inc., 2323 Sycamore Drive, Knoxville, TN 37921, USA.

3.2.7. Energy-dispersive X-ray Spectroscopy (EDS)

EDS analysis was used to supplement and verify the cross-sectional analysis carried out with Raman microscopy. Measurements were performed using a Bruker Quantax 50 energy dispersive spectrometer attached to a Hitachi TM-3000 scanning electron microscope. The EDS spectrometer was calibrated with a copper standard prior to use. All samples were dried under vacuum at 50 °C for 4 hours, prior to the measurements. The acceleration voltage in the SEM was 10kV and the spectra acquisition time for all samples was 100 seconds. The sampling area of the EDS analysis was approximately 3 µm. Cross-sectioning of the polymer beads was identical to the one described in the Cross-sectional Analysis using Raman Microscopy section.

3.2.8. High Performance Liquid Chromatography (HPLC)

The activity of the solid acid catalysts towards cellulose depolymerization was inferred from analysis of the soluble products post hydrolysis reaction. Quantification of the cellulose hydrolysates was performed on an Agilent 1200 HPLC series equipped with Diode Array Detector (DAD), Refractive Index Detector (RID), and Bio-Rad Aminex HPX-87H column. The mobile phase was 5 mM sulfuric acid at 0.6 mL/min flowrate. The separation column and the RID detector were both kept at 35 °C during analytical runs. The hydrolysates were analyzed for cellulose depolymerization products, mainly glucose as it is the main product (see Scheme 3.5.). In addition, considering that glucose can decompose in hydrothermal environment catalyzed by Brønsted acid catalysts to HMF, levulinic and formic acids, those were also quantified. Calibration curves of the compounds of interest were obtained by analyzing 8 standards of known concentrations (0.1, 0.2, 0.4, 0.5, 0.6, 0.8, 0.9, and 1 g/L).

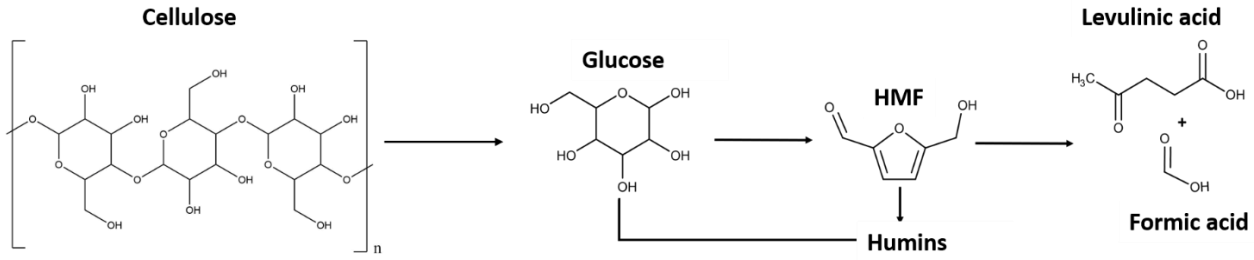

Scheme 3.8. Cellulose hydrolysis to glucose and subsequent degradation to HMF, humins, levulinic acid, and formic acid. The HPLC analysis quantified glucose as the main cellulose hydrolysis product and HMF, levulinic acid, and formic acid as glucose degradation products. The sum of all compounds was used as an indication of the extent of cellulose hydrolysis.

3..2.9. Cellulose and Cellobiose Hydrolysis

Cellulose or cellobiose hydrolysis experiments were performed in analogy to a procedure published by Zuo et al.[23] Reactions were carried out in batch reactors, typically used for catalyst performance analysis. Polymer catalyst (0.20 g), cellobiose (0.10 g) or cellulose (0.10 g), water (2.0 mL; 17.7 MΩ resistivity), and a magnetic stir bar were added to a 15 mL heavy wall pressure vial and the vial was sealed with a screw cap with a Viton O-ring seal. The vial was submerged in an oil bath that had been preheated to 150 °C (or 175 °C). The reaction mixture was stirred at 150 rpm for 5 h (or 10 h) at this temperature. At the end of the reaction, the vial was placed in an ice bath to quench the reaction. Additional 8 mL of DI water were used to dilute the sample. 1 mL aliquot of the diluted sample was further diluted with DI water to a total of 10 mL. The second dilution was analyzed with HPLC as described in the General Procedures section: The soluble products were detected and quantified with HPLC as already described. Cellobiose conversion was calculated based on the difference of the initial amount and the amount measured by HPLC analysis after the reaction. Glucose yields were calculated as $Y_g = \frac{m_{g*}M_{gu}}{m_{c*}M_g} * 100\%$, where m_g is the glucose mass determined by HPLC, M_g is the molecular weight of glucose, m_c is the mass of

cellulose or cellobiose, and M_{gu} is the molecular weight of the glucose unit in the cellulose chain or cellobiose molecule. Levulinic acid yields were calculated as $Y_{la} = \frac{m_{la} * M_{gu}}{m_c * M_{la}} * 100\%$, where m_{la} is the mass of levulinic acid determined by HPLC, M_{la} is the molecular weight of levulinic acid. No stoichiometric adjustment is necessary since the stoichiometric ratio between glucose and its degradation products is unity. Formic acid yields were calculated as $Y_{fa} = \frac{m_{fa} * M_{gu}}{m_c * M_{fa}} * 100\%$; m_{fa} is mass of formic acid determined by HPLC, M_{fa} is the molecular weight of formic acid. The mass balance of soluble carbon was calculated based on the sum of the mass of carbon atoms of all soluble products divided by the carbon present in starting cellulose or cellobiose substrate, $S.C.B. = \frac{\sum_i^n C_i}{C_c} * 100$. Yields are tabulated as averages and standard deviations of yields obtained from three independent catalytic runs.

3.2.10. Characterization of Leached Homogeneous Acid

As it was discovered that the pH of the reaction solution decreases it was necessary to determine the extent of catalyst degradation and its propensity to form liquid acid. In addition, the activity of the liquid acid needed to be accounted for as the homogeneous acid species would remain in the batch reactors contributing to the hydrolysis of cellulose. To determine the extent of liquid acid generation, the polymers were hydrothermally treated as described below. The reaction conditions were identical to the reaction conditions of cellulose and cellobiose hydrolysis as described in the previous section. Polymer (0.20 g), water (2.0 mL; 17.7 MΩ resistivity), and a magnetic stir bar were added to a 15 mL heavy wall pressure vial and the vial was sealed with a screw cap with a Viton O-ring seal. The vial was submerged in an oil bath that had been preheated to the desired temperature (120 °C, 150 °C, or 175 °C). The reaction mixture was stirred at 150

rpm for 10 h. After the reaction was over, the reaction was cooled to room temperature and the pH was measured with a pH meter (VWR Scientific Model 8000).

3.2.11. Ion Chromatography

The leached acids were characterized, and their anions quantified with Dionex ICS-2100 Ion Chromatographer equipped with AERS 500 anion electrolytically regenerated suppressor and DS6 heated conductivity cell. Anions were separated with AS153 250 mm column equipped with IonPac AG 2x50 mm guard. The mobile phase was 38.00 mM KOH at 0.25 ml/min. Separation was carried at column temperature of 30 °C and detection at cell temperature of 35 °C.

Concentration of the chloride ion was quantified by using five-point calibration curves. Concentrations are plotted as averages and standard deviations of concentrations obtained from three independent runs.

3.2.12. Hydrolysis of Cellulose with Catalysts Leachate

Polymer catalyst (0.5 g), water (5 mL, 17.7 MΩ resistivity), and a magnetic stir bar were placed into a 15 mL, heavy wall pressure vial and the vial was sealed with a Viton O-ring seal. The vial was submerged in an oil bath that had been preheated to 175 °C. The reaction mixture was stirred for 10 hours at 150 rpm. After the reaction time was complete, the vial was cooled in an ice bath. The liquid was recovered with a syringe equipped 22G needle and the solids were separated and stored. 2 mL of the leachate (corresponding from leach liquor obtained from 0.20 g of polymer, the amount of catalyst used in prior reactions), cellulose (0.100 g), and a magnetic stir bar were placed in 15 mL heavy wall pressure vial and the vial was sealed with a Viton O-ring seal. The vial was submerged in an oil bath that had been preheated to 175 °C. The reaction mixture was stirred for 10 hours at 150 rpm at 175 °C. After the reaction time, vials were cooled in an ice bath

to stop the hydrolysis reaction. The liquid was filtered and further analyzed with HPLC for quantifying hydrolysis products.

3.3. Results and Discussion

In this work we investigated a polymer solid acid catalyst, labeled here CMP-SO_3H-0.3, whose synthesis, for the purpose of reproducibility, was adapted from a well-known polymer functionalization procedure.[23, 47, 48] Since Zuo et al. first used this material for cellulose hydrolysis and reported several structural modifications, with varying chloromethyl and sulfonic acid group compositions, we focused on reproducing the catalyst structure that exhibited greatest cellulose hydrolysis activity.[23] CMP-SO_3H-0.3 does not bear any additional functional groups (such as the amine substructure in Pan's catalyst) other than C−Cl and C−SO_3H moieties.[22, 23] We reasoned that the relative simplicity of CMP-SO_3H-0.3 would enable a more straightforward analysis of structure−activity relationships.

For the purpose of preparing the CMP-SO_3H-0.3 catalyst, we began with chloromethyl polystyrene (CMP) polymer beads, bearing only benzyl chloride groups. The functionalization was monitored at each step of the synthesis procedure by ATR-FTIR, to observe the changes in the spectrum and verify the reduction of -Cl signal and the presence of -SO_3H signal. Figure 3.1. shows infrared spectra of the polymer at each stage of modification. Specifically, the characteristic signal at 1265 cm^{-1} attributed to -CH_2-Cl groups is reduced in intensity following attachment of thiourea. After oxidation to sulfonic acid, a signal appears at 1040 cm^{-1}, consistent with -SO_3H vibrations.

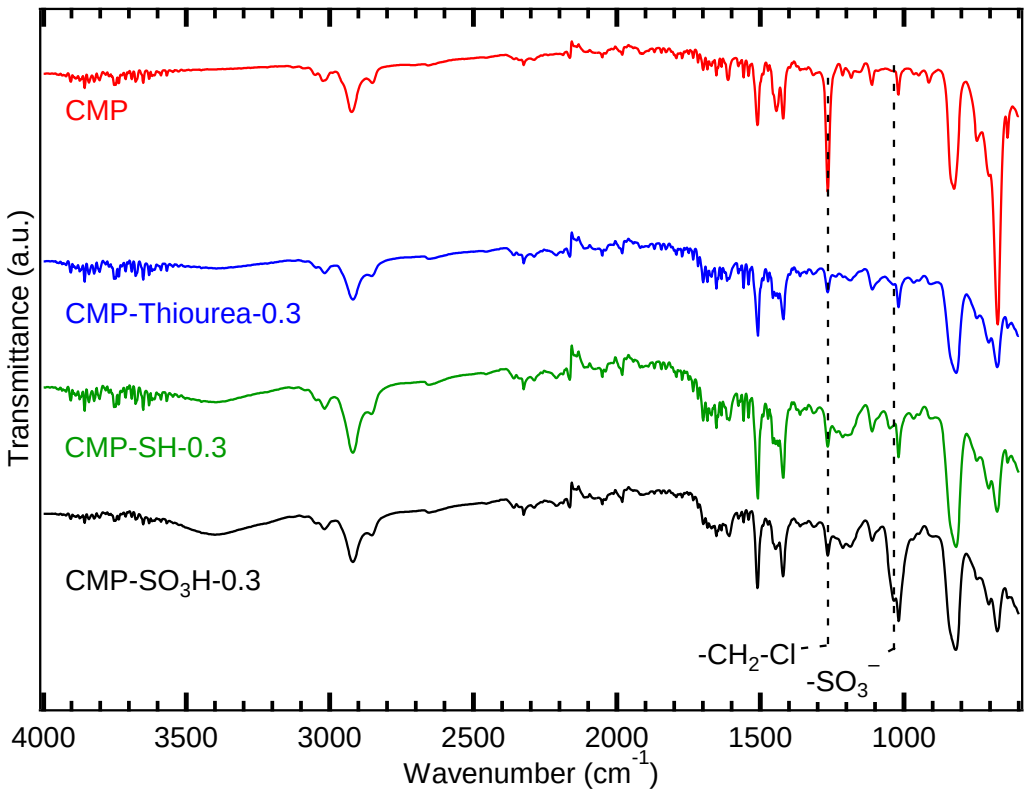

Figure 3.5. ATR-FTIR spectra of CMP-SO_3H-0.3 and intermediates at different stages of the catalyst preparation procedure. The characteristic chloromethyl and sulfonic acid peaks are marked.

To further verify successful functionalization of the polymer beads we performed elemental analysis. Table 3.1. presents the experimental results and compares them to the stoichiometric predictions assuming only the desired functionalization reactions took place and 100% conversion at each step. The starting CMP precursor has 5.5 mmol/g of Cl loading. The elemental analysis results confirm that catalyst synthesis procedure successfully substitutes, but retains some of the chloride, and introduces sulfur moieties. However, the content of both the chlorine and the sulfur is lower than the predictions, suggesting incomplete functionalization and side reactions taking place. The results are consistent with the structural analysis reported by Zuo et al.[23]

Table 3.1. Elemental analysis of CMP-SO_3H-0.3.

		Predicted*		Experimental Results	
Element	**Mass**	**Mass %**	**mmol/g**	**Mass %**	**mmol/g**
Cl	0.117	11.1	3.14	8.75	2.47
S	0.0528	5.02	1.57	4.51	1.41
O	0.088	8.36	5.22	8.74	5.46
C	0.72864	69.2	57.7	69.83	58.2
H	0.06628	6.30	63.0	5.86	58.6
Total	1.05272	100		97.7	

***** Based on assumption that 100% thiourea attachment is achieved during polymer modification and no side reactions occur.

In addition to verifying the structural reproducibility, we sought to confirm the cellulose hydrolysis activity was identical to that reported by Zuo et al.[23] The observed catalytic activities of CMP-SO_3H-0.3 in the hydrolysis of cellulose were in close agreement with literature data as shown in Figure 3.2., instilling confidence that the obtained material was suitable for more detailed structural analysis.

After the successful activity tests, CMP-SO_3H-0.3 and its precursor resin CMP were both analyzed using quantitative solid-state ^{13}C NMR spectroscopy to determine the concentration of functional groups present within the modified polymer beads. The spectra presented in Figure 3.3. confirmed the desired partial substitution of the benzylic C−Cl groups in CMP-SO_3H-0.3. Specifically, the intensity of the signal at 138 ppm attributed to the carbon bonded to the chloromethyl groups decreased and a new signal appeared at around 58 ppm, consistent with the formation of the expected benzyl sulfonic acid moiety. In addition, a polymer catalyst that had

been treated with excess thiourea in order to fully substitute the chloromethyl groups with sulfonic acids (CMP-SO_3H-1.2) was also analyzed. For reference, the ATR-FTIR and NMR spectra are presented in Appendix A (Figures A1 and A2). Figures A1 and A2 d) confirm full sulfonation of CMP-SO_3-1.2 as no chloromethyl signal was observed, but sulfonic acid signal was present.

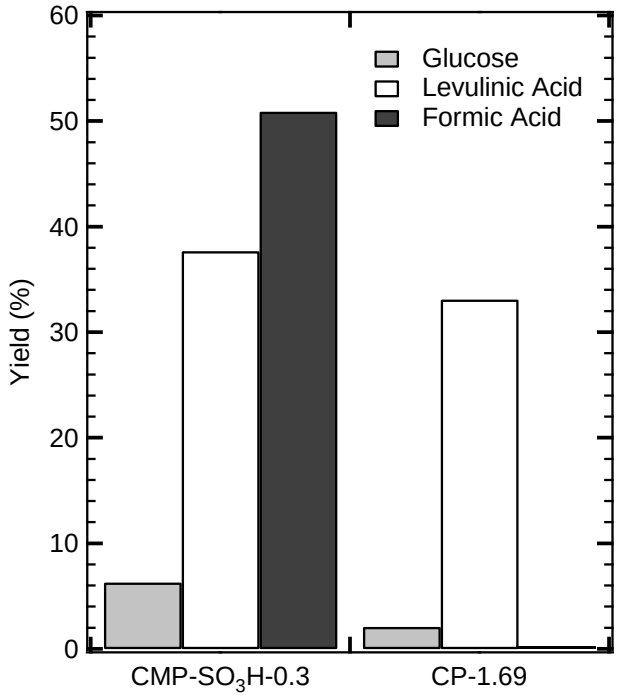

Figure 3.6. Comparison of the soluble product yields after cellulose hydrolysis with CMP-SO_3H-0.3 synthesized in the current study and CP-1.69 reported by Zuo et al. Zuo et al. did not quantify formic acid.[23]

Quantification of the NMR signals indicated that ~30% of the C−Cl functionalities in CMP had been converted to C− SO_3H moieties in CMP-SO_3H-0.3. Interestingly, in addition to the signals of the benzylic C−Cl and C−SO_3H groups, the MAS NMR spectrum of CMP-SO_3H-0.3 contains a band at 62 ppm, consistent with the presence of benzylic CH_2−OH groups constituting ~14% of the total benzylic functional groups. The presence of C−OH groups is further supported by a weak band observed in the ATR-IR spectrum at 3400 cm^{-1} (see Figure 3.1.). On the other

hand, signal consistent with CH_2-OH groups was not detected in the NMR spectrum of the fully sulfonated CMP-SO_3H-1.2 (see Figure A3 d).

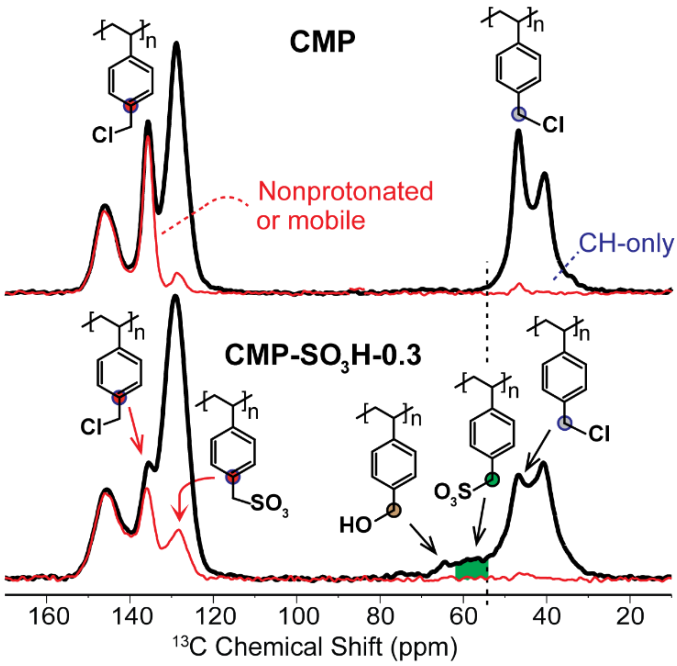

Figure 3.7. ^{13}C NMR spectra of polymer precursor (CMP) (top) and CMP-SO_3H-0.3 (bottom). Thick black line: all C; thin red line: nonprotonated or mobile C.

These observations indicate that the benzylic C−Cl functionalities, previously hypothesized to act as "binding groups", hydrolyze partially to produce benzylic alcohols under typical polymer modification conditions. To explore further the possibility of C-Cl hydrolysis especially during reaction conditions, we subjected CMP-SO_3H-0.3 to a reaction with cellobiose and analyzed the changes of the NMR spectrum. Notably, after employing CMP-SO_3H-0.3 to catalyze cellobiose hydrolysis, the C−OH signal intensity further increased, while the C−Cl signal intensity decreased as shown in Figure 3.4., consistent with the general instability of benzylic C−Cl groups under catalytic conditions.

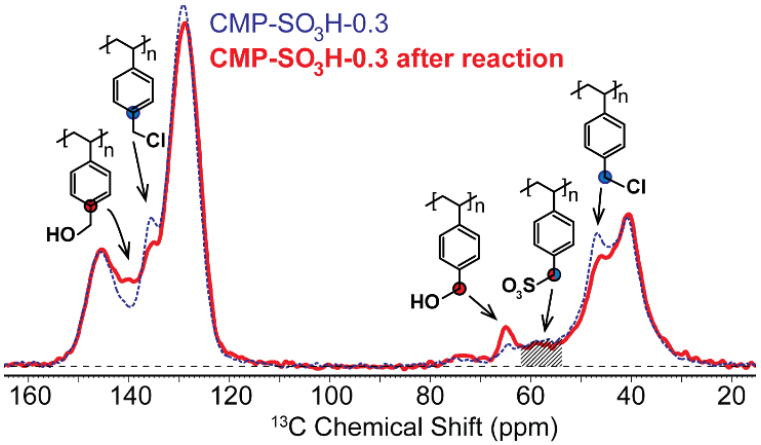

Figure 3.8. ^{13}C NMR spectrum of CMP-SO_3H-0.3 before (blue, dotted line) and after (red line) cellobiose hydrolysis. Catalysis conditions: 5 h, 175 °C, 0.2 g catalyst, 0.1 g cellobiose, 2 mL H_2O.

The NMR spectra presented in Figures 3.3. and 3.4. imply that both hydroxyl and chloromethyl groups are present in the catalyst structure and, therefore, can participate in hydrogen bonding with cellulose. However, NMR provides bulk detection of the chemical moieties and does not provide additional structural information on the three-dimensional distribution of the groups. Considering that the interactions between the solid acid catalyst and solid cellulose substrate are limited to the external surfaces, two questions arise: what is the spatial distribution of C−OH and C−Cl groups and which of these two groups (if either) is available for binding carbohydrates during hydrolysis? To investigate, polymer beads of CMP-SO_3H-0.3 (particle sizes ~500 μm) were sectioned in half; Raman microscopy and energy-dispersive spectroscopy analysis were performed on the sectioned beads to gain insight into the spatial distribution of functional groups.

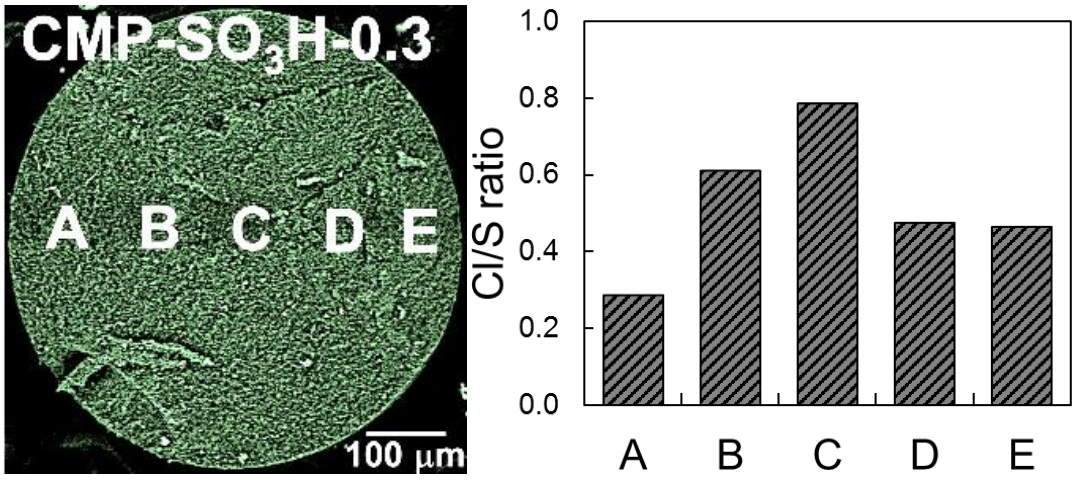

Figure 3.9. Cross-sectional EDS analysis of CMP-SO_3H-0.3 catalyst bead.

Figure 3.5. provides a SEM image and indicates the locations of EDS spectra acquired along the bead cross-section and the obtained Cl/S ratios. Interestingly, the Cl/S ratio is not uniform, with the values measured near the polymer bead's exterior being lower than those observed in its interior. Detailed cross-sectional Raman microscopy characterization is shown in Figure 3.6. The spectrum of the precursor CMP polymer shows an intense band attributable to -CH_2Cl at 1265 cm^{-1}. After functionalization to CMP-SO_3H-0.3, the -CH_2-Cl band decreases in intensity toward the outside of the bead. The opposite trend is observed for the -SO_3^- band at 1040 cm^{-1}. For reference, the cross-sectional Raman spectra of CMP-SO_3H-1.2 are provided in Figure A reveals a uniform distribution of -SO_3^- and no -CH_2-Cl signal, consistent with complete sulfonation of the polymer beads (see Figure A3). Together, these data indicate that the C−Cl moieties in the center of the polymer beads remain mostly intact, while the chemical modifications occur more completely in the outer regions of the beads than in the interior.

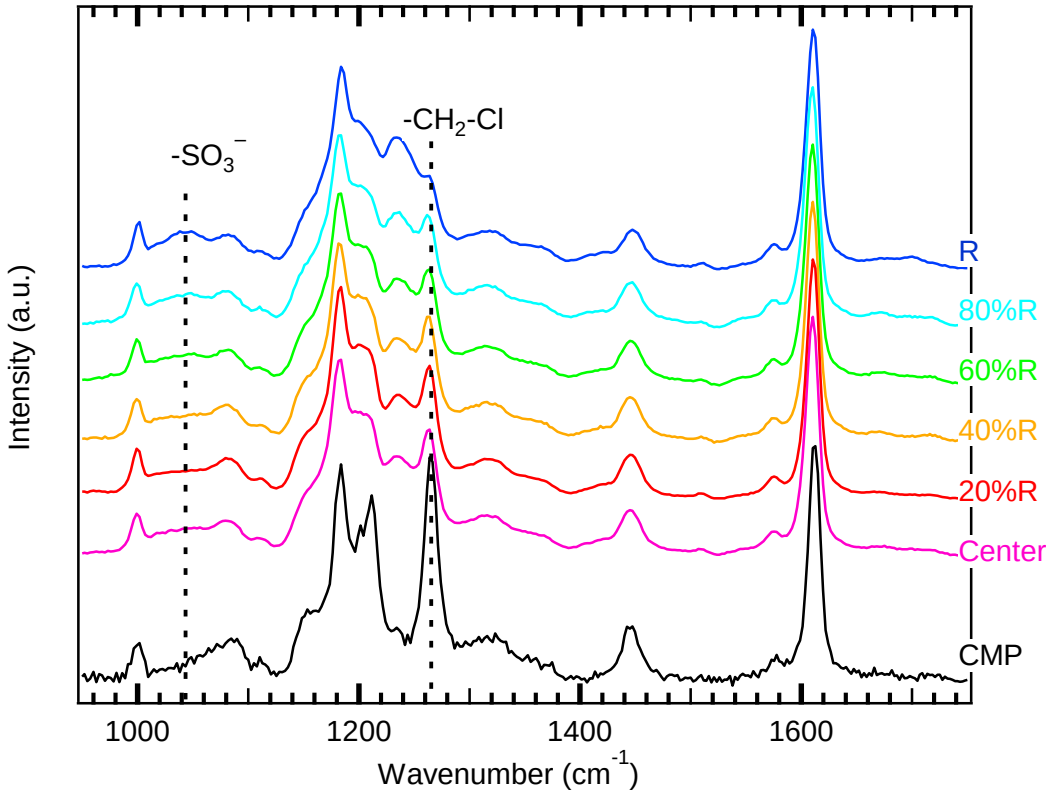

Figure 3.10. Cross-sectional Raman analysis of CMP-SO_3H-0.3. Marked bands: 1265 cm^{-1} (CH_2−Cl; decreasing from inside to outside of the bead), 1040 cm−1 (CH_2−SO_3H, increasing from inside to outside of the bead). The value R signifies the distance of the measurement from the center of the polymer bead.

EDS and Raman cross-sectional analyses further suggest that access to the inside of the beads is limited for the aqueous reagent mixtures used for polymer modification as well as the polysaccharide hydrolysis reaction mixture. This is most likely due to the hydrophobic environment in the beads' interior, especially during the modification steps employing aqueous environment such as the NaOH hydrolysis of the thoiuronium salt and H_2SO_4 treatment. Notably, with more C−Cl bonds in the interior of the particle, the previously postulated hydrogen-bonding contact between C−Cl moieties and cellulose fibers during hydrolysis seems less like to occur than if the C−Cl groups were to remain intact on the polymer surface. Thus, for the resin under

investigation, attributing their superior catalytic activity to the presence of supramolecular interactions between the polysaccharides and the benzyl chloride groups seems inconsistent with the spatially resolved structural data.

Despite these new insights, the structural analysis does not clearly establish the source of the significant catalytic activity exhibited by CMP-SO_3H-0.3 in cellulose hydrolysis. In is not clear whether the detected hydroxyl groups in the structure of CMP-SO_3H-0.3 participate in hydrogen bonding interactions with the hydroxyl group present in cellulose. To test whether the measured activity in cellulose hydrolysis is simply due to the presence of the sulfonic acid groups, the catalytic activity of CMP-SO_3H-0.3 was compared to that of a fully sulfonated counterpart, CMP-SO3H-1.2. In CMP-SO_3H-1.2, the C−Cl groups are completely substituted with C−SO_3H groups, as verified by ATR-FTIR solid-state 13C NMR, FTIR, and Raman analyses (for details, see Figures A1, A2, A3, in Appendix A). If sulfonic acid groups are the sole source of catalytic activity towards cellulose hydrolysis, and if neither the chloride nor the hydroxyl groups contribute to the observed activity, then CMP-SO_3H-1.2 would be expected to show greater activity than CMP-SO_3H-0.3, simply due to the greater amount of C−SO_3H groups present. However, yields of glucose, LA, and formic acid (3%, 7%, and 12%, respectively) obtained using CMP-SO3H-1.2 for cellulose hydrolysis were lower than those with CMP-SO_3H-0.3 (6%, 38%, and 51%, respectively) as shown in Figure 3.7. The soluble carbon balance was also lower for CMP-SO_3H-1.2 (see section 2.10 for details on calculating soluble carbon). Furthermore, the reaction solution using CMP-SO_3H-1.2 as catalyst clearly contained residual cellulose as a white powder (Figure 3.8B), while CMP-SO3H-0.3 yielded a yellow solution with little cellulose visible left in the reaction mixture (Figure 3.8A).

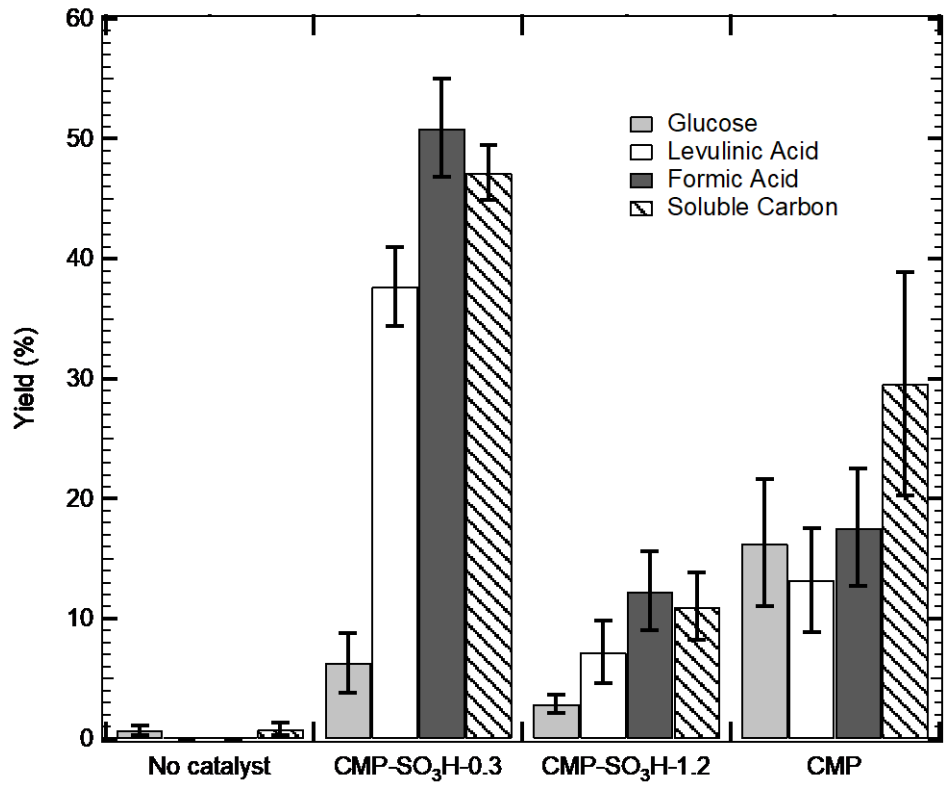

Figure 3.11. Comparison of catalytic activity of CMP-SO_3H-0.3, CMP-SO_3H-1.2, and catalyst polymer precursor CMP in cellulose hydrolysis.

These differences in activity of the two catalysts contradict the hypothesis that only the sulfonic acid groups in CMP-SO_3H-0.3 are responsible for hydrolysis activity. Interestingly, cellulose hydrolysis experiments employing the precursor polymer CMP with nonmodified benzylic C−Cl moieties and no -SO_3H groups also resulted in appreciable cellulose conversion. The use of CMP as catalyst produced less LA (13%) and formic acid (18%), and soluble carbon balance (~30%) than what was obtained with CMP-SO_3H-0.3 (Figure 7; 38% LA and 51% formic acid, and 47% soluble carbon balance, respectively), but more glucose (17%) than when using CMP-SO_3H-0.3 as catalyst (6%). NMR spectra in Figure 3.4. revealed -C-Cl bond hydrolysis at reaction conditions the result of which was introduction of additional hydroxyl groups in the polymer structure. Another product of this reaction is hydrochloric acid.[49, 50] The structural analysis along with the

cellulose hydrolysis observations made for CMP suggest as a new hypothesis – in situ HCl generation is likely responsible for part of the observed hydrolysis activity with CMP-SO_3H-0.3.

To confirm that the hydroxyl groups presence in CMP-SO_3H-0.3 do not contribute to the observed the activity of hydroxymethyl polystyrene polymer bearing only benzylic hydroxyl groups was evaluated. Notably, none of the typical products of cellulose hydrolysis (glucose, levulinic acid, formic acid, HMF) were observed in these tests, indicating that CMP−OH is catalytically inactive in the absence of additional stronger acid groups.

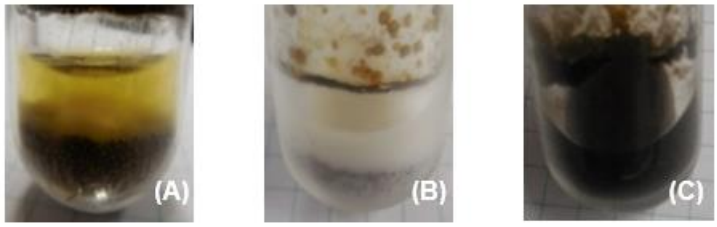

Figure 3.12. Visual Comparison of Cellulose Hydrolysis Suspensions for (A) CMP-SO_3H-0.3, (B) CMP-SO_3H-1.2, and (C) Leachate from CMP-SO_3H-0.3.

The results obtained after cellulose hydrolysis with CMP-SO_3H-1.2 and hydroxymethyl polystyrene indicate that the presence of -CH_2-Cl moieties in CMP-SO_3H-0.3 contributes to the apparent catalytic activity of the polymer. Along with the structural insights provided by Raman (no -CH_2-Cl groups on the surface) and NMR (hydrolysis of -CH_2-Cl groups) these observations point to the previously state hypothesis of HCl generation and hydrolysis by the homogeneous acid. To directly test whether formation of HCl occurs in reaction mixtures employing CMP-SO_3H-0.3 as catalyst, chloride concentrations were measured in these mixtures after hydrolysis of cellobiose and cellulose and the values are presented in Table 3.2. As expected, both reaction mixtures showed significant concentrations of chloride (0.051 M for cellobiose hydrolysis at 150 °C after 5 h; 0.195 M for cellulose hydrolysis at 175 °C after 10 h). Moreover, the H^+

concentrations, as determined by pH measurements, showed a similar trend (0.042 and 0.141 M, respectively). These data confirm that HCl is formed from CMP-SO_3H-0.3 when using this material as solid acid catalyst. The formation of HCl is due to hydrolysis of the -CH_2-Cl groups in the hydrothermal environment used for cellulose hydrolysis.

Table 3.2. Ion Concentrations in reaction solution after catalytic hydrolysis of cellobiose and cellulose substrates. Conditions: 0.100 g substrate, water (2.0 mL), CMP-SO_3H-0.3 (0.200 g), sealed pressure glass vial.

Substrate	Time [h]	Temperature [°C]	$[Cl^-]$	$[H^+]$
Cellobiose	5	150 °C	0.051 ± 0.002 M	0.042 ± 0.006 M
Cellulose	10	175 °C	0.195 ± 0.007 M	0.141 ± 0.005 M

Hydrolysis experiments utilizing CMP-SO_3H-1.2 revealed that the catalyst, exclusively decorated with -SO_3H groups, is also capable of depolymerizing cellulose. However, since we already established CMP-SO_3H-0.3 also possesses such functionalities on its external surface, it is not clear how much they contribute to the apparent cellulose hydrolysis and what part of the activity can be attributed to the action of HCl as a homogeneous acid. Accordingly, we investigated if HCl formed by leaching CMP-3H-0.3 can affect cellulose hydrolysis at similar catalytic levels as the polymer beads. To simulate the effects of HCl, CMPSO_3H-0.3 was treated with H_2O at 175 °C for 10 h, mimicking cellulose hydrolysis conditions without the presence of the catalytic substrate. The polymer beads were then removed, and the resulting leachate was used for cellulose hydrolysis studies. In a first set of experiments, cellulose was hydrolyzed only with the leachate as reagent and the data is shown in Figure 3.9. Importantly, these experiments resulted in significantly higher yields of levulinic acid (57%), formic acid (60%), and soluble carbon (59%) than those determined for the tests using CMP-SO_3H-0.3 as catalyst. Figure 3.8C shows that the

solution of the leachate catalyzed cellulose hydrolysis turned black post reaction which indicates formation of carbohydrate degradation species and insoluble humins. This suggests that HCl formed through hydrolysis of benzylic C−Cl sites on CMP-SO_3H-0.3 is a powerful catalyst for cellulose hydrolysis. Furthermore, gradual HCl release from CMPSO_3H-0.3 under cellulose hydrolysis conditions would lead to a lower average HCl concentration over the reaction time than found in the HCl-containing leachate, providing a reason for the overall lower activity observed for CMP-SO3H-0.3, compared to the activity of the leachate.

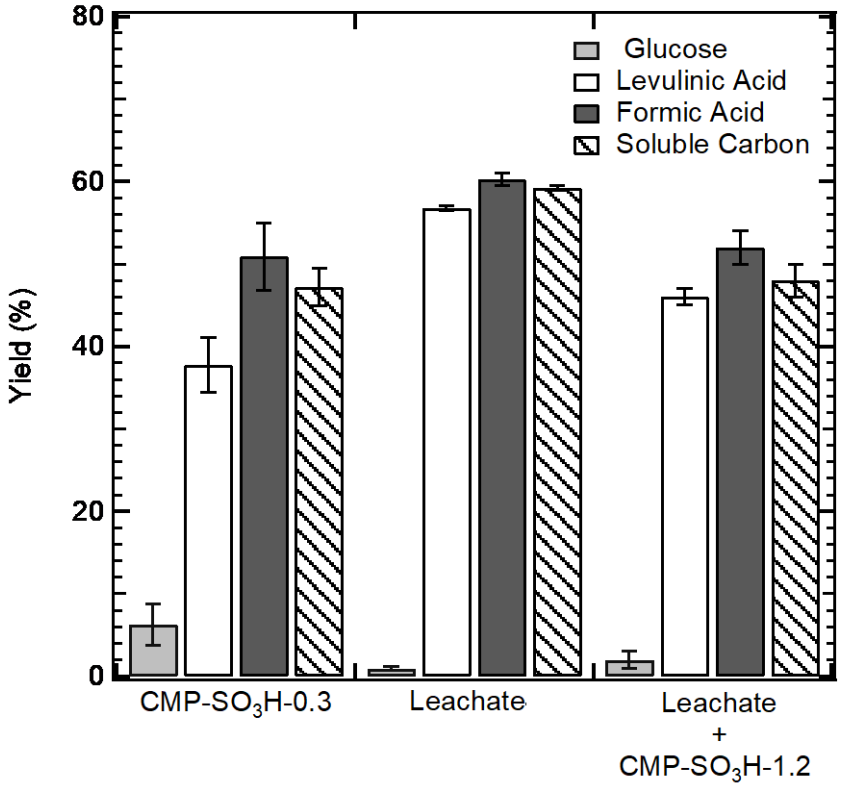

Figure 3.13. Comparison of catalytic activity of CMP-SO_3H-0.3, leachate from treating CMP-SO_3H-0.3 with H_2O (175 °C, 10 h), and leachate + CMP-SO_3H-1.2 for cellulose hydrolysis.

Interestingly, high activity (46% levulinic acid, 52% formic acid, and 58% soluble carbon) of the leachate was still observed after the solution was combined with polymeric CMP-SO_3H-1.2 and employed in cellulose hydrolysis. However, both CMP-SO_3H-0.3 and CMP-SO_3H-1.2 appear

to play an additional role during cellulose hydrolysis. The polymer beads undergo a color change, possibly consistent with adsorption of humin side products. Such adsorption possibilities are not present in the reaction mixtures employing the leachate, which leads to humin precipitation (Figure 3.8C).

The hydrothermal environment used in the cellulose hydrolysis experiments presented so far is rather severe. It is not clear whether application of the chloromethyl polystyrene based catalysts would leach at lower temperatures. To test this, we subjected CMP, CMP-SO_3H-0.3, and CMP-SO_3H-1.2 to hydrothermal treatments at three temperatures (120, 150, and 175 °C) and measured the pH of the liquid and the results are presented in Table 3.3. CMP and CMP-SO_3H-0.3 result in progressive generation of homogeneous acid with increasing temperature. On the other hand, CMP-SO_3H-1.2 is a lot more stable and results in moderate pH decrease with increasing temperature, consistent with relative stability of benzyl sulfonic acid groups.[44]

Table 3.3. Hydrothermal treatment of chloromethyl polystyrene based polymers and pH characterization of aqueous media post reaction.

Polymer	175 °C	150 °C	120 °C
CMP-SO_3H-0.3	0.91 ± 0.02	1.15 ± 0.02	1.33 ± 0.04
CMP-SO_3H-1.2	1.84 ± 0.03	1.89 ± 0.05	2.14 ± 0.05
CMP	1.34 ± 0.06	1.86 ± 0.05	2.46 ± 0.03

3.4. Conclusion

The studies presented herein suggest that benzylic chloride functionalities are hydrothermally labile and mostly absent from the surface of the polymer beads used as solid acid catalysts. As such, benzylic C−Cl groups are unlikely to be involved in supramolecular interactions with polysaccharide substrates such as cellulose. Alternatively, our data suggest that residual benzylic

chloride moieties within the polymer beads release HCl under the hydrolysis reaction conditions, providing a homogeneous acid source to catalyze cellulose hydrolysis. Furthermore, our analyses indicate that previously unreported functional groups−specifically benzylic C−OH moieties−are present in the polymer and that their concentration increases upon use of the catalyst in cellobiose hydrolysis. Overall, our results question the commonly accepted role of benzylic C−Cl groups acting as hydrogen bond acceptors and present an alternative explanation for high catalytic activities through a combination of sulfonic acid catalysis and in situ release of HCl; notably, humin adsorption on the polymer surface was observed, which in turn may affect glucan-polymer interactions. Generally, this work highlights the need for caution when interpreting catalytic results with polymer-based solid acids without a detailed, quantitative analysis of polymer structure and spatial distribution of functional groups.

3.5. References

1.D. M. Alonso, J. Q. Bond and J. A. Dumesic, *Green Chemistry*, 2010, **12**.

2.F. H. Isikgor and C. R. Becer, *Polymer Chemistry*, 2015, **6**, 4497-4559.

3.M. Hall, P. Bansal, J. H. Lee, M. J. Realff and A. S. Bommarius, *FEBS J*, 2010, **277**, 1571-1582.

4.S. Sun, S. Sun, X. Cao and R. Sun, *Bioresour Technol*, 2016, **199**, 49-58.

5.M. Foston and A. J. Ragauskas, *Industrial Biotechnology*, 2012, **8**, 191-208.

6.G. Brodeur, E. Yau, K. Badal, J. Collier, K. B. Ramachandran and S. Ramakrishnan, *Enzyme Res*, 2011, **2011**, 787532.

7.U. Bornscheuer, K. Buchholz and J. Seibel, *Angew Chem Int Ed Engl*, 2014, **53**, 10876-10893.

8.X. Zhao, L. Zhang and D. Liu, *Biofuels, Bioproducts and Biorefining*, 2012, **6**, 465-482.

9.R. Rinaldi and F. Schuth, *ChemSusChem*, 2009, **2**, 1096-1107.

10.H. Zhao, J. Kwak, Z. Conradzhang, H. Brown, B. Arey and J. Holladay, *Carbohydrate Polymers*, 2007, **68**, 235-241.

11.O. Bobleter, W. Schwald, R. Concin and H. Binder, *Journal of Carbohydrate Chemistry*, 1986, **5**, 387-399.

12.R. Weingarten, J. Cho, R. Xing, W. C. Conner, Jr. and G. W. Huber, *ChemSusChem*, 2012, **5**, 1280-1290.

13.B. Yang, D. M. Willies and C. E. Wyman, *Biotechnology and Bioengineering*, 2006, **94**, 1122-1128.

14.N. Sweygers, N. Alewaters, R. Dewil and L. Appels, *Sci Rep*, 2018, **8**, 7719.

15.J. Nill, N. Karuna and T. Jeoh, *Process Biochemistry*, 2018, **74**, 108-117.

16.E. Johnson, *Biofuels, Bioproducts and Biorefining*, 2016, **10**, 164-174.

17.D. Gomes, A. C. Rodrigues, L. Domingues and M. Gama, *Applied Microbiology and Biotechnology*, 2015, **99**, 4131-4143.

18.A. Aden and T. Foust, *Cellulose*, 2009, **16**, 535-545.

19.L. R. Lynd, X. Liang, M. J. Biddy, A. Allee, H. Cai, T. Foust, M. E. Himmel, M. S. Laser, M. Wang and C. E. Wyman, *Curr Opin Biotechnol*, 2017, **45**, 202-211.

20.Y.-B. Huang and Y. Fu, *Green Chemistry*, 2013, **15**.

21.A. Shrotri, H. Kobayashi and A. Fukuoka, *Acc Chem Res*, 2018, **51**, 761-768.

22.L. Shuai and X. Pan, *Energy & Environmental Science*, 2012, **5**.

23.Y. Zuo, Y. Zhang and Y. Fu, *ChemCatChem*, 2014, **6**, 753-757.

24.Q. Yang and X. Pan, *BioEnergy Research*, 2016, **9**, 578-586.

25.B. Wiredu and A. S. Amarasekara, *Catalysis Communications*, 2014, **48**, 41-44.

26.F. Parveen, K. Gupta and S. Upadhyayula, *Carbohydr Polym*, 2017, **159**, 146-151.

27.X. Qian, J. Lei and S. R. Wickramasinghe, *RSC Advances*, 2013, **3**.

28.S. Suganuma, K. Nakajima, M. Kitano, D. Yamaguchi, H. Kato, S. Hayashi and M. Hara, *Journal of the American Chemical Society*, 2008, **130**, 12787-12793.

29.M. Yabushita, H. Kobayashi, J. Y. Hasegawa, K. Hara and A. Fukuoka, *ChemSusChem*, 2014, **7**, 1443-1450.

30.G. S. Foo and C. Sievers, *ChemSusChem*, 2015, **8**, 534-543.

31.S. Hu, T. J. Smith, W. Lou and M. Zong, *J Agric Food Chem*, 2014, **62**, 1905-1911.

32.P.-W. Chung, M. Yabushita, A. T. To, Y. Bae, J. Jankolovits, H. Kobayashi, A. Fukuoka and A. Katz, *ACS Catalysis*, 2015, **5**, 6422-6425.

33.P.-W. Chung, A. Charmot, T. Click, Y. Lin, Y. Bae, J.-W. Chu and A. Katz, *Langmuir*, 2015, **31**, 7288-7295.

34.G. S. Foo and C. Sievers, *ChemSusChem*, 2015, **8**, 534-543.

35.L. Hu, Z. Li, Z. Wu, L. Lin and S. Zhou, *Industrial Crops and Products*, 2016, **84**, 408-417.

36.S. Van de Vyver, L. Peng, J. Geboers, H. Schepers, F. de Clippel, C. J. Gommes, B. Goderis, P. A. Jacobs and B. F. Sels, *Green Chemistry*, 2010, **12**.

37.G. Akiyama, R. Matsuda, H. Sato, M. Takata and S. Kitagawa, *Adv Mater*, 2011, **23**, 3294-3297.

38.J. M. Geremia, B. M. Baynes and A. Dhawan, *Journal*, 2013.

39.F. Shen, R. L. Smith, L. Li, L. Yan and X. Qi, *ACS Sustainable Chemistry & Engineering*, 2017, **5**, 2421-2427.

40.G. Fei, J. Shin, S.-A. Kang, B.-S. Ko, P.-H. Kang, Y.-S. Lee and Y. C. Nho, *Journal of Polymer Science Part A: Polymer Chemistry*, 2010, **48**, 563-569.

41.C. Ji, R. Qu, C. Sun, C. Wang, Q. Xu, Y. Sun, C. Li and S. Guo, *Journal of Applied Polymer Science*, 2007, **103**, 3220-3227.

42.R. L. Johnson and K. Schmidt-Rohr, *Journal of Magnetic Resonance*, 2014, **239**, 44-49.

43.J. M. Anderson, R. L. Johnson, K. Schmidt-Rohr and B. H. Shanks, *Carbon*, 2014, **74**, 333-345.

44.J. M. Anderson, R. L. Johnson, K. Schmidt-Rohr and B. H. Shanks, *Catalysis Communications*, 2014, **51**, 33-36.

45.J.-D. Mao and K. Schmidt-Rohr, *Environmental science & technology*, 2004, **38**, 2680-2684.

46.K. Schmidt-Rohr and J. D. Mao, *Journal of the American Chemical Society*, 2002, **124**, 13938-13948.

47.M.-L. Hwang, J. Choi, H.-S. Woo, V. Kumar, J.-Y. Sohn and J. Shin, *Nuclear Instruments and Methods in Physics Research Section B: Beam Interactions with Materials and Atoms*, 2014, **321**, 59-65.

48.J. M. Fréchet, M. D. de Smet and M. J. Farrall, *Polymer*, 1979, **20**, 675-680.

49.G. W. Beste and L. P. Hammett, *Journal of the American Chemical Society*, 1940, **62**, 2481-2487.

50.W. Mabey and T. Mill, *Journal of Physical and Chemical Reference Data*, 1978, **7**, 383-415.

Chapter 4

Implications of homogeneous acid catalysis and criteria for interpretation of solid acid catalyst activity for cellulose hydrolysis

4.1. Introduction

As a renewable and sustainable feedstock lignocellulosic biomass has gained significant interest as an alternative to fossil resources to produce carbon-based fuels and chemicals.[1] The ultimate success of biomass utilization is dependent on the development of economically competitive strategies and processes for its deconstruction.[2] As a major component of lignocellulosic biomass, cellulose has attracted major research effort for its depolymerization.[3-5] Cellulose is a homopolymer made up of glucose units connected via β-1,4 glycosidic ether bonds and currently its depolymerization to low molecular weight species represents a bottleneck for economically competitive production of renewable fuels and chemicals such as ethanol.[6-9]

Widely investigated approach for cellulose depolymerization is hydrolysis where the main goal is selective conversion to glucose or its decomposition products which can subsequently be upgraded.[10-14] Hydrolysis can be carried out by high temperature water in sub or supercritical state; less severe temperature conditions employ the use of inorganic homogeneous acids or enzymes as catalysts in aqueous environment.[4, 15-20] Depolymerization of cellulose in high temperature water and by liquid acid catalysts occurs in reaction times ranging from seconds to tens of minutes.[21-24] However, at those conditions the products of hydrolysis are more reactive than the polymer and subsequent product decomposition and loss of yields and selectivity complicate controlled deconstruction of cellulose.[25, 26] Overcoming this issue requires sophisticated reactor design, while

the use of homogeneous acid promote side reactions.[27, 28] On the other hand, enzymes are very selective, but the reaction rate of cellulose hydrolysis is very slow.[18, 29-31] Furthermore, both acids and enzymes are not recyclable, which effectively renders them reactants, resulting in costs that prevent commercialization of cellulose hydrolysis.[32, 33]

Solid acid catalysts have emerged as a recyclable alternative to liquid acids and enzymes for hydrolysis of cellulose.[34, 35] Application of solid acid catalysts for cellulose hydrolysis is typically carried out in hydrothermal conditions (120-200 °C) at which cellulose is a solid.[34-37] Therefore, the reaction would occur at the contact interface of the two solids and will be severely mass transfer limited. However, the interactions between the two solids at these reaction conditions have not been directly elucidated which prevents development of reaction mechanism and rational catalyst design.[38] Most commonly structure-activity relationships are inferred from bulk characterization, adsorption of soluble cellulosic molecules such as glucose and cellobiose or soluble oligomers, and quantification of cellulose conversion and product yields after hydrolysis.[36, 39-48] Based on such correlations a proposed reaction mechanism suggests supramolecular binding interactions between cellulose and the solid acid catalysts which increase the probability for splitting the glycosidic bond.[36, 46] This explanation is supported by the observation that catalysts with chemical moieties hypothesized to bind to cellulose appear to outperform catalysts without such chemical functionalities that can participate in binding.[36, 39, 49, 50]

However, despite attempts to model the interactions between cellulose and solid acid catalyst using colloid suspension stabilization theory,[51] no direct evidence has been presented of such interactions occurring at the hydrothermal environment used in cellulose hydrolysis. Furthermore, in Chapter 3 we showed that chloromethyl polystyrene based catalysts could degrade and leach homogeneous acid which is active towards cellulose hydrolysis, revealing that in reality the

reaction network is more complicated than the hypothesized adsorption-reaction-desorption mechanism.[38] It is not clear whether the aforementioned conclusions can be extended to other catalytic structures that have been proposed for cellulose hydrolysis since leaching analysis is not typically carried out. Considering the continuing interest in proposed solid catalyst structures for cellulose hydrolysis, it is necessary to address the implications of acid leaching.[47, 48, 52-58] Few studies have considered leaching of acid sites as a mode of catalyst deactivation, but the effect of leaching on the hydrolysis has not been investigated.[50, 59, 60] Leaching of catalytically active homogenous acid can result in inappropriately attributing observed cellulose hydrolysis activity to solid acid catalysts and overall misinterpretation of the structure-activity correlations.[61]

In this case, two questions arise - do catalysts leach homogeneous acid that catalyzes cellulose hydrolysis and how can the intrinsic activity of the solid acid towards hydrolysis of solid cellulose substrate be determined. Determining the intrinsic activity of a solid acid catalyst is an important step towards unraveling the underlying mechanism of action. Since direct measurements of the solid-solid interactions under hydrothermal conditions are experimentally challenging, interpreting the activity of proposed catalyst structures must account for the potential contribution of leaching to the observed hydrolysis. Specifically, in the context of batch reactors usually used for testing the activity of catalyst, leaching and accumulation of homogeneous acid can significantly impact the interpretation of the solid acid catalyst activity.[36, 52, 56] Subtracting the effects of side reactions should elucidate the solid-solid interactions and allow for quantification of the intrinsic activity of solid acid catalysts, the development of structure-activity relationships, mechanism elucidation, and rational catalyst design.[60]

The objective of this work was to determine whether solid acid catalysts from various structural classes leach homogeneous acid species that are catalytically active towards cellulose hydrolysis.

In addition, we investigated how leaching of homogeneous acid affects the interpretation of the activity of solid acid catalysts. For these purposes, we selected several solid acid catalysts representative of different structural classes reported in the literature to hydrolyze cellulose. The materials of choice were subjected to the hydrothermal environment used for cellulose hydrolysis to determine whether they leach homogeneous acid. Furthermore, we tested the activity of the leached acid towards cellulose hydrolysis and addressed the implications towards interpreting solid acid catalyst activity. We developed an overall reaction model that includes leaching and proposed criteria for accounting for the effects of homogeneous acid hydrolysis and attributing activity to solid acid catalysts. We used kinetic modeling to predict the activity of homogeneous acid with increasing concentration due to accumulation from continuous solid acid leaching. In addition, we considered the effects of soluble products and catalyst charring on the release of homogeneous acid. Overall, the results presented here argues that the mechanism of cellulose hydrolysis of various solid acid catalysts involves hydrothermal degradation and leaching of homogeneous acid which in turn carries out the deconstruction of cellulose. The approach towards the experimental analysis of the solid acid catalysts used here provides motivation for updating methodologies for solid acid catalyst testing and the development of structure-activity relationships.

4.2. Methodology

4.2.1. Materials

Avicel PH-101 cellulose, Amberlyst-15, H_2SO_4 (98%), 0.1 M HCl, 0.1 M NaOH, cellobiose, glucose, xylose, hydroxymethyl furfural (HMF), levulinic acid, and formic acid were purchased from Sigma-Aldrich. Sulfated Zirconia, Norit, and HZSM-5 (Si/Al=38) were purchase from MEL Chemicals, Cabot Corporation, and ACS Material, respectively. 13C-enriched glucose was purchased from Cambridge Isotope Laboratories Inc.

4.2.2. Catalysts Preparation

4.2.2.1. Sulfonated Humins (SH)

Xylose (20 grams) and 98% H_2SO_4 (7 mL) were mixed with deionized water (17.7 MΩ·cm) to create a 100ml solution of molar ratio of sugar to acid of 1:1. This was then stirred at room temperature for 30 minutes. The resulting solution was then placed 160 mL Teflon vessel, which was deposited into a Teflon-lined aluminum autoclave for 24 hours at 120 °C. The resulting mixture was allowed to cool for 12 hours and then washed with a 300ml equimolar mixture of DI water and ethanol. The solid char phase was separated from the aqueous phase via vacuum filtration and dried for 24 hours at 65 °C.

4.2.2.2. Sulfonated Activated Carbon (SAC)

Norit activated carbon was sulfonated in a similar fashion to a procedure used by Foo et al.[44] Briefly, 10 grams of Norit SX-1 were washed with 500 mL deionized water overnight, after which they were dry at 65 °C. The activated carbon was then mixed with 78 mL deionized water, 54 grams of 98% H_2SO_4 and put in a Teflon-lined aluminum autoclave. The mixture was placed in a preheated oven at 200 °C and allowed to react for 24 hours after which the autoclave was cooled in an ice bath. Following the treatment, the solids were filtered and washed twice with 1800 mL of deionized water for 24 hours. To remove any residual H_2SO_4 after which the solid material was filtered again and dried at 65 °C.

4.2.2.3. Sulfated Zirconia (SZ)

Sulfuric acid doped zirconia oxide (MEL Chemicals Inc) was activated at 550 °C for 16 hours.

4.2.2.4. HZSM-5

HZSM-5 with Si/Al ratio of 38 (ACS Materials) was calcined at 550 °C for 16 hours.

4.2.2.5. CMP-SO_3H-0.3

Bifunctional polymer solid acid bearing chloromethyl and sulfonic acid groups was prepared according to the procedure reported by Tyufekchiev et al. and Zuo et al.[38, 39] For more details refer to the respective references.

4.2.2.6. Vinyl-Sulfonic Acid Glucose Char (VSGC)

Vinyl sulfonic acid glucose char preparation procedure was adopted from Demir-Cakan et al who prepared carboxylate rich glucose char by hydrothermally cocarbonizing glucose and acrylic acid.[62] Specifically, glucose (36 g) and vinyl sulfonic acid sodium salt (3.6 g) were dissolved in 60 mL of water and put in a Teflon-lined aluminum autoclave. The autoclave was placed in a pre-heated oven at 190 °C and the mixture was allowed to react for 21 hours after which the autoclave was cooled for 30 minutes in an ice bath and under running cold water. The resultant solid material was washed with 2L of acetone and 2L of water after which it was dried at 65 °C overnight. To acidify the carbonaceous material, the solids were put in 1M HCl and stirred for 20 hours at room temperature. The material was then washed with 2L of water and filtered and was followed by 500 mL of ethanol washing overnight. Finally, the solids were dry at 65 °C overnight.

4.2.3. Catalyst wash

The catalysts were washed extensively with water to remove any soluble acidic species present on the catalyst. Briefly, 1.5 grams of catalyst was washed with 50 mL of water in a centrifuge tube. The pH of the suspension was measured until the value stopped changing with further wash. After the wash, the catalysts were dried at 65 °C overnight. This treatment eliminated the contribution from any residual homogeneous acid species that were present on the catalyst structures, likely remnants from the catalyst preparation procedure, to the hydrolysis of cellulose.

4.2.4. Solid State Titration

Since solid acid catalysts were exposed to hydrothermal environment that potentially resulted in leaching of soluble acid species, it was necessary to confirm that the acid generated was leached from the solid materials. Therefore, the ion concentration in the liquid medium post reaction had to be compared to the acid site content of the solid catalysts. For this purpose, we employed solid state titration to quantify the acid sites on the solid materials. Solid state titration of the catalysts was carried out according to the Boehm's procedure.[63] Briefly, predetermined amounts of 0.1M NaOH standard solution and solid acid catalyst were mixed. The mixture was shaken and allowed to ion exchange for 24 hours. After that an aliquot was taken and acidified with a predetermined volume of 0.1M HCl. The acidified solution was then titrated with 0.05 NaOH, while the pH was monitored with a digital pH meter (Denver Instruments, model 225). The amount of acid sites in the solid catalyst was then calculated.

4.2.5. Hydrothermal Degradation and Homogeneous Acid Leaching

To determine whether the solid acid catalysts are stable in the hydrothermal environment used for cellulose hydrolysis and whether they are leaching homogeneous acid, the catalyst were treated at the same reaction conditions used for cellulose hydrolysis, but in the absent of cellulose substrate. Briefly, solid acid catalyst (0.2 grams) were mixed with water (2 mL) and were treated in hydrothermal conditions at 150 °C for 15 hours (10 hours for Amberlyst-15, Sulfated Zirconia and CMP-SO_3H-0.3). After the reaction, the pH of the liquid was measured; the liquid and the solid were centrifuged and the liquid was extracted with a syringe. The liquid was then analyzed with Ion Chromatography (IC) to characterize the leached species and stored for cellulose hydrolysis tests.

4.2.6. Cellulose Hydrolysis

Cellulose was hydrolyzed to determine the activity of the solid acid catalyst and the leached homogeneous acid. Solid acid catalyst (0.2 grams) was mixed with cellulose (0.1 grams) and water (2 mL) in a 15 mL glass reactor vial and sealed with a Teflon cap and Viton O-ring. The reactor vial was submerged in an oil bath and reacted at 150 °C for 15 hours (10 hours for CMP-SO_3H-0.3, Amberlyst-15 and Sulfated Zirconia). After the reaction the vial was centrifuged, and the liquid was extracted with as syringe. The soluble products of the hydrolysis were analyzed with HPLC.

In a similar fashion the activity of the leached homogeneous acid was determined by mixing 2 mL of the liquid from hydrothermally treated solid catalyst with cellulose (0.1 grams) and reacted at the same conditions as above. The soluble products were quantified with High Performance Liquid Chromatography (HPLC).

4.2.7. Hydrolysate Analysis

The activity of the solid acid catalysts and the leached liquid acid species was inferred from the analysis of the hydrolysate solutions post hydrolysis reaction. Products of cellulose hydrolysis were analyzed and quantified with high performance liquid chromatography (HPLC). Agilent 1200 Series equipped with a refractive index detector (RID) and a diode array detector (DAD) for quantifying carbohydrates and furanic compounds. Rezex ROA-Organic acid column (Phenomenex) maintained at 35 °C was used for separation and the mobile phase was deionized water at 0.6 mL/min. The RID detector operated at 35 °C and the DAD UV-Vis detection wavelength was set to 284 nm. Calibration curves for cellobiose, glucose, HMF, levulinic acid, and formic acid were prepared by analyzing standardized solutions at 0.25, 0.5, 0.75, 1, 1.25, 1.5, 1.75, 2, and 2.5 g /L.

Product yields were calculated based on the formula: $\frac{m_p * M_{gu}}{m_c * M_p} * 100\%$, where m_c is mass of cellulose, m_p is mass of the soluble product in the solution determined by HPLC, M_{gu} is molecular weight of glucose unit in cellulose, and M_p is molecular weight of the soluble products. Calculation of the yields of hydroxymethyl furfural, levulinic acid, and formic acid were carried out in a similar fashion. Soluble carbon balance was calculated by the following formula: $\frac{\sum_i^n C_i}{C_c} * 100\%$, where C_i is the amount of carbon atoms expressed in moles present in product i and C_c is the amount of carbon expressed in moles present in cellulose.

4.2.8. Ion Analysis

Quantification of the ionic species in the liquid medium post hydrothermal stability tests of the solid acid catalysts was necessary to characterize the nature of the leached acids. For this purpose, the anions present in the leachates analyzed with ion chromatography with Dionex ICS-2100 Ion Chromatographer equipped with AERS 500 anion electrolytically regenerated suppressor and DS6 heated conductivity cell. Anions were separated with AS153 250 mm column equipped with IonPac AG 2x50 mm guard. The mobile phase was 38.00 mM KOH at 0.25 ml/min. Separation was carried at column temperature of 30 °C and detection at cell temperature of 35 °C.

To confirm that the anions were balanced by an acidic hydronium ion, the pH of the leachates was measured by a pH meter (Denver Instruments, model 225) equipped with a glass, Ag/AgCl reference, 0-14 pH probe (Symphony pH Probes), calibrated with buffers of pH of 4 and 7.

4.2.9. Kinetic Modeling of Cellulose Hydrolysis by a Homogeneous Acid

In a typical cellulose hydrolysis tests using solid acid catalysts carried out in batch reactors, the leaching of homogeneous acid will contribute to the observed hydrolysis. We hypothesized that if the effects of the homogeneous acid are quantified and subtracted, it would potentially reveal if there is contribution to the observed cellulose hydrolysis due to solid-solid interactions between

the solid acid catalyst and the cellulose substrate. For this purpose, we modeled cellulose hydrolysis by a homogeneous acid.

Hydrolysis of solid cellulose substrates catalyzed by a liquid acid is a complex heterogeneous process that depends on the structural characteristics of cellulose in addition to temperature, acid concentration, and time. Saeman, however, found that acid catalyzed hydrolysis of wood cellulose substrates obeys first order kinetics within a particle size range between 75 μm and 850 μm and can be treated as a homogeneous reaction.[64] As a result, cellulose hydrolysis has been widely modeled by the pseudo first order approximation, despite additional models that include structural characteristics such as degree of polymerization or account for the heterogeneity of the reaction by modeling it as a shrinking-core process.[65-67] The cellulose average particle size in the current study was 100 μm, which is within the range studied by Saeman. Therefore, we reasoned that to model cellulose hydrolysis by homogeneous acid with the pseudo first order kinetics would be an adequate approximation.

We reviewed the literature was to identify kinetic studies that have investigated hydrolysis conditions similar to the conditions in this work such as acid concentration and temperature and select relevant kinetic parameters.[24, 64, 68] Several kinetic models exist and can be distinguished based on the conditions and substrates studied. Table 4.1. shows the kinetic parameters of selected studies treating cellulose hydrolysis as a pseudo first order reaction. In addition, the pseudo first order kinetic models accounted for the acid concentration with a pre-exponential term in the expression for the kinetic rate constant; the general expression for the kinetic rate constant is a modified Arrhenius equation $k = A * [H^+]^n * \exp\left(\frac{-E_a}{R*T}\right)$. However, the power functionality of the acid concentration term varies widely depending on the conditions each specific kinetic model

explored as is shown in Table 4.1. For our purposes, it was necessary to select a kinetic model which was developed within the temperature and acid concentration range studied in this work.

Table 4.4. Substrates, reaction conditions, and kinetic parameters of pseudo first order models for cellulose hydrolysis to glucose.

Substrate	Reaction conditions	A (min^{-1})	E_a (kJ/mol)	n	Ref.
Douglas fir	Acid: 0.4-1.6 wt% Temp: 170-190 °C	$1.73x10^{19}$	179.5	1.34	64
Microcrystalline cellulose	Acid: 30-70 wt% Temp: 25-40 °C	$2.946x10^{10}$	127.2	6.0	69
Paper refuse	Acid: 0.2-1.0 wt% Temp:180-240 °C	$28x10^{19}$	188.7	1.78	70
Filter paper	Acid: 0.4-1.5 wt% Temp: 200-240 °C	$1.22x10^{19}$	178.9	1.16	71
Microcrystalline cellulose	Acid: 0.05-1 M Temp: 175 °C	N.A.	151.5	0.96	72

It can be seen from Table 4.1. that all reference models are outside the temperature range used in this work (150 °C). The model closest to the conditions encountered here was Saeman's model. In his study Saeman used sulfuric acid of concentration between 0.4 and 1.6 wt %, corresponding to a molarity of 0.04 and 0.16 M, which is within the range of the homogeneous acid concentrations observed here. With respect to the substrate, in our study we used Avicel PH-101 microcrystalline cellulose. While Table 4.1. entries 2 and 5 have also employed microcrystalline cellulose, the conditions they used exceed those used here. Further, the microcrystalline cellulose used in entry 5 by Girisuta et al had average particle size of 20 μm, far below the particle size of 100 μm used here.[72] Additionally, Avicel PH-101 is microcrystalline cellulose derived from wood sources, which instills confidence that it can be approximated to the Douglas fir woody substrate used by

Saeman.[64] Additionally, Saeman's approach utilized glass batch reactors similar to the reactors used in this work.[64]

For those reasons, the kinetic models proposed by Saeman[64] was selected as the conditions used in developing Saeman's cellulose hydrolysis pseudo first order kinetic model were in closest agreement with the current study. This instilled confidence that modeling the cellulose hydrolysis of homogeneous acid release by a solid acid catalyst would be best approximated by Saeman's model. Therefore, cellulose hydrolysis reaction in a batch reactor is modeled by a first order reaction equation: $\frac{d[C]}{dt} = -k * [C]$, where the expression for the reaction rate constant and its dependence on acid concentration is defined by $k = A * [H^+]^n * \exp\left(\frac{-E_a}{2.303*R*T}\right)$.[64] The value of 2.303 encountered in the exponential is resultant from Saeman's mathematical treatment where the base of 10 was used for logarithmic plotting and calculations.[64] The values of the kinetic parameters are shown in Table 4.1. entry 1 and are as follows: A=1.73_x10^{19} min/$M^{1.34}$, n=1.34, and *Ea*=179.5 kJ/mol.[64] Specific focus of the model was quantifying cellulose conversion and comparing it to the soluble carbon balance obtained from experiments.

The time dependence of the concentration of the homogeneous acid was accounted for by doing a kinetic study of the leaching of solid acid catalysts. For that purpose, solid acid catalysts were treated in the hydrothermal environment used for cellulose hydrolysis for varying time up to 10 hours and the pH was measured as already described in section 2.5. The acid concentration data was then fitted to first order kinetics by treating the final acid concentration at 10 hours as 100% conversion of hydrothermally unstable groups in the solid acid catalyst structure. To calculate the average kinetic rate of leaching the first order kinetic expression $\ln\left(\frac{[H^+]_f - [H^+]}{[H^+]_f}\right)$ was plotted versus reaction time and the slope, representative of the average leaching constant, was obtained. The

time functionality expression of the acid concentration was then used in the equations for the kinetic rate constants replacing the acid concentration term. The reaction temperature in the vial was accurately measured with modified screw top cap equipped with an Omega K-type thermocouple and it was measured to vary between 150 °C and 155 °C.

Modelling the cellulose hydrolysis kinetics was carried out in MATLAB. The script is provided in Appendix B. The variation in temperature and the deviation for the concentration of homogeneous acid were simulated by using a *rand* function that generates a matrix with specified dimensions and filled with random numbers between 0 and 1. The model calculated a random temperature within the temperature range and homogeneous acid leaching constant which later used to solve the differential equation. In order to simulate the uncertainty of the conditions and the resultant cellulose conversion the system was solved for with 25 different randomly generated temperatures (within the measured temperature range) and 25 randomly generated kinetic constants describing acid leaching (calculated within the standard deviation determined from the leaching analysis) for a total of 625 conditions. Cellulose conversion was calculated for each condition; following the 625 iterations, the cellulose conversion was averaged, and standard deviation was calculated. For comparison, a kinetic study of cellulose hydrolysis using selected solid acid catalysts was carried out. The quantification of soluble products and soluble carbon balance was as described in section 2.7.

4.2.10. Solid-state Nuclear Magnetic Resonance (ss-NMR)

To determine whether the solid acid catalysts interact with the soluble products from cellulose hydrolysis we performed solid-state nuclear magnetic resonance analysis of CMP-SO_3H-0.3 catalyst after reaction with ^{13}C-enriched glucose. Experiments were performed on a Bruker Avance 400 spectrometer at a 100 MHz ^{13}C resonance frequency with high-power ^{1}H decoupling, with

magic-angle spinning (MAS) of 4-mm zirconia rotors in a double-resonance probe head at ambient temperature. ^{13}C chemical shifts were calibrated to TMS, using 1-13C-α-glycine at 176.49 ppm as secondary reference. All the samples were packed as received. Composite-pulse multiCP pulse sequence[73] was used at 14 kHz MAS to obtain quantitative ^{13}C NMR spectra, with a 4-s recycle delay, ten 1.1-ms cross polarization periods and a final 0.55-ms CP time, each separated by a ^{1}H repolarization time of 1.5 s. Corresponding spectra of nonprotonated C and mobile segments were obtained after 68 μs recoupled ^{1}H-^{13}C dipolar dephasing before detection[74]. To detect the connectivities between protonated and nonprotonated carbons in coked CMP-SO_3H-0.3, two-dimensional exchange with protonated and nonprotonated spectral editing (EXPANSE) NMR spectra[75] were recorded with a mixing time of 10 ms. Since small residual diagonal peaks of arenes do not interfere with detection of most of the cross peaks, the dipolar dephasing difference was not recorded, which maximized the signal-to-noise ratio. Standard 4.2-μs ^{1}H and ^{13}C 90º pulses were used in the experiments described above.

4.3. Results and Discussion

4.3.1. Catalyst Selection

The field of solid acid catalyzed cellulose hydrolysis abounds with various catalytic structures ranging from organic polymers, inorganic metal oxides and heteropolyacids, functionalized magnetic particles, and carbonaceous materials.[34, 35, 50, 56, 76, 77] Despite various success in depolymerizing cellulose, there is still little direct evidence of the mechanism of catalysis of those catalysts. Some studies have considered the hydrothermal stability of solid catalysts, but the leaching of homogeneous acid and its effects on the observed cellulose hydrolysis have not been investigated.[50, 59, 78, 79] It is practically prohibitive to test every single catalyst that has been

proposed for cellulose hydrolysis. Accordingly, we focused on catalysts that are representative of the various structural classes.

CMP-SO_3H-0.3 and Amberlyst-15 are polystyrene based catalyst, bearing benzyl chloride, benzyl alcohol, and benzyl sulfonic acid groups or sulfonic acid groups directly attached to an aromatic ring, respectively.[38, 80] In addition, CMP-SO_3H-0.3 is an example of a specific group of chlorinated bifunctional solid catalyst, where chloromethyl groups and hydroxyl groups could potentially participate in binding interactions with cellulose.[39] Amberlyst-15 has been used as a model sulfonated polymer catalyst for cellulose hydrolysis with high acid site content, meant to be compared to other catalysts with fewer acid sites, but with other structural characteristics hypothesized to affect cellulose depolymerization in a beneficial way.[43, 50, 81]

The sulfonated activated carbon (SAC) and the sulfonated humins (SH) represent the class of sulfonated carbonaceous catalysts.[35, 48, 55, 77, 82] In this group, materials can be prepared in two main ways: 1) sulfonation of highly graphitic carbon structures,[77, 83, 84] or 2) hydrothermal or pyrolysis carbonization of carbon feedstocks (typically biomass) and *in-situ* or post synthesis sulfonation.[46, 76, 85, 86] Carbonaceous materials possess structurally rich functionalities which are implicated in interpreting the cellulose hydrolysis mechanism.[46, 77, 87] To simulate the former sub-class we prepared SAC and for the latter we used SH. Considering that the sulfonated carbonaceous catalysts represent probably the largest structural class of materials applied for cellulose hydrolysis, it was important to investigate the effects of leaching of homogeneous acid and the implications on the interpretation of the activity of those materials.

Similarly to the carbonaceous catalysts, the class of inorganic materials applied for cellulose hydrolysis abound with various catalytic structures. Sulfated Zirconia (SZ) was used as a representative of acidic metal oxide catalyst. It has been applied for cellulose depolymerization as

well as conversion of glucose to hydroxymethyl furfural.[50, 88-90] While it was found that SZ leaches sulfate ions in the hydrothermal environment, their effect on the cellulose hydrolysis and interpretation of catalyst activity was not elucidated.[91] As such, SZ represents a hydrothermally unstable catalyst capable of hydrolyzing cellulose, but whose activity has not been unambiguously attributed to the solid acid species.

We also investigated hydrothermally stable solid acid catalysts and interpret their activity. For this purpose, we selected zeolite HZSM-5 which has been established to be stable in liquid water at conditions of up to 300 °C and which has been previously applied for cellulose hydrolysis.[34, 35, 92] On the other hand, we sought to synthesize a hydrothermally stable sulfonated amorphous carbonaceous material. Anderson et al. showed that alkyl sulfonic acids are hydrothermally stable at temperatures of up to 160 °C.[78] To synthesize such a material bearing stable sulfonic acid groups we co-carbonized glucose with vinyl sulfonic acid sodium salt with a procedure similar to the one reported by Demir-Cakan for preparing carboxylate rich carbonaceous materials.[62] We hypothesized that the vinyl-sulfonic acid sodium salt would result in the formation of alkyl sulfonic acid groups in the carbonaceous catalyst. The imparted hydrothermal stability of a sulfonated carbonaceous material will eliminate contributions from leached homogeneous acid. This will elucidate if there indeed are interactions between cellulose and the carbonaceous material as inferred from structural studies and adsorption of soluble cellulosic molecules.[44, 93]

While the list of catalysts tested is not exhaustive, we sought to use these materials as examples of catalysts applied for cellulose hydrolysis. Furthermore, the catalysts were investigated with the purpose to develop an experimental methodology for future testing of proposed structures and for the development of criteria for interpreting the solid-solid interactions between catalysts and

cellulose substrates.[60] Simplified representation of the catalytic structure is provide in Scheme 4.1. as a visual guide.

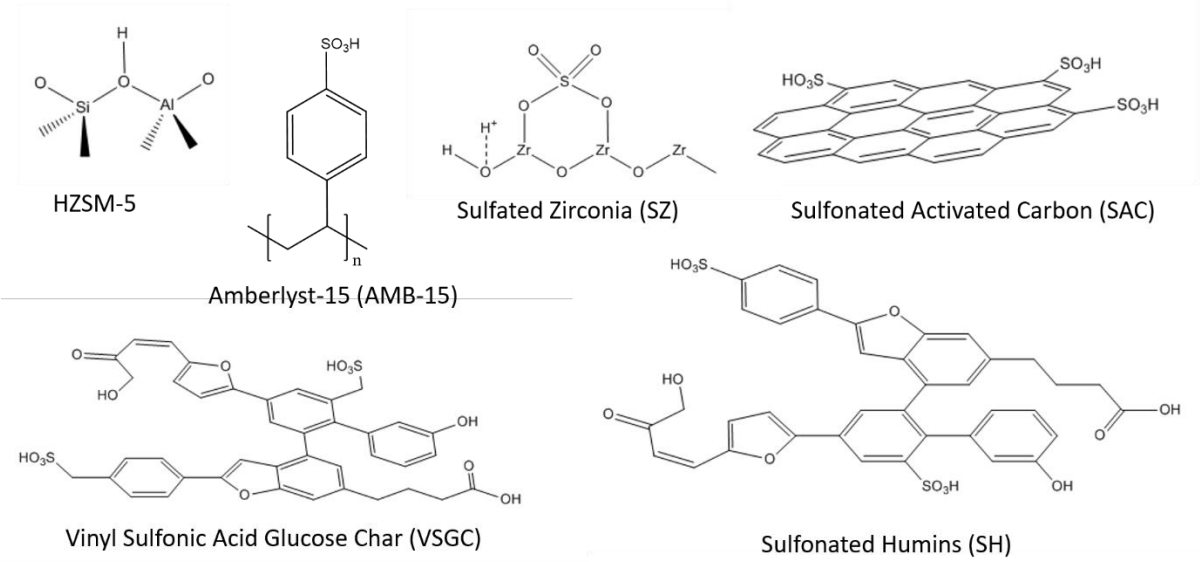

Scheme 4.9. Simplified structures of the solid acid catalysts used in the current study. The structures of SAC, VSGC, and SH are highly exaggerated due to the difficulties of accurate characterization of carbonaceous materials and their structure is provided only as a visual guide.

4.3.2. Apparent Catalyst Activity and Leaching of Homogeneous Acid

Prior to attributing the observed cellulose hydrolysis results to the activity of solid acid catalysts towards solid cellulose substrates, we sought to answer a simple question: do catalysts leach homogeneous acid that is active towards cellulose hydrolysis. Considering that in a typical catalytic activity test, where a reaction mixture consists of solid acid catalyst, solid cellulose, and the water medium and that the reaction is carried out in batch reactors,[36, 39, 43, 46] homogenous acid leaching and cellulose hydrolysis, catalyzed by both solid acid catalyst and the leached homogenous acid, will occur simultaneously.[38] In order to test the activity of the leached homogenous acid, the solid acid catalyst and the homogenous acid should be separated to properly assign the activity to the respective species.

Accordingly, we devised a set of experiments addressing those considerations as shown in Scheme 4.2. First, the solid acid catalysts were used to hydrolyze cellulose at 150 °C for 15 hours (10 hours in the case of AMB-15, CMP-SO_3H-0.3, and SZ) in water. Quantification and characterization of the products provides information about the apparent activity of the solid acid catalysts. In a separate set of experiments the fresh catalysts were treated at the same hydrothermal conditions (temperature, time, water content), but in the absence of cellulose, to determine whether the solid acid catalysts generate liquid acid species. After the treatment, the liquid and the solid were separated via centrifugation and filtering; the liquid was used to hydrolyze cellulose at the same reaction conditions that were used for the solid acid catalysts. This set of experiments reveals if catalytically active acid is generated by the solid catalyst at the hydrothermal conditions used for cellulose hydrolysis. The liquid from the hydrothermally treated solid acid catalysts will be referred to as leachate henceforth.

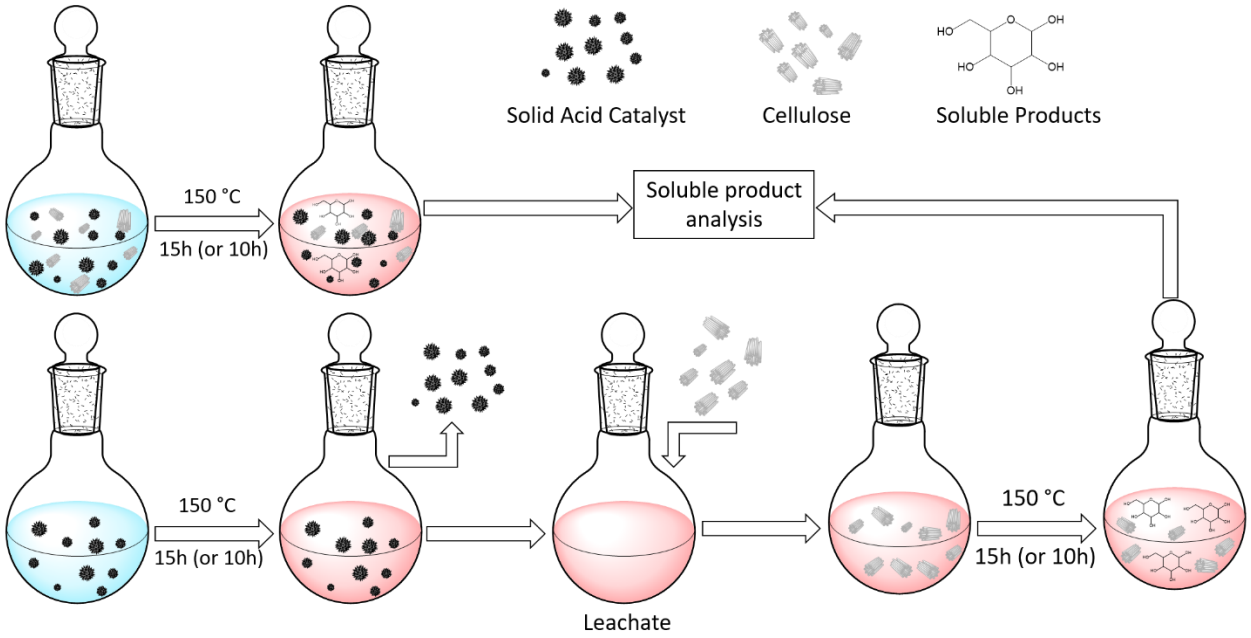

Scheme 4.10. Experimental approach for analyzing solid acid catalyst leaching and cellulose hydrolysis activity. Red color of the liquid indicates elevated acid concentration due to leaching.

The soluble products from hydrolysis were quantified as an indication of the activity of solid acid catalysts and their leachates and the extent of cellulose hydrolysis. The detailed distribution of the soluble products is presented in Table B1. The distribution of soluble products is not directly indicative of the solid-solid interactions between solid catalyst and cellulose since the soluble products can undergo additional reactions; therefore, the best measure for this should be cellulose conversion. However, quantifying cellulose conversion is challenging – solid catalyst-cellulose separation is unpractical and catalyst degradation and cellulose darkening during drying even at low temperature such as 65 °C, indicative of degradation and mass loss, prevent accurate quantification. Instead, we used the total soluble carbon balance (the ratio of the carbon contained in the soluble products over the carbon content in cellulose) as an indication of the conversion of cellulose. The low apparent activity of the solid acid catalysts and the relatively low temperature prevented the formation of solid char residue, allowing for the use of this approach.[25] Figure 4.1. plots the soluble carbon balance obtained from hydrolysis with fresh solid catalysts and with their leachates. The extent to which water hydrolyzes cellulose and generates soluble products is indicated by a line and is used as a baseline for comparing and determining catalyst activity.

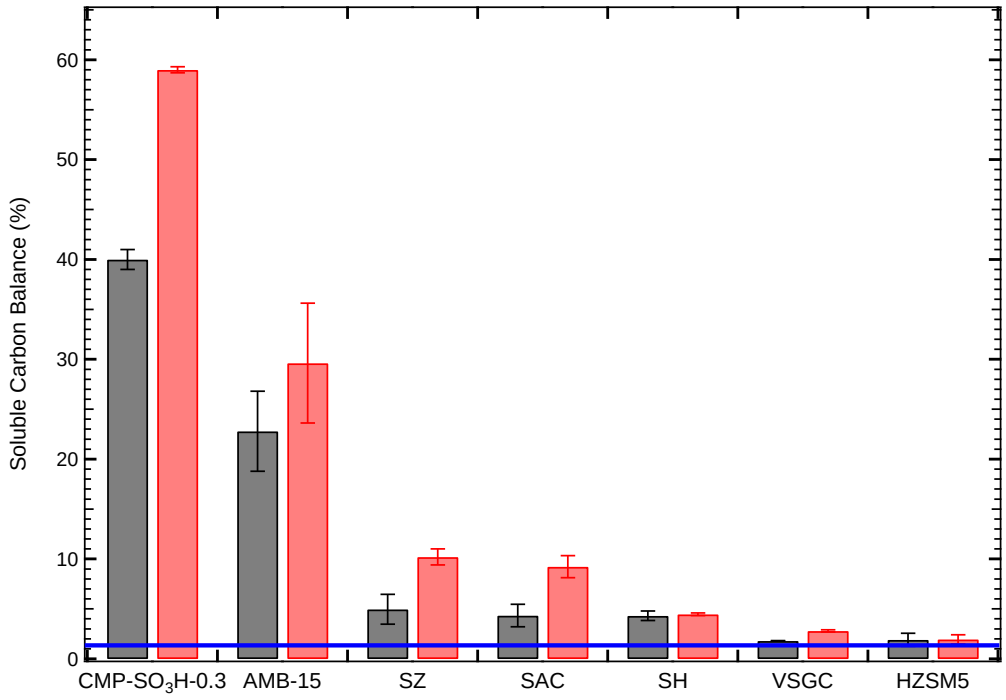

Figure 4.14. Comparison of the soluble carbon balance of cellulose hydrolysis with fresh solid acid catalyst (grey bars) and homogeneous acid leachate (red bars). The blue line represents the cellulose hydrolysis activity of water.

Figure 4.1. reveals that every catalyst resulted in cellulose hydrolysis and release of soluble products. It is also evident that the leachate, too, can hydrolyze cellulose, resulting in release of soluble products. It should be noted that water at those conditions is also capable of hydrolyzing cellulose that results in release of soluble products. Furthermore, cellulose hydrolysis catalyzed by the leachate results in equal or greater conversion and yields of soluble products than when the fresh solid acid catalyst is used at the same conditions. Regardless of the catalytic structure, the fresh solid acid catalysts leach catalytically active homogeneous acid in hydrothermal conditions; therefore, its observed activity towards cellulose hydrolysis in batch system is a combination of its intrinsic activity and the activity of the homogeneous acid. The only exception appears to be VSGC and HZSM-5 whose activities (both the solid acid catalyst and its leachate) do not differ

significantly from that of water. This observation suggests that the catalyst is hydrothermally stable which is consistent with literature reports of the stability of HZSM-5 and the hypothesized stability of alkyl sulfonic acids.[78, 92] Furthermore, it appears that there are no interactions between those catalysts and solid cellulose as the release of soluble products of hydrolysis products greater than water.

The cellulose hydrolysis results obtained by the leachates of the solid acid catalysts indicate presence of homogeneous acid. To understand the nature of the acid species and its propensity to hydrolyze cellulose, we measured the pH and used ionic chromatography to characterize and quantify the ion content in the leachate. Based on the chemical structure of the solid acid catalysts we focused on three main ions – chloride, hydrogen sulfate, and hydronium ions. Figure 4.2. a) shows the changes of the pH of the liquid after hydrothermal treatment of solid acid catalysts in the absence of cellulose. Prior to treatment, the pH of the suspension of solid catalysts is greater than 3 for each catalyst. However, after exposure to the hydrothermal conditions at which hydrolysis takes place (150° C, 10 or 15 hours) the pH of the suspension decreases significantly for every catalyst.

Figure 4.2. b) plots the ion concentrations in the leachate of each catalyst. CMP-SO_3H-0.3 releases mainly chloride ions, whose concentration is parallel to the concentration of the hydronium ion, consistent with hydrolysis of the chloromethyl group and relative stability of the sulfonic acid attached to a benzylic carbon atom.[38, 78] The rest of the catalysts release mainly hydrogen sulfate ions resultant from degradation of the sulfonic acid groups in AMB-15, SAC, and SH and the sulfate ions from SZ. We were not able to identify the anionic species leached from HZSM-5; literature reports suggest it could be formation of Al_3^+ species.[61] VSGC is also

relatively stable as the H^+ concentration in the leachate is the same as that of HZSM-5 and very little sulfates have leached.

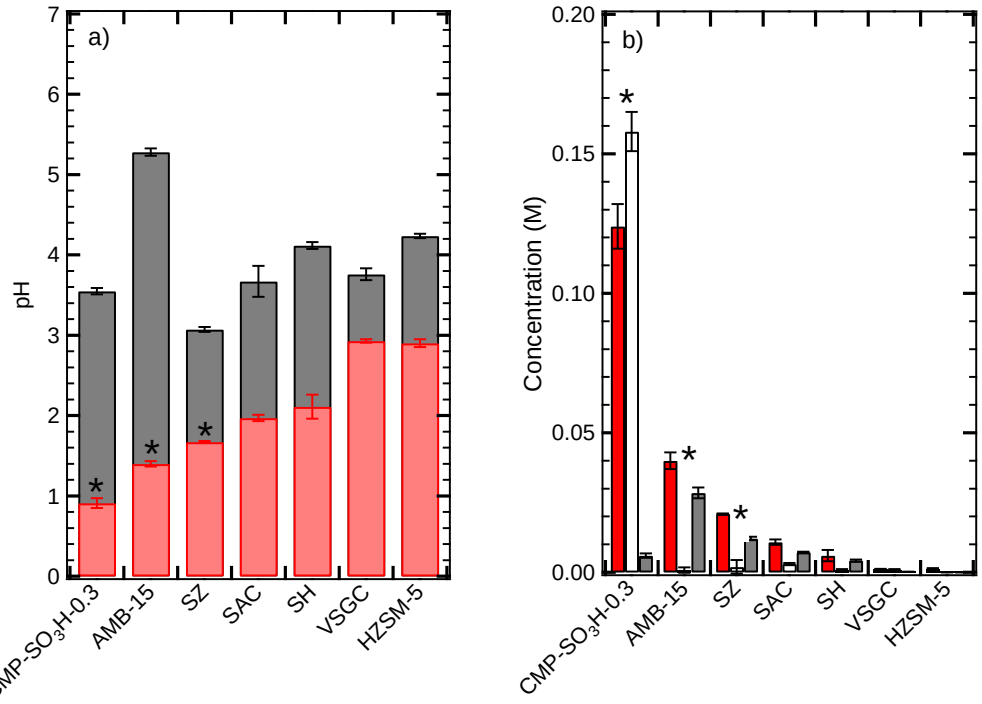

Figure 4.15. Hydrothermal stability of catalysts and leached acid characterization. In a), grey bars indicate pH of catalyst suspension on water after wash and red pH after treatment in hydrothermal conditions (0.2 g catalyst, 2 mL water, 150 °C, 15 h.). In b), red bars represent H^+, white – Cl^-, and grey – HSO_4^- ions. Asterisk indicates time of hydrothermal treatment was 10 h. for those catalyst.

The ion analysis indicates that the leachates consist of either hydrochloric acid (in the case of CMP-SO_3H-0.3) or sulfuric acid. These observations imply that: 1) the leaching is due to hydrolysis and loss of acid sites, rather than ion exchange mechanism and 2) interpretation of the apparent activity of solid acid catalysts towards cellulose hydrolysis cannot be directly attributed to the solid-solid interactions. The former could explain the observations of decreased activity towards cellulose hydrolysis after catalyst reuse as fewer acid sites are left on the catalyst that can participate in hydrolysis reaction or leach to form homogeneous acid.[43] Titration of the solid acid

catalysts before and after hydrothermal treatment confirmed the acid site loss. More details of the solid-state titration could be found in Figure B1 in Appendix B.

Sulfonic acid is widely used as a catalytic group;[35, 46, 54] however, the carbon sulfur bond is rather unstable in hydrothermal conditions, with alkyl sulfonic acids being more stable than aromatic ones.[59, 94] This suggests that the activity of sulfonated catalysts has been inappropriately attributed solely to the solid catalyst, while the contribution of the leached homogenous acid has not been investigated. Similarly, a chloride group in the catalytic structure, often used as a potential binding group, also degrades in the severe environment used for cellulose hydrolysis.[38, 42, 47] The observations of solid acid catalyst degradation and leaching in the hydrothermal environment made in the current study point to a necessary consideration of hydrothermal stability for solid acid catalyst design.[60] Specifically, the sulfonic acid widely used as a catalytic group is not stable. This has implications not only for interpretation of the solid acid catalyst activity, but also for the recyclability of solid acid catalyst applied hydrothermal conditions.

Considering that the solid acid catalysts, representative of the catalytic structures used in literature, degrade in the hydrothermal environment and leach homogeneous acid that is active at hydrolyzing cellulose, correlating the structural characteristics of the solid acid catalysts and the apparent activity is not indicative of the solid-solid interactions between the catalyst and the solid cellulose substrate. For example, a common literature approach is to correlate the apparent activity of the solid acid catalyst to a structural parameter such as number of acid sites or presence of binding groups.[36, 39, 40, 43, 45, 95] In a similar fashion, we calculated the apparent first order kinetic rate constant (k_{cat}) of solid acid catalyzed cellulose hydrolysis using the soluble carbon balance and related it to the initial number of acid sites measured by solid state titration. The data, plotted in Figure 4.3. a), reveals a weak correlation between the two. Conversely, correlating to the

concentration of the leached homogeneous acid, as shown in Figure 4.3. b), reveals a direct proportionality. Consequently, this analysis suggest that apparent activity is a result of the propensity of the catalysts to leach, preventing interpretation of the solid-solid interactions and development of structure-activity relationships.

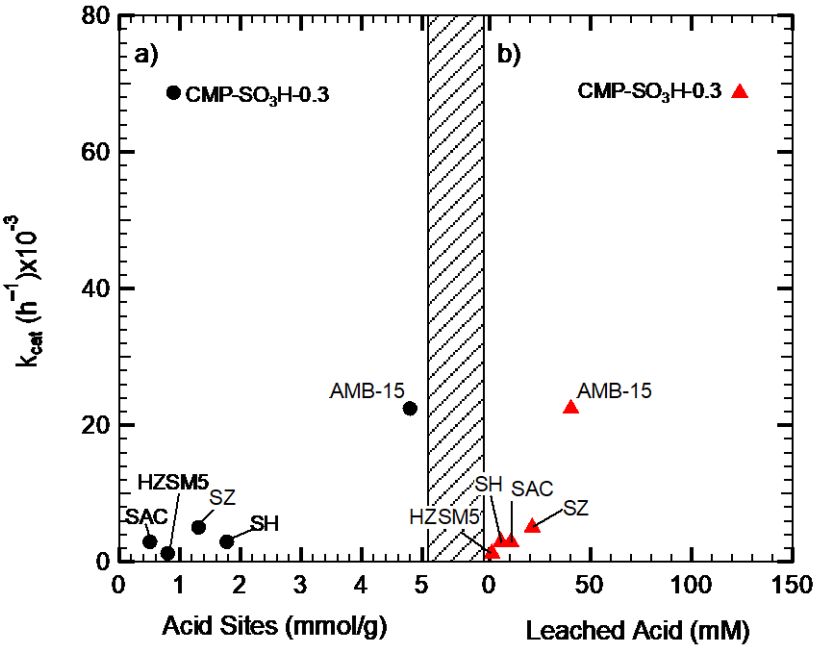

Figure 4.16. Correlation between apparent rate constant of cellulose hydrolysis using fresh solid acid catalyst and amount of acid sites in a) and concentration of leached homogeneous acid in b). The data points for VSGC and HZSM-5 overlap in this figure.

Therefore, accounting for the catalyst degradation, the leaching of homogeneous acid, and cellulose hydrolysis catalyzed by the homogeneous acid should allow for estimating the intrinsic activity of the solid acid catalyst and characterizing the solid-solid interactions. As already stated, the apparent cellulose hydrolysis activity of the solid acid catalysts in a batch system is a combination of the solid and homogeneous catalysts. Conversely, cellulose hydrolysis by the leachate is a result of the homogeneous acid alone. Interestingly, the apparent activity when the

solid acid catalysts were used, quantified by the soluble carbon after cellulose hydrolysis, was consistently lower than the activity of the leachates as shown on Figure 4.1. We hypothesized that due to additive effects cellulose hydrolysis by solid and homogeneous acid would result in greater activity compared to the leachate which would be representative of the activity of the homogenous acid alone. To investigate further we treated AMB-15 at the hydrothermal environment for intermediate periods of time and monitored the pH and quantified the concentration of the homogeneous acid. Figure 4.4. reveals that the concentration increases over the period of 6 hours after which it appears to level off. This indicates that the solid acid catalyst is continuously releasing homogeneous acid which builds up in the batch reactor.

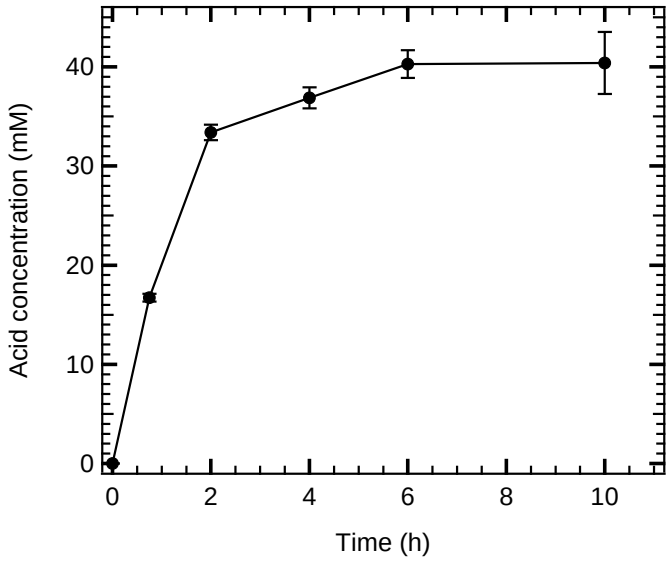

Figure 4.17. Concentration of the leached homogeneous acid for AMB-15 as a function of treatment time at 150 °C.

Therefore, the contribution of the homogeneous acid to cellulose hydrolysis varies with time, increasing as the concentration increases. Conversely, the leachate used for hydrolysis of cellulose was obtained after 10 hours (or 15 hours in the case of SAC, SH, HZSM-5) and its concentration is constant throughout the catalytic test and is greater than the concentration of the homogeneous

acid released during hydrothermal degradation of the solid acid catalyst. This explains the observed greater cellulose hydrolysis activity of the leachate. Therefore, a more detailed mechanistic analysis is necessary to unravel the underlying reactions and extract information on the solid-solid interactions. Specifically, the contribution of the homogeneous acid to the observed cellulose hydrolysis must consider the time dependence of the concentration.

4.3.3. Criteria for Activity Assessment and Kinetic Modeling

So far, we established that solid acid catalysts with different chemical structures decompose in hydrothermal environment and release homogeneous acid that hydrolyzes cellulose. However, the effects of those two reactions obscure any possible interactions between the cellulose and the solid acid catalyst. The question arises – how can the activity of the solid acid catalyst be determined in the presence of leaching?

Based on the observations made here an overall mechanism of cellulose hydrolysis using solid acid catalysts can be described. In a typical batch reactor cellulose is mixed with water and the solid catalyst; following the reaction the conversion and soluble products are quantified and the observed activity is attributed to the solid acid catalyst. However, as already elucidated this process involves additional reactions. The underlying reactions that occur are summarized in Scheme 4.3. The apparent activity constitutes of solid acid catalyst leaching (R_1), homogeneous acid catalyzed cellulose hydrolysis (R_2), hydrolysis of cellulose due to water (R_3), and, potentially, cellulose hydrolysis catalyzed by the solid acid catalyst (R_4). Since the focus is on the elucidating the interactions between the solid catalyst and solid cellulose substrate, the reactions involving the soluble hydrolysis products, such as glucose and HMF decomposition, are not considered in this model. Development of catalytic structures and structure-activity relationships is dependent on

observations attributed to R_4. Therefore, in order to assign conversion and soluble product yields to hydrolysis of cellulose catalyzed by the solid acid catalyst certain criteria should be met.

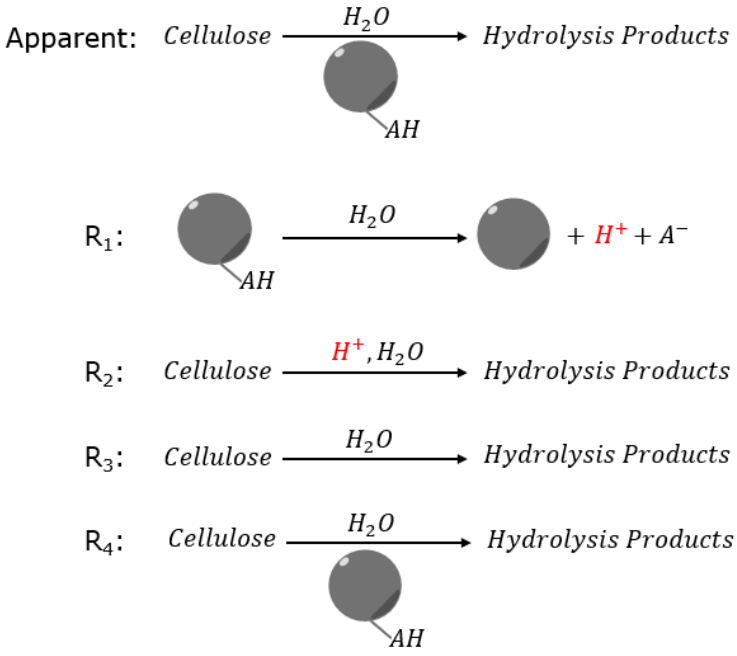

Scheme 4.11. Reaction network for cellulose hydrolysis using solid acid catalysts.

In the simplest case, unambiguous assessment of the intrinsic activity of the solid acid catalyst could be made if R_1 and R_2 are zero or have negligible contribution to cellulose hydrolysis. This implies that the catalyst is hydrothermally stable and does not leach homogenous acid that could hydrolyze cellulose. Therefore, interpretation of solid acid and solid cellulose interactions (R_4) could be made only if the apparent overall activity is greater than the activity of water at the same conditions (R_3). Then by subtraction the solid acid catalyzed cellulose hydrolysis could be estimated and structure-activity relationships and reaction mechanism could be studied. On the other hand, if R_3 accounts for all of the apparent hydrolysis, there are likely no solid-solid interactions capable of hydrolyzing cellulose. In the current study, the closest example to a hydrothermally stable solid acid catalysts are HZSM-5 and VSGC, which do not result in

significant acid leaching as evident from Figure 4.1. and Figure 4.2. However, their activity towards cellulose hydrolysis is almost indistinguishable from that of water at the same conditions, indicating lack of solid acid catalyzed cellulose hydrolysis.

The second case for interpreting the intrinsic activity of the solid acid catalyst is when leaching is present, i.e. $R_1>0$. Further, the leached acid would be catalytically active, therefore, $R_2>0$. In this case, cellulose hydrolysis would be a result of R_2 and potentially R_4. Practically, distinguishing contributions from R_2 and R_4 cannot be made as it cannot be determined whether conversion was due to or a product formed was from R_2 or R_4. Indirectly, the contribution of R_4 can be estimated by carrying out the catalyst leaching, and the cellulose hydrolysis analysis presented in this study. Specifically, the data of the leachate and the solid acid catalysts can be utilized. This facile approach could serve as a rapid screening for solid acid catalyst and improving the interpretation of the apparent catalytic activity.

To determine if R_4 is indeed occurring when $R_1>0$ we devised criteria by comparing the activities of the leachate and the apparent activity of a fresh solid acid catalyst. The initial rate of cellulose hydrolysis using the leachate is a result of the intrinsic activity of the homogeneous acid at constant concentration and the specified temperature. On the other hand, the initial rate calculated when a fresh solid acid catalyst is used the observed initial rate of cellulose hydrolysis would have contributions from the continuously leaching homogeneous acid and potentially from the intrinsic activity of the solid acid. Furthermore, the concentration of the acid in the leachate is greater than the concentration of the homogeneous acid continuously leached by the solid catalyst. Accordingly, the leachate would hydrolyze cellulose to a greater extent as the activity of homogeneous acid is directly proportional to its concentration.[24] Therefore, if the apparent initial rate is greater than the initial rate of the leachate, then at those conditions the solid acid catalyst

would have definite contribution to the hydrolysis. This interpretation would be valid only if the concentration of the homogeneous acid of the leachate at the selected conditions is greater than or equal to the concentration of the continuously leaching acid when a fresh solid acid catalyst is used. This requirement ensures that the activity could be properly assigned to the combinatorial effects of the solid and homogeneous acids.

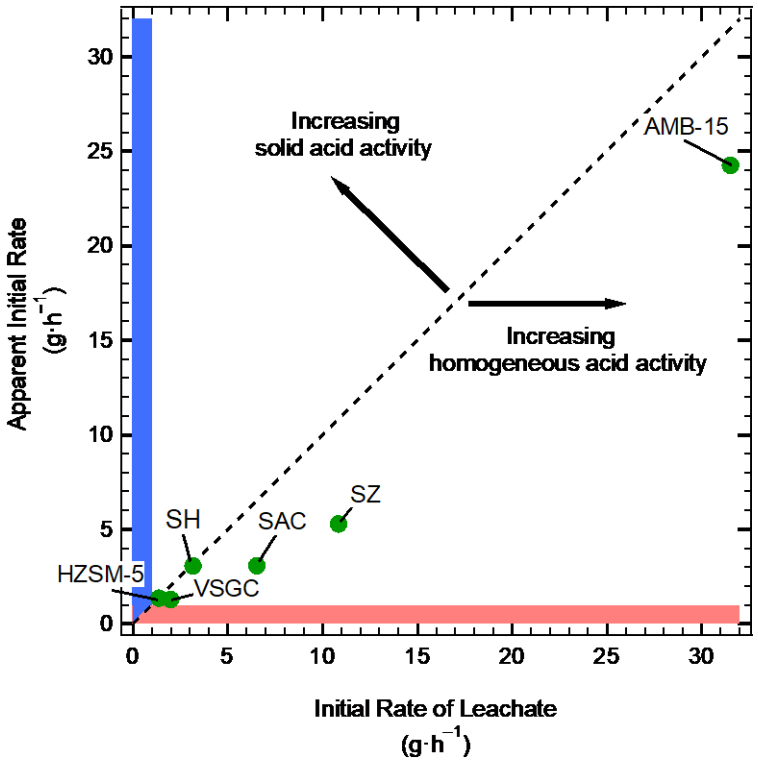

Figure 4.18. Parity plot of the apparent initial rate of hydrolysis with fresh solid acid catalyst and the initial rate of hydrolysis with leachate at constant acid concentration normalized by the initial rate of cellulose hydrolysis due to water. Blue region indicates hydrothermally stable catalyst that is more active than water. Red region represents hydrothermally stable catalyst whose leachate is more active than water, an impossible case if the catalyst doesn't leach homogeneous acid. Arrows indicate the directions in which the activity of the solid acid or homogeneous acid increase. CMP-SO_3H-0.3 is omitted for clarity.

The solid catalysts tested in the current study meet the conditions described in the second case. Figure 4.5. presents a parity plot of the apparent initial rate of hydrolysis of the fresh solid acid catalyst and the initial rate of cellulose hydrolysis with the leachate normalized by the initial rate of cellulose hydrolysis by water. The parity plot is separated into four different regions. The region colored in blue represents the case where the leachate has the same activity as water, but the solid acid has an apparent activity greater than that of the leachate. Therefore, this region is identical to the case where $R_1=0$, i.e. the solid acid catalyst is hydrothermally stable, and there are solid-solid interactions between the catalyst and cellulose. On the other hand, the region colored in red is where the leachate exhibits high activity, but the apparent activity of the solid acid catalyst is identical to that of water. This region represents an impossible scenario where the solid acid catalyst does not leach homogeneous acid, but the leachate is highly active at hydrolyzing cellulose.

The two intermediate regions lying above and below the parity line represent the case where $R_1>0$ and the leached homogeneous acid is active at hydrolyzing cellulose. In the region above the parity line the apparent initial rate of cellulose hydrolysis by a fresh solid acid catalyst is greater than the initial rate of the leachate. Since the concentration of the homogeneous acid in the leachate is greater at all times than the concentration of the continuously generated homogeneous acid in the presence of the solid acid catalyst, this region could unambiguously be interpreted as definite contribution of the solid acid catalyst to the observed hydrolysis activity. Conversely, the region below the parity line is where the initial rate of the leachate is greater than the apparent initial rate of the fresh solid acid catalyst. This could be due to the greater concentration of the homogeneous acid provided that all of the observed activity is due to the homogeneous acid species. Or, on the other hand, it could be due to the leachate being more active than the combination of the activity

continuously release homogeneous acid and the intrinsic activity of the solid acid catalyst. Therefore, the interpretation of this region is ambiguous, and activity cannot be clearly attributed to the solid acid catalyst alone.

Amberlyst-15 (AMB-15), Sulfated Zirconia (SZ), and sulfonated activated carbon (SAC), lie in the region below the parity line, hence, direct interpretation of solid acid activity cannot be made. Similarly, CMP-SO_3H-0.3 also lies in that region (data not shown for clarity of presentation) with coordinates of (62.5; 42.5). Sulfonated humins (SH) catalyst lie on the parity line. This line could be interpreted as a region where leaching is very rapid or where there is activity by the solid catalyst. Thus, it requires further leaching analysis, specifically, determining the rate of acid leaching. On the other hand, HZSM-5 and VSGC also lie on the parity line, but also near the region of activity of water, indicating low activity towards cellulose hydrolysis, despite being hydrothermally stable. The solid acid activity of the catalysts tested here cannot be interpreted unambiguously as they reside in the region below the parity line with an increasing contribution of the leached homogenous acid to the apparent cellulose hydrolysis activity and, furthermore, are not practically applicable.

Regardless, even if a catalyst resides in the region below the parity line, there could still be contribution from the intrinsic activity of the solid acid catalyst. Therefore, interpretations about R_4 can still be made which could allow for studying the solid catalyst solid cellulose interactions. To quantify contribution of solid acid catalyst in such cases the activity of the homogeneous acid should be calculated and compared to and subtracted from the experimental results of cellulose hydrolysis.

Cellulose hydrolysis by the homogenous acid depends on the concentration of the hydronium ion, which increases throughout the reaction. Previous studies have investigated the effects of acid

concentration on the kinetics of cellulose hydrolysis and soluble products degradation.[24, 64, 72] The effect of acid concentration on the reaction rates has been modeled by introducing a pre-exponential factor in the expression for the reaction rate constant.[68] Therefore, defining the pre-exponential factor to be a function of time can capture the changes of the homogeneous acid concentration throughout the reaction. The time functionality can be described by measuring the homogenous acid concentration leached from the solid acid at different time points and regressing the data. Therefore, the activity of the leached homogeneous acid can be mathematically modelled and compared to experimental results. If the observed cellulose hydrolysis activity is greater than the modelled, the difference should be indicative of the solid-solid interactions between the catalyst and cellulose.

In order to calculate the hydrolysis activity of the homogenous acid, it is imperative to select a proper cellulose hydrolysis model. Several kinetic expressions and respective parameters have been reported in the literature spanning wide range of reaction conditions.[68] Since a unified theoretical kinetic model capable predicting cellulose hydrolysis has not been verified, we selected cellulose hydrolysis model that most closely resembles the conditions such as temperature and acid concentration observed in the current study.[68] For the purpose of modelling cellulose hydrolysis, we used the kinetic model proposed by Saeman as the temperature and acid concentrations are in agreement with conditions of cellulose hydrolysis in the current study (see more details of the justification for selecting Saemans kinetic model in the Methodology section).[64] Details of the kinetic modelling are provided in the Methodology section.

To verify that the kinetic model that we chose can predict the hydrolysis of homogeneous acid, we compared the cellulose conversion predicted by the kinetics to the observed soluble carbon balance obtained from the constant acid concentration leachate experiments. A parity plot of the

measured soluble carbon balance and cellulose conversion predicted by the hydrolysis model is presented in Figure 4.6. There is a good agreement between the predictions of the Saeman model and the experimental results obtained in the current study which indicates that this model can be used to a good approximation for calculating the hydrolysis of acid with time dependent concentration. Furthermore, these results support the use of soluble carbon balance as a measurement of cellulose conversion by a solid acid catalyst.

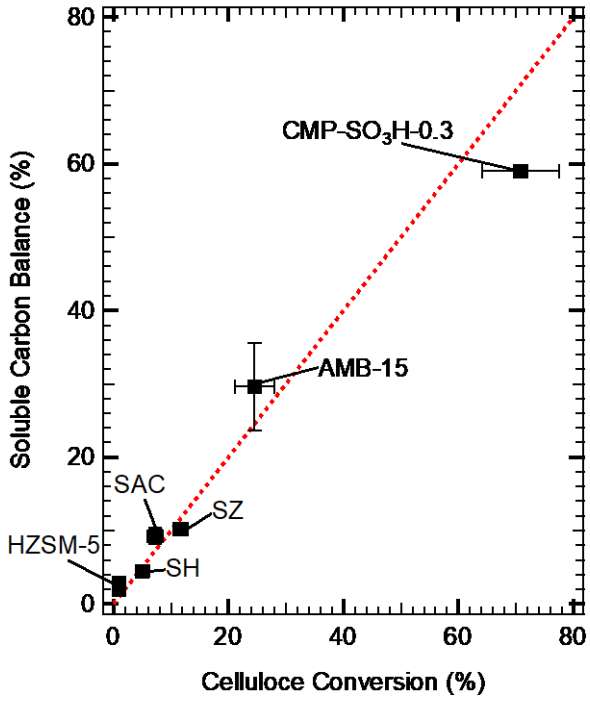

Figure 4.19. Parity plot of measured soluble carbon balance versus predicted cellulose conversion by homogeneous acid hydrolysis model. The dotted red line represents parity between the two metrics. The black squares datapoints represent the results obtained from acid hydrolysis with the leachates of each catalyst, where the acid concentration remains constant throughout the reaction. The datapoints for HZSM-5 and VSGC overlap. Reaction temperature range simulated was 150-155 °C to capture the temperature variations in the glass reactor heated by an oil bath.

For the purpose of quantifying the effects of the continuously leaching homogeneous acid we performed a kinetic study of the leaching of two catalysts – AMB-15 and CMP-SO_3H-0.3. The

two catalysts were selected for the following reasons: 1) they represented catalysts possessing only catalytic and catalytic and binding groups, respectively and 2) they exhibited greater apparent activity, which allowed for temporal resolution for an experimental kinetic study of cellulose hydrolysis. Similarly to AMB-15, a time study of the acid leaching of CMP-SO_3H-0.3 was carried out; for reference the plot of acid concentration versus time data for CMP-SO_3H-0.3 is provided in Appendix B, Figure B2.

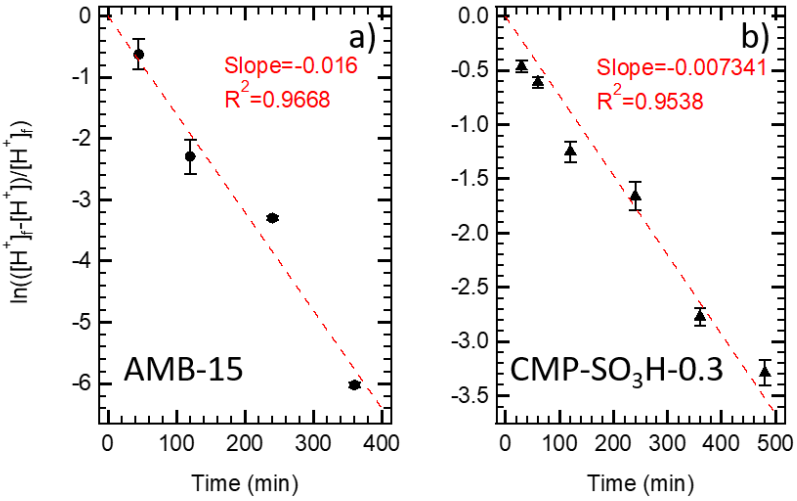

Figure 4.20. Kinetic analysis of homogeneous acid leaching from AMB-15 in a) and CMP-SO_3H-0.3 in b) assuming the leaching obeys first order kinetics. The slope, indicative of the leaching rate constant, is used in the kinetic modeling for cellulose hydrolysis catalyzed by time dependent acid concentration.

The acid concentration as a function of time for two catalysts, namely AMB-15 and CMP-SO_3H-0.3, was used to extract a leaching rate constant. For this purpose, the leaching was approximated to first order kinetics within the time range tested and the first order kinetic rate was calculated. Specifically, since the acid concentration appears to reach an asymptote value at the end of the reaction, we considered the final acid concentration as the initial value of the most reactive and hydrolysable acid sites. Therefore, the conversion of the acid sites in the solid acid catalyst to homogeneous ionic species could be represented as the final acid concentration minus

the momentary acid concentration both divided by the final acid concentration. The natural logarithm of the conversion was plotted against reaction time to extract the first order kinetic constant. This analysis is for AMB-15 and CMP-SO_3H-0.3 is plotted in Figure 4.7. a) and b). In addition, we carried out a kinetic study of the cellulose hydrolysis in the presence of the solid acid catalysts to compare the experimental results to the predictions of the kinetic model.

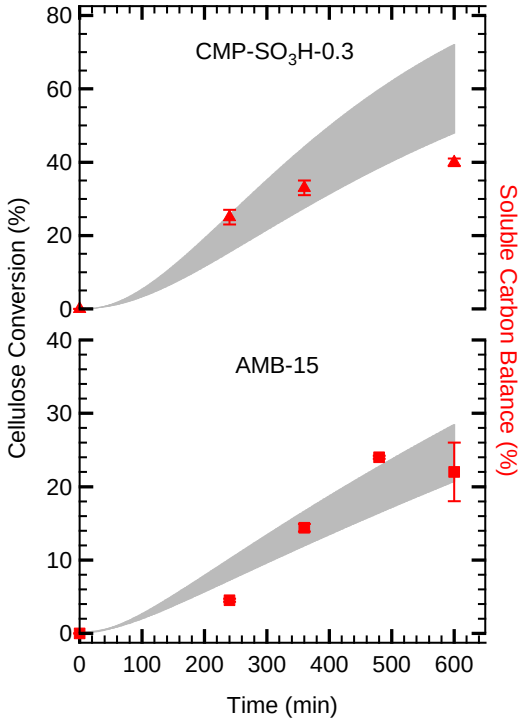

Figure 4.21. Comparison of cellulose conversion (grey) predicted by using Saeman's homogeneous acid cellulose hydrolysis model with time dependent acid concentration and measured soluble carbon balance (red) as a function of reaction time. Data presented are for CMP-SO_3H-0.3 (top) and AMB-15 (bottom).

Figure 4.8. shows the soluble carbon balance obtained after cellulose hydrolysis with CMP-SO_3H-0.3 and AMB-15 superimposed on the predictions from the kinetic modelling of cellulose hydrolysis with time dependent acid concentration. The model and the experimental results are in a good agreement indicating that accounting for the homogeneous acid activity captures all of the apparent cellulose hydrolysis activity of the two solid acid catalysts. Based on this analysis it can

be concluded that there is little to no contribution from the intrinsic activity of the two solid acid catalyst and, thus, no solid-solid interactions between the solid acid catalysts and the cellulose substrate. While accounting for the effects of the homogeneous acid on the cellulose hydrolysis revealed that AMB-15 and CMP-SO_3H-0.3 do not act as true solid catalysts for depolymerizing solid cellulose substrates, the same approach can be applied for investigating other proposed catalytic structures.

4.3.4. Effect of Soluble Products on Solid Acid Leaching

Figure 4.8. reveals a good agreement between kinetic modelling and experimental results. However, the experimental data for both catalysts suggest that the soluble carbon balance appear to reach a plateau near the end of the reaction, while the kinetic modelling predicts ever increasing conversion. This suggest that the cellulose hydrolysis reaction rate is reducing. However, considering that the solid acid catalysts continue to leach, and the concentration of the homogeneous acid would increase further, the rate of cellulose hydrolysis should also increase, since it is dependent on the acid concentration. Therefore, it precludes the interpretation of reduced cellulose hydrolysis rate.

On the other hand, the data could be interpreted as balance between production of soluble products from cellulose hydrolysis and their degradation. That interpretations supposes that the soluble products undergo further reactions that remove them from the solution and are, thus, not captured by the soluble carbon balance. A possible reaction is the production of humins.[25] We explored the possibility of a reaction between the soluble products and the solid acid catalysts. Considering that the CMP-SO_3H-0.3 and AMB-15 catalysts analyzed kinetically possess either chloromethyl and benzylsulfonic acid groups or aromatic sulfonic acid groups, respectively, it is conceivable that a potential reaction between the soluble products would occur at those sites. In

that case, potential further degradation of the catalyst could result in further acid leaching which will have additional implications on the apparent catalytic activity and its interpretation.

To test this hypothesis, we measured the acid concentration after 10 hours of cellulose hydrolysis with either CMP-SO_3H-0.3 and AMB-15. Figure 4.9. plots the homogeneous acid concentration in the liquid media after hydrothermal treatment of CMP-SO_3H-0.3 and AMB-15 and after cellulose hydrolysis. The homogeneous acid concentration after cellulose hydrolysis is higher than when the catalysts are treated in the hydrothermal environment. While for CMP-SO_3H-0.3 the increase is modest (from 0.124 M to 0.14M), form AMB-15 it is nearly double (from 0.04M to 0.078M). These results reveal that the catalyst can leach homogeneous acid not only due to hydrolysis by water, but also due to reaction with the soluble products released from cellulose hydrolysis. This implies that the reaction network for describing cellulose hydrolysis with solid acid catalyst that can leach catalytically active homogeneous acid is more complicated and the reactions between the solid acid catalyst and the soluble products also need to be considered for proper interpretations of the potential solid-solid interactions between the catalysts and the solid cellulose substrate.

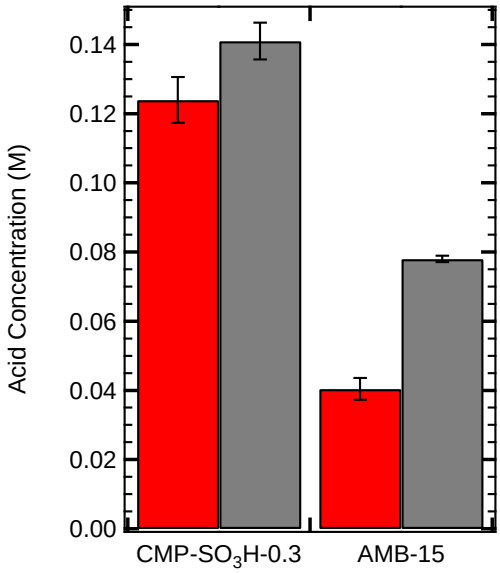

Figure 4.22. Acid concentration in the liquid medium after hydrothermal treatment of CMP-SO_3H-0.3 and AMB-15 in the absence of cellulose (red) and after cellulose hydrolysis at the same conditions. Reaction was carried out at 150 °C for 10 hours.

To elucidate products of the reaction between the solid acid catalyst and the soluble cellulose hydrolysis species, we subjected ^{13}C enriched glucose to hydrolysis with CMP-SO_3H-0.3 at the same conditions as before (150 °C, 10 h.) and analyzed the solid catalyst after the reaction with solid-state NMR. The 2D NMR spectra correlating protonated and non-protonated carbons, plotted in Figure 4.10., reveals presence of mainly HMF and levulinic acid. However, further signal indicative of complex carbon functionality including aromatic rings, aromatic carboxylic acids, biphenyl, and linkages between aromatic and furan rings. The spectra suggest that the products from the reaction between glucose and its decomposition products and the solid acid catalysts are char-like species physically adsorbed and potentially covalently bonded to the structure of the solid acid catalyst. This data in combination with Figure 4.9. indicate: 1) interactions between soluble products and solid acid catalyst, 2) interaction between insoluble species by adsorption and potentially further reaction with solid acid catalyst, and 3) additional release of homogeneous acid

into the bulk solution. A secondary route of solid acid catalyst leaching and subsequent cellulose depolymerization obscure even further interpretations of the intrinsic activity of solid acid catalyst and its interactions with the solid cellulose substrate.

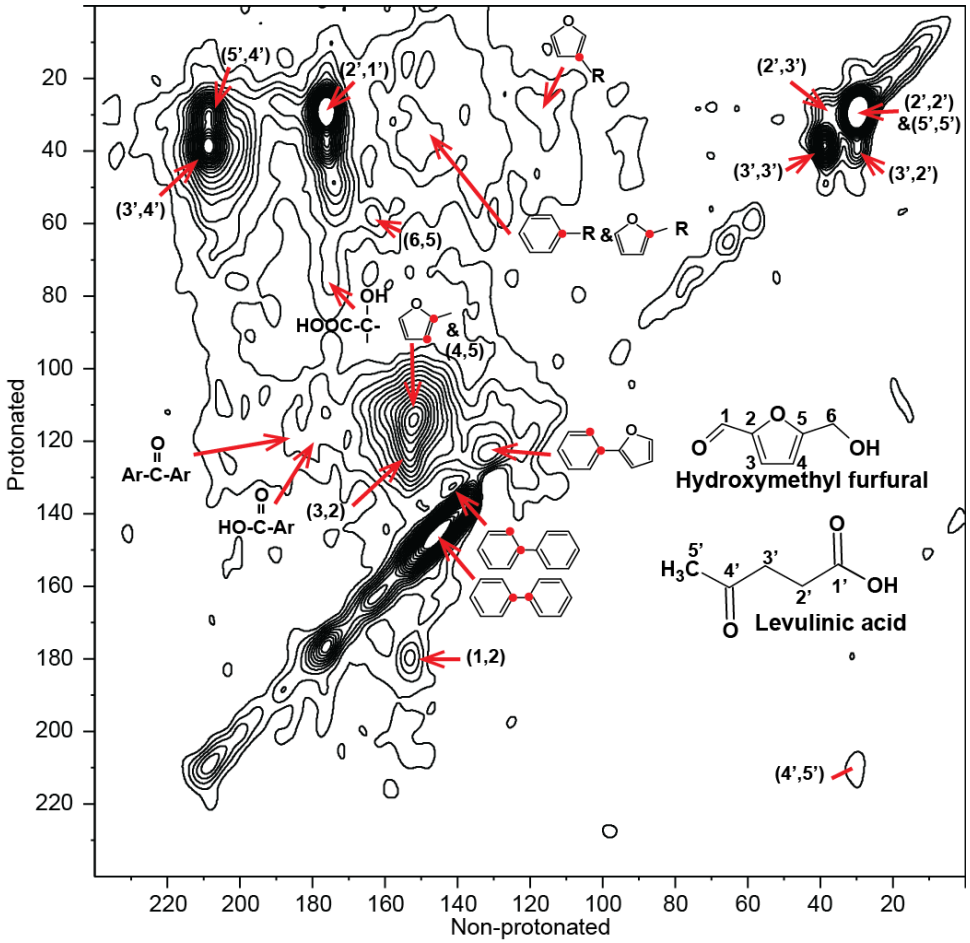

Figure 4.23. 2D solid-state NMR analysis of CMP-SO_3H-0.3 after reaction with ^{13}C enriched glucose (150 °C, 10 h.). Presented is correlation between protonated and non-protonated carbons present in the glucose degradation species.

The results of the analysis presented in this study can be summarized in Scheme 4.4. Chemical moieties of solid acid catalyst are hydrolyzed in water, releasing homogeneous acid species. The leached homogeneous acid in turn depolymerizes cellulose to soluble molecules. In addition, the soluble products generated react or catalyze further release of homogeneous acid. These results

call into question the observations presented in the literature. For this reason, we propose a shift of the experimental approach for testing solid acid catalysts for cellulose hydrolysis. Rather than the current approach which attempts sophisticated characterization of structures proposed for solid acid catalysts followed by cellulose hydrolysis tests, we recommend first a stability test and analysis of the cellulose hydrolysis interpretation. Should a catalyst provide evidence for solid-solid interactions, then it is rational to proceed with structural analysis.

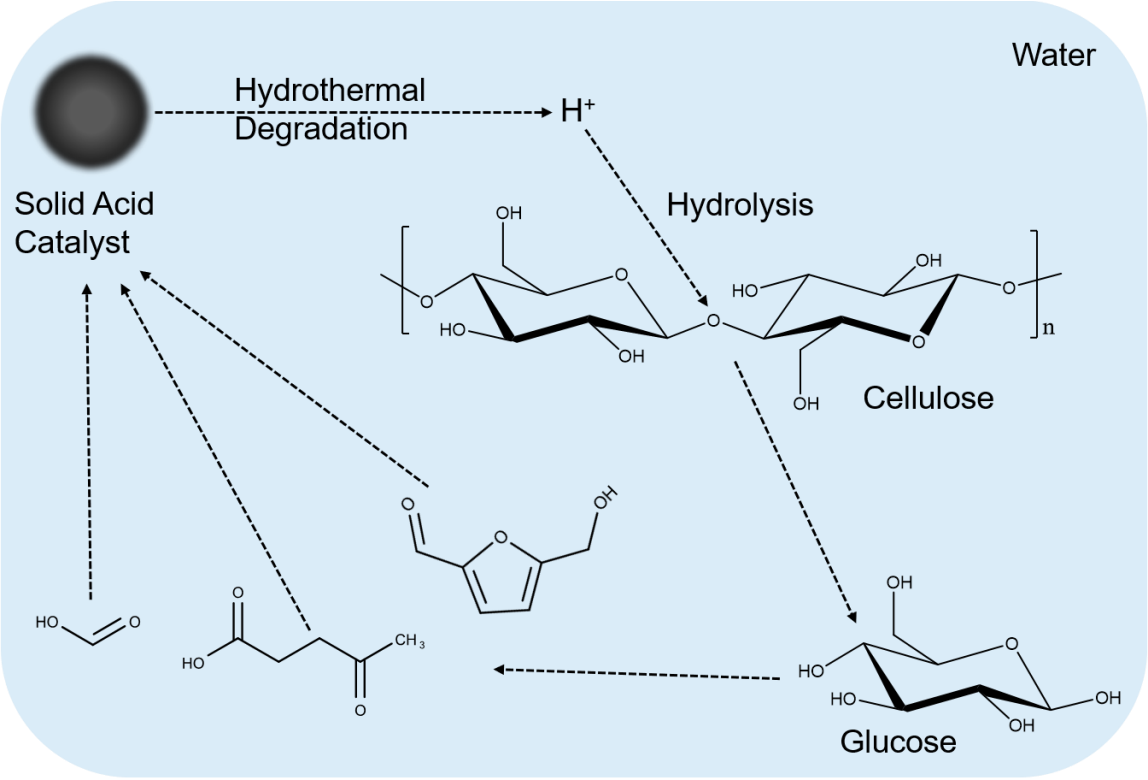

Scheme 4.12. Summary of solid acid catalyzed cellulose hydrolysis mechanism via leaching of homogeneous acid species.

4.4. Conclusions

In this study we examined the implications of potential solid acid catalyst degradation in the hydrothermal environment used for cellulose hydrolysis. The focus was on catalytic structures

which are representative of the type of catalysts used in the field of solid acid catalyzed cellulose hydrolysis. Treating such materials at the hydrothermal conditions used for depolymerization of cellulose results in leaching of catalytically active homogeneous acid the reaction medium. Specifically, the acid species are not a result of an ion exchange process but are due to hydrolysis of chemical moieties in the solid catalysts. We found that the sulfonated materials are releasing sulfuric acid, while a chlorine-based catalyst releases hydrochloric acid.

The leaching of homogeneous acid prevents direct interpretation of intrinsic activity of the solid acid catalysts towards cellulose hydrolysis and the development of structure-activity relationships. Indeed, structural features such as number of acid sites does not provide a meaningful correlation with activity; on the contrary, activity appears to be directly proportional to the propensity of the solid material to leach homogeneous acid.

In order to attribute cellulose hydrolysis observations to the intrinsic activity of the solid acid catalyst we devised simple criteria for catalyst assessment. The solid materials were treated at the same hydrothermal conditions used for cellulose hydrolysis. The activity of the homogeneous acid obtained after such a treatment can be compared to the apparent activity of a solid acid catalyst. If the apparent activity is greater, that conclusive indicates contribution from the solid-solid interactions between solid acid catalyst and solid cellulose substrate. However, almost all catalyst exhibited a lower apparent activity. Hydrothermally stable catalyst did not result in activity greater than that of the cellulose hydrolysis potential of water, indicating no solid-solid interactions.

We modeled the cellulose hydrolysis catalyzed by the homogeneous acid that is continuously leached from the solid catalysts in order to compare it to the apparent activity and conclude on potential contribution from solid catalyst solid cellulose interactions. However, the model captured the experimental results, further confirming lack for contribution from the solid acid material to

the observed cellulose hydrolysis, beyond serving as a source of homogeneous acid. Furthermore, we found that the soluble products of cellulose depolymerization react with the solid catalysts, promoting additional leaching of homogeneous acid. Overall, we found no evidence solid-solid interactions between the solid acid catalysts and cellulose, implying that observations reported in the scientific literature of solid acid catalyzed cellulose hydrolysis are likely due to the effects of homogeneous acids. The current study could serve for the development of catalyst testing framework that would appropriately account for all reactions and allow for improved interpretation of catalytic observations. The analysis applied and conclusions obtained from the current study are not limited only to these specific catalysts and to cellulose hydrolysis but can be transferred to reactions involving soluble reactants both in hydrothermal medium.

4.5. References:

1.V. Balan, D. Chiaramonti and S. Kumar, *Biofuels, Bioproducts and Biorefining*, 2013, **7**, 732-759.

2.D. M. Alonso, S. H. Hakim, S. Zhou, W. Won, O. Hosseinaei, J. Tao, V. Garcia-Negron, A. H. Motagamwala, M. A. Mellmer and K. Huang, *Science advances*, 2017, **3**, e1603301.

3.H. Kawamoto, *Current Organic Chemistry*, 2016, **20**, 2444-2457.

4.B. Yang, Z. Dai, S.-Y. Ding and C. E. Wyman, *Biofuels*, 2011, **2**, 421-449.

5.S. Park, J. O. Baker, M. E. Himmel, P. A. Parilla and D. K. Johnson, *Biotechnology for biofuels*, 2010, **3**, 10.

6.Y. Nishiyama, P. Langan and H. Chanzy, *Journal of the American Chemical Society*, 2002, **124**, 9074-9082.

7.L. R. Lynd, *Nat Biotechnol*, 2017, **35**, 912-915.

8.Y. Zhu, M. J. Biddy, S. B. Jones, D. C. Elliott and A. J. Schmidt, *Applied Energy*, 2014, **129**, 384-394.

9.T. R. Brown, *Bioresource Technology*, 2015, **178**, 166-176.

10.R. Rinaldi and F. Schuth, *ChemSusChem*, 2009, **2**, 1096-1107.

11.L. Vaquerizo, N. Abad-Fernández, R. B. Mato and M. J. Cocero, *Chemical Engineering Journal*, 2018, **350**, 463-473.

12.H. B. Aditiya, T. M. I. Mahlia, W. T. Chong, H. Nur and A. H. Sebayang, *Renewable and Sustainable Energy Reviews*, 2016, **66**, 631-653.

13.R. A. Sheldon, *Green Chem.*, 2014, **16**, 950-963.

14.P. C. Torres-Mayanga, D. Lachos-Perez, A. Mudhoo, S. Kumar, A. B. Brown, M. Tyufekchiev, G. Dragone, S. I. Mussatto, M. A. Rostagno, M. Timko and T. Forster-Carneiro, *Biomass and Bioenergy*, 2019, **130**, 105397.

15.M. A. Rostagno, J. M. Prado, A. Mudhoo, D. T. Santos, T. Forster-Carneiro and M. A. Meireles, *Crit Rev Biotechnol*, 2015, **35**, 302-312.

16.G. Chen, X. Wang, Y. Jiang, X. Mu and H. Liu, *ACS Sustainable Chemistry & Engineering*, 2018, **6**, 10999-11007.

17.N. Sweygers, N. Alewaters, R. Dewil and L. Appels, *Sci Rep*, 2018, **8**, 7719.

18.A. Peciulyte, K. Karlstrom, P. T. Larsson and L. Olsson, *Biotechnol Biofuels*, 2015, **8**, 56.

19.M. Z. Karim, Z. Z. Chowdhury, S. B. A. Hamid and M. E. Ali, *Materials (Basel)*, 2014, **7**, 6982-6999.

20.M. Möller, F. Harnisch and U. Schröder, *RSC Advances*, 2013, **3**.

21.D. A. Cantero, M. D. Bermejo and M. J. Cocero, *The Journal of Supercritical Fluids*, 2013, **75**, 48-57.

22.A. Orozco, M. Ahmad, D. Rooney and G. Walker, *Process Safety and Environmental Protection*, 2007, **85**, 446-449.

23.Y. Yu and H. Wu, *Energy & Fuels*, 2010, **24**, 1963-1971.

24.J. Shen and C. E. Wyman, *AIChE Journal*, 2012, **58**, 236-246.

25.R. Weingarten, J. Cho, R. Xing, W. C. Conner, Jr. and G. W. Huber, *ChemSusChem*, 2012, **5**, 1280-1290.

26.O. Bobleter, W. Schwald, R. Concin and H. Binder, *Journal of Carbohydrate Chemistry*, 1986, **5**, 387-399.

27.D. A. Cantero Sposetti, DOI: 10.35376/10324/5374info:eu-repo/semantics/doctoralThesis, 2014.

28.R. W. Torget, J. S. Kim and Y. Y. Lee, *Industrial & Engineering Chemistry Research*, 2000, **39**, 2817-2825.

29.P. Bansal, M. Hall, M. J. Realff, J. H. Lee and A. S. Bommarius, *Biotechnol Adv*, 2009, **27**, 833-848.

30.K. Kafle, H. Shin, C. M. Lee, S. Park and S. H. Kim, *Sci Rep*, 2015, **5**, 15102.

31.B. Yang, D. M. Willies and C. E. Wyman, *Biotechnology and Bioengineering*, 2006, **94**, 1122-1128.

32.D. Gomes, A. C. Rodrigues, L. Domingues and M. Gama, *Applied Microbiology and Biotechnology*, 2015, **99**, 4131-4143.

33.D. Humbird, R. Davis, L. Tao, C. Kinchin, D. Hsu, A. Aden, P. Schoen, J. Lukas, B. Olthof, M. Worley, D. Sexton and D. Dudgeon, *Process Design and Economics for Biochemical Conversion of Lignocellulosic Biomass to Ethanol: Dilute-Acid Pretreatment and Enzymatic Hydrolysis of Corn Stover*, United States, 2011.

34.A. Shrotri, H. Kobayashi and A. Fukuoka, *Acc Chem Res*, 2018, **51**, 761-768.

35.Y.-B. Huang and Y. Fu, *Green Chemistry*, 2013, **15**.

36.L. Shuai and X. Pan, *Energy & Environmental Science*, 2012, **5**.

37.S. Chu, L. n. Yang, X. Guo, L. Dong, X. Chen, Y. Li and X. Mu, *Molecular Catalysis*, 2018, **445**, 240-247.

38.M. Tyufekchiev, P. Duan, K. Schmidt-Rohr, S. Granados Focil, M. T. Timko and M. H. Emmert, *ACS Catalysis*, 2018, **8**, 1464-1468.

39.Y. Zuo, Y. Zhang and Y. Fu, *ChemCatChem*, 2014, **6**, 753-757.

40.B. Wiredu and A. S. Amarasekara, *Catalysis Communications*, 2014, **48**, 41-44.

41.O. M. Gazit and A. Katz, *J Am Chem Soc*, 2013, **135**, 4398-4402.

42.L. Hu, Z. Li, Z. Wu, L. Lin and S. Zhou, *Industrial Crops and Products*, 2016, **84**, 408-417.

43.S. Hu, T. J. Smith, W. Lou and M. Zong, *J Agric Food Chem*, 2014, **62**, 1905-1911.

44.G. S. Foo and C. Sievers, *ChemSusChem*, 2015, **8**, 534-543.

45.Q. Yang and X. Pan, *BioEnergy Research*, 2016, **9**, 578-586.

46.S. Suganuma, K. Nakajima, M. Kitano, D. Yamaguchi, H. Kato, S. Hayashi and M. Hara, *Journal of the American Chemical Society*, 2008, **130**, 12787-12793.

47.S. Yuan, T. Li, Y. Wang, B. Cai, X. Wen, S. Shen, X. Peng and Y. Li, *Fuel*, 2019, **237**, 895-902.

48.X. Wang, X. Wu, K. Guo, J. Ren, Q. Lin, H. Li, X. Wang and S. Liu, *Catalysis Letters*, 2019, DOI: 10.1007/s10562-019-02912-6.

49.X. Qian, J. Lei and S. R. Wickramasinghe, *RSC Advances*, 2013, **3**.

50.A. Onda, T. Ochi and K. Yanagisawa, *Green Chemistry*, 2008, **10**, 1033-1037.

51.N. Tarabanko, V. E. Tarabanko, S. V. Kukhtetskiy and O. P. Taran, *ChemPhysChem*, 2019, **20**, 706-718.

52.H.-X. Li, W.-J. Shi, X. Zhang, P. Liu, Q. Cao and L. e. Jin, *Journal of Chemical Technology & Biotechnology*, 2019, **n/a**.

53.K. Mohammed Hello and E. Kadhim Hlial, *Journal of Physics: Conference Series*, 2019, **1294**, 052013.

54.D. Scholz, J. Xie, O. Kröcher and F. Vogel, *RSC Advances*, 2019, **9**, 33525-33538.

55.R. Gong, Z. Ma, X. Wang, Y. Han, Y. Guo, G. Sun, Y. Li and J. Zhou, *RSC Advances*, 2019, **9**, 28902-28907.

56.Q. Xu, W. Yang, G. Liu, C. Liang, S. Lu, Z. Qi, J. Hu, Q. Wang and W. Qi, *ACS omega*, 2019.

57.I. Kurnia, A. Yoshida, N. Chaihad, A. Bayu, Y. Kasai, A. Abudula and G. Guan, *Fuel Processing Technology*, 2019, **196**, 106175.

58.Z. Tang and J. Su, *Carbohydrate Research*, 2019, **481**, 52-59.

59.D. Scholz, O. Krocher and F. Vogel, *ChemSusChem*, 2018, **11**, 2189-2201.

60.I. Sádaba, M. López Granados, A. Riisager and E. Taarning, *Green Chemistry*, 2015, **17**, 4133-4145.

61.D. W. Gardner, J. Huo, T. C. Hoff, R. L. Johnson, B. H. Shanks and J.-P. Tessonnier, *ACS Catalysis*, 2015, **5**, 4418-4422.

62.R. Demir-Cakan, N. Baccile, M. Antonietti and M.-M. Titirici, *Chemistry of materials*, 2009, **21**, 484-490.

63.S. L. Goertzen, K. D. Thériault, A. M. Oickle, A. C. Tarasuk and H. A. Andreas, *Carbon*, 2010, **48**, 1252-1261.

64.J. F. Saeman, *Industrial & Engineering Chemistry*, 1945, **37**, 43-52.

65.M. Mosteiro-Romero, F. Vogel and A. Wokaun, *Chemical Engineering Science*, 2014, **109**, 220-235.

66.K. Wu, G. Feng, Y. Liu, C. Liu, X. Zhang, S. Liu, B. Liang and H. Lu, *Bioresour Technol*, 2018, **261**, 28-35.

67.P. Calvini, A. Gorassini and A. L. Merlani, *Cellulose*, 2007, **15**, 193-203.

68.G. SriBala and R. Vinu, *Industrial & Engineering Chemistry Research*, 2014, **53**, 8714-8725.

69.F. Camacho, P. González-Tello, E. Jurado and A. Robles, *Journal of Chemical Technology & Biotechnology*, 1996, **67**, 350-356.

70.R. D. Fagan, H. E. Grethlein, A. O. Converse and A. Porteous, *Environmental Science & Technology*, 1971, **5**, 545-547.

71.J.-P. Franzidis, A. Porteous and J. Anderson, *Conservation & Recycling*, 1982, **5**, 215-225.

72.B. Girisuta, L. Janssen and H. Heeres, *Industrial & engineering chemistry research*, 2007, **46**, 1696-1708.

73.P. Duan and K. Schmidt-Rohr, *Journal of Magnetic Resonance*, 2017, **285**, 68-78.

74.J.-D. Mao and K. Schmidt-Rohr, *Environmental science & technology*, 2004, **38**, 2680-2684.

75.R. L. Johnson, J. M. Anderson, B. H. Shanks, X. Fang, M. Hong and K. Schmidt-Rohr, *Journal of Magnetic Resonance*, 2013, **234**, 112-124.

76.F. Guo, Z. Fang, C. C. Xu and R. L. Smith, *Progress in Energy and Combustion Science*, 2012, **38**, 672-690.

77.G. S. Foo and C. Sievers, *ChemSusChem*, 2015, **8**, 534-543.

78.J. M. Anderson, R. L. Johnson, K. Schmidt-Rohr and B. H. Shanks, *Catalysis Communications*, 2014, **51**, 33-36.

79.V. C. Nguyen, A. Dandach, T. T. H. Vu, P. Fongarland and N. Essayem, *Molecular Catalysis*, 2019, **476**.

80.R. Rinaldi, N. Meine, J. vom Stein, R. Palkovits and F. Schuth, *ChemSusChem*, 2010, **3**, 266-276.

81.P. Lanzafame, D. M. Temi, S. Perathoner, A. N. Spadaro and G. Centi, *Catalysis Today*, 2012, **179**, 178-184.

82.P. Chen, A. Shrotri and A. Fukuoka, *ChemSusChem*, 2019, **12**, 2576-2580.

83.H. Kobayashi, M. Yabushita, T. Komanoya, K. Hara, I. Fujita and A. Fukuoka, *Acs Catalysis*, 2013, **3**, 581-587.

84.O. L. Li, R. Ikura and T. Ishizaki, *Green Chemistry*, 2017, **19**, 4774-4777.

85.B. Zhang, J. Ren, X. Liu, Y. Guo, Y. Guo, G. Lu and Y. Wang, *Catalysis Communications*, 2010, **11**, 629-632.

86.S. Li, Z. Gu, B. E. Bjornson and A. Muthukumarappan, *Journal of Environmental Chemical Engineering*, 2013, **1**, 1174-1181.

87.A. B. Brown, B. J. McKeogh, G. A. Tompsett, R. Lewis, N. A. Deskins and M. T. Timko, *Carbon*, 2017, **125**, 614-629.

88.A. Osatiashtiani, A. F. Lee, M. Granollers, D. R. Brown, L. Olivi, G. Morales, J. A. Melero and K. Wilson, *ACS Catalysis*, 2015, **5**, 4345-4352.

89.S. Kassaye, C. Pagar, K. K. Pant, S. Jain and R. Gupta, *Bioresour Technol*, 2016, **220**, 394-400.

90.A. Kristiani, K. C. Sembiring, F. Aulia and H. Abimanyu, *Energy Procedia*, 2015, **65**, 8-13.

91.A. Onda, T. Ochi and K. Yanagisawa, *Topics in Catalysis*, 2009, **52**, 801-807.

92.A. R. Maag, G. A. Tompsett, J. Tam, C. A. Ang, G. Azimi, A. D. Carl, X. Huang, L. J. Smith, R. L. Grimm and J. Q. Bond, *Physical Chemistry Chemical Physics*, 2019, **21**, 17880-17892.

93.M. Yabushita, H. Kobayashi, J. Y. Hasegawa, K. Hara and A. Fukuoka, *ChemSusChem*, 2014, **7**, 1443-1450.

94.J. M. Anderson, R. L. Johnson, K. Schmidt-Rohr and B. H. Shanks, *Carbon*, 2014, **74**, 333-345.

95.F. Parveen, K. Gupta and S. Upadhyayula, *Carbohydr Polym*, 2017, **159**, 146-151.

CHAPTER 5

Reaction Engineering Implications of Cellulose Crystallinity and Water-Promoted Recrystallization

5.1. Introduction

Cellulose is an abundant and renewable source of carbon with potential to serve as a feedstock for the production of fuels and chemicals.[1-3] In addition, due to its physicochemical properties cellulose finds high value applications in the polymer, pharmaceutical, and nanomaterial fields.[4-6] Depolymerization of cellulose using hydrolysis and other methods is deemed essential for economical production of lignocellulose-based products, and accordingly it has received attention as a research area for decades.[5, 7-9] Various approaches have been studied to depolymerize cellulose to monosaccharides that can be converted and upgraded to fuels and chemicals. One of the most promising routes involves cellulose hydrolysis to glucose.[7, 10-16] However, cellulose, particularly cellulose that is part of lignocellulosic biomass, exhibits low chemical and biological reactivity, making necessary severe conditions, excess biocatalysts, and energy intensive pretreatments to break down its structure.[8, 14, 17-22] As a result, cellulose depolymerization remains a technological and economic bottleneck for commercialization of otherwise promising second generation biofuel technologies, including cellulosic bioethanol.[9, 23]

Cellulose depolymerization approaches are either energy intensive, slow, or result in degradation of valuable products.[24-27] To identify approaches that increase cellulose reactivity, many studies have investigated the relationships between cellulose's reactivity and its polymer structure.[28-30] Cellulose reactivity has been attributed to many different physicochemical structural

characteristics, including the chemical composition of the lignocellulosic complex itself;[29] the interconnectedness of lignin, hemicellulose, and cellulose;[31, 32] cellulose particle size,[33, 34] surface area,[30, 34] pore structure,[34, 35] degree of polymerization,[34] accessibility,[34, 36] and especially crystallinity,[28-30, 37-41] i.e., the relative amount of crystalline and amorphous regions present in the cellulose. In particular, decrystallization of cellulose has been reported to increase the cellulose conversion rate, an empirical observation which implies that crystallinity is important to cellulose recalcitrance.[28, 30, 37, 38, 42-44]

Observations of decreasing hydrolysis rates with increasing conversion have motivated the development of qualitative and quantitative models with separate reaction rates for amorphous and crystalline cellulose.[45] Kinetic models that explicitly relate cellulose reactivity to its crystallinity date back to at least 1947 when Philipp et al.[45] proposed a two-parameter amorphous-crystalline cellulose hydrolysis model to fit rate data obtained from acid-catalyzed cellulose solubilization. In the Philipp et al.[45] model, the first order rate constant for amorphous cellulose hydrolysis (k_a) is an order of magnitude greater than that for hydrolysis of crystalline domains (k_c). Following its introduction, the theory of differential reactivity of amorphous and crystalline regions has been used to explain numerous experimental results, especially the observation of increased cellulose conversion and glucose yield associated with decreasing cellulose crystallinity.[11, 28, 30, 38, 42, 43, 46-50] The differential reactivity model has similarly been used to explain the observation that cellulose crystallinity increases after hydrolytic treatment, an observation which has typically been attributed to preferential removal of the supposedly more reactive amorphous regions during hydrolysis, one of the key predictions of the theory.[38, 42, 51, 52]

Reaction engineering models that include explicit differences in the reactivity of crystalline and amorphous cellulose are confounded by the fact that exposure of decrystallized cellulose to

liquid water or water vapor promotes recrystallization, even under non-hydrolyzing conditions.[53-56] Even though the molecular-level details of this re-structuring are not fully understood, the phenomenon itself is empirically well established, having been reported several times previously by investigators using different characterization techniques.[57-61] Despite the fact that many cellulose depolymerization techniques involve a liquid or vapor water phase,[8, 38, 60, 62, 63] cellulose hydrolysis models do not account for a water-promoted cellulose recrystallization pathway. In fact, correlations between crystallinity and reactivity are based on crystallinity measured prior to sample exposure to the aqueous conditions of hydrolysis.[28, 38, 40, 43, 64] Considering the fact that decrystallized cellulose recrystallizes on contact with water, the actual crystallinity of the sample undergoing hydrolysis is not clear. As a result, the common observation that cellulose crystallinity increases after water-based conversion processes[38, 40, 42] might plausibly be due in part – or in total – to non-hydrolytic recrystallization,[60] placing in doubt one of the core pieces of supporting evidence used for the differential reactivity theory. These considerations point to a gap in the current understanding of cellulose hydrolysis reaction mechanisms, even at the most qualitative level of determining which steps are required for a physically meaningful mechanism.

The objective of this work was to determine the effect of water-induced recrystallization on cellulose reactivity and provide fundamental understanding of the relevant physical and chemical phenomena that occur during hydrolysis. To do so, we ball-milled microcrystalline cellulose for different durations and quantified the relative crystallinity of the resulting samples using X-ray diffraction (XRD). We then subjected these samples to hydrolysis treatment to reproduce literature results and replicate a correlation between measured crystallinity and reactivity commonly reported in the literature.[28, 38, 40, 42] Next, these same samples were subjected to water-induced recrystallization under non-hydrolytic conditions to examine the effect of water exposure on

crystallinity and attempt to measure the crystallinity of the samples at the onset of hydrolysis. Raman spectroscopy was used to provide support for XRD data and expand molecular-level understanding. Solid-state ^{13}C nuclear magnetic resonance (ssNMR) was applied to distinguish cellulose I, cellulose II, non-crystalline chains on the crystallite surface, and truly amorphous cellulose. Through spectral editing based on spin–lattice relaxation, peaks of cellulose I and II could be separated from overlapping non-crystalline bands and quantified fairly accurately.[65] Finally, reactivity under ethanolysis conditions was evaluated in an attempt to differentiate the reactivity of recrystallized cellulose from amorphous cellulose. These results guide the development of quantitative and predictive cellulose hydrolysis reaction engineering models and provide new motivation for developing methods for overcoming the challenge of cellulose recalcitrance.

5.2. Methodology

5.2.1. Materials

Avicel PH101 cellulose (average particle size of 50 μm, 100% purity with 3-5% moisture content), 0.1 M hydrochloric acid standard, cellobiose >98%, glucose >99.5% , hydroxymethyl furfural (HMF) >99% purity, levulinic acid >98%, formic acid >98%, were purchased from Sigma Aldrich. Acetone and ethanol ACS grade were purchased from Pharmco-Aaper. All chemicals were used as received.

5.2.2. Ball Milling

Microcrystalline cellulose (MCC) was ball-milled for different durations to generate a family of samples with varying degrees of crystallinity. Briefly, 1.0 gram of MCC was placed in a stainless-steel cylinder (18 mm diameter×55.5 mm length, 10 mL). Three stainless-steel balls (2×9.5 mm diameter and 1×15.85 mm diameter) were placed in the cylinder. The cylinder was

clamped in the holder of a vibratory shaker Retsch MM2000 and samples were ball-milled for 10, 20, 30, 40, and 50 minutes. The temperature was not controlled during milling. The initial temperature was the same as ambient (22-26 °C). Temperature increased during treatment, rapidly reaching a maximum of 50-60 °C after several minutes. This temperature appears to be a steady state between frictional heating and ambient loss.

5.2.3. Acid Hydrolysis

Cellulose samples were depolymerized using hydrochloric acid to determine the relationship between cellulose structure and reactivity. Acid treatment conditions were as follows: 0.25 g of cellulose, 5.0 mL of 0.1 M HCl, and a magnetic stir bar were added to a 15 mL heavy wall pressure vial sealed by a screw cap with a Viton O-ring seal. The vial was submerged in an oil bath to heat the reaction mixture to 150 °C, as measured by a thermocouple inserted directly into the reaction mixture through a modified screw cap. The reaction mixture was stirred at 200 rpm for the duration of the reaction time. After the desired reaction time, the vial was removed from the oil bath and quenched in cold water. The reactor vials were centrifuged at 1400 rpm for 15 minutes, and the supernatant liquid was extracted with a syringe for further analysis. After removal of the supernatant liquid, the solids were washed with acetone to remove any residual water. The samples were centrifuged, and the acetone was removed by syringe and the remaining solids were transferred into a pre-weighed crucible. The crucible containing the solid product was covered and placed in an oven held at 65 °C until the weight stops changing. The total amount of residual solids was determined gravimetrically.

Concentrations of water-soluble products were determined by HPLC analysis of the liquid recovered from centrifugation. The glucose yield was calculated based on the following formula: $\frac{m_g * M_{gu}}{m_c * M_g} * 100\%$, where m_c is mass of cellulose, m_g is mass of glucose determined by HPLC, M_{gu}

is molecular weight of glucose unit in cellulose, and M_g is molecular weight of glucose. All experiments were carried out at least in triplicate. Error bars are reported as the standard deviation of replicated experiments.

5.2.4. Hot Liquid Water Treatment

Cellulose samples were treated in hot liquid water to determine the effect of the treatment on the structure of cellulose and to determine the glucose yield under conditions in the absence of acid. The hydrothermal, hot liquid water treatment was identical to the acid treatment described previously, with the exception that no HCl was added to the reaction mixture.

5.2.5. Recrystallization Tests

To test whether recrystallization in hot liquid water conditions recovers recalcitrance, cellulose was ball-milled for 50 minutes as described before. The ball-milled cellulose (0.50 grams) and 5.0 mL of water were placed in high-pressure glass reactor vials, which were then placed in a preheated oil bath. The treatment was carried out at three different temperatures of 110 °C, 130 °C, and 150 °C. The treated cellulose was recovered and dried as described before. Following the treatment, the cellulose samples (0.25 grams) were hydrolysed by 0.1 M HCl (5.0 mL) for one hour at 150 °C reaction temperature, again as described previously. The liquid sample was extracted and analyzed using HPLC.

5.2.6. Liquid Product Analysis and Quantification

The liquid products obtained from both acid and liquid hot water treatments of cellulose were analyzed for water-soluble compounds using High Performance Liquid Chromatography (HPLC, Agilent 1200 series). A diode array detector (DAD) was used for organic acids and furanic compounds and a refractive index detector (RID) for carbohydrate detection. The column was a Bio-Rad Aminex HPX-87H; the mobile phase was 5 mM sulfuric acid; and the mobile phase

flowrate was 0.6 mL min^{-1}. The column and the RID detector were both kept at 35 °C during analytical runs, while the UV-Vis detection wavelength was set to 284 nm. Calibration curves were determined from analysis of mixtures containing known concentrations of standards at 0.25, 0.5, 0.75, 1, 1.25, 1.5, 1.75, 2, and 2.5 g L^{-1}.

5.2.7. X-Ray Diffraction (XRD)

X-Ray diffraction (XRD) analysis was carried out with Rigaku Geigerflex diffractometer using CuKα radiation at 37.5 kV and 25 mA. A step size of 0.05° was used with 1 second accumulation time. Diffractograms of different samples were compared after area normalization and baseline subtraction. A crystallinity index was calculated by the widely used method first developed by Segal.[66] In this method, the crystalline contribution is determined by the intensity of the 002 peak at 22.5° and the amorphous by the intensity at 18.3°.[66] The crystallinity index was calculated based on the following equation $CI = \frac{I_{200} - I_A}{I_{200}} * 100\%$.

5.2.8. Raman Microscopy

As a complementary technique to X-ray diffraction Raman spectral analysis of cellulose samples was carried out to observe changes in crystallinity. Spectra were obtained with a Horiba Xplora Raman Microscope using 785 nm excitation laser and 10× Olympus magnification lens.

5.2.9. Solid-state Nuclear Magnetic Resonance (ss-NMR)

Additional analysis of the cellulose structure was carried out with NMR due it its ability to more accurately quantify cellulose conformations compared to XRD or Raman. Experiments were performed using a Bruker Advance Neo 400WB spectrometer operating at a ^{13}C resonance frequency of 100 MHz, using a 4-mm magic-angle spinning probe in double-resonance mode at a spinning frequency of 9 kHz and at room temperature. The ^{13}C chemical shifts were externally referenced on the neat TMS scale using the carboxyl peak of α-glycine at 176.49 ppm. Typical 90°

pulse lengths were 3.6 μs for ^{1}H and 4 μs for ^{13}C. MultiCP[67] with composite-pulse excitation and storage[68] was used to obtain nearly quantitative ^{13}C spectra. Five blocks of CP were implemented with 90–100% amplitude ramps on the ^{1}H channel. The contact time for each CP period was 1.1 ms, resulting in a total combined CP contact time of 5.5 ms. The delays for ^{1}H repolarization were 4 s for all samples, while the recycle delay was 8 s. A rotation-synchronized Hahn spin echo[69] was used to achieve dead-time-free detection, generated by a 180° pulse with EXORCYCLE[70] phase cycling after the last multiCP block. During the 18.7-ms detection, proton decoupling with the SPINAL64 scheme[71] was applied, at a ^{1}H strength of $\nu_1 \approx 85$ kHz. The number of scans averaged was 512 for MCC, 1280 for MCC-BM50, 768 for MCC-BM50-SP, and 832 for MCC-BM50-AC (see nomenclature defined below in 2.11).

A 5-s T_{1C} filter[72] was used to remove signals from segments with short ^{13}C spin-lattice relaxation times T_{1C} due to fast segmental motions, such as non-crystalline cellulose C6 side groups, retaining the sharp crystalline-C6 peaks of cellulose I and II, which are well resolved. The same numbers of scans as for the multiCP spectra were averaged. Direct polarization with 2-s recycle delay was used to select signals of mobile segments with fast T_{1C} relaxation, yielding the band of non-crystalline cellulose C6 complementary to the T_{1C}-filtered crystalline peaks. For all four samples 4096 scans were averaged. Zirconia rotors (Bruker Biospin) were used as received for magic-angle spinning of all samples.

5.2.10. Ethanolysis

Cellulose was converted using ethanolysis to test the reactivity of cellulose in the absence of solvent-promoted recrystallization. Briefly, 37% HCl was diluted to 0.1M in ethanol. Cellulose (0.25 grams) was mixed with 5 mL of 0.1M HCl-ethanol solution in a manner similar to the hydrolysis experiments and reacted at 130 °C for 1.5 hours. Ethanol vapor pressure limited

temperature selection as higher temperatures resulted in pressures that exceed the limits of the glass reactors used in this study. After the reaction, the mixture was centrifuged and the solid and liquid products were separated. The solid residue was additionally washed with ethanol, dried at 65 °C and weighed to determine conversion.

5.2.11. Sample Nomenclature

MCC is used as an abbreviation for microcrystalline cellulose throughout the text. For convenient reference, Table 5.1. provides suffixes that are used to denote various treatments of MCC.

Table 5.5. Suffixes used to denote treatment of microcrystalline cellulose (MCC).

Suffix to MCC	Sample Treatment
-BM50	Ball-milled for the indicated time duration
-BM50-HLW150	Ball-milled for the indicated time duration, then subjected to hot liquid water treatment at the indicated temperature
-BM50-AC	Ball-milled for the indicated time duration, then subjected to acid hydrolysis with 0.1 M HCl, for 1 hour, at 150 °C
-BM50-SP	Ball-milled for the indicated time duration, then subjected to simulated sample treatment. The simulated sample treatment involved exposure of sample to 0.1 M HCl at room temperature for 10 minutes followed by 5 minute heating up to 150 °C. After reaching temperature, sample was cooled rapidly and washed with acetone.

5.3. Results and Discussion

Reaction engineering models require qualitative knowledge of the relevant reaction pathways and quantitative knowledge of the relevant transport, thermodynamic, and especially kinetic parameters. Cellulose hydrolysis models typically have one or more parallel pathways describing

hydrolysis of amorphous and crystalline cellulose, each with its own rate parameter.[41, 45, 73, 74] The rate constants used to describe hydrolysis of amorphous cellulose are typically greater than those describing hydrolysis of crystalline cellulose, which has been justified by rapid initial weight loss and decrease of degree of polymerization, followed by a leveling of reaction rate.[40, 41, 45, 75, 76] Such reasoning has been used to explain the observation of greater conversion rates of samples with lower crystallinity and motivates the use of decrystallizing pretreatments to increase cellulose reactivity.[28, 30, 39, 49] However, hydrolysis models that ascribe reactivity based on relative amounts of amorphous and crystalline cellulose do not take into account the fact that exposure to water promotes recrystallization of amorphous cellulose,[59, 60] meaning that even the qualitative features of the corresponding cellulose hydrolysis models may not be accurate. Models consisting of incorrect pathways can only aspire to data fitting, meaning that models that miss key pathways will lack predictive power. Development of predictive, structure-based models must account for all of the relevant underlying physical and chemical phenomena that affect reactivity. Accordingly, we began this study with a simple question: do current cellulose hydrolysis models contain all the pathways required for more than data fitting?

5.3.1. XRD Crystallinity and Reactivity

The first aim of this study was to reproduce the observations that cellulose decrystallization increases conversion and soluble product yields. The focus of this part of the study was measuring the reactivity of cellulose crystalline allomorph type I as it is the form that is present in lignocellulosic plant biomass.[77] Ball milling was selected as a mechanical method for decrystallizing cellulose.[24, 63] Accordingly, a family of cellulose samples with varying crystallinity was generated by subjecting Avicel microcrystalline cellulose (labeled MCC), a commonly studied cellulose I model substrate, to vibratory ball milling for varying amounts of time, from 10 to 50

min in 10 min increments ; Table 5.1. (section 5.2.11) provides sample naming conventions. Figure 5.1. provides representative X-ray diffractograms obtained for MCC and the ball-milled samples. As expected, XRD indicates that ball milling progressively decreases MCC crystallinity. More specifically, the sharp peaks of MCC, assigned in the literature to diffraction from the 101, 10$\bar{1}$, 021, 200, and 040 crystalline planes[47] broaden and decrease in intensity after ball milling.[78] The x-ray diffractogram of the most aggressively treated sample, MCC-BM50, is nearly featureless. Ball milling for durations greater than 50 min resulted in sample darkening which we took as evidence of formation of degradation products. Charring would have added unwanted complexity to the analysis and visual discoloration therefore placed an upper limit on the duration of the ball milling treatment.

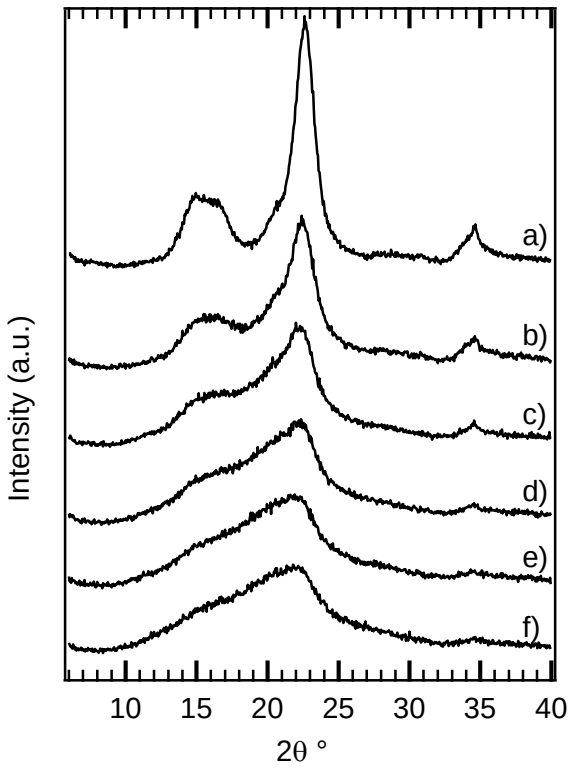

Figure 5.24. X-ray diffractograms of progressively ball-milled cellulose samples: a) Avicel-PH101, b) MCC-BM10, c) MCC-BM20, d) MCC-BM30, e) MCC-BM40, f) MCC-BM50.

Numerous methods have been proposed for quantifying cellulose crystallinity using characterization techniques such as XRD (peak height, amorphous subtraction, peak fitting, Rietveld modelling), NMR (peak integration), Raman spectroscopy (peak heights), and infrared spectroscopy.[47, 79-81] Estimated crystallinity values can be method dependent, pointing to issues of absolute quantification of non-crystalline cellulose.[47] To estimate crystallinity and correlate its trends to observed reactivity, we used Segal's method as a facile and a popular method, with the caveat that the method is best used as a qualitative indicator of crystallinity rather than a quantitative one.[47, 66] For precision, we term crystallinity measured using the Segal analysis method of XRD data, "Segal crystallinity". XRD data were used to calculate cellulose relative crystallinity and corresponding values are plotted in Figure 5.2. (black triangles). Segal crystallinity decreased with increasing ball milling time from 92% for MCC to 35% for MCC-BM50.

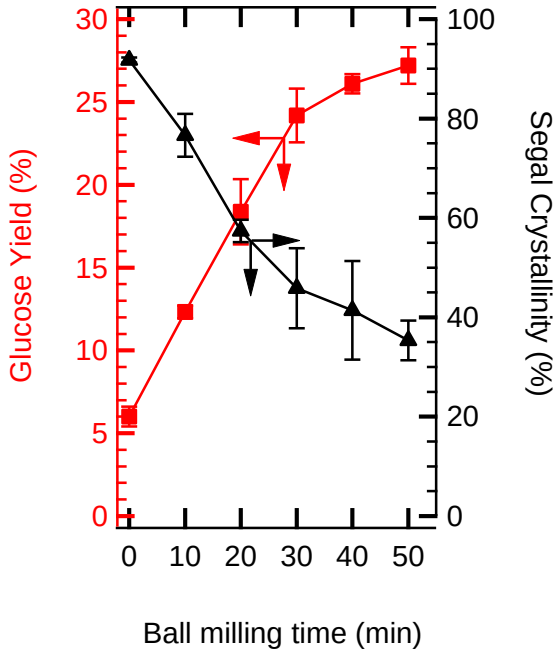

Figure 5.25. Glucose yield (■) and XRD Segal crystallinity (▲) of ball-milled cellulose samples plotted versus ball milling time.

To determine the effect of the mechanical treatment on reactivity, the ball-milled samples were subjected to acid hydrolysis at standard conditions (0.1 M HCl, 150 °C, 1 hour) and soluble product yields and conversion were measured. In all cases, glucose was the main product, with trace amounts of HMF and cellobiose. Accordingly, measured glucose yields are plotted alongside the Segal crystallinity data in Figure 5.2. (red squares). As expected,[38] glucose yields increased with increasing ball milling time, with the maximum obtained for MCC-BM50 (27±1 %). Water-soluble glucose oligomers were minor byproducts; this was further supported by the fact that cellobiose yields were always less than 0.1% and measurable oligosaccharide yields were less than the estimated detection limit (0.005%). Mass balance details of the solid residue and liquid products can be found in Appendix C in Figure C1 showing closure to within 8% further supporting the above arguments. Accordingly, Figure 5.2. confirms that decreased Segal crystallinity and a commensurate increase of glucose yield are the apparent main effects associated with ball milling pretreatment, consistent with previous literature reports and establishing a baseline for more detailed experiments.[38, 43]

After the acid treatment, the residual solids were collected, washed with acetone, dried, and analyzed to determine the effect of the treatment on cellulose crystallinity. Acetone wash was employed to remove water from the sample and prevent changes in crystallinity during water drying, as reported previously.[82] In control tests, the XRD diffractogram did not change appreciably after treatment with acetone and subsequent drying, indicating that the method successfully avoided introduction of artifacts (X-ray diffractograms are shown in Figure C2 in Appendix C).[61, 82, 83] Figure 5.3. provides the corresponding x-ray diffractograms of the acid hydrolyzed samples (see Table 5.1. for nomenclature). The characteristic profile of MCC is recovered after acid treatment, and the broad features of the ball-milled samples are no longer

observable after treatment (compare to Figure 5.1.). While the intensities of the main peaks are less than observed for the precursor MCC, the main diffraction peaks are clearly identifiable after acid treatment of even the most aggressively ball-milled sample, indicating that the acid hydrolysis treatment at least partially restores cellulose crystallinity.

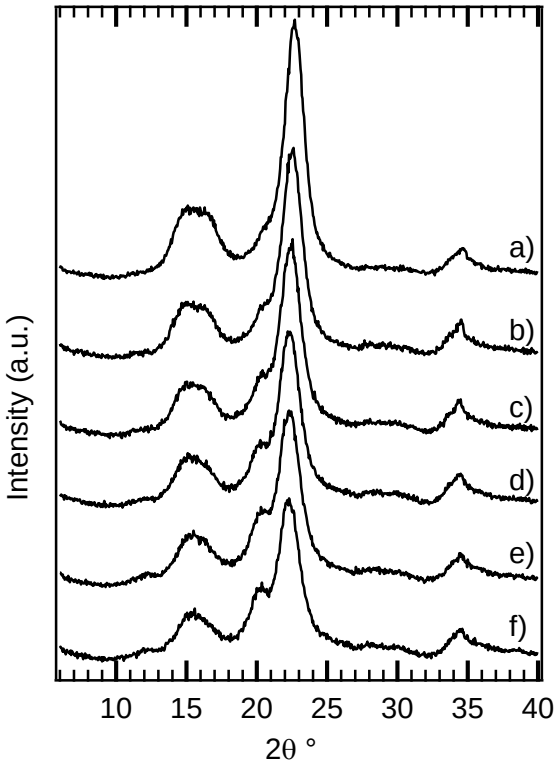

Figure 5.26. X-ray diffractograms of progressively ball-milled cellulose samples after 0.1 M HCl acid treatment at 150 °C for 1 hour: a) Avicel-PH101, b) MCC-BM10-AC, c) MCC-BM20-AC d) MCC-BM30-AC, e) MCC-BM40-AC, f) MCC-BM50-AC.

XRD Segal crystallinities of the acid treated samples were calculated as before and are plotted in Figure 5.4. as red squares. As expected from Figure 5.3., Segal crystallinity increases following acid hydrolysis compared to the ball-milled samples (black triangles); for example, the calculated Segal crystallinity of MCC-BM50, the most aggressively treated MCC sample, increases from 35% to nearly 86% after acid treatment. The magnitude of the Segal crystallinity increase depends

on the ball milling time, with the greatest increase observed for the most aggressively ball-milled samples. The amorphous-crystalline cellulose reactivity theory would explain the observation of increased crystallinity as preferential hydrolysis of amorphous cellulose during acid treatment.[45] However, this explanation does not account for the spontaneous recrystallization of cellulose that occurs during water exposure under non-hydrolytic conditions, a phenomenon reported several times but never connected directly with cellulose reactivity.[59, 60] Accordingly, we continued our study by attempting to isolate the effects of water-promoted recrystallization from hydrolytic effects.

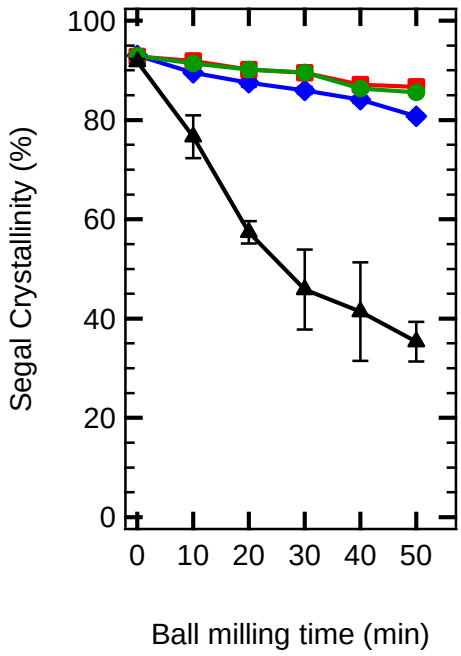

Figure 5.27. XRD Segal crystallinity of cellulose samples after ball milling (▲), acid hydrolysis (AC) (■), hot liquid water (HLW) (◆), and simulated sample preparation (SP) (●) treatments.

5.3.2. Water-Promoted Recrystallization

To isolate the effects of water-promoted recrystallization from hydrolysis of amorphous cellulose, we treated the MCC-BM samples by exposing them to hot liquid water (HLW, see Table 5.1.) at the same temperature and reaction time as in the acid hydrolysis treatment, but without

acid. For brevity the X-ray diffractograms of HLW treatment are shown in Appendix C in Figure C3. The qualitative XRD features obtained for the HLW are similar to those corresponding to samples subjected to acid hydrolysis, with the HLW treatment promoting recovery of the sharp diffraction peaks ascribed to crystalline cellulose. Figure 5.4. plots the Segal crystallinity values of samples that have undergone HLW treatment (blue diamonds), showing that HLW treatment increases crystallinity to values similar to those observed after acid hydrolysis treatment. Unlike acid hydrolysis, HLW treatment resulted in soluble product yields of less than 0.5%. Mass balance closure was 103±2% (see Figure C1 blue diamonds), indicating that preferential conversion of amorphous regions to soluble products could not possibly account for the increased crystallinity. Instead, phase transition from amorphous to crystalline cellulose is implicated.

Comparing diffractograms obtained after hydrolytic and HLW treatments indicate that water-promoted cellulose recrystallization must occur in parallel with hydrolysis. The implication therefore is either that crystallinity plays at most a secondary role in reactivity or that cellulose hydrolysis models should be modified to include a cellulose recrystallization pathway that competes with hydrolysis. To differentiate between these two scenarios, the next step was to investigate the differences in the soluble product yields of decrystallized and recrystallized samples. MCC-BM50 was selected for studying the effects of recrystallization on product yields as the most highly decrystallized sample considered in this work that was therefore expected to elicit the greatest response to recrystallization treatment. Samples with varying degrees of recrystallization were generated by treating MCC-BM50 in HLW at 110, 130, and 150 °C (labeled as MCC-BM50-HLW110, 130, and 150 respectively). These samples were then subjected to acid hydrolysis at the same conditions as before (0.1 M HCl, 150 °C, 1 hour). Table 5.2. provides glucose yields and Segal crystallinity values obtained for the three HLW-treated samples. The

same data are provided for MCC, MCC-BM50, and MCC-BM10 for comparison. After HLW treatment, the Segal crystallinities of MCC-BM50-HLW110, 130, and 150 are similar to one another and are significantly greater than that of MCC-BM50 prior to acid or water treatment. However, glucose yields obtained from acid hydrolysis of the HLW samples are the same to within uncertainty as those obtained for MCC-BM50. Reaction models that explain reactivity using different rate constants for amorphous and crystalline cellulose would predict that the yields obtained from hydrolysis of the HLW samples should be similar to those obtained for MCC-BM10, which is not observed and is a clear breakdown of existing cellulose hydrolysis models.

Table 5.6. XRD Segal crystallinities and glucose yields obtained from hydrolysis of MCC subjected to different treatments. Reaction conditions: 0.1M HCl, 150 °C, 1 hour.

Sample	**Segal Crystallinity (%)**	**Glucose Yield (%)**
MCC	92	6 ± 1
MCC-BM10	77 ± 4	12 ± 0.4
MCC-BM50	35 ± 4	27 ± 1
MCC-BM50-HLW110	77 ± 1	28 ± 2
MCC-BM50-HLW130	79 ± 1	26 ± 2
MCC-BM50-HLW150	81 ± 1	24 ± 3

The data in Figure 5.4. and Table 5.2. suggest that the crystallinity of ball-milled cellulose prior to contact with water may not be the most appropriate measurement for understanding reactivity. In particular, the rate of water-promoted recrystallization of amorphous cellulose is not clear and simply contacting water may be sufficient to recrystallize amorphous cellulose.[59] The effects of water-promoted recrystallization thereby make cellulose crystallinity a moving target,

even before the potential effects of hydrolysis on crystallinity are considered. To estimate cellulose crystallinity at the onset of hydrolysis, MCC-BM samples were subjected to a treatment identical to that used to generate glucose yield data, including a 10-min mixing period and a 5-min heating period. However, instead of permitting the reaction mixture to remain at temperature for 1 h, the reaction mixture was rapidly quenched in an ice bath, filtered, and the solid rinsed with acetone to prevent further exposure to the aqueous solution. Samples treated in such a manner were labeled with an additional -SP descriptor to denote the sample preparation treatment and analyzed for the effects of the simulated sample treatment on crystallinity (See Table 5.1.).

The x-ray diffractograms obtained for SP samples (provided as Figure C4 in Appendix C) are qualitatively similar to those obtained from the HLW and AC samples, indicative of crystallinity recovery after the simulated sample treatment. Figure 5.4. plots the values of Segal crystallinity of the samples subjected to simulated sample preparation treatment (green circles), showing that the estimated crystallinities of the SP samples agree within error with those of the HLW and AC samples. As before, mass balance considerations do not support the theory of preferential solubilization of amorphous cellulose during sample preparation (both cellulose conversion and yields of soluble products were <1%). Therefore, results from the simulated sample treatment indicate that water promoted cellulose recrystallization is nearly complete during sample preparation and heat up. In comparison, any changes in crystallinity due to conversion of amorphous cellulose to soluble products within that timeframe occur more slowly – if at all. These results provide an explanation for the similar glucose yields of MCC-BM50 and MCC-BM50-HLW samples presented in Table 5.2. By the time release of soluble products has begun, MCC-BM50 has reached the same level of crystallinity as MCC-BM50-HLW150, suggesting that the samples are structurally identical during hydrolysis, hence, the equivalence of their reactivity.

Moreover, Figure 5.4. suggests that crystallinity of the dry sample fed to the reactor is not even especially relevant to the state of the sample being converted to soluble products and instead that the more meaningful correlation might be between reactivity and the crystallinity measured after the simulated sample preparation treatment as it is the state that undergoes hydrolysis.

Figure 5 re-plots the glucose yields versus their corresponding values of Segal crystallinity measured for ball-milled (black triangles) and SP samples (green circles). As expected, based on the literature in this field[38, 40] and as anticipated from Figure 5.2., glucose yields increase with decreasing substrate Segal crystallinity, provided that crystallinity is measured for the dry sample prior to contacting water. In contrast, when glucose yields are plotted with values of crystallinity measured after simulated sample preparation treatment instead of a linear relationship with finite slope, the glucose yields are nearly invariant with crystallinity. While glucose yields increase, the Segal crystallinity does not, indicating a lack of predictive correlation, when crystallinity is measured correctly at the onset of hydrolysis. As a result, including parallel pathways for hydrolysis of amorphous and crystalline domains in hydrolysis reaction models may be a numerical approach to capture observed glucose yield data, but parallel pathways are not physically meaningful.

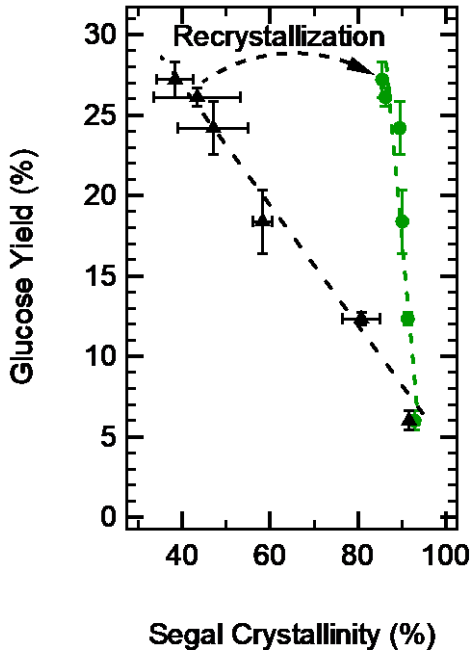

Figure 5.28. Glucose yield plotted as a function of XRD Segal crystallinity measured after ball milling (▲) and after sample preparation and heat up (●). The arrow indicates the effect of recrystallization on the reactivity-crystallinity correlation.

Figure 5.5. suggests a complete re-interpretation of cellulose hydrolysis models; however, the validity and strength of that conclusion may be limited by the method selected for analyzing cellulose structure and estimating crystallinity, as the Segal method has shortcomings for quantitative measurements of crystallinity. Moreover, mechanical decrystallization clearly results in structural changes that increase cellulose reactivity, while water-promoted recrystallization restores apparent Segal crystallinity but with negligible effects on reactivity. This leads to two simple questions: 1) can Segal crystallinity measurements be trusted on their own for model development? and 2) what occurs during decrystallization-recrystallization that affects XRD diffractograms reversibly, but not reactivity?

5.3.3. Raman and ss-NMR Analysis

To answer these questions, we expanded the analysis of the various cellulose samples to include additional instrumentation. As a starting point, we initially selected the Segal method for quantifying crystallinity, as this is the most widely used cellulose characterization technique.[47] However, cellulose is a complex polymer with several different allomorphs, and many different techniques have been developed for probing cellulose structure, and especially estimating its crystallinity.[47] Based on this rationale, Raman spectroscopy and solid-state nuclear magnetic resonance (ss-NMR) were selected as well-documented cellulose crystallinity estimation techniques that probe qualitatively different aspects of cellulose structure than does XRD.[47, 80] Whereas XRD is sensitive to the periodic arrangement of atoms in the cellulose lattice, Raman is sensitive to chain vibrations attributable to skeletal configuration[84] and NMR can detect differences in atomic environment associated with polymer conformation and packing.[85] The distinct physical basis of the three methods means that making qualitatively (and quantitatively) similar observations from all three can answer the question about the reliability of different methods of crystallinity estimations for model development. Considering that Raman and especially NMR provide additional information not captured by XRD, the complementary techniques also have potential for answering the question about the different reversible and irreversible changes that cellulose undergoes during ball milling.

Figure 5.6. plots the Raman spectra of MCC and MCC-BM50 after various treatments and specific peaks at 380 and 1096 cm^{-1} associated with crystallinity are highlighted. Detailed Raman spectra of the entire series of samples are presented in Figures C5 to C8 in Appendix C. The Raman spectrum of MCC-BM50 exhibits a general loss of intensity and blurring of fine spectral features compared with MCC; both of these changes are attributable to a loss of crystallinity.[80] Spectra b,

c and d, in Figure 5.6. show that exposure to aqueous conditions, including acid hydrolysis (MCC-BM50-AC), hot liquid water (MCC-BM50-HLW150), or simulated sample preparation (MCC-BM50-SP) all result in increased intensity of the bands characteristic of crystallinity, specifically those appearing at 380 and 1096 cm^{-1}.[80] In fact, the Raman spectra of the various water-treated samples are nearly indistinguishable from one another, though recrystallization does not recover the intensities of the crystalline peaks to the levels of the precursor MCC sample. Accordingly, Raman analysis shows the same qualitative behavior as does XRD, lending credibility to the Segal interpretation of the XRD data.

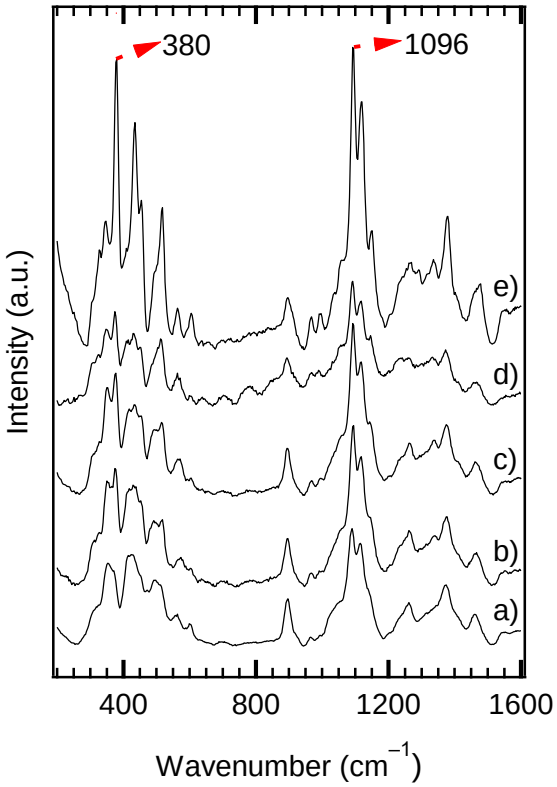

Figure 5.29. Raman spectra of selected cellulose samples: a) MCC-BM50, b) MCC-BM50-HLW, c) MCC-BM50-SP, d) MCC-BM50-AC, and e) Avicel MCC. Peaks associated with crystallinity at 380 cm─1 and 1096 cm─1 are indicated with red arrows.

To gain greater insight, selected samples were further analyzed using quantitative ^{13}C ssNMR. Specific focus was placed on the C4 and C6 regions of the NMR spectrum, as these regions contain distinguishable contributions from carbons in crystalline interior chains and non-crystalline surface or truly amorphous chains.[85] In fact, heretofore, we have adopted typical convention and not differentiated between non-crystalline and amorphous cellulose, as XRD and Raman cannot distinguish them from each other. The most severely decrystallized sample, MCC-BM50, and its recrystallized analogs were studied and compared to the untreated MCC. Their C4 and C6 signals are plotted in Figure 5.7., showing that ball milling results in almost complete elimination of the crystalline cellulose I signals between 87 and 92 ppm and 64 and 68 ppm. The bands between 80 and 87 ppm and 58 and 64 ppm are broader than those of the non-crystalline surface chains in untreated MCC and can therefore be assigned to truly amorphous cellulose; surface chains are indeed not to be expected since almost no crystals exist. Non-hydrolytic or hydrolytic treatment using any of the previously described methods increases the relative intensity of the C4 signal of the crystalline chains (see spectra of MCC-BM50-SP and MCC-BM50-AC), again consistent with water-promoted recrystallization. After recrystallization, the band between 80 and 87 ppm was displaced to a lower field chemical shift and recovered the narrower features of the non-crystalline surface chains, rather than amorphous cellulose. Consistent with XRD and Raman, NMR indicates that most of the recovery of the crystallinity occurs after contact with water and heat up with only minor additional increase after prolonged acid hydrolysis.

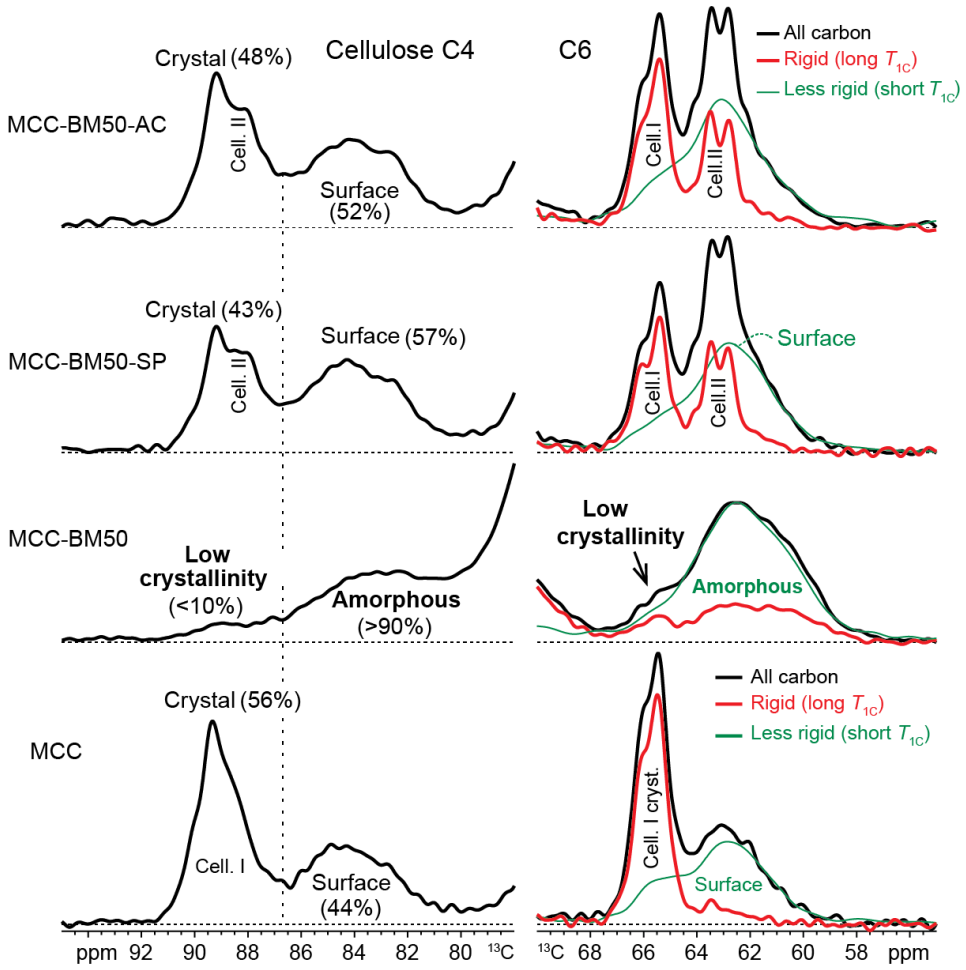

Figure 5.30. The C4 and C6 ^{13}C NMR spectra of selected cellulose samples. The black curve represents the overall spectrum; the red curve is signal from domains with long T_{1C} relaxation times, and the green curve is signal from regions with short T_{1C} relaxation times.

Comparing the C6 regions of MCC and MCC-BM50 shown in Figure 5.7. (right column) confirms that ball milling decrystallization decreases the signal of interior crystalline regions and increases the amorphous content. All previous arguments led us to expect that recrystallization would result in recovery of spectral intensity and peak shape in the C6 carbons analogously to those observed for C4 carbons. However, while the interior crystalline signal partially recovered its initial shape and intensity, the intensity between 60 and 64 ppm also increased. Moreover, the shape of the features in the C6 surface region changed from a single broad band to include a

narrower doublet. The new feature can be attributed to crystalline cellulose II,[85] a distinct allomorph of cellulose not present in lignocellulosic plant biomass.[77] This assignment is confirmed by spectral editing in Figure 5.7., which resolves the cellulose II doublet when the band of the more mobile non-crystalline chains is suppressed based on their faster spin–lattice relaxation. Although formation of cellulose II after ball milling is not specifically considered in common cellulose hydrolysis models,[74] recrystallization of amorphous cellulose as both cellulose I and II have been reported previously in the literature.[56, 86] Our study now shows that recrystallization of cellulose I and II must have reactivity implications.

Coexistence of cellulose I and cellulose II is crucially important for reactivity and the reaction mechanism since cellulose II is often the more reactive allomorph.[87] In the NMR spectra, cellulose II interior signal coincides with surface signal from cellulose I. By separating cellulose C6 signals with long (crystalline) and short (non-crystalline) T_{1C} relaxation filters, see Figure 5.7., we deconvolved the spectra and quantified the cellulose I, II, and non-crystalline surface content. The results, presented in Table 5.3., show that after one hour of hydrolysis (MCC-BM50-AC) the cellulose I content is increased by 3% relative to simulated sample treatment (MCC-BM50-SP), the non-crystalline decreases by about the same amount, while cellulose II appears to remain the same. However, the observed changes cannot account for the glucose yield (28%), which indicates that both cellulose I and II fractions are being hydrolyzed to glucose. Both C6 deconvolution and the C4 region show that the recrystallized cellulose has ~4-5% greater non-crystalline surface content when compared to the starting MCC. Since overlap between interior and surface chain signals from either allomorph in the C4 region is minor, estimation of the surface content based on C4 region could be more reliable. This could imply that in addition to the more reactive cellulose II, the composite cellulose sample could have greater accessible surface area available

for hydrolysis. Greater relative surface chain content could potentially mean smaller crystallite size, and cellulose with smaller crystallite size has been reported to exhibit greater swelling and solubility,[88] suggesting possible correlation with reactivity towards acid hydrolysis.

Table 5.7. Cellulose I, cellulose II, and non-crystalline content calculated by deconvolution of the C6 signal in the NMR spectra.

Sample	Cellulose I (%)	Cellulose II (%)	Non-crystalline (%)
MCC	47±1	0	53±1
MCC-BM50	3.5±1	0	96.5±1
MCC-BM50-SP	25±2	18±2	57±3
MCC-BM50-AC	28±2	17.5±2	54.5±3

Given the surface chain content and the presence of cellulose II in recrystallized cellulose, we revisited the XRD and Raman spectra for additional insight that might have been missed on first analysis. In fact, a distinguishable peak at 12.2° (see Figure C9 in Appendix C) can be attributed to the $1\bar{1}0$ crystalline planes of cellulose II. The full width at half maximum (FWHM) of the main peak at 22.5° increases with increasing ball milling time (shown in Figure C10 in Appendix C), indicating decreasing crystallite size. Literature XRD analysis of cellulose I and II mixtures has been carried out by mixing pure allomorphs and varying their content.[89]

We explored using Figure C9 in Appendix C for quantification. Cellulose II exhibits characteristic XRD features that distinguish it from cellulose I[90] which can allow deconvolution of the diffractograms to estimate the content of each allomorph and correlate it to the reactivity of a sample.[89] In addition, the crystallite size can be estimated from the FWHM of corresponding

diffraction peaks, which provides further structural information that can be accounted for in developing a hydrolysis model.[89] This approach, however, is not applicable here since crystallite size likely varies with decrystallization and potentially recrystallization.[44] Furthermore, the interlayer distance has been shown to vary with crystallite size,[88] thus affecting the angular position of the Bragg's peak. Quantitative data of cellulose I and II from NMR analysis could be used to decrease the number of variables, but the positions of the underlying cellulose I and II peaks remain unknown. Unfortunately, due to the many degrees of freedom of fitting the XRD diffractograms an unambiguous deconvolution by fitting diffraction peaks of the cellulose I and cellulose II and calculating their crystallite size cannot be achieved, preventing correlation of crystallite size to reactivity. In the end, XRD diffractograms allow us to conclude that decrystallization-recrystallization leads to formation of a complex mixture of cellulose I and II, potentially with reduced crystallite size compared with the starting material – all of which are qualitatively in agreement with ss-NMR.

5.3.4. Conversion of Cellulose in Non-Recrystallizing Solvent

Having answered the question about XRD reliability, the next question then becomes: Are the cellulose I/II and potentially size-reduced crystallites simply a more specific description of the reactive form of cellulose that accounts for the effects of mechanical decrystallization on hydrolysis reactivity? Or, is the reactivity of truly amorphous cellulose different from that of either the starting material or the cellulose I/cellulose II mixture? Hydrolysis treatment cannot answer this question since exposure to water collapses amorphous cellulose into the cellulose I/cellulose II mixture. Instead, ethanolysis is a suitable model reaction for studying the reactivity of amorphous cellulose compared with that of the recrystallized mixture. The mechanism of ethanolysis is similar to hydrolysis[91] and yet previous work indicates that organic solvents do not

promote rapid recrystallization of amorphous cellulose under non-hydrolytic conditions.[60] Figure C11 in Appendix C provides the XRD diffractogram of MCC-BM50 treated in ethanol at elevated temperature (130 °C, 1.5 h). The XRD diffractogram sharpens slightly after the treatment, although not to the extent that occurs in water, indicating that solvent-promoted recrystallization is less active in ethanol than in water, as desired.

Comparing ethanolysis rates for MCC, ball-milled MCC, and ball-milled and recrystallized MCC can provide relative reactivity information for crystalline cellulose I, amorphous cellulose, and the recrystallized cellulose I/cellulose II mixture, respectively. Accordingly, the ethanolysis conversions of MCC (as a baseline), MCC-BM50 (decrystallized), and MCC-BM50-HLW150 (recrystallized) were measured at standardized conditions (0.1M HCl in ethanol, 130 °C, 1.5 h). The primary products of ethanolysis, ethyl glucopyranoside, ethoxymethyl furfural and ethyl levulinate, are ethanol soluble[91] so that conversion measurements alone provide unambiguous indications of reactivity. Accordingly, Table 5.4. provides ethanolysis conversion data, showing that MCC, MCC-BM50, and MCC-BM50-HLW indeed exhibit differences in reactivity under conditions where solvent-promoted recrystallization does not occur. Specifically, the amorphous cellulose content of MCC-BM50 is more reactive than the recrystallized substrate, resulting in 41% conversion of the decrystallized sample compared with 13% under the same conditions for the recrystallized one. In comparison, cellulose I (MCC) is nearly unreactive. The data in Table 5.4., therefore, establish that the cellulose I/cellulose II mixture is much less reactive than amorphous cellulose, i.e., cellulose I/cellulose II is not simply a more specific description of the reactivity of ball milled cellulose, but actually distinct.

Table 5.8. Conversion, change in XRD Segal crystallinity values, and apparent kinetic rate constant of selected cellulose samples subjected to ethanolysis treatment. Studied samples were MCC, ball-milled cellulose MCC-BM50, and ball-milled and hot liquid water recrystallized MCC-BM50-HLW.

Sample	Conversion (%)	Initial crystallinity (%)	Final crystallinity (%)	Crystallinity change (%)	Ethanolysis k (h^{-1})
MCC (baseline)	2 ± 1	92	93	1	0.016 ± 0.009
MCC-BM50 (decrystallized)	41 ± 2	35	81	46 ± 1	0.35 ± 0.024
MCC-BM50-HLW150 (recrystallized)	13 ± 1	81	84	3 ± 1	0.09 ± 0.012

To investigate ethanolyzed cellulose further, the treated samples were analyzed using XRD. The corresponding diffractograms are presented in Figure C12 in Appendix C, and estimated changes in crystallinities are provided in Table 5.4. Cellulose I Segal crystallinity is not affected by ethanolysis, as MCC crystallinity remains unchanged at 93% after treatment. In contrast, the Segal crystallinity of MCC-BM50 increases sharply from 35 to 81% after ethanolysis. The low solvent recrystallization potential of ethanol as shown in Figure C11 suggests that the increase in Segal crystallinity of MCC-BM50 after ethanolysis could be attributed partly to preferential conversion of amorphous cellulose to soluble products. A potential parallel mechanism for increasing crystallinity could be scission of reactive bonds and relaxation of chains into crystalline organization.[92] In contrast, the rapid increase of cellulose crystallinity during hydrolysis is primarily due to solvent-induced recrystallization and not conversion of amorphous cellulose to soluble products as revealed by Figure C1 and Figure 5.4. Remarkably, the results and interpretation are similar to the original model suggested by Philipp et al.,[45] i.e. differential rates

of conversion of amorphous and crystalline cellulose, except we find that this occurs only under ethanolysis and not hydrolysis conditions. Finally, the x-ray diffractogram and Segal crystallinity of MCC-BM50-HLW150 do not change after ethanolysis, again consistent with water-promoted recrystallization reaching effective completion after water exposure even before the onset of hydrolysis.

5.3.5. Updating the Cellulose Hydrolysis Model

Table 5.3. establishes that the reaction mechanism describing hydrolysis of amorphized cellulose must include a recrystallization step for formation of the cellulose I/cellulose II mixture. However, what is less clear for reaction models is if a single rate constant can be used to describe the reactivity of the cellulose I/cellulose II mixture, irrespective of the degree of amorphization the sample had undergone prior to water-induced recrystallization. Put another way, is the cellulose I/cellulose II mixture functionally a single material or does it encompass a range of materials, each with different reactivities? In particular, previous work on cellulose reactivity implicates a potential role of degree of polymerization (DP).[34, 46] Previous studies indicate that ball milling cellulose leads to a reduction of DP, with DP decreasing monotonically with increasing ball milling intensity and duration.[34, 37, 54] Therefore, the decrystallization-recrystallization process might result in a family of materials with different DP characteristics and hence reactivities that differ based on the duration of the initial ball milling treatment that cannot be captured simply as a mixture of cellulose I and cellulose II.

To investigate further, hydrolysis yield data were converted into rate constants assuming a first order hydrolysis rate law, as is typically reported in the literature.[93] Further, we assumed that the hydrolysis data obtained from treatment of MCC were representative of highly recalcitrant crystalline cellulose and calculated its rate constant. Based on this assumption we then normalized

Segal crystallinity values to estimate the amount of the two cellulosic species assuming that the amorphous content completely converts to active recrystallized cellulose at the time of onset for hydrolysis, as XRD, Raman, and NMR indicate that MCC-BM50 consists almost completely of amorphous cellulose. Avicel MCC was assumed as a 100% crystalline cellulose with low reactivity and the samples ball-milled for intermediate durations were normalized to be a mixture of Avicel MCC and MCC-BM50 based on their Segal crystallinity.

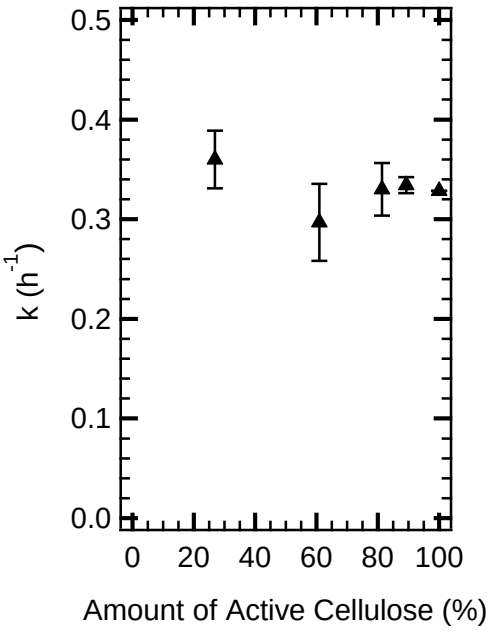

Figure 5.31. Kinetic rate constant of hydrolysis of active recrystallized cellulose plotted versus its amount calculated from XRD Segal crystallinities of ball-milled cellulose.

Following this analysis method, the rate constant for hydrolysis of active recrystallized cellulose mixture could be determined by difference for all of the ball-milled samples, as shown in Figure 8. Interestingly, the data indicate that the rate constant is at most a weak function of the amount of active cellulose initially present, suggesting that – to within the limits of uncertainty – a single rate constant is appropriate for describing the reactivity of the recrystallized cellulose I/cellulose II mixture. Using the NMR data of cellulose I and II content and the glucose yields, we

calculated the hydrolysis rate constants as 0.22 h^{-1} for cellulose I and 0.48 h^{-1} for cellulose II. Further we calculated a composite rate constant by weight averaging the contribution of each allomorph, arriving at 0.36 h^{-1} for active cellulose, which is consistent with the values presented in Figure 5.8., supporting the above interpretation.

While the current data are sufficiently explained using a single rate constant for active cellulose hydrolysis, the values of this rate constant may depend on additional sample-dependent factors, such as degree of polymerization. In particular, the active cellulose formed here must have DP equal to or less than that of the parent material since formation of new glycosidic bonds during any of the thermal or acidic treatments used here is not expected. Therefore, the reactivity of active cellulose found here may in part be a reflection of DP effects, as well as coexistence of cellulose I and cellulose II. Careful study of the effect of DP on cellulose I and cellulose II reactivity is recommended to clarify this issue. The work presented here should be considered during development of the DP study, since just as crystallinity changes under non-solubilizing conditions, so too might DP.[46] Lastly, cellulose reactivity depends on source, which is another factor to be considered.[94]

Structural characterization and reactivity data presented here suggest revision of the classical hydrolysis mechanism of decrystallized cellulose. Specifically, addition of two new pathways – recrystallization of amorphous cellulose and hydrolysis of recrystallized cellulose to glucose – should be included in the overall reaction network. Figure 5.9. summarizes the new model. Exposure of amorphous cellulose to aqueous conditions leads to water-promoted recrystallization as a new form of cellulose, which is a combination of cellulose I and cellulose II with greater surface content and/or decreased crystallite size compared with the original. Since its structural characteristics are not yet entirely clear, Figure 5.9. retains the label of the recrystallized material

as “active cellulose”, echoing previous terminology used in the pyrolysis literature.[95] Hydrolysis occurs via parallel pathways involving crystalline cellulose I, active cellulose, and any trace amorphous cellulose remaining in the sample during and after water-induced recrystallization.

The rates of all reactions shown in Figure 5.9. can be described by their own rate constants. The current study did not aim to quantify these rates; however, the data presented here allow identification of the relative order of their magnitudes. Specifically, the experimental data make clear that the rate constant for recrystallization of amorphous cellulose to active cellulose (k_2) is much greater than the rate constant for active cellulose hydrolysis (k_4). The rate constant for hydrolysis of crystalline cellulose I (k_1) is less than either k_2 or k_4. If recrystallization could somehow be prevented, ethanolysis data suggest that hydrolysis rate constant of amorphous cellulose, k_3, would be greater than all other hydrolysis rate constants. Future studies can be performed to measure these rate constants, with these general trends as guidance. As mentioned previously, the effect of DP on hydrolysis rate constants should be included in these studies.

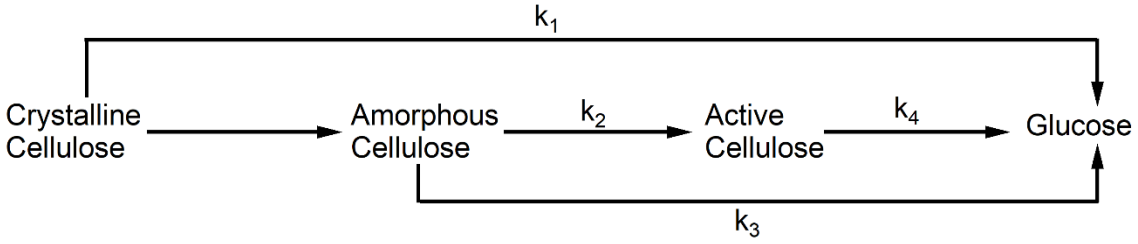

Figure 5.32. Proposed updated cellulose hydrolysis model that includes a decrystallization pathway with conversion of crystalline to amorphous cellulose. Water-promoted recrystallization is incorporated by a transformation of amorphous cellulose to active crystalline cellulose. The three types of cellulose exhibit different reactivity described by a respective rate constant.

The updated hydrolysis model presented here implies that studies interpreting the reactivity of decrystallized cellulose in aqueous conditions as hydrolysis of amorphous cellulose are likely

observing hydrolysis of what we have termed active cellulose. Since mechanical amorphization is a common method of increasing cellulose reactivity, the results of this study can be generalized.[28, 38] Recrystallization of amorphous cellulose in liquid water has been reported to occur even at room temperature.[59-61] Similarly, we observed sharpening of the XRD peaks of cellulose wetted for 1 hour at room temperature (data not shown), although not to the same extent as the hot liquid water treated samples. This indicates that water-induced recrystallization is an activated process; presence of acid could increase the rate of recrystallization by a scission-relaxation mechanism.[92] This rapid transformation suggests that depolymerization of truly amorphous cellulose cannot be realized in aqueous conditions. This indicates that the benefits of decrystallization are diminished when water is used as the reaction medium. Consequently, the recrystallizing effect of water renders mechanical decrystallization less effective than it has the potential to be. Therefore, an alternative approach for cellulose deconstruction is depolymerization of decrystallized cellulose in solvents that do not promote recrystallization. In fact, this may account partially for the success of co-solvent based biomass deconstruction approaches.[96] Regardless of how it is achieved, circumventing water-promoted recrystallization can permit direct conversion of the highly reactive amorphous cellulose, with potential benefits such as use of more moderate reaction conditions, increased yields and selectivities of soluble products, and decreased processing costs.

5.4. Conclusions

The most common reaction model describing cellulose hydrolysis proposes that reaction occurs via parallel pathways involving amorphous and crystalline cellulose. Invariably in these models, the hydrolysis rate of amorphous cellulose is much greater than that of crystalline cellulose. While this reaction model appears to match the available data, experiments to date have not confirmed the reaction network that it implies. To examine the effects of decrystallization on

the cellulose hydrolysis reaction network, we investigated mechanical decrystallization and water-promoted recrystallization on cellulose reactivity. Ball milling cellulose decreases crystallinity and increases its hydrolysis reactivity, both of which appear to support the theory of highly reactive amorphous and recalcitrant crystalline regions. However, by exposing decrystallized cellulose to the aqueous environment of acid hydrolysis we discovered that rapid recrystallization occurs and that the phase transition is complete before the onset of hydrolytic solubilization. These results contradict the current hydrolysis models describing cellulose hydrolysis as parallel reactions of amorphous and crystalline regions.

Ball-milled and recrystallized cellulose can be structurally distinguished from crystalline cellulose I precursor as a mixture of cellulose I and II using ssNMR. Decrystallization and recrystallization may also decrease crystallite size, confounding quantification of the various cellulose forms. Reacting decrystallized cellulose under ethanolysis conditions where solvent-promoted recrystallization is suppressed confirms that the reactivity of amorphous cellulose is greater than that of the recrystallized form. Consequently, we modified the current cellulose hydrolysis models by incorporating a pathway for recrystallization of amorphous cellulose to active crystalline cellulose. The reactivities of crystalline cellulose I, amorphous cellulose, and active cellulose can be described using distinct reaction rate constants. Furthermore, the rate of recrystallization is greater than any of the hydrolysis rates. The knowledge provided here can serve for further development of structure-activity relationships and cellulose conversion models and for design of processes that avoid cellulose recrystallization.

5.5. References

1.M. H. Langholtz, B. J. Stokes and L. M. Eaton, *2016 Billion-ton report: Advancing domestic resources for a thriving bioeconomy, Volume 1: Economic availability of feedstock*, 2016.

2.F. H. Isikgor and C. R. Becer, *Polymer Chemistry*, 2015, **6**, 4497-4559.

3.M. J. Climent, A. Corma and S. Iborra, *Green Chemistry*, 2014, **16**, 516-547

4.J. George and S. N. Sabapathi, *Nanotechnol Sci Appl*, 2015, **8**, 45-54.

5.H. Kargarzadeh, M. Mariano, D. Gopakumar, I. Ahmad, S. Thomas, A. Dufresne, J. Huang and N. Lin, *Cellulose*, 2018, **25**, 2151-2189.

6.H. Kang, R. Liu and Y. Huang, *Polymer*, 2015, **70**, A1-A16.

7.D. M. Alonso, J. Q. Bond and J. A. Dumesic, *Green Chemistry*, 2010, **12**, 1493-1513

8.R. Rinaldi and F. Schuth, *ChemSusChem*, 2009, **2**, 1096-1107.

9.L. R. Lynd, X. Liang, M. J. Biddy, A. Allee, H. Cai, T. Foust, M. E. Himmel, M. S. Laser, M. Wang and C. E. Wyman, *Curr Opin Biotechnol*, 2017, **45**, 202-211.

10.T. Endo, E. M. Aung, S. Fujii, S. Hosomi, M. Kimizu, K. Ninomiya and K. Takahashi, *Carbohydr Polym*, 2017, **176**, 365-373.

11.K. Wu, G. Feng, Y. Liu, C. Liu, X. Zhang, S. Liu, B. Liang and H. Lu, *Bioresour Technol*, 2018, **261**, 28-35.

12.B. Mostofian, C. M. Cai, M. D. Smith, L. Petridis, X. Cheng, C. E. Wyman and J. C. Smith, *J Am Chem Soc*, 2016, **138**, 10869-10878.

13.M. Mohan, R. Timung, N. N. Deshavath, T. Banerjee, V. V. Goud and V. V. Dasu, *RSC Advances*, 2015, **5**, 103265-103275.

14.J. A. Geboers, S. Van de Vyver, R. Ooms, B. Op de Beeck, P. A. Jacobs and B. F. Sels, *Catalysis Science & Technology*, 2011, **1**, 714-726

15.S. Sun, S. Sun, X. Cao and R. Sun, *Bioresour Technol*, 2016, **199**, 49-58.

16.R. W. Torget, J. S. Kim and Y. Y. Lee, *Industrial & Engineering Chemistry Research*, 2000, **39**, 2817-2825.

17.S. Deguchi, K. Tsujii and K. Horikoshi, *Green Chem.*, 2008, **10**, 191-196.

18.S. P. Chundawat, G. Bellesia, N. Uppugundla, L. da Costa Sousa, D. Gao, A. M. Cheh, U. P. Agarwal, C. M. Bianchetti, G. N. Phillips, Jr., P. Langan, V. Balan, S. Gnanakaran and B. E. Dale, *J Am Chem Soc*, 2011, **133**, 11163-11174.

19.D. Klemm, B. Heublein, H. P. Fink and A. Bohn, *Angew Chem Int Ed Engl*, 2005, **44**, 3358-3393.

20.G. SriBala, R. Chennuru, S. Mahapatra and R. Vinu, *Cellulose*, 2016, **23**, 1725-1740.

21.E. Johnson, *Biofuels, Bioproducts and Biorefining*, 2016, **10**, 164-174.

22.N. Sweygers, N. Alewaters, R. Dewil and L. Appels, *Sci Rep*, 2018, **8**, 7719.

23.L. R. Lynd, *Nat Biotechnol*, 2017, **35**, 912-915.

24.A. Bychkov, E. Podgorbunskikh, E. Bychkova and O. Lomovsky, *Biotechnol Bioeng*, 2019, **116**, 1231-1244.

25.S. P. Chundawat, G. T. Beckham, M. E. Himmel and B. E. Dale, *Annu Rev Chem Biomol Eng*, 2011, **2**, 121-145.

26.M. A. Rostagno, J. M. Prado, A. Mudhoo, D. T. Santos, T. Forster-Carneiro and M. A. Meireles, *Crit Rev Biotechnol*, 2015, **35**, 302-312.

27.B. Yang, Z. Dai, S.-Y. Ding and C. E. Wyman, *Biofuels*, 2014, **2**, 421-449.

28.M. Hall, P. Bansal, J. H. Lee, M. J. Realff and A. S. Bommarius, *FEBS J*, 2010, **277**, 1571-1582.

29.X. Zhao, L. Zhang and D. Liu, *Biofuels, Bioproducts and Biorefining*, 2012, **6**, 465-482.

30.L. T. Fan, Y.-H. Lee and D. R. Beardmore, *Biotechnology and Bioengineering*, 1981, **23**, 419-424.

31.Y. Pu, F. Hu, F. Huang, B. H. Davison and A. J. Ragauskas, *Biotechnol Biofuels*, 2013, **6**, 15.

32.R. Kumar, G. Mago, V. Balan and C. E. Wyman, *Bioresour Technol*, 2009, **100**, 3948-3962.

33.A.-I. Yeh, Y.-C. Huang and S. H. Chen, *Carbohydrate Polymers*, 2010, **79**, 192-199.

34.A. P. Sinitsyn, A. V. Gusakov and E. Y. Vlasenko, *Applied Biochemistry and Biotechnology*, 1991, **30**, 43-59.

35.J. S. Luterbacher, J. Y. Parlange and L. P. Walker, *Biotechnol Bioeng*, 2013, **110**, 127-136.

36.T. Jeoh, C. I. Ishizawa, M. F. Davis, M. E. Himmel, W. S. Adney and D. K. Johnson, *Biotechnol Bioeng*, 2007, **98**, 112-122.

37.V. P. Puri, *Biotechnology and Bioengineering*, 1984, **26**, 1219-1222.

38.H. Zhao, J. H. Kwak, Y. Wang, J. A. Franz, J. M. White and J. E. Holladay, *Energy & Fuels*, 2006, **20**, 807-811.

39.H. Zhao, J. Kwak, Z. Conradzhang, H. Brown, B. Arey and J. Holladay, *Carbohydrate Polymers*, 2007, **68**, 235-241.

40.L. T. Fan, Y. H. Lee and D. H. Beardmore, *Biotechnology and Bioengineering*, 1980, **22**, 177-199.

41.P. Calvini, A. Gorassini and A. L. Merlani, *Cellulose*, 2007, **15**, 193-203.

42.M. Möller, F. Harnisch and U. Schröder, *RSC Advances*, 2013, **3**, 11035-11044

43.Y. Yu and H. Wu, *AIChE Journal*, 2011, **57**, 793-800.

44.P. Phanthong, G. Guan, Y. Ma, X. Hao and A. Abudula, *Journal of the Taiwan Institute of Chemical Engineers*, 2016, **60**, 617-622.

45.H. J. Philipp, M. L. Nelson and H. M. Ziifle, *Textile Research Journal*, 1947, **17**, 585-596.

46.O. A. Battista, *Industrial & Engineering Chemistry*, 1950, **42**, 502-507.

47.S. Park, J. O. Baker, M. E. Himmel, P. A. Parilla and D. K. Johnson, *Biotechnology for Biofuels*, 2010, **3**, 10.

48.A. P. Dadi, S. Varanasi and C. A. Schall, *Biotechnol Bioeng*, 2006, **95**, 904-910.

49.J. Zhang, B. Zhang, J. Zhang, L. Lin, S. Liu and P. Ouyang, *Biotechnol Adv*, 2010, **28**, 613-619.

50.Q. Zhang, M. Benoit, K. De Oliveira Vigier, J. Barrault, G. Jégou, M. Philippe and F. Jérôme, *Green Chemistry*, 2013, **15**, 963-969

51.M. Foston and A. J. Ragauskas, *Biomass and Bioenergy*, 2010, **34**, 1885-1895.

52.F. Hu and A. Ragauskas, *BioEnergy Research*, 2012, **5**, 1043-1066.

53.P. H. Hermans and A. Weidinger, *Journal of the American Chemical Society*, 1946, **68**, 1138-1138.

54.J. A. Howsmon and R. H. Marchessault, *Journal of Applied Polymer Science*, 1959, **1**, 313-322.

55.I. L. Wadehra and R. S. J. Manley, *Journal of Applied Polymer Science*, 1965, **9**, 2627-2630.

56.D. F. Caulfield and R. A. Steffes, *TAPPI*, 1969, **52**, 1361-1366.

57.H. Hatakeyama and T. Hatakeyama, *Makromol Chem*, 1981, **182**, 1655-1668.

58.M. Kimura, Hatakeya.T and J. Nakano, *Journal of Applied Polymer Science*, 1974, **18**, 3069-3076.

59.P. Wormald, K. Wickholm, P. T. Larsson and T. Iversen, *Cellulose*, 1996, **3**, 141-152.

60.S. Ouajai and R. A. Shanks, *Cellulose*, 2006, **13**, 31-44.

61.U. P. Agarwal, S. A. Ralph, C. Baez, R. S. Reiner and S. P. Verrill, *Cellulose*, 2017, **24**, 1971-1984.

62.D. A. Cantero, M. D. Bermejo and M. J. Cocero, *The Journal of Supercritical Fluids*, 2013, **75**, 48-57.

63.M. J. Taherzadeh and K. Karimi, *Int J Mol Sci*, 2008, **9**, 1621-1651.

64.P. Bansal, M. Hall, M. J. Realff, J. H. Lee and A. S. Bommarius, *Bioresour Technol*, 2010, **101**, 4461-4471.

65.D. M. Mowery, D. J. Harris and K. Schmidt-Rohr, *Macromolecules*, 2006, **39**, 2856-2865.

66.L. Segal, J. J. Creely, A. E. Martin and C. M. Conrad, *Textile Research Journal*, 1959, **29**, 786-794.

67.R. L. Johnson and K. Schmidt-Rohr, *J Magn Reson*, 2014, **239**, 44-49.

68.P. Duan and K. Schmidt-Rohr, *J Magn Reson*, 2017, **285**, 68-78.

69.E. L. Hahn, *Physical Review*, 1950, **80**, 580-594.

70.G. Bodenhausen, R. Freeman and D. L. Turner, *Journal of Magnetic Resonance*, 1977, **27**, 3, 511-514.

71.B. M. Fung, A. K. Khitrin and K. Ermolaev, *J Magn Reson*, 2000, **142**, 97-101.

72.D. A. Torchia, *Journal of Magnetic Resonance (1969)*, 1978, **30**, 613-616.

73.D. D. Y. Ryu, S. B. Lee, T. Tassinari and C. Macy, *Biotechnology and Bioengineering*, 1982, **24**, 1047-1067.

74.S. E. Jacobsen and C. E. Wyman, in *Twenty-First Symposium on Biotechnology for Fuels and Chemicals: Proceedings of the Twenty-First Symposium on Biotechnology for Fuels and Chemicals. Applied Biochemistry and Biotechnology.*, eds. M. Finkelstein and B. H. Davison, Humana Press, Totowa, NJ, 2000, DOI: 10.1007/978-1-4612-1392-5_6, pp. 81-96.

75.M. L. Nelson, *Journal of Polymer Science*, 1960, **43**, 351-371.

76.P. Bansal, M. Hall, M. J. Realff, J. H. Lee and A. S. Bommarius, *Biotechnol Adv*, 2009, **27**, 833-848.

77.A. C. O'Sullivan, *Cellulose*, 1997, **4**, 173-207.

78.Z. Ling, T. Wang, M. Makarem, M. Santiago Cintrón, H. N. Cheng, X. Kang, M. Bacher, A. Potthast, T. Rosenau, H. King, C. D. Delhom, S. Nam, J. Vincent Edwards, S. H. Kim, F. Xu and A. D. French, *Cellulose*, 2019, **26**, 305-328.

79.C. Driemeier and G. A. Calligaris, *Journal of Applied Crystallography*, 2011, **44**, 184-192.

80.U. P. Agarwal, R. S. Reiner and S. A. Ralph, *Cellulose*, 2010, **17**, 721-733.

81.M. L. Nelson and R. T. O'Connor, *Journal of Applied Polymer Science*, 1964, **8**, 1325-1341.

82.U. P. Agarwal, S. A. Ralph, R. S. Reiner and C. Baez, *Cellulose*, 2015, **23**, 125-144.

83.R. H. Newman, *Cellulose*, 2004, **11**, 45-52.

84.J. H. Wiley and R. H. Atalla, *Carbohyd Res*, 1987, **160**, 113-129.

85.R. H. Newman and T. C. Davidson, *Cellulose*, 2004, **11**, 23-32.

86.P. Bhama Iyer, S. Sreenivasan, P. K. Chidambareswaran and N. B. Patil, *Textile Research Journal*, 1984, **54**, 732-735.

87.B. F. Wood, A. H. Conner and C. G. Hill, *Journal of Applied Polymer Science*, 1989, **37**, 1373-1394.

88.M. Ioelovich, A. Leykin and O. Figovsky, *Bioresources*, 2010, **5**, 1393-1407.

89.S. Nam, A. D. French, B. D. Condon and M. Concha, *Carbohydr Polym*, 2016, **135**, 1-9.

90.M. Akerholm, B. Hinterstoisser and L. Salmen, *Carbohydr Res*, 2004, **339**, 569-578.

91.J.-H. Lin, Y.-H. Chang and Y.-H. Hsu, *Food Hydrocolloids*, 2009, **23**, 1548-1553.

92.R. N. Ibbett, D. Domvoglou and D. A. S. Phillips, *Cellulose*, 2007, **15**, 241-254.

93.L. T. Fan, M. M. Gharpuray and Y. H. Lee, *Cellulose hydrolysis. Biotechnology monographs. Volume 3*, Springer-Verlag,New York, NY; None, 1987.

94.B. B. Hallac and A. J. Ragauskas, *Biofuels, Bioproducts and Biorefining*, 2011, **5**, 215-225.

95.F.-X. Collard and J. Blin, *Renewable and Sustainable Energy Reviews*, 2014, **38**, 594-608.

96.C. M. Cai, T. Zhang, R. Kumar and C. E. Wyman, *Green Chemistry*, 2013, **15,** 3140-3145

CHAPTER 6

Rapid Depolymerization of Decrystallized Cellulose to Soluble Products via Ethanolysis under Mild Conditions

6.1. Introduction

As the main structural component of plant matter, cellulose is the most abundant biopolymer on earth and its depolymerization to platform molecules is essential for the utilization of lignocellulose biomass as a renewable resource.[1, 2] However, processes that convert cellulose into its constituent monomers are not economically competitive,[3, 4] due in part to the highly crystalline structure that confers chemical and biochemical recalcitrance.[5] The enzymatic hydrolysis route suffers from low reaction rates while homogeneous acid catalyzed hydrolysis necessitates severe reaction conditions that promote undesirable degradation reactions.[6-8] Pyrolysis achieves rapid depolymerization rates, but at the expense of selectivity.[9-11]

Approaches to increase product yields and avoid degradation include reactor design, catalyst use, or addition of reactants and co-solvents that aim to limit the exposure of desired products to the severe environment.[12-15] Nevertheless, the overall goals of cellulose utilization strategies – maximizing conversion, product yields and selectivities, while simultaneously minimizing process requirements and costs have not been commercially successful, leaving the potential of second generation biofuels unrealized.[3]

Physically altering the structural organization of cellulose can impact its reactivity and facilitate subsequent efforts to depolymerize it.[16-21] Accordingly, decrystallization pretreatments such as mechanochemical (milling) or swelling in acids, ionic liquids, or ammonia increase the

reactivity of cellulose.[16-23] Greater cellulose reactivity increases monomer yields and selectivity at mild conditions but must be balanced with the increased energy input and/or chemical waste production.[24]

The increased reactivity observed post decrystallization has been attributed to increased content of highly reactive amorphized cellulose regions.[16, 17, 20, 25] However, in chapter 5 we showed that amorphous cellulose undergoes rapid recrystallization in water during hydrolysis, significantly reducing reactivity.[26] Therefore, the benefits of decrystallization for enhancing cellulose depolymerization are not fully realized in aqueous-based processes, since the amorphized cellulose recrystallizes at greater rates than cellulose depolymerization.[26, 27] Water-induced cellulose recrystallization likely renders decrystallization pretreatments, especially mechanochemical decrystallization, economically uncompetitive.

Unlike water, organic solvents have not been found to induce recrystallization.[27] Therefore, ethanolysis, splitting the glycosidic bond with ethanol, rather than water, has the potential to increase cellulose conversion and yields by circumventing the solvent induced recrystallization that is a barrier to hydrolysis-based processes.[28-31] The associated benefit of reduced reaction severity can thus compensate for the energy required for decrystallization as part of an economically competitive and energy efficient process. As shown in Scheme 1, products from ethanolysis are ethyl-glucopyranoside, 5-ethoxymethylfurfural (EMF), and ethyl levulinate, direct analogs to the well-known platform chemicals obtained from hydrolysis.[28, 30, 32] Ethanol is an especially attractive reactant and solvent as it is inexpensive and already produced at a commercial scale from renewable feeds.[33] The heat capacity of ethanol is significantly lower than that of water, thereby reducing heat duties and potentially offsetting energy consumption by ball milling or other decrystallization methods.[34]

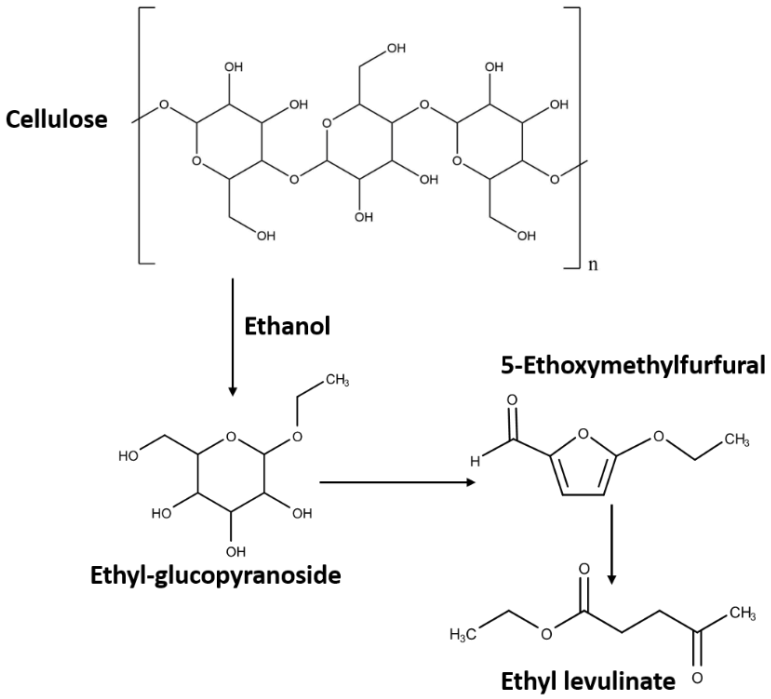

Scheme 6.13. Ethanolysis of cellulose to ethyl-glucopyranoside and decomposition to 5-Ethoxymethylfurfural and Ethyl levulinate. Ethanolysis is an analogous reaction to hydrolysis where instead of the breaking of glycosidic bond by addition of a water molecule, an ethoxy group is added.

Previous attempts at cellulose ethanolysis employed conditions that promoted byproduct formation, including formation of diethyl ether and diethoxy methane.[28, 35] Conversion to diethyl ether is especially problematic as the economics and environmental benefits of the solvent-based process rely on ethanol reuse. Considering that diethyl ether production rates increase with increasing temperature and/or acid concentration,[36, 37] we examined the combination of mechanical decrystallization and ethanolysis at mild conditions where byproduct formation should not be problematic and realize the full potential of ethanolysis-based cellulose depolymerization.

In this study, cellulose was first ball-milled to produce highly amorphous substrate and then subjected to mild ethanolysis conditions using hydrochloric acid as the catalyst. Cellulose conversion and soluble product yields were quantified to demonstrate potential benefits. Residual

cellulose was analyzed with X-ray diffraction and solid state nuclear magnetic resonance (ss-NMR) to understand structural changes in the cellulose that occur during ethanolysis and provide mechanistic insight. The results presented here suggest that ethanolysis of decrystallized cellulose could be a promising approach for the selective production of renewable platform chemicals that will guide future work in this promising area.

6.2. Methodology

6.2.1. Materials

Avicel PH101 cellulose (average particle size of 50 μm, 100% purity with 3–5% moisture content), 0.1 M hydrochloric acid standard, cellobiose > 98%, glucose > 99.5%, 5-hydroxymethyl furfural (HMF) > 99% purity, 5-ethoxymethyl furfural (EMF) > 99%, purity ethyl levulinate> 99%. Acetone and ethanol ACS grade were purchased from Pharmco-Aaper. All chemicals were used as received.

6.2.2. Cellulose ball milling

Microcrystalline cellulose (Avicel PH101) was decrystallized via ball milling pretreatment. Briefly, 1.0 gram of cellulose was put in a stainless-steel cylinder (18 mm diameter x 55.5 mm length, 10 mL total volume). Three stainless steel balls, two balls with 9.5 mm diameter and one ball with 15.85 mm diameter, were put in the ball milling cylinder. The cylinder was attached to a Retsch MM200 vibratory shaker and the cellulose was milled for 50 minutes. The temperature of the milling was not controlled.

6.2.3. Cellulose ethanolysis

Cellulose was depolymerized under ethanolysis conditions to determine the effects of decrystallization on the conversion and soluble product yields. The treatment was similar to the one carried out in our previous study.[26] The ethanolysis solvent was prepared by diluting 37% HCl

to 0.1 M in ethanol. Cellulose substrate (0.25 grams) was mixed with 5 mL of the ethanol solution in a 15 mL heavy wall pressure glass reactor sealed with a screw cap and a Viton O-ring. The glass reactor was submerged in a preheated oil bath. The reaction temperature was set to 410 K. Using a modified screw top with an inserted omega K type thermocouple it was determined that the reaction temperature was reached within 200 seconds. After the reaction, the mixture was cooled in ice bath, centrifuged, and the solid and liquid products were separated. The liquid product was analyzed with HPLC. The solid residue was additionally washed with acetone twice to remove any remaining soluble products, centrifuged, dried at 340 K, and weighed to determine conversion. The solid residue was subjected to further structural analysis.

6.2.4. Cellulose hydrolysis

Cellulose was hydrolyzed at the same conditions and in the similar manner as ethanolysis and described previously. Instead of ethanol, however, the solvent was 0.1M HCl in water. The liquid and solid products were separated analyzed as previously described.

6.2.5. Cellobiose and glucose ethanolysis

Small carbohydrates such as glucose and cellobiose were subjected to ethanolysis to determine the cause for the stoichiometric ratio of the α and β ethyl-glucopyranoside ethanolysis products. The ethanolysis conditions were identical to those used for cellulose. Cellobiose and glucose did not dissolve in the ethanol solvent at room temperature. The mixture was treated at 410 K for 30 minutes. After 30 minutes the reactor was cooled in ice bath. After cooling there was no solid residue left, indicating all of the substrate was converted. The liquid was analyzed with HPLC to determine the quantities of alpha and beta ethyl-glucopyranoside.

6.2.6. X-ray diffraction

X-Ray diffraction (XRD) analysis was carried out with Rigaku Geigerflex diffractometer. Cu Kα radiation at 37.5 kV and 25 mA was used for sample irradiation. Accumulation time of 1 second and step size of 0.05° were used for recoding diffraction data. The areas of the diffractograms of all samples were normalized prior to plotting and analysis.

6.2.7. Solid-State Nuclear Magnetic Resonance (ss-NMR)

NMR experiments were performed using a Bruker DSX400 spectrometer operating at a ^{13}C resonance frequency of 100 MHz, using a 4-mm magic-angle spinning probe in double-resonance mode at a spinning frequency of 9 kHz and at room temperature. The ^{13}C chemical shifts were externally referenced on the neat TMS scale using the carboxyl peak of α-glycine at 176.49 ppm. Typical 90° pulse lengths were 3.6 μs for ^{1}H and 4 μs for ^{13}C. MultiCP[38] with composite-pulse excitation and storage[39] was used to obtain nearly quantitative ^{13}C spectra. Five blocks of CP were implemented with 90–100% amplitude ramps on the ^{1}H channel. The contact time for each CP period was 1.1 ms, resulting in a total combined CP contact time of 5.5 ms. The delays for ^{1}H repolarization were 4 s for all samples, while the recycle delay was 8 s. A rotation-synchronized Hahn spin echo[40] was used to achieve dead-time-free detection, generated by a 180° pulse with EXORCYCLE[41] phase cycling after the last multiCP block. During the 18.7-ms detection, proton decoupling with the SPINAL64 scheme[42] was applied, at a ^{1}H strength of $\nu_1 \approx 85$ kHz. The number of scans averaged was 512 for MCC, 1280 for MCC-BM50, 768 for MCC-BM50-SP, and 832 for MCC-BM50-AC (see nomenclature defined below in 2.11).

A 5-s T_{1C} filter[43] was used to remove signals from segments with short ^{13}C spin-lattice relaxation times T_{1C} due to fast segmental motions, such as non-crystalline cellulose C6 side groups, retaining the sharp crystalline-C6 peaks of cellulose I and II, which are well resolved. The

same numbers of scans as for the multiCP spectra were averaged. Direct polarization with 2-s recycle delay was used to select signals of mobile segments with fast T_{1C} relaxation, yielding the band of non-crystalline cellulose C6 complementary to the T_{1C}-filtered crystalline peaks. For all samples 4096 scans were averaged. Zirconia rotors (Bruker Biospin) were used as received for magic-angle spinning of all samples.

6.2.8. High Performance Liquid Chromatography (HPLC) analysis

The liquid obtained after ethanolysis and hydrolysis was analyzed for soluble products using HPLC (Agilent 1200 series) equipped with a diode array detector (DAD) and refractive index detector (RID). Phenomenex Rezex ROA-Organic Acid H+ (8%) column was used for separation of product molecules. The mobile phase used for analysis was deionized chromatography water (Sigma) flowrate was 0.6 mL/min. The column and the RID detector were both kept at 35 °C during analytical runs, while the UV-Vis detection wavelength was set to 284 nm. Calibration curves were determined from analysis of mixtures containing known concentrations of standards at 0.25, 0.5, 0.75, 1, 1.25, 1.5, 1.75, 2, and 2.5 g/L.

6.2.9. Gas Chromatography Mass Spectrometry Analysis (GC-MS)

Analysis of the liquid after ethanolysis reaction for detection and quantification of diethylether and dietoxymethane was carried out by GC-MS. Briefly, the liquid was diluted 10 times in dichloromethane and analyzed using a GC equipped with a mass spectrometer detector (QP 2010 SE system, Shimadzu) and a SHRXI-5MS column (30 m × 0.25 mm ID × 0.5 μm film thickness). Helium was the carrier gas (2 sccm). The initial column temperature was 40 °C, which was increased by 3 °C/min until reaching a maximum temperature of 300 °C. The injector temperature was held at 300 °C and the injected sample volume was 3 μL.

6.2.10. Sample Nomenclature

Table 6.1. provides the sample labeling rules to be used as reference further in the text.

Table 6.9. Nomenclate of cellulose samples subjected to different treatments

Suffix to MCC	Sample Treatment
-BM50	Ball-milled for the indicated duration.
-E60	Ethanolyzed with 0.1M HCl in ethanol at 410 K for the indicated duration of time.
-H60	Hydrolyzed with 0.1M HCl in water at 410 K for the indicated duration of time.
-E90-E90	Ethanolyzed with 0.1M HCl in ethanol for the indicated duration of time; washed with acetone, dried at 340 K, and ethanolyzed a second time for the indicated duration.
-HLW60	Subjected to treatment in hot liquid water at 430 K for the indicated duration of time
-E/DMSO60	Ethanolyzed with 0.1M HCl in 90% ethanol and 10% DMSO for the indicated duration of time
-E/EG60	Ethanolyzed with 0.1M HCl in 90% ethanol and 10% ethylene glycol for the indicated duration of time
-E/H_2O60	Ethanolyzed with 0.1M HCl in 90% ethanol and 10% water for the indicated duration of time

6.3. Results and Discussion

Mechanical decrystallization can overcome cellulose recalcitrance towards depolymerization attributed to its crystallinity.[16, 44] Unfortunately, contacting decrystallized cellulose with water leads to rapid recrystallization and an associated decrease in its reactivity.[26] Replacing water used for depolymerization of cellulose via hydrolysis with ethanol and ethanolysis can overcome some

of the problems associated with cellulose resistance to chemical depolymerization previously attributed to its crystallinity and other structural features.[26]

Ethanolysis has been the subject of only a handful of previous studies, possibly due to concerns about co-production of diethyl ether under the acidic reaction conditions required for depolymerization.[28, 35, 45] Therefore, mechanical decrystallization followed by ethanolysis may permit depolymerization at mild conditions which avoid diethyl ether formation.

We performed a series of experiments to examine ethanolysis of mechanically decrystallized cellulose. Table 6.2. provides cellulose conversion and product yields measured for key ethanolysis experiments. As a starting point, we subjected microcrystalline cellulose (MCC) to ethanolysis treatment at a reaction time of 60 minutes, MCC-E60, (Table 6.2., entry 1) to determine the reactivity of highly crystalline cellulose. Ethanolysis of MCC resulted in 3±1% cellulose conversion with ethyl-glucopyranoside as the sole product formed at yields greater than 0.1%. Both the α and β forms of ethyl-glucopyranoside were formed, always in a 1:2 molar ratio; based on experiments with glucose and cellobiose (details contained in the Methodology section), the 1:2 molar ratio appears to be determined by thermodynamic equilibrium and indicative of rapid interconversion between the two isomers. Accordingly, ethyl-glucopyranoside yields are reported as the sum of the two isomers.

Table 6.10. Results of cellulose depolymerization to soluble products via ethanolysis.

Sample[a]	Cellulose Conversion (%)	Ethyl-Glucopyranoside Yield (%)
1. MCC-E60	3 ± 1	2.04 ± 0.04
2. MCC-BM50-E60	38 ± 2	24.5 ± 0.2
3. MCC-BM50-H60	21 ± 1	18 ± 1[b]
4. MCC-BM50-E90	38 ± 2	26.7 ± 0.3
5. MCC-BM50-E90-E90	53 ± 2	34 ± 1
6. MCC-BM50-E90-E90-HLW60	62 ± 1	35.2 ± 0.2
7. MCC-BM50-E/DMSO60	15 ± 2	4.1 ± 0.1
8. MCC-BM50-E/EG60	40 ± 1	25 ± 0.4
9. MCC-BM50-E/H_2O60	48 ± 1	26 ± 2
10. MCC-BM50-E60-BM50-E60	62 ± 1	42.4 ± 0.2

[a] See nomenclature in Table 6.1.
[b] Hydrolysis yielded glucose

Cellulose ethanolysis was performed at 410 K using 0.1 M HCl as an ethanol-stable catalyst. These conditions are milder than typically used for hydrolysis or previously studied for ethanolysis and were selected in part because they were not expected to promote diethyl ether formation. Ethanolysis of MCC confirms that the conditions selected are not severe enough for depolymerization of crystalline cellulose consistent with literature observations.

Having confirmed that the conditions were sufficiently mild, MCC was milled for 50 min in a vibratory ball mill, a treatment which we previously[26] found resulted in near complete

amorphization of MCC. The ball milled sample was then subjected to the same ethanolysis treatment as before (Table 6.2., entry 2). Remarkably, cellulose conversion increased to 38±2%, while the yield of ethyl-glucopyranoside to 24.5%. The discrepancy between ethyl-glucopyranoside yield and the conversion can be attributed to formation of unidentified soluble products, potentially oligomeric species and other carbohydrate isomers.

The only degradation products observed in yields greater than detection limits (0.01%) were 5-EMF, 5-HMF, and furfural. A previous study on ethanolysis observed similar byproducts, but with co-production of ethyl levulinate and other side products that are not formed here due to the much milder depolymerization temperatures made effective by ball milling (443 K vs 410 K).[28] The presence of the furanic compounds at trace levels indicates that the carbohydrate products are relatively stable under the mild reaction conditions; the stability of the primary products is further supported by the absence of ethyl levulinate, indicating that EMF conversion is also suppressed, meaning that these conditions are suitable for selective carbohydrate production.

Diethyl ether was not detected in the reaction mixture at concentrations greater than its detection limit (detection limit was 0.5% due to partial co-elution with ethanol), satisfying the need to minimize ethanol consumption by dimerization and in contrast with a previous study that used crystalline cellulose as a feed and reported 0.2% diethyl ether yield at 473 K (60 min reaction time and 1 wt% sulfuric acid). Similarly, diethoxymethane, the undesired product formed by ethanolysis of formic acid, was found in a previous study after reaction at 473 K, but was not observed here. Collectively, these results confirm that mild conditions can prevent undesirable side reactions of the ethanol solvent, surmounting a major problem that previous studies encountered due to the more aggressive reaction conditions they examined.

As a further control, ball-milled MCC was subjected to hydrolysis conditions, again for 60 min and at 410 K with 0.1 M HCl as catalyst (Table 6.2., entry 3). As expected, hydrolytic conversion of decrystallized cellulose was much less than observed under ethanolysis conditions (21±1%), consistent with water-induced recrystallization resulting in re-stabilization of the cellulose.[26]

To increase ethanolysis conversion and yields, the ethanolysis reaction time was increased from 60 to 90 min, while holding all other reaction variables constant (Table 6.2., entry 4). Surprisingly, increasing the reaction time by 50% did not result in a commensurate increase of the conversion and only a marginal increase of the ethyl-glucopyranoside yield was observed. Comparison of entries 2 and 4 in Table 6.1., therefore, suggests that ethanolytic conversion of decrystallized cellulose reaches a limit of approximately 40%, potentially due to exhaustion of reactive amorphous cellulose. To investigate further we performed a time study of cellulose ethanolysis and analyzed both the liquid products and the solid residue.

Figure 6.1. plots the conversion and the yield of ethyl-glucopyranoside of MCC-BM50 after ethanolysis as function of reaction time (410 K, 0.1 M HCl). Most conversion and release of soluble products occurred within the first 30 min of the reaction; for reaction times greater than 30 min, only minor increases of the ethyl-glucopyranoside are observed and conversion ceases. As expected, soluble product yields increase in parallel with cellulose conversion. Degradation products such as ethoxymethyl furfural, HMF, and furfural had a combined yield of less than 0.6% even after 120 minutes of reaction time. For reference, the yield of degradation products as a function of time is provided in Figure D1 in Appendix D. Since the yield of ethyl-glucopuranoside does not converge with the measured conversion, it is unlikely that the discrepancy could be due to presence of oligomers, as they would be ethanolyzed otherwise. HPLC chromatograms presented in Appendix D Figure D2 showing ethanolysis solutions after 5 and 15 minutes of

ethanolysis illustrate the disappearance of oligomeric species and their conversion to ethyl-glucopyranoside with prolonged reaction time.

A reference kinetic study was carried out for cellulose hydrolysis at the same temperature and acid concentration conditions. Unlike ethanolysis, cellulose hydrolysis results in conversion and yields that are lower than those obtained with ethanolyssis. Even after 120 minutes of hydrolysis the conversion is only 28%. Detailed kinetic data is available in Figure D3 in Appendix D for reference. Unlike ethanolysis, hydrolysis data suggest that further increases of reaction time beyond 120 min may lead to further increases in cellulose conversion and soluble product yield; however, since ethanolysis significantly outperforms hydrolysis in this time interval, further increases of conversion and yields are not sufficient to justify extending reaction times.

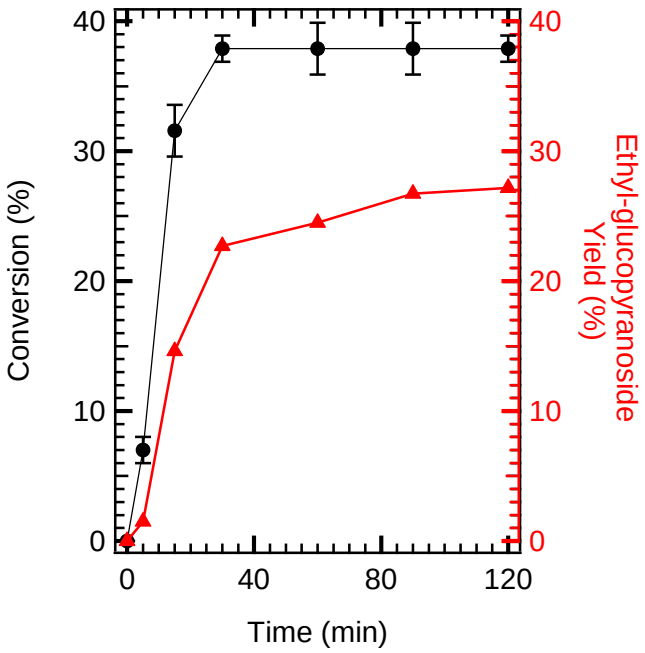

Figure 6.33. Time study of ethanolysis of ball-milled cellulose. Plotted are conversion (●) and ethyl-glucopyranoside yield (▲). Reaction conditions – 0.1M HCl in ethanol, 410 K.

Figures 6.1. and Figure D3 show that the initial rate of ethanolysis is approximately 3-times greater than the initial hydrolysis rate. Figure 6.1. does not make clear why increasing cellulose

conversion and yield level off for times greater than 30 min. To investigate further, the ball-milled and ethanolyzed sample was subjected to a second ethanolysis treatment (Table 6.2., Entry 5), with the result that the cumulative conversion increased to 53±2%. This observation implies that either an equilibrium of the ethanolysis reaction exists between the soluble products and the solid substrate or that solubility limit of the soluble products is reached ceasing further release.

To address potential solubility issues, we treated a sample subjected previously to two ethanolysis treatments to treatment in hot liquid water (Table 6.2., Entry 6). The hot liquid water treatment increased cellulose conversion to 62±1%, but without a corresponding increase in monomer yield. This observation suggests the presence of trapped oligomers within the cellulose matrix that cannot be accessed by the ethanol solvent but are accessible to water. Confirming this explanation, a chromatogram of the liquid products revealed the presence of oligomers as soluble products in the water medium after the hot liquid water treatment of the ethanolyzed sample. The raw chromatogram data is available in Figure D4 in Appendix D.

The limiting conversion behavior shown in Figure 6.1. suggests that ethanolysis of ball-milled decrystallized cellulose involves a complex mechanism consisting of reactions, product solubilization, and potentially solid-state phase changes including recrystallization. To elucidate the structural changes that the solid cellulose substrate undergoes, the samples obtained after ethanolysis were analyzed using X-ray diffraction (XRD) and solid-state NMR. Figure 6.2. shows the XRD diffractograms of MCC-BM50 ethanolyzed at different reaction times. The diffractogram of MCC-BM50 consists of a single broad peak, characteristic of amorphous cellulose. The broad band does not change in either intensity or location after 5 minutes of ethanolysis, confirming that solvent-induced recrystallization is suppressed. After 30 minutes (38% cellulose conversion), sharp peaks characteristic of cellulose I are well formed in the diffractogram, indicating increase

of the relative content of crystalline regions. The increased crystallinity observed after 30 min of ethanolysis treatment is presumably due in part to preferential removal of amorphous chains, leaving behind crystalline regions.

Further increases in ethanolysis reaction time lead to continued sharpening and increase of the relative intensity of the cellulose I peaks. Since the sharpening of these peaks occurs without increases in cellulose conversion, the increased crystallinity observed after 30 min must be due to solid state re-arrangement of the cellulose chains or recombination of crystallite surfaces. Accordingly, Figure 6.2. implies that ethanolysis depolymerization competes kinetically with cellulose restructuring to assume a more stable form, a competition which could be limiting conversion and yields. Regardless, the rate of re-structuring found in ethanol is much less than that observed in water; as we showed in Chapter 5 ball-milled cellulose recrystallizes rapidly in aqueous environment (see Figure D5 in Appendix D for X-ray diffractograms for reference of hydrolyzed ball-milled samples), supporting the hypothesis that ethanolysis effectively avoids the undesired effects of water-induced recrystallization occurring under hydrolytic conditions.

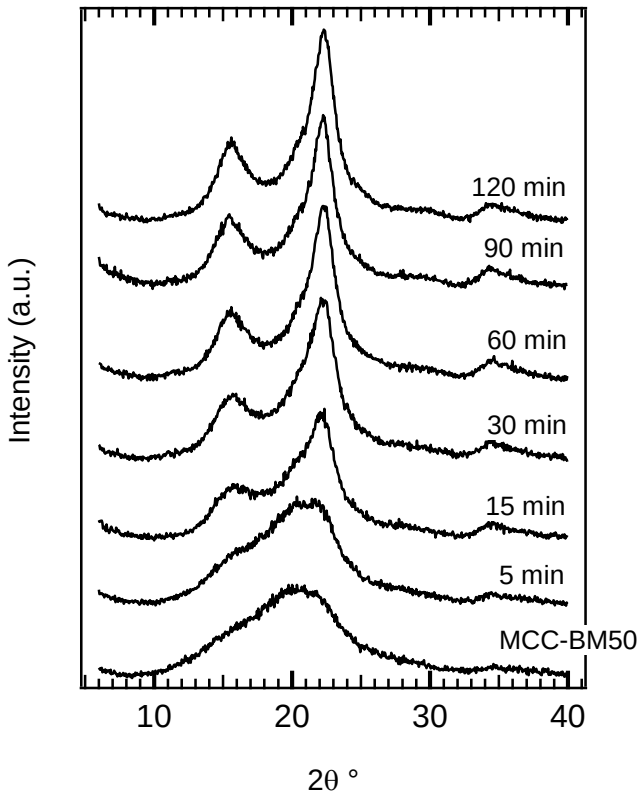

Figure 6.34. X-ray diffractograms of ball-milled cellulose subjected to ethanolysis for different periods of time.

To provide further structural detail we analyzed select cellulose samples with solid-state NMR. Figure 6.3. plots the spectra of MCC, MCC-BM50, and MCC-BM50-E90-E90. Comparison between the signals of MCC and MCC-BM50 reveals that ball milling reduces the spectral complexity consistent with sample amorphization. The regions between 80 and 92 ppm and 60 and 67 ppm assigned to C4 and C6 carbons in the glucose unit. The regions between 87 and 92 ppm and 64 and 67 ppm, attributed to crystalline interior cellulose chains, nearly completely disappear after ball milling. The signals between 80 and 87 ppm and 60 and 64 ppm, attributed to surface chains and amorphous cellulose remain, indicating that the substrate nearly completely decrystallized. Treating MCC-BM50 in ethanol at the same conditions as used for

depolymerization, but in the absence of acid, does not result in significant spectral changes indicative of crystallinity increase (reference NMR spectra of ball-milled cellulose before and after ethanol treatment in the absence of acid are provided in Figure D6 in Appendix D). After subjecting the sample to two ethanolysis treatments, however, the crystalline peaks partially recover in intensity confirming the increase in crystallinity as revealed by XRD. Interestingly, the signals at 80 and 87 ppm and 60 and 64 ppm are greater in intensity than the highly crystalline MCC, suggesting greater content of non-crystalline domains and surface chains in the ethanolyzed sample and indicating crystallites with smaller size than MCC. Most importantly, the NMR analysis reveals that little, if at all, presence of cellulose II after ethanolysis. This contrasts with depolymerization of decrystallized cellulose in water where structural transformation of amorphous to crystalline cellulose results in both cellulose I and II allomorphs.

The increased crystalline content from 5% to 37%, as calculated by integrating the crystalline and non-crystalline regions of the C4 signal, cannot be fully accounted for by conversion of amorphous cellulose. Assuming the only mechanism to increase the substrate's crystallinity is depolymerization of amorphous cellulose to soluble products and recalling that the initial crystallinity 5%, 53% conversion of MCC-BM50-E90-E90 should result in a final crystallinity of 11% – not 37%. The apparent discrepancy indicates that crystallinity must increase due to a

mechanism other than solubilization of amorphous cellulose, which we hypothesize is scission of strained bonds and relaxation of the polymer chains to crystalline organization.

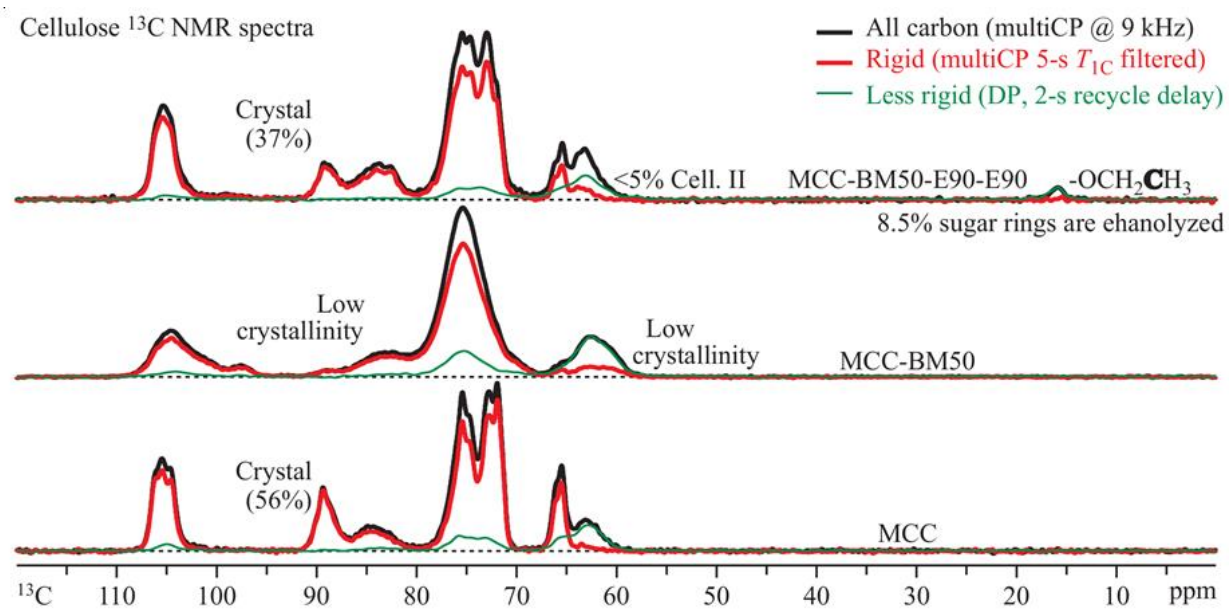

Figure 6.35. Solid state NMR spectra of MCC, MCC-BM50, MCC-BM50-E90 comparing the effects of decrystallization and ethanolysis on cellulose structure. The signals between 80-90 ppm and 60-70 ppm attributed to C4 and C6 carbons in the glucose unit, respectively. Each of the two signals exhibit a sharp peak associated with crystalline and a broad peak attributed to amorphous or non-crystalline cellulose

In addition to crystallinity features, NMR analysis reveals a peak near 15 ppm that indicates presence of aliphatic carbon in the residual cellulose. We attribute the aliphatic peak to ethoxy groups that are the product of glycosidic bond scission followed by attachment of ethanol to the C1 carbon in the solid state. This finding indicates that ethanol is incorporated both in soluble products as well as in the cellulose itself. The effect of the ethoxy chain ends on the reactivity of cellulose towards ethanolysis depolymerization is not clear.

The data presented in Figures 6.1.-6.3. clearly indicate that substantial recrystallization occurs during ethanolysis of ball-milled cellulose substrates. Furthermore, comparison of NMR data with

mass balance indicates solid state recrystallization occurs in parallel with depolymerization. Accordingly, we hypothesized that recrystallization occurs preferentially at the solvent-cellulose interface, resulting in a nanoscale crystalline barrier which limits further access of the ethanol reactant to the underlying oligomeric chains, likely due to surface interactions between cellulose crystallites. This hypothesis motivates approaches which disrupt the recrystallization and formation of the crystalline barrier by preventing collapse of amorphous chains undergoing ethanolysis depolymerization into crystalline organization and interaction between crystallite surfaces. Hypothetically, this would improve reactant access to the cellulose chains, thereby increasing conversion. Two approaches were evaluated: 1) use of cellulose swelling co-solvents and 2) repetitive ball milling.

Cellulose swelling co-solvents have the potential to decrystallize crystalline cellulose and/or prevent recrystallization of amorphous cellulose in the first place.[27, 46, 47] Unfortunately, ethanol on its own has limited cellulose capacity and a co-solvent must be selected that can swell cellulose without decreasing the activity of the acid proton catalyst.[47, 48] Entries 7-9 in Table 6.2. provide guidance. Entry 7 utilizes a DMSO co-solvent at 10 wt% relative to ethanol. DMSO appears to be an obvious selection for a swelling co-solvent, due to its ability to swell cellulose by 200% on a volume basis.[49] Interestingly, Entry 7 indicates that DMSO is a poor choice for co-solvent, resulting in decreased conversion from 38±2% to 15±1%. Figure 6.4. shows the x-ray diffractogram of the sample ethanolyzed with DMSO as a co-solvent. The diffraction peaks are less resolved when compared to 60 min ethanolysis in pure ethanol, suggesting successfully suppressing relaxation of the structure; however, use of DMSO decreased conversion, consistent with proton association with the highly basic DMSO co-solvent rather than cellulose.[48]

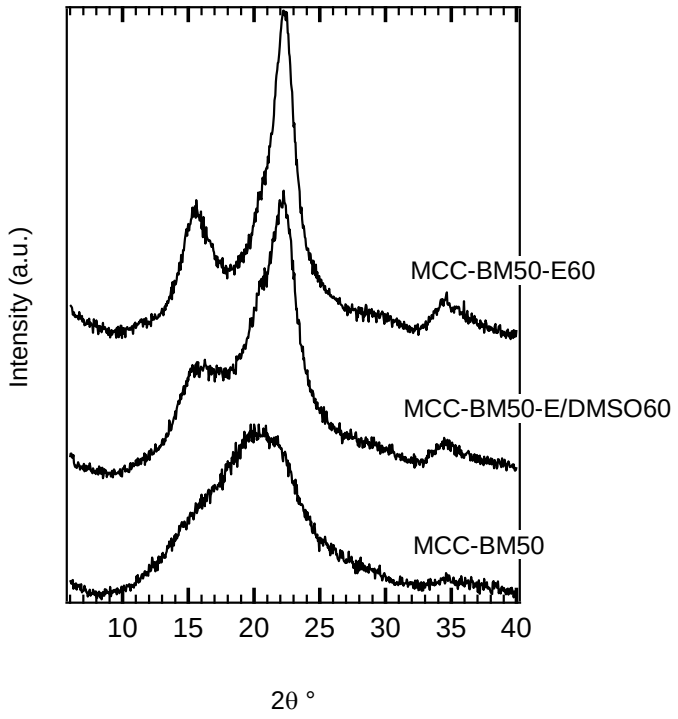

Figure 6.36. Investigating the effects of adding a co-solvent to ethanol on the cellulose structure during ethanolysis. Comparison of the X-ray diffractograms of cellulose samples subjected to ball milling (MCC-BM50), ball milling and ethanolysis in 90% etnanol and 10% DMSO for 60 minutes (MCC-BM50-E/DMSO60), and ball milling after ethanolysis for 60 minutes (MCC-BM50-E60). The

Based on the observations made with DMSO, the effects of swelling co-solvents with less proton affinity than DMSO were investigated, specifically ethylene glycol[50] and water (Entries 8 and 9 in Table 6.2.), both of which swell cellulose more effectively than ethanol and neither of which is strongly basic.[48] Both of the weakly basic co-solvents achieved the desired effect of increasing cellulose conversion. Interestingly, water was more effective than ethylene glycol as a co-solvent, increasing cellulose conversion from 38±2% to 48±2% under the same conditions. Entry 6 (Table 6.2.) suggests that water may play dual roles of cellulose swelling and oligomer solubilization, accounting for the superior performance of water compared with ethylene glycol. Moreover, the swelling and solubilization effects of water apparently counter balance its tendency

to promote spontaneous cellulose recrystallization.[26, 48] Interestingly, X-ray analysis shown in Figure 6.5. reveals that the use of ethylene glycol and water as co-solvents results cellulose residue with similar crystallinity as was found after similar treatment in pure acidified ethanol. Accordingly, the conversion in ethanol-water may be interpreted as suppressed solvent-induced recrystallization due to increased cellulose swelling.

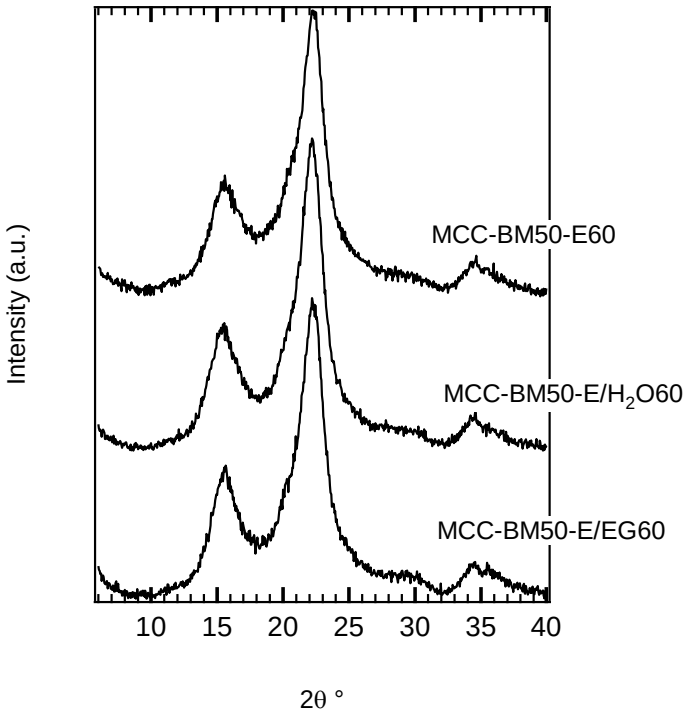

Figure 6.37. Investigating the effects of adding a co-solvent to ethanol on the cellulose structure during ethanolysis. Comparison of the X-ray diffractograms of cellulose samples subjected to ball milling and ethanolysis (MCC-BM50-E60), ethanolysis with 90% ethanol and 10% water (MCC-BM50-E/H_2O60), ethanolysis with 90% ethanol and 10% ethylene glycol (MCC-BM50-E/EG60).

Repeated ball milling and ethanolysis was also investigated as an alternative to the use of co-solvents for disruption of the crystalline cellulose nanobarrier. Entry 10 consists of sequential treatment by ball milling, ethanolysis, ball milling, and ethanolysis. Consistent with the disruption hypothesis, cellulose conversion for the repetitive treatment corresponds to 62±1% with 42%

monomer carbohydrate yield, still with less than 1% yield of degradation products such as EMF. Accordingly, sequential ball milling and ethanolysis is an effective approach for rapid cellulose depolymerization for selective production of monomers under mild reaction conditions, a performance combination that other depolymerization techniques have not yet produced.

The conversion, yield, XRD, and NMR data provide sufficient evidence to devise a reaction scheme, as summarized in Scheme 2. Ball milling results in cellulose decrystallization, yielding a reactive substrate. Unlike reaction under hydrolytic conditions, ethanolytic depolymerization of decrystallized cellulose results in rapid formation of soluble products. Ball milling and use of ethanol solvent enables cellulose depolymerization to occur at mild temperature (410 K), which limits carbohydrate degradation and unwanted reaction of the solvent to form byproducts to maintain high yield. Cellulose recrystallization occurs under ethanolysis conditions, albeit at much slower rates than under hydrolytic conditions and via a reactive mechanism that involves chain scission and relaxation. Cellulose recrystallization occurs at the solvent-substrate interface, resulting in formation of a nanoscale barrier that prevents further depolymerization and traps oligomers within the crystalline cellulose matrix. The formation of crystalline barrier can be disrupted by the use of cellulose swelling co-solvents. Alternatively, a sequential depolymerization and ball milling decrystallization is an effective strategy for increasing cellulose conversion and yields of soluble products – without promoting their subsequent degradation.

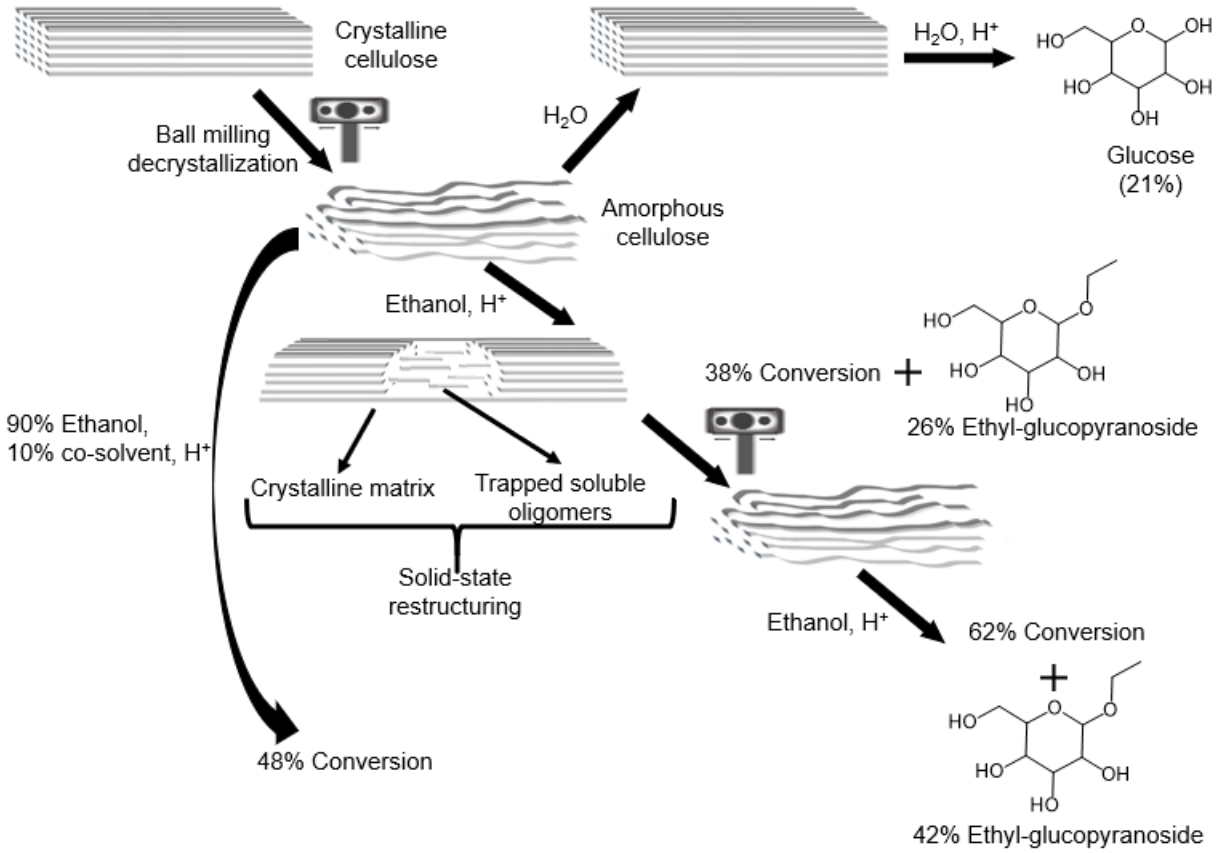

Scheme 6.14. Summary of conversion of decrystallized cellulose via ethanolysis at mild conditions.

6.4. Conclusions

Combining ball milling and ethanolysis constitutes a new approach to mild cellulose de-polymerization, potentially reducing the costs of producing second generation biofuels and bio-based chemicals. Further process advantages include the ease of post-reaction separation of products, solvent, and catalyst; elimination of clean-up steps typically required prior to fermentation; and more favorable energy balance compared with hydrolysis due to the lower temperatures that can be used and the much lower heat capacity of ethanol compared with water. Insight into the formation of the crystalline barrier will guide future work to optimize the process and make it commercially viable, for example by continuous ball milling under ethanolytic conditions.

6.5. References

1. E. M. Rubin, *Nature*, 2008, **454**, 841-845.

2. F. H. Isikgor and C. R. Becer, *Polymer Chemistry*, 2015, **6**, 4497-4559.

3. L. R. Lynd, *Nat Biotechnol*, 2017, **35**, 912-915.

4. L. R. Lynd, X. Liang, M. J. Biddy, A. Allee, H. Cai, T. Foust, M. E. Himmel, M. S. Laser, M. Wang and C. E. Wyman, *Curr Opin Biotechnol*, 2017, **45**, 202-211.

5. X. Zhao, L. Zhang and D. Liu, *Biofuels, Bioproducts and Biorefining*, 2012, **6**, 465-482.

6. B. Yang, Z. Dai, S.-Y. Ding and C. E. Wyman, *Biofuels*, 2014, **2**, 421-449.

7.U. Bornscheuer, K. Buchholz and J. Seibel, *Angew Chem Int Ed Engl*, 2014, **53**, 10876-10893.

8.J. A. Geboers, S. Van de Vyver, R. Ooms, B. Op de Beeck, P. A. Jacobs and B. F. Sels, *Catalysis Science & Technology*, 2011, **1**.

9.M. S. Mettler, D. G. Vlachos and P. J. Dauenhauer, *Energy & Environmental Science*, 2012, **5**.

10.A. D. Paulsen, M. S. Mettler and P. J. Dauenhauer, *Energy & Fuels*, 2013, **27**, 2126-2134.

11.G. SriBala, H.-H. Carstensen, K. M. Van Geem and G. B. Marin, *Wiley Interdisciplinary Reviews: Energy and Environment*, 2019, **8**, e326.

12.Y.-B. Huang and Y. Fu, *Green Chemistry*, 2013, **15**.

13.D. A. Cantero Sposetti, DOI: 10.35376/10324/5374info:eu-repo/semantics/doctoralThesis, 2014.

14.R. W. Torget, J. S. Kim and Y. Y. Lee, *Industrial & Engineering Chemistry Research*, 2000, **39**, 2817-2825.

15.H. Tadesse and R. Luque, *Energy & Environmental Science*, 2011, **4**.

16.H. Zhao, J. H. Kwak, Y. Wang, J. A. Franz, J. M. White and J. E. Holladay, *Energy & Fuels*, 2006, **20**, 807-811.

17.M. Hall, P. Bansal, J. H. Lee, M. J. Realff and A. S. Bommarius, *FEBS J*, 2010, **277**, 1571-1582.

18.S. P. Chundawat, G. Bellesia, N. Uppugundla, L. da Costa Sousa, D. Gao, A. M. Cheh, U. P. Agarwal, C. M. Bianchetti, G. N. Phillips, Jr., P. Langan, V. Balan, S. Gnanakaran and B. E. Dale, *J Am Chem Soc*, 2011, **133**, 11163-11174.

19.H. Xu, X. Che, Y. Ding, Y. Kong, B. Li and W. Tian, *Bioresour Technol*, 2019, **279**, 271-280.

20.K. Wu, G. Feng, Y. Liu, C. Liu, X. Zhang, S. Liu, B. Liang and H. Lu, *Bioresour Technol*, 2018, **261**, 28-35.

21.T. Endo, E. M. Aung, S. Fujii, S. Hosomi, M. Kimizu, K. Ninomiya and K. Takahashi, *Carbohydr Polym*, 2017, **176**, 365-373.

22.H. Zhao, C. L. Jones, G. A. Baker, S. Xia, O. Olubajo and V. N. Person, *Journal of Biotechnology*, 2009, **139**, 47-54.

23.M. Lu, J. Li, L. Han and W. Xiao, *Bioresource Technology*, 2019, **273**, 1-7.

24.P. Alvira, E. Tomas-Pejo, M. Ballesteros and M. J. Negro, *Bioresour Technol*, 2010, **101**, 4851-4861.

25.Y. Yu and H. Wu, *AIChE Journal*, 2011, **57**, 793-800.

26.M. Tyufekchiev, A. Kolodziejczak, P. Duan, M. Foston, K. Schmidt-Rohr and M. T. Timko, *Green Chemistry*, 2019, **21**, 5541-5555.

27.S. Ouajai and R. A. Shanks, *Cellulose*, 2006, **13**, 31-44.

28.G. Xu, C. Chang, S. Fang and X. Ma, *Renewable Energy*, 2015, **78**, 583-589.

29.J.-H. Lin, Y.-H. Chang and Y.-H. Hsu, *Food Hydrocolloids*, 2009, **23**, 1548-1553.

30.K. Garves, *Journal of Wood Chemistry and Technology*, 1988, **8**, 121-134.

31.A. S. Klimentov, A. L. Fedorov, N. E. Kotel'nikova, G. A. Petropavlovskij, L. A. Volkova and B. G. Ershov, *Zhurnal Prikladnoj Khimii*, 1981, **54**, 686-690.

32.S. Saravanamurugan and A. Riisager, *Catalysis Communications*, 2012, **17**, 71-75.

33.K. Tekin, N. Hao, S. Karagoz and A. J. Ragauskas, *ChemSusChem*, 2018, **11**, 3559-3575.

34.J. M. Smith, H. C. Van Ness and M. Abbott, *Introduction to Chemical Engineering Thermodynamics*, McGraw-Hill Education, 2005.

35.M. Mascal and E. B. Nikitin, *ChemSusChem*, 2010, **3**, 1349-1351.

36.X. Xu, C. P. De Almeida and M. J. Antal Jr, *Industrial & engineering chemistry research*, 1991, **30**, 1478-1485.

37.T. K. Phung and G. Busca, *Chemical Engineering Journal*, 2015, **272**, 92-101.

38.R. L. Johnson and K. Schmidt-Rohr, *Journal of Magnetic Resonance*, 2014, **239**, 44-49.

39.P. Duan and K. Schmidt-Rohr, *Journal of Magnetic Resonance*, 2017, **285**, 68-78.

40.E. L. Hahn, *Physical Review*, 1950, **80**, 580-594.

41.G. Bodenhausen, R. Freeman and D. L. Turner, *Journal*, **27**, 511-514-511-514.

42.B. M. Fung, A. K. Khitrin and K. Ermolaev, *Journal of Magnetic Resonance*, 2000, **142**, 97-101.

43.D. A. Torchia, *Journal of Magnetic Resonance (1969)*, 1978, **30**, 613-616.

44.L. T. Fan, Y.-H. Lee and D. H. Beardmore, *Biotechnology and Bioengineering*, 1980, **22**, 177-199.

45.C. Chang, G. Xu and X. Jiang, *Bioresour Technol*, 2012, **121**, 93-99.

46.L. C. Fidale, N. Ruiz, T. Heinze and O. A. E. Seoud, *Macromolecular Chemistry and Physics*, 2008, **209**, 1240-1254.

47.O. A. El Seoud, L. C. Fidale, N. Ruiz, M. L. O. D'Almeida and E. Frollini, *Cellulose*, 2007, **15**, 371-392.

48.C. P. Kelly, C. J. Cramer and D. G. Truhlar, *The Journal of Physical Chemistry B*, 2007, **111**, 408-422.

49.G. I. Mantanis, R. A. Young and R. M. Rowell, *Cellulose*, 1995, **2**, 1-22.

50.E. Jasiukaitytė, M. Kunaver and M. Strlič, *Cellulose*, 2009, **16**, 393-405.

CHAPTER 7

Conclusions and Recommendations

In this thesis we addressed the topic of cellulose depolymerization to monomer sugars for the production of renewable fuels and chemicals. Motivated by the necessity to reduce conversion costs two technologically relevant routes were investigated. Specifically, the application of solid acids as recyclable catalysts and the effect of water on the cellulose structure were studied in detail. The studies involving solid acid catalysts attempted to answer two questions that were posed by the field: what is the structure-activity relationships of solid acid catalysts and what is the catalytic mechanism of cellulose hydrolysis. On the other hand, this work addressed the effects of water-induced recrystallization of decrystallized cellulose on its reactivity, a phenomenon known for decades, but not directly tested before. As a result, an alternative to hydrolysis, namely depolymerization of cellulose in ethanol was explored to circumvent limitations imposed by water-induced recrystallization.

In **Chapter 3**, a bifunctional polymer solid acid catalyst CMP-SO_3H-0.3, a chloromethyl polystyrene polymer-based material bearing benzyl chloride groups and benzylsulfonic acid groups, was structurally characterized and its cellulose hydrolysis activity evaluated in order to relate its structural characteristics to its activity and attempt to elucidate its catalytic mechanism. CMP-SO_3H-0.3 exhibited remarkable activity towards cellulose hydrolysis at 175 °C which was consistent with the original literature report. The original report attributed the activity of the catalyst to binding via hydrogen bonding between the benzyl chloride groups and the hydroxyl groups of cellulose. However, nuclear magnetic resonance analysis revealed that the functionalization procedure for the catalyst preparation resulted in the formation of benzylic

hydroxyl groups in the catalyst structure. Like their chlorinated counterpart, the hydroxyl groups in the catalyst could potentially form hydrogen bonds with cellulose. In order for any binding interactions to occur the groups that would interact with cellulose have to be located at an accessible to the solid cellulose substrate part of the catalyst, which is the external surface.

Detailed three-dimensional analysis using Raman microscopy and energy dispersive X-ray spectroscopy elucidated the spatial distribution of the chemical moieties in the catalyst particle. Interestingly, the benzyl chloride groups were not present on the external surface of the polymer beards, precluding any interactions between the chlorine groups and cellulose, suggesting that benzyl hydroxyl group could participate in hydrogen bonding with cellulose. This hypothesis was supported by the greater activity of CMP-SO_3H-0.3 than a catalyst bearing only sulfonic acid groups. However, structural analysis after reaction revealed reduction of benzyl chloride groups and further increase of hydroxyl groups in the catalyst. This indicated hydrolysis of the chloride moieties at the hydrothermal environment and *in situ* release of hydrochloric acid. To confirm this, the catalyst was treated in the hydrothermal environment used for cellulose hydrolysis. Characterization of the liquid confirmed the presence of hydrochloric acid. The acidic supernatant was used to hydrolyze cellulose to determine its contribution to the observed activity of the solid acid catalyst and it was revealed that the homogeneous acid was fully responsible for the depolymerization and solubilization of cellulose.

These results motivate adoption of a new synthesis and a characterization approach for the development of solid acid catalysts for cellulose hydrolysis. Solid acid catalysts are typically extensively characterized by procedures which might not provide relevant structural information to the activity of the catalyst. We propose a more focused characterization, specifically, of the external surface of newly prepared catalyst since this would be the part of the catalyst that would

interact with the solid cellulose substrate. The interior water-accessible sites while catalytically active will only interact with soluble species. In the current study, Raman microscopy and energy dispersive spectroscopy (EDS) were used to analyze the polymer beads of catalyst with particle size in the range of 0.3 to 1.2 mm. Other catalyst may exhibit even smaller particle sizes which may preclude the use of Raman microscopy due to limitations of the spatial resolution. We recommend surface characterization with EDS, which is gaining attention for the characterization of solid acid catalysts for cellulose hydrolysis since 2019.

In addition to the necessity to improve catalyst characterization, we recommend the selection and incorporation of hydrothermally stable groups into the catalyst structure. Furthermore, despite the wide use of chlorinated groups as hypothetical binding groups, we caution against the use of chlorine-based catalyst as the results reveal they are labile and result in the release of hydrochloric acid. While we show here that the benzyl chloride groups decompose, sulfonic acid groups typically used as catalytic sites can also be hydrothermally unstable, depending on their local chemical environment. For this we propose the synthesis of catalyst that have stable sulfonic acid groups, for example, attached to an aliphatic carbon atom, rather than aromatic one, or the use of the more stable carboxylic acids.

In **Chapter 4**, we explored further the implications of catalyst degradation and leaching of homogeneous acid on the interpretation of solid acid catalyst activity towards cellulose hydrolysis. Due to experimental challenges for measuring catalytic events between solid cellulose and solid acid catalysts, there was no direct evidence of the solid-solid interactions and the hypothesized mechanism involving binding had no support apart from correlations between characterization, activity, and adsorption of cellulosic molecules at lower temperature. However, catalyst degradation and *in situ* release of homogeneous acid which in turn hydrolyzes cellulose was a

viable interpretation of the observed catalytic activity and that reaction pathway called into question the interpretation of the activity of the all catalysts proposed in the field.

We selected representative catalysts from various structural classes and tested their activity towards cellulose hydrolysis to identify if leaching reaction is occurring. To determine the effect of leaching, we treated the catalysts were treated in the hydrothermal conditions used for cellulose hydrolysis and the activity of the supernatant was tested. We discovered that the catalysts degraded primarily by hydrolysis of acid sites leaching sulfuric acid which in turn carried out hydrolysis. Two catalysts remained relatively stable and did not result in significant release of homogeneous acid species, namely VSGC and HZSM-5. Despite that, we considered the possibility of solid-solid interactions between the catalyst and the cellulose substrate. We provided a kinetic framework that allows for testing and deconvoluting the effects of homogenous acid hydrolysis and attributing activity to the solid catalyst. Accounting for homogenous acid catalyzed cellulose hydrolysis by means of kinetic modeling revealed no contribution from the solid acid catalyst. The hydrothermally stable catalyst did not exhibit activity greater than water which is evidence that there are no solid-solid interactions that results in the depolymerization of cellulose. Even more, the data indicated that additional leaching was occurring for hydrothermally unstable catalyst due to the presence of cellulose hydrolysis soluble products in the reaction environment. This was confirmed by measuring the acid concentration of the hydrolysate and by nuclear magnetic resonance analysis of the catalyst post-reaction.

We recommend the adoption of our approach for analysis of solid acid catalysts for cellulose hydrolysis prior to structural characterization. Adoption of this methodology would allow for quick screening of solid acid catalysts in hydrothermal environments and selection of stable structures for further studies.

Hydrothermal stability only ensures that the cellulose hydrolysis activity can be correctly attributed to the solid acid catalyst. However, as revealed by the results obtained from HZSM-5 and VSGC the stable solid acid catalysts do not hydrolyze cellulose. For future work, instead of laborious catalyst synthesis, characterization, and performance evaluation, we propose a more theoretical approach that can provide the design specifications for new catalysts and address the challenges for measuring interactions at the severe hydrothermal environment. Specifically, we recommend characterization of the cellulose substrate followed by theoretical calculations of the forces between cellulose particles and theoretical catalysts. For example, cellulose is slightly acidic and negatively charged due to small amount of carboxylic acid functionalities; similarly, the typical Brønsted solid acid catalysts used are also negatively charged due to dissociation of the strong acidic groups. This suggests that the two substrates are more likely to repel each other in water rather than interact via adsorptive binding; for instance, water soluble anionic polyelectrolytes do not adsorb on cellulose, while cationic do. However, utilizing developed and established theoretical descriptions of colloid intermolecular interactions that model short and long range forces such as electrostatic, polar, and van der Waals forces and allow for simulating the ionic strength, particle size, and temperature effects, can result in a description of a system where the solid cellulose substrate would be attracted to and bind to a hypothetical solid acid catalyst. Once a mathematical model of a solid particle and conditions resulting in interactions with cellulose is described, follow-up efforts will attempt to synthesize such a material that also meets the requirements for hydrothermal stability. Provided that successful preparation of such material is achieved, it may then be proceeded to evaluation of catalytic performance and elucidation of cellulose hydrolysis mechanism.

Chapter 5 addressed the effect of water-induced recrystallization on the structure-reactivity relationship of cellulose. Ball milling followed by hydrolysis seemed to support long-standing theory attributing cellulose reactivity to the relative content of amorphous and crystalline regions in its structure. However, hydrothermal treatment that resulted in increase of crystallinity, but no release of soluble sugars, did not decrease cellulose susceptibility to acid catalyzed hydrolysis. Further analysis revealed that decrystallized cellulose recrystallizes rapidly when exposed to water, contradicting the crystallinity-based theory. Nuclear magnetic resonance analysis detected the presence of cellulose allomorphs type I and II with greater crystal surface content after recrystallization. Ethanolysis, as a probe reaction, was carried out and showed that crystalline, decrystallized, and recrystallized indeed exhibit different reactivities, with decrystallized being the most reactive. Based on these findings we proposed un update to cellulose hydrolysis models that include water-induced recrystallization of amorphous cellulose. The results imply that recrystallization diminishes the effectiveness of decrystallization pretreatments on cellulose depolymerization.

Since cellulose is a solid substrate in typical hydrolysis or solvolysis conditions and its reactivity depends on several structural parameters, the reversibility of crystallinity due to water-induced recrystallization can serve as a means to test and establish the effects of other structural parameters on the reactivity, especially degree of polymerization. Pretreatments such as ball milling affect both crystallinity and degree of polymerization and, while crystallinity is reversible, degree of polymerization isn't. Therefore, substrates can be prepared with varying degree of polymerization, but relatively similar crystallinity followed by acid hydrolysis can reveal the effects of degree of polymerization on the reactivity. As a result, more targeted pretreatment processes that maximize reactivity can be designed.

While here we show that water-induced recrystallization reduces reactivity for pure cellulose substrate, it is not clear whether those conclusions can be extended to complex lignocellulosic biomass or to the technologically relevant process of enzymatic hydrolysis. For this purpose, we recommend a similar study as the one carried out here, involving whole biomass substrates that include cellulose, hemicellulose, and lignin. Comparison of the enzymatic hydrolysis of ball-milled decrystallized and ball-milled and water-recrystallized biomass will elucidate whether water-induced recrystallization reduces the biomass susceptibility to depolymerization via enzymes.

Provided that cellulose recrystallization effects are not limited only to pure substrates, it will become necessary to establish kinetics and molecular aspects of water-induced recrystallization of cellulose in liquid water. Here we showed that at elevated temperature cellulose recrystallizes very rapidly. However, enzymatic hydrolysis is carried out at much lower temperatures where hydrolysis rate can potentially compete with recrystallization rate. For this purpose, a technique that has the temporal resolution and which is transparent to water is necessary. While nuclear magnetic resonance is an analytical tool that can reveal molecular details with quantitative capabilities, the time to obtain ^{13}C spectra can far exceed the time for recrystallization to take place as recrystallization in liquid water occurs in the matter of minutes. Accordingly, we propose the use of Raman microscopy which can have the temporal resolution of seconds with high spectral resolution. Raman vibrations occur from inelastic scattering due to changes of polarizability caused by excitation from electromagnetic wave; water on the other hand is highly polar and does not result in significant changes of polarizability and is thus Raman transparent. Therefore, *in situ* studies of water-induced recrystallization can be carried out using Raman and provide both vibrational information that can be converted to kinetic data.

Fundamental knowledge on cellulose reactivity, effects of recrystallization on enzymatic hydrolysis of biomass, and recrystallization rate of cellulose will inform the design of pretreatment processes and hydrolysis conditions that maximize cellulose conversion and glucose yields while simultaneously minimizing costs.

Chapter 6 builds on the conclusions from **Chapter 5** and explores cellulose depolymerization via ethanolysis to ethyl glucopyranoside as means to maximizing conversion and yields by circumventing the effects of water-induced recrystallization on the reactivity of cellulose. We used ball-milled cellulose and deconstructed it in ethanol with hydrochloric acid as a catalyst. The rate of conversion and the product yields were greater than those obtained by hydrolysis at the same conditions. Interestingly, ethanolysis rapidly reached a maximum conversion after 30 minutes, which we attributed to either solubility and equilibrium limits or exhaustion of amorphous cellulose as the crystallinity of the ethanolyzed substrate had increased. Further ethanolysis with fresh solvent provided support of the solubility-equilibrium hypothesis. Treating ethanolyzed cellulose in hot liquid water resulted in the release of soluble oligomers, indicating that they were trapped in the crystalline matrix during ethanolysis, suggesting scission-relaxation mechanism of increase of crystallinity. We explored additional ways to increase soluble product yields by using co-solvents capable of swelling cellulose that we hypothesized would suppress cellulose structural relaxation during ethanolysis. The swelling capability had to be balanced by the affinity of the co-solvent to the acidic proton. The use of water as a co-solvent, despite its capability to recrystallize amorphous cellulose, increase the conversion and yield of soluble products. Alternatively, further deconstruction was achieved by repetitive ball milling and ethanolysis.

Ethanolysis is an attractive alternative to water-based hydrolysis for depolymerization of decrystallized cellulose substrates for the production of monomer sugars. However, this reaction

has not been studied as extensively as hydrolysis. One of the major knowledge gaps appear to be the limits of conversion which are reached likely due to scission-relaxation of the decrystallized cellulose substrate. For future work we recommend further investigation into this process. Specifically, we propose studies of ethanolysis of decrystallized cellulose at conditions where glycosidic bonds are broken but that do not produce monomer species; this would prevent interpreting any structural changes being attributed to solubilization of decrystallized regions. Such conditions would employ elevated acid concentrations, but lower temperatures, analogous to degree of polymerization studies with hydrolysis and would result in lower rate of structural relaxation and solubilization allowing better temporal resolution and potentially *in situ* experiments. The focus will be on structural characterization of the solid substrate. Molecular details of the changes can be described by X-ray and nuclear magnetic resonance analysis, which can be observed over time. A specific focus of the structural studies will be elucidating the mechanism of structural relaxation – whether it is due to reformation of hydrogen bonds or accretion of cellulose chains and crystallites along the hydrophobic planes of the polymer. This will provide information for the use of a co-solvent that hinders the relaxation pathway.

The experimental studies on the scission-relaxation of decrystallized cellulose during ehtanolysis can be supplemented by molecular dynamics simulations. Specifically, models of cellulose chains lacking crystalline order and exhibiting strained bonds to mimic the effects of decrystallization can be created. Ethanol can be implicitly or explicitly introduced in the simulations and controlled scission of a strained glycosidic bond can be modeled to elucidate the mechanism and thermodynamics of the relaxation process. Studies of simulating cellulose crystallite bending have been carried out previously and can serve as a reference point for the design of similar simulations.

In addition, we recommend studies employing pack bed reactors where the cellulose substrate is packed in the reaction zone with acidic ethanol solution flowing through. This will circumvent the solubility limits reached by the batch reactors used in the current study, and extend the conversion and yields, and minimize product degradation even further.

Appendices

Appendix A

Cellulase-Inspired Solid Acids for Cellulose Hydrolysis: Structural Explanations for High Catalytic Activity

ATR-FTIR Comparison of CMP-SO_3H-0.3 and CMP-SO_3H-1.2

CMP-SO_3H-0.3 and CMP-SO_3H-1.2 were synthesized under different conditions. The preparation of CMP-SO_3H-0.3 involved substituting chloromethyl groups of chloromethyl polystyrene (CMP) precursor with thiourea where the stoichiometric ratio of chloromethyl groups to thiourea was 0.3. On the other hand, of CMP with thiourea at stoichiometric ratio of 1.2 aimed at substituting all the chloromethyl groups with thiourea, which would later be converted to sulfonic acid groups. To verify the successful removal and sulfonation of CMP-SO_3H-1.2 ATR-FTIR analysis was carried out. The spectra of CMP-SO_3H-0.3 and CMP-SO_3H-1.2 are compared in Figure A1. In can be seen that the two differ significantly in the region between 1000 cm^{-1} and 1200 cm^{-1} wavenumbers. CMP-SO_3H-1.2 exhibits a significantly stronger signal at 1040 cm^{-1} than CMP-SO_3H-0.3. This signal is resultant from -SO_3H vibrations. On the other hand, signal at 1265 cm^{-1} attributed to -CH_2-Cl groups is not present in the spectrum of CMP-SO_3H-1.2. ATR-FTIR confirms complete sulfonation of CMP-SO_3H-1.2. Accordingly, CMP-SO_3H-1.2 can be used as a catalyst bearing only -SO_3H groups that could serve as a control to the bifunctional CMP-SO_3H-0.3, which has both -CH_2-Cl and -SO_3H groups.

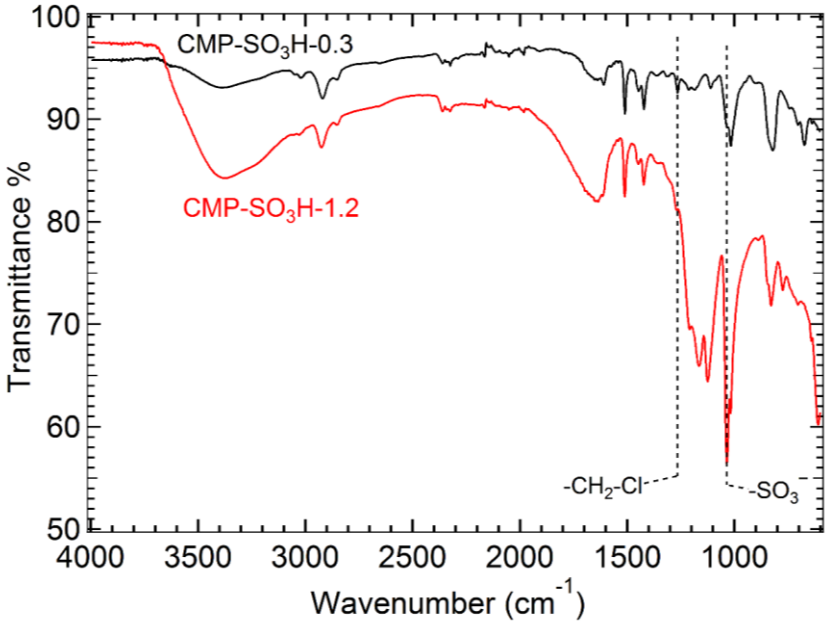

Figure A38. ATR-FTIR comparison of CMP-SO_3H-0.3 and CMP-SO_3H-1.2.

Assignment of NMR Signal and Structural Comparison of CMP, CMP-SO_3H-0.3, and CMP-SO_3H-1.2

Solid-state nuclear magnetic resonance analysis of the polymer catalysts was carried out. Specifically, CMP precursor, CMP-SO_3H-0.3, and CMP-SO_3H-1.2 were compared. Spectrum from polystyrene was also obtained to validate peak assignment. Spectra are shown in Figure A2. The spectrum in Figure A2 a) serves to identify the signals resultant from carbons in the polymer backbone. The signals between 140-150 ppm and the peak centered at 40 ppm are indicative of the aromatic carbon connected to the aliphatic chain and the aliphatic carbon present in the polystyrene backbone, respectively. The spectra presented of CMP, CMP-SO_3H-0.3, and CMP-SO_3H-1.2 are presented in Figure A2 b through d. The CMP exhibits a signal at chemical shift of 138 ppm and of 50 ppm attributed to the aromatic and aliphatic carbons of the chloromethyl group. CMP-SO_3H-0.3 exhibits additional signals at 58 ppm and 63 ppm assigned to -SO_3H and -OH groups, confirming successful functionalization. On the other hand, the spectra of CMP-SO_3H-1.2 exhibits only one additional signal at 58 ppm, confirming it is fully sulfonated. This corroborates the interpretation of the ATR-FTIR spectrum. The structural analysis validates that CMP-SO_3H-1.2 can be used as a control catalyst exhibiting only acidic groups for comparison to the activity of the bifunctional CMP-SO_3H-0.3 catalyst.

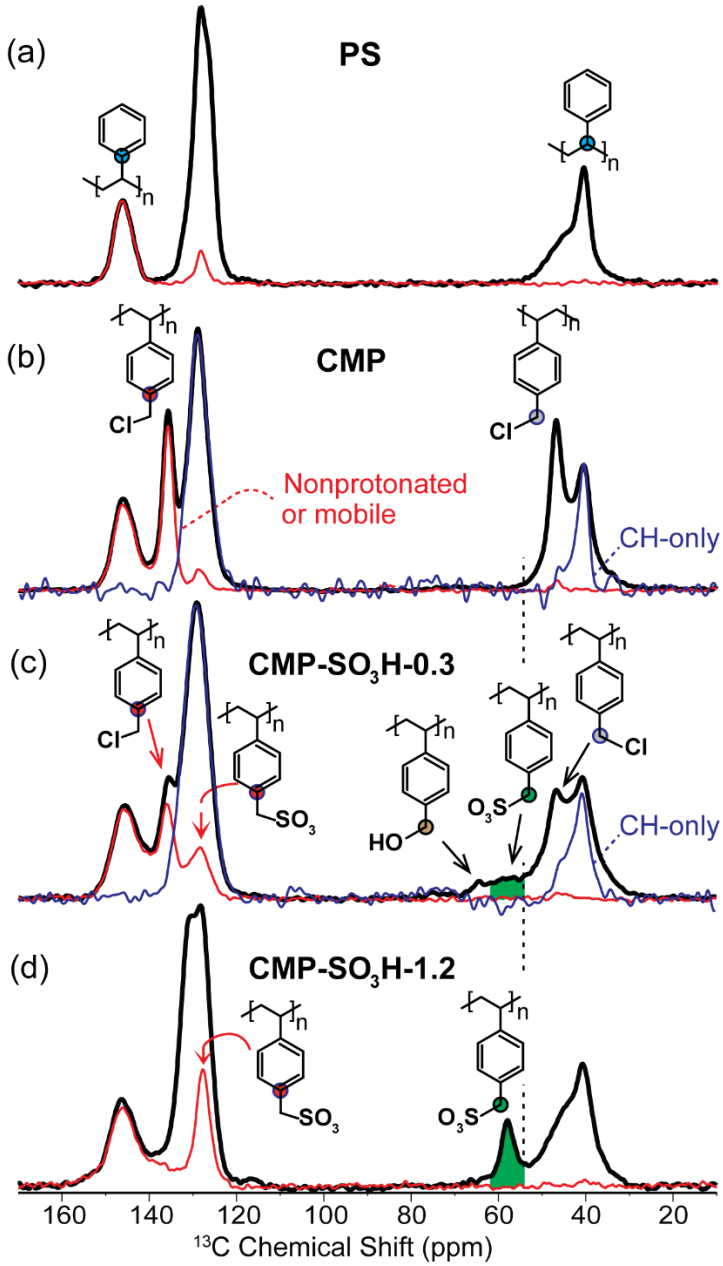

Figure A39. Solid-state 13C NMR spectra of (a) polystyrene; (b) catalyst precursor (CMP); (c) partially sulfonated polymer CMP-SO_3H-0.3, (d) fully sulfonated polymer CM-SO_3H-1.2. Thick black lines: Quantitative multiCP spectra of all C; thin red lines: Quantitative multiCP spectra of nonprotonated C; thin blue lines: Spectra of CH (methine) carbons, scaled to match the aromatic C-H peak intensity. The dotted line shows the cut-off of the CH_2Cl signal; the green shaded area shows the signal range corresponding to CH_2SO_3H.

Cross-sectional Raman Microscopy Analysis of CMP-SO_3H-1.2

Cross-sectional analysis of CMP-SO_3H-1.2 was carried out with Raman microscopy to determine whether there are spatial variations of the -SO_3H groups in that catalyst. Figure A3 shows Raman spectra obtained at various locations of a dissected polymer bead. In addition, the spectrum of the precursor CMP is plotted for comparison. The spectra of CMP-SO_3H-1.2 do not exhibit a signal at 1265 cm^{-1}, confirming complete substitution. Furthermore, the peak at 1040 cm^{-1} attributed to -SO_3^- vibration does not vary in intensity with respect to the location where the spectrum was obtained. This confirms that CMP-SO_3H-1.2 is fully sulfonated and uniform polymer catalyst.

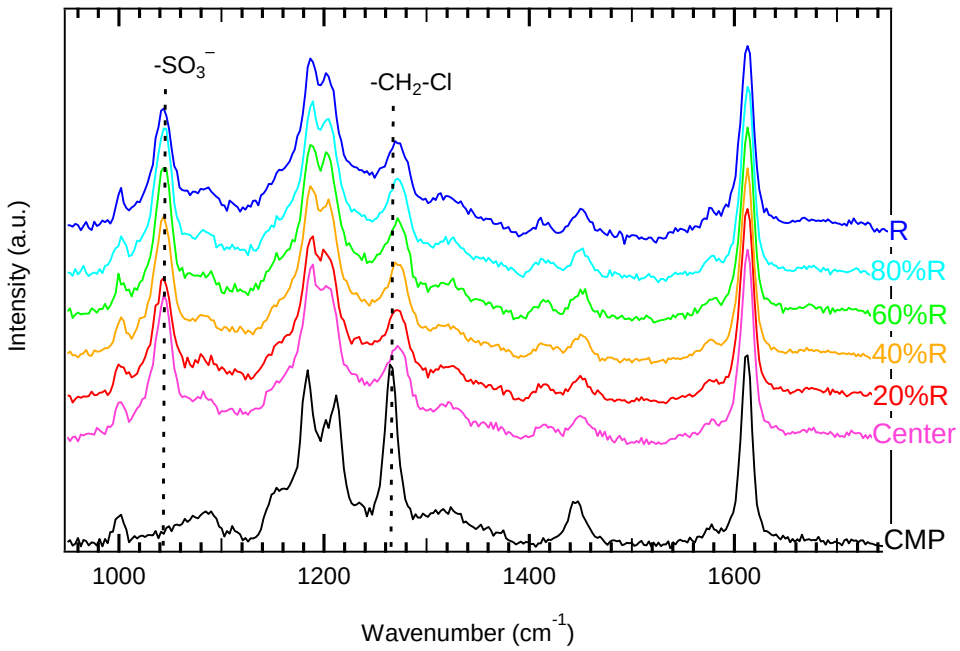

Figure A40. Cross-sectional Raman analysis of CMP-SO_3H-1.2. Marked bands: 1265 cm^{-1} (CH_2−Cl; decreasing from inside to outside of the bead), 1040 cm−1 (CH_2−SO_3H, increasing from inside to outside of the bead). The value R signifies the distance of the measurement from the center of the polymer bead.

Appendix B

Implications of homogeneous acid catalysis and criteria for interpretation of solid acid catalyst activity for cellulose hydrolysis

Detailed Compositional Analysis of Cellulose Hydrolysates

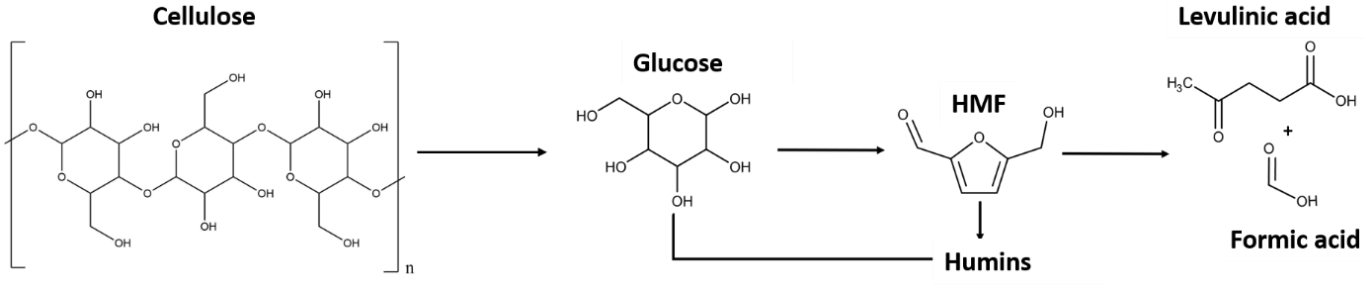

Scheme B15. Cellulose hydrolysis to glucose and glucose degradation to HMF, levulinic acid, and formic acid.

Following cellulose hydrolysis, the soluble products in the liquid medium were quantified by HPLC. Detailed product yields are presented in Table B1. Since all the products are due to hydrolysis of cellulose as shown in Scheme B1, the total carbon content of the products would be indicative of cellulose conversion. Due to experimental challenges to quantify cellulose conversion the carbon balance that is the carbon contained in the soluble products as a ratio of the carbon contained initially in the cellulose was used as a metric.

Table B11. Comparison of the yields (%) of most abundant soluble products generated by solid acid and leached homogeneous acid catalyzed cellulose hydrolysis.

Sample		Glucose	Levulinic Acid	Formic Acid	HMF
CMP-SO_3H-0.3	**Solid**	12 ± 3	27 ± 4	36 ± 5	trace
	Leachate	1 ± 1	57 ± 0.3	60 ± 1	trace
AMB-15	**Solid**	8.8 ± 1	13 ± 4	17 ± 4	0.1
	Leachate	18 ± 2.5	10.5 ± 4	16 ± 4	0.5
SZ	**Solid**	1 ± 0.1	3 ± 1	5 ± 2	1
	Leachate	8 ± 1	1 ± 0.4	5 ± 0.3	0.3
SAC	**Solid**	3 ± 1	0.1 ± 0.1	5 ± 2	trace
	Leachate	6 ± 1	1.4 ± 0.4	6 ± 0.5	1
SH	**Solid**	2.4 ± 1	1 ± 0.2	4 ± 1	trace
	Leachate	3 ± 0.2	0.2 ± 0.1	4 ± 1	0.2
HZSM-5	**Solid**	1 ± 0.2	trace	3.6 ± 1	trace
	Leachate	1 ± 0.4	trace	1 ± 0.5	0.1
Water		1 ± 0.1	trace	0.5 ± 0.1	trace

***trace indicates yields less than 0.05%**

Mass Balance of Solid Acid Catalyst Leaching – Comparison of the Quantity of Acid Sites and Ions in the Liquid Medium

The solid acid catalysts were treated in the hydrothermal environment employed for cellulose hydrolysis. The pH of the aqueous media decreased following treatment indicating leaching of homogeneous acid species. The leachate and the solid acid were characterized after the reaction. From a mass balance perspective, the release of the acid species in the medium had to match the loss of the acid sites of the solid acid catalysts, assuming it was the acid sites that were hydrolyzed. Figure B1 plots the acid sites lost from four catalysts and compares them to the sulfate and hydronium ions leached per gram of catalyst post reaction. The results show a relatively good agreement and indicate that the acid sites are being hydrolyzed and not ion exchanged.

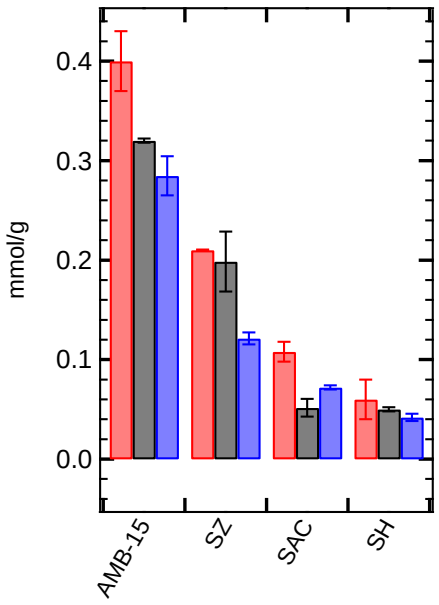

Figure B41. Comparison of the leached homogeneous acid concentration per gram of catalyst (red bars), the decrease of acid sites of the catalysts after hydrothermal treatment (grey bars), and the concentration of the leached sulfate species per gram of catalyst (blue bars). CMP-SO_3H-0.3 is not included in this analysis

since it leaches chloride and soli- state titration would not capture this change. HZSM-5 and VSGC were not analyzed due to very low leaching of homogeneous acid.

MATLAB Script for Cellulose Hydrolysis Model

```
% Kinetic Model for Acid Catalyzed Hydrolysis of Cellulose
based on
% Saeman w/ time dependent acid concentration,
% variable T, and variable H+

clear; clc; close all;

CellMW = 162.1406; %g/mol MW of cellulose

% Reaction Conditions
R = 8.314E-3;
WeightCellulose = 0.1; %Initial weight (g) of cellulose in
reactor
VolumeWater = 2/1000; %Initial volume of water in reactor
in L
CelluloseO = WeightCellulose/VolumeWater/CellMW;

Hpluslb = 0.03997;%Lower Bound H+ of AMB-15 leaching
Hplusub = 0.044;%Upper Bound H+ of AMB-15 leaching
h = @(r) Hpluslb + (Hplusub-Hpluslb)*r;%Pre-exponential
factor for time dependent H+ equation w/ variability given
by standard deviation
klave=0.016; %average leaching constant of AMB-15 leaching
CHplus = @(t,r) h(r)*(1-exp(-klave*t)); %CHplus
concentration bas
%CHplus = @(t,r) Aconc; %constant acid concentration of
leachate (used to simulate leachate hydrolysis)

Xintermediate = @(t,r) CHplus(t,r)*(98.079); %Convert mole
H+ to grams H2SO4
Yintermediate = @(t,r) Xintermediate(t,r)*(1/1.84);
%Convert grams H2SO4 to mL H2SO4
Zintermediate = @(t,r) (1000-Yintermediate(t,r))*(0.99823);
%Convert remaining L to g of water

Hpluswt = @(t,r)
(Xintermediate(t,r)/(Xintermediate(t,r)+Zintermediate(t,r))
)*100; %converts to concentration expressed as wt%
```

```
Tlb = 273+150;%Lower Bound Temperature
Tub = 273+155;%Upper Bound Temperature
T = @(a) Tlb + (Tub-Tlb)*a;%random selection of temperature
within the temperature range measured

k1 = @(t,a,r) 1.73E19*(Hpluswt(t,r)^1.34)*10^(-
(179.5/(2.303*R*T(a)))); %kinetic rate constant for
cellulose hydrolysis

% Hydrolysis of Cellulose to Glucose ;

n = 25; %number of interations
a = rand(n,1); %generates random 25x1 matrix with numbers
between 0 and 1; used in concentration
r = rand(n,1); %generates random 25x1 matrix with numbers
between 0 and 1; used in temperature

tspan = linspace(0, 600, 601); %generates linearly spaced
vectors
fun1 = @(t,z,r,a) [-(k1(t,r,a)*z(1))];
%defining a column vector of the reaction equations
%Solving system of ODEs
for iter1 = 1:length(a)%temperature selection
    for iter2 = 1:length(r)%concentration selection
    [t,z] = ode45(@(t,z)
fun1(t,z,a(iter1),r(iter2)),tspan,[CelluloseO]); %solving
the system of differential equations
    tz1(iter1,iter2,:,:) = [t  z];%defining a matrix with
results
    end
end

%%

%Plotting results
for x = 1:n
    for y = 1:n
        figure(1)
        hold on
        grid on
        time = tz1(x,y,:,1);
        time1 = squeeze(time);
        Cell = tz1(x,y,:,2);
```

```
        Cell1 = squeeze(Cell);
        Cellconv = ((CelluloseO - Cell1)/CelluloseO)*100;
        plot(t,Cellconv,'black')
        end
end
hold on
%Calculating average values
Cellulose=tz1(:,:,:,2);
Celave=mean(mean(Cellulose));
CellAverage=squeeze(Celave);
%Calculating standard deviation
for i=1:601
    Celldev(i,1)=std2(Cellulose(:,:,i));
end
```

Kinetic Study of CMP-SO_3H-0.3 Leaching

Kinetic study of the leaching of CMP-SO_3H-0.3 was carried out in order to determine the concentration of the leached homogeneous acid variation with time shown in Figure B2. The data was then used to fit a first order kinetic model in order to extract a rate constant that was later used in the kinetic modeling of cellulose hydrolysis by a homogenous acid.

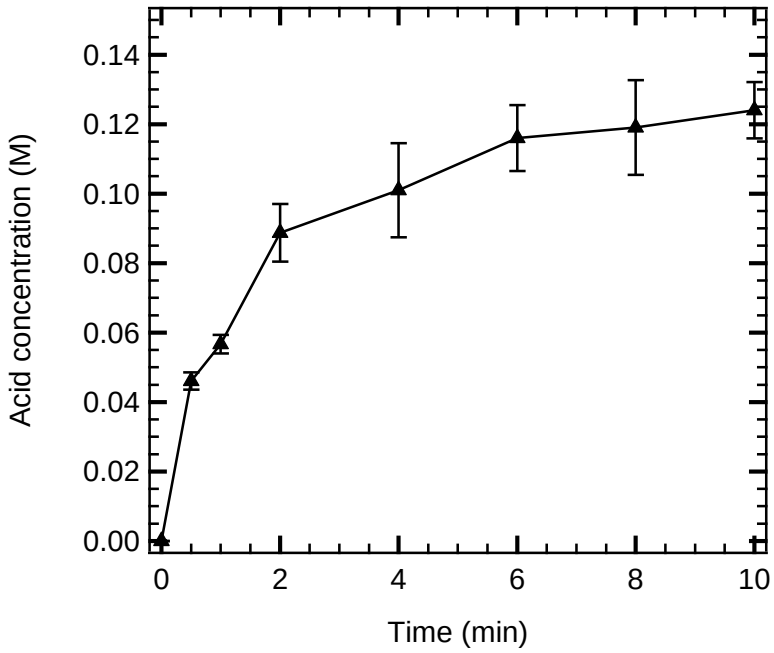

Figure B42. Concentration of the leached homogeneous acid for CMP-SO_3H-0.3 as a function of treatment time at 150 °C.

Appendix C

Reaction Engineering Implications of Cellulose Crystallinity and Water-Promoted Recrystallization

Mass Balance after Acid Hydrolysis or Hot Liquid Water Treatments

Following cellulose treatments either by acid or liquid hot water, the solid residues and the liquid products were quantified to determine whether there are products that are unaccounted for. The mass balance for each ball-milled sample after hydrolysis or liquid hot water treatment is shown in Figure C1. The mass balance of the acid hydrolyzed samples accounted for minimum of 92% for the sample ball-milled for 50 minutes. It was determined that for acid hydrolyzed samples the mass balance differed from 100% due to losses of the solid residue during drying and weighing.

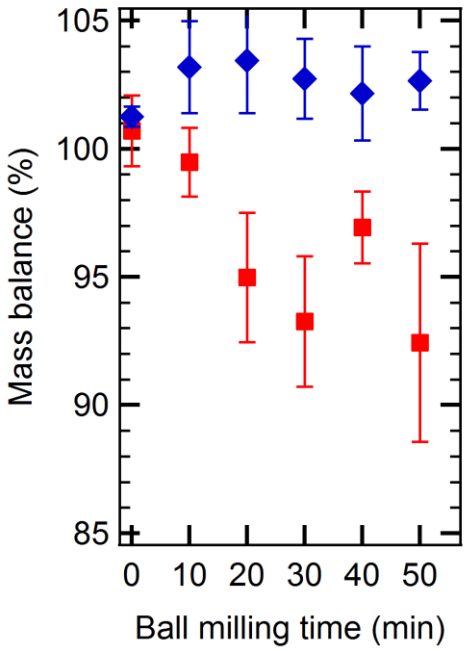

Figure C43. Mass balance closure for acid (red squares) and hot liquid water (blue diamonds) treated ball-milled cellulose samples.

Determining the Effects of Cellulose Drying

Following acid hydrolysis or liquid hot water treatments, the cellulose samples were washed with acetone and dried. To eliminate the possibility of crystallinity increases due to drying, a sample ball-milled for 50 minutes was washed both with acetone and water and then dried at 65 °C. The samples were then analyzed using XRD to determine if there were any changes of the crystalline organization. X-ray diffractograms are showed in Figure C2. The sample dried with acetone did not show any changes of its diffractogram, while the sample dried with water exhibited sharp diffraction peaks. This confirmed that drying with acetone did not increase the crystallinity and that washing of samples with acetone was an adequate procedure to assign the structural changes to the effects of hydrolysis or liquid hot water treatments.

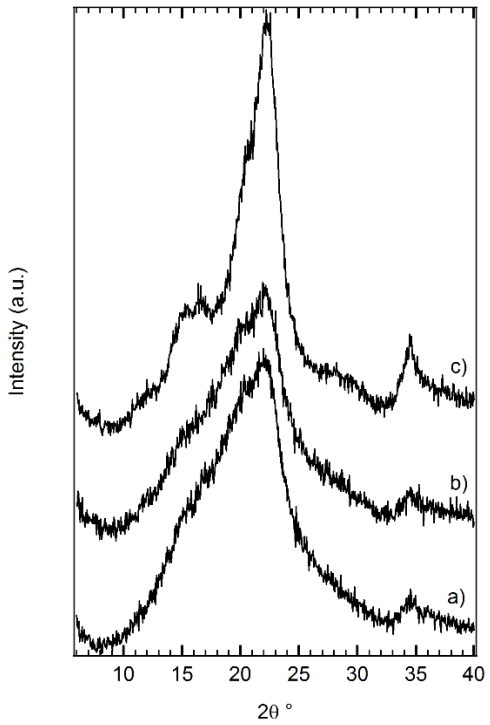

Figure C44. X-ray diffractograms of a) MCC-BM50, b) MCC-BM50 washed with acetone and dried at 65 °C, c) MCC-BM50 washed with water and dried.

XRD Analysis of Cellulose Samples after Hot Liquid Water or Sample Preparation Treatments

To determine the structural changes of cellulose that occur after treatment in hot liquid water in the absence of acid or after sample preparation (0.1M HCl, 5-minute heat-up time to reaction temperature), the samples were analyzed by XRD. The diffractograms are plotted in Figure C3 and Figure C4. It can be seen that in both figures all analyzed samples exhibit sharp diffraction peaks, indicating crystalline organization of the analyzed samples. The changes are similar to the changes occurring after full acid hydrolysis.

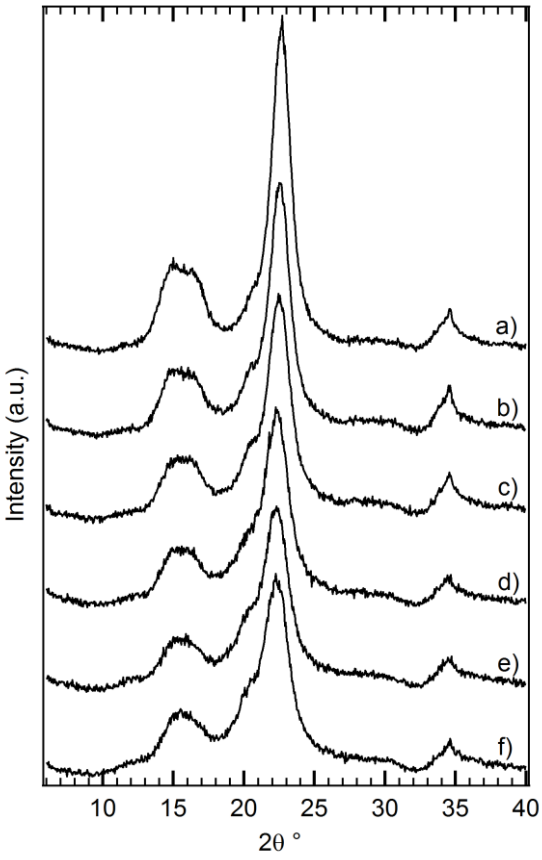

Figure C45. X-ray diffractograms of progressively ball-milled cellulose samples after liquid hot water treatment at 150 °C for 1 hour: a) Avicel-PH101, b) MCC-BM10-HLW, c) MCC-BM20-LHW, d) MCC-BM30- HLW, e) MCC-BM40- HLW, f) MCC-BM50-HLW.

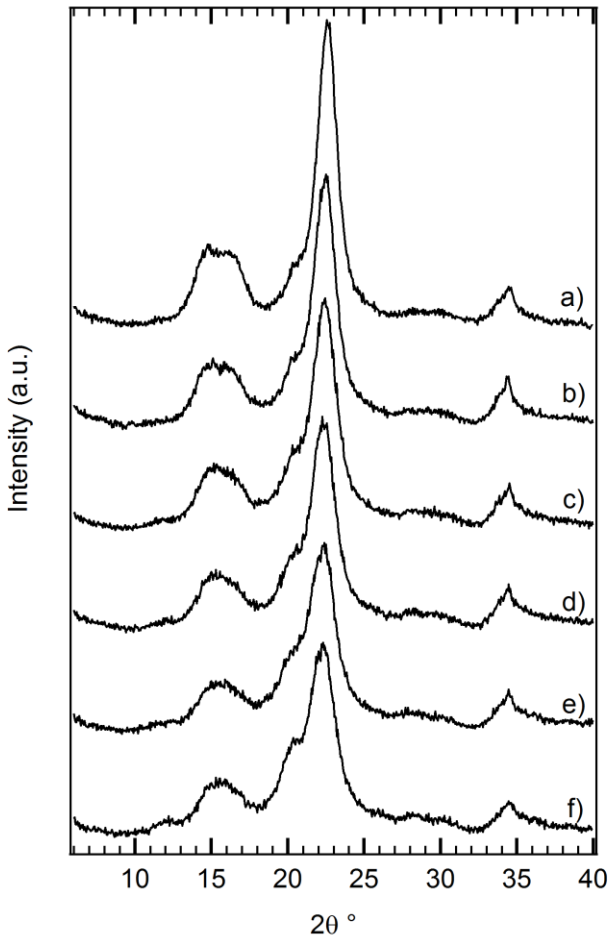

Figure C46. X-ray diffractograms of progressively ball-milled cellulose samples after sample preparation simulated conditions: a) Avicel-PH101, b) MCC-BM10-SP, c) MCC-BM20-SP, d) MCC-BM30-SP, e) MCC-BM40-SP, f) MCC-BM50-SP.

Raman Spectroscopy Analysis of Ball-milled Cellulose after Various Treatments

To supplement the XRD analysis and prevent technique bias that could affect the structure-reactivity conclusions, the cellulose samples subjected to various treatments were also analyzed with Raman spectroscopy. Detailed spectra of each ball-milled sample are presented in Figures C5 through C8.

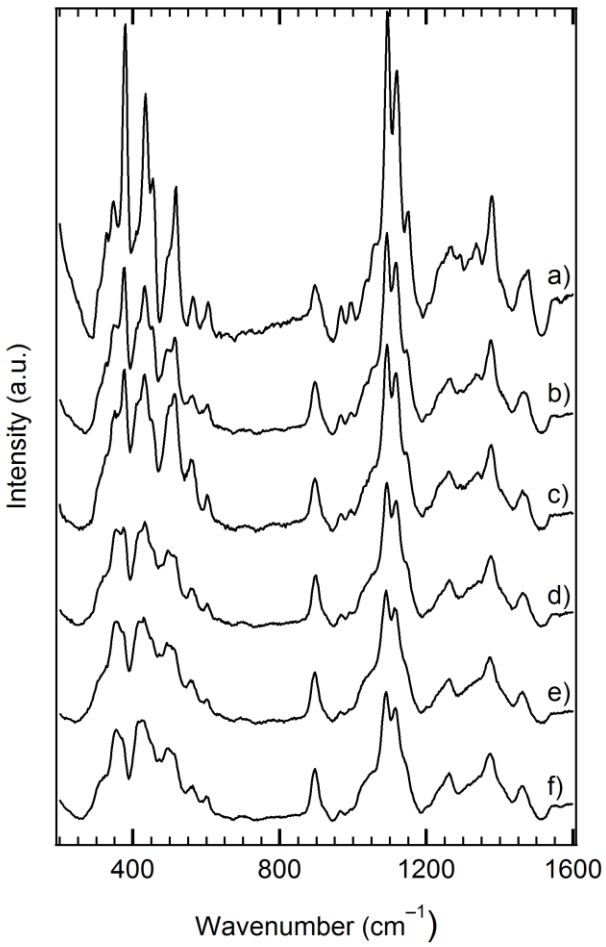

Figure C47. Raman spectra of progressively ball-milled cellulose samples: a) Avicel-PH101, b) MCC-BM10, c) MCC-BM20, d) MCC-BM30, e) MCC-BM40, f) MCC-BM50.

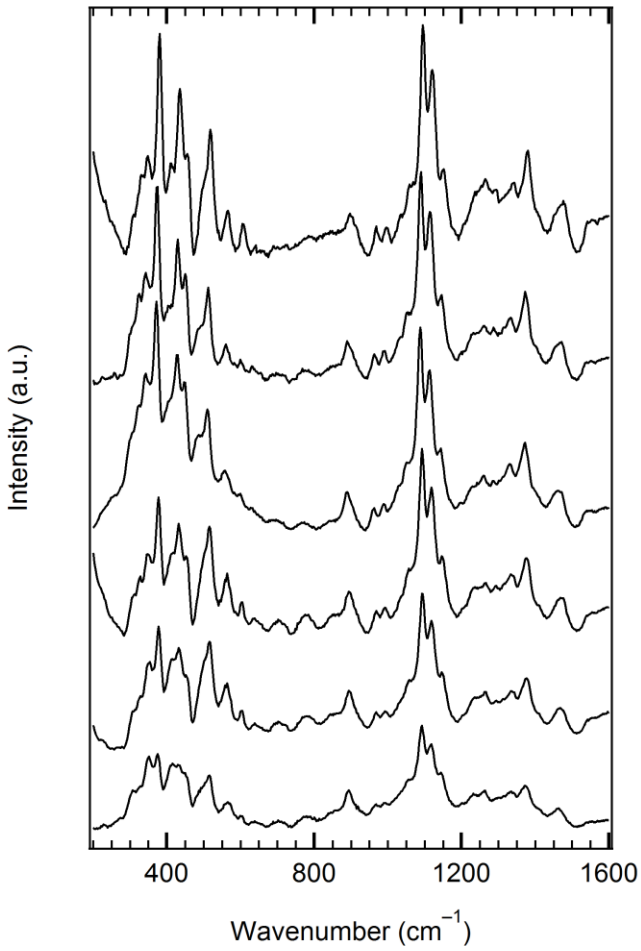

Figure C48. Raman spectra of progressively ball-milled cellulose samples after 0.1 M HCl acid treatment at 150 °C for 1 hour: a) Avicel-PH101, b) MCC-BM10-AC, c) MCC-BM20-AC d) MCC-BM30-AC, e) MCC-BM40-AC, f) MCC-BM50-AC.

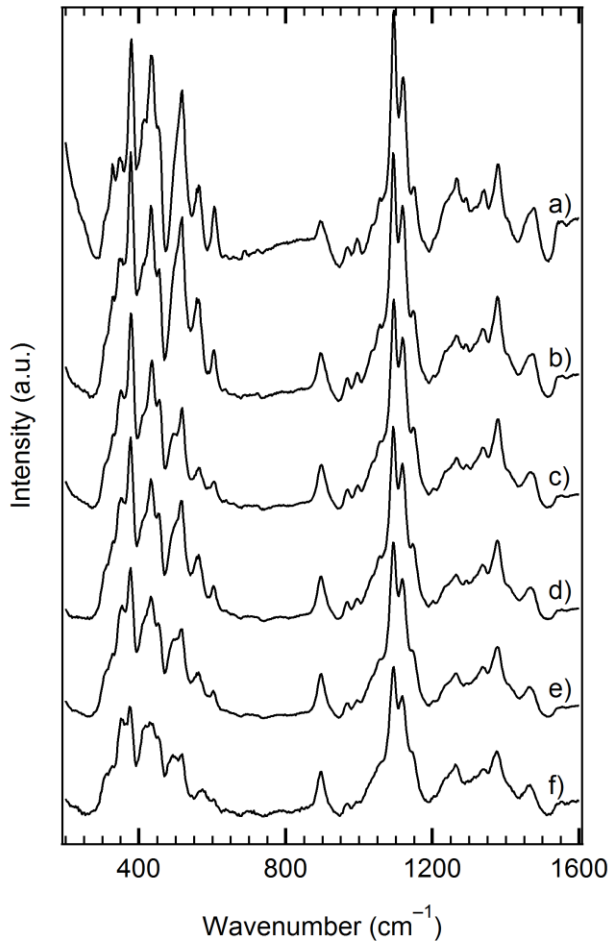

Figure C49. Raman spectra of progressively ball-milled cellulose samples after liquid hot water treatment at 150 °C for 1 hour: a) Avicel-PH101, b) MCC-BM10- HLW, c) MCC-BM20- HLW, d) MCC-BM30- HLW, e) MCC-BM40- HLW, f) MCC-BM50- HLW.

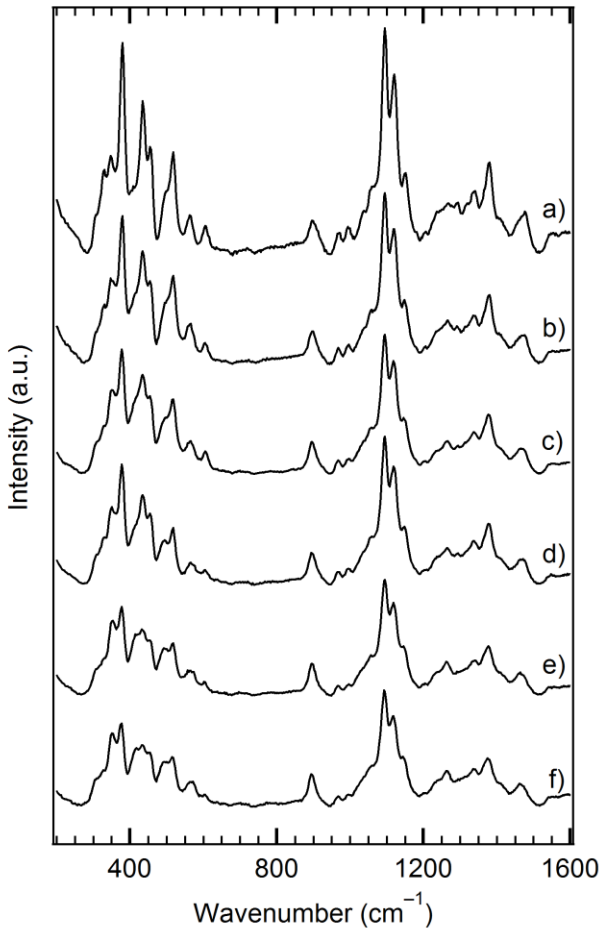

Figure C50. Raman spectra of progressively ball-milled cellulose samples after samples after sample preparation simulated conditions: a) Avicel-PH101, b) MCC-BM10-SP, c) MCC-BM20-SP, d) MCC-BM30-SP, e) MCC-BM40-SP, f) MCC-BM50-SP.

XRD Detection of Cellulose II

Following the detection of cellulose II by ss-NMR analysis, X-ray diffractograms were revisited. Cellulose I and cellulose II have overlapping diffraction peaks, which complicates distinguishing the two allomorphs. However, cellulose II exhibits a characteristic diffraction peak at 12.2°. Accordingly, the X-ray diffractograms of samples subjected to sample preparation treatment were investigated for the presence of this diffraction peak and are plotted in Figure C9. The peak was observable in ball-milled samples and grew in intensity for samples ball-milled for longer periods.

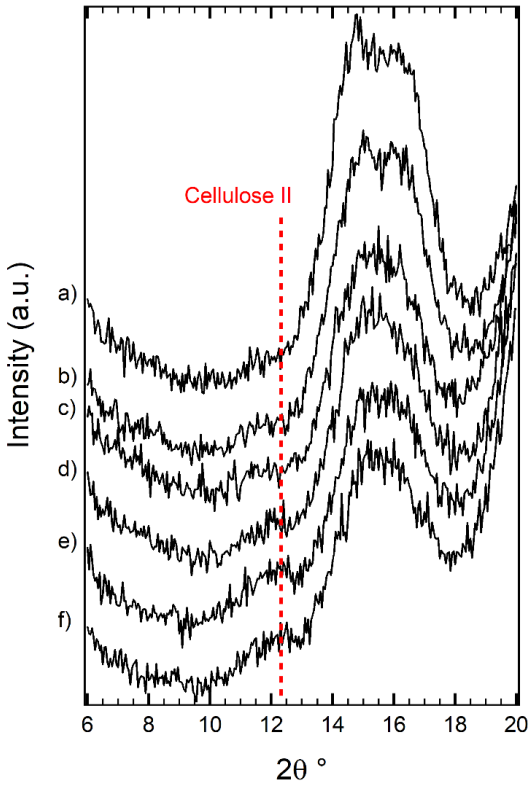

Figure C51. Expanded region of the X-ray diffractograms of progressively ball-milled cellulose samples after sample preparation simulated conditions: a) Avicel-PH101, b) MCC-BM10-SP, c) MCC-BM20-SP, d) MCC-BM30-SP, e) MCC-BM40-SP, f) MCC-BM50-SP. The peak at approximately 12.2° is identified as cellulose II.

Correlating the XRD Full-Width-Half-Max to Ball Milling Time of Recrytallized Cellulose Samples

The full-width-half-max (FWHM) of ball-milled cellulose samples recrystallized after sample preparation treatment varied proportionally with the ball milling time of the sample. This suggested potential correlation to reactivity of cellulose substrates. The FWHM was calculated and is plotted versus ball milling time in Figure C10.

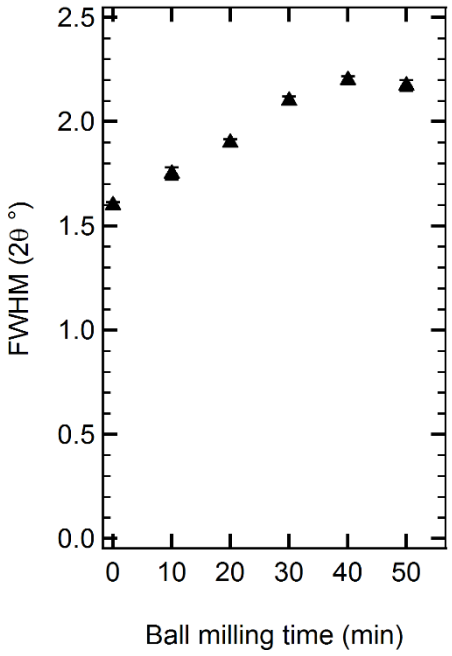

Figure C52. Full-width-halfmax (FHWM) of 200 diffraction plane plotted versus ball milling time for ball-milled cellulose samples recrystallized by sample preparation and heat up treatment.

Determining the Recrystallization Potential of Ethanol at Elevated Temperature

Ethanol does not recrystallize amorphous cellulose at room temperature conditions. However, no studies were carried out with ethanol at elevated temperature. To determine whether there is solvent-induced recrystallization of amorphous cellulose by ethanol at elevated temperature, cellulose, ball-milled for 50 minutes, was subjected to treatment with ethanol at 130 °C for 1 hour. The sample was then cooled, washed with acetone, dried, and analyzed with XRD. The X-ray diffractograms of the sample before and after treatment are shown in Figure C11. While some sharpening is observed, it is not as drastic as if the sample was treated in water.

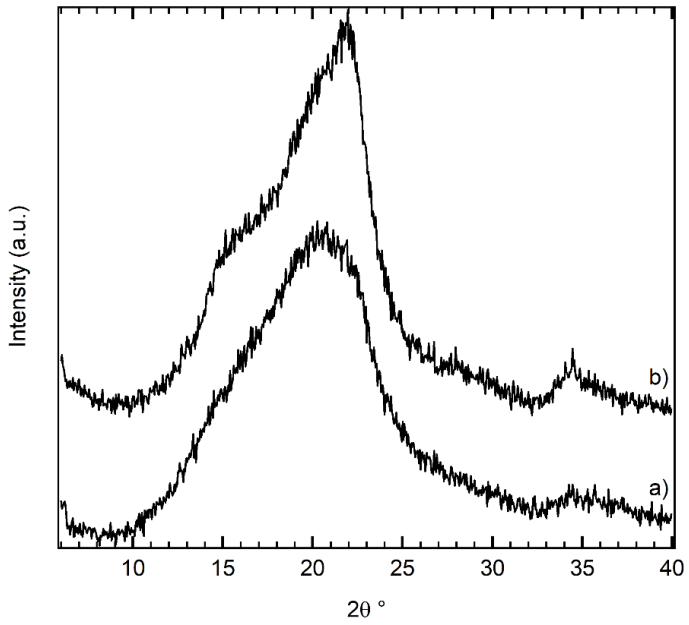

Figure C53. X-ray diffractograms of selected samples: a) MCC-BM50 and b) MCC-B50 after treatment in ethanol (130 °C, 1 hour).

Comparison of Hydrolyzed and Ethanolyzed Ball-milled Cellulose

Cellulose was ball-milled for 50 minutes and then subjected to hydrolysis or ethanolysis treatments and the residual substrate was characterized with XRD. The X-ray diffractograms are plotted in Figure C12. Highly crystalline Avicel cellulose is provided for comparison. Both ethanolyzed and hydrolyzed samples exhibit sharp diffraction peaks. However, while the hydrolyzed cellulose recrystallizes due to contact with water, the ehtanolyzed recrystallizes due to solubilization of highly reactive amorphous regions.

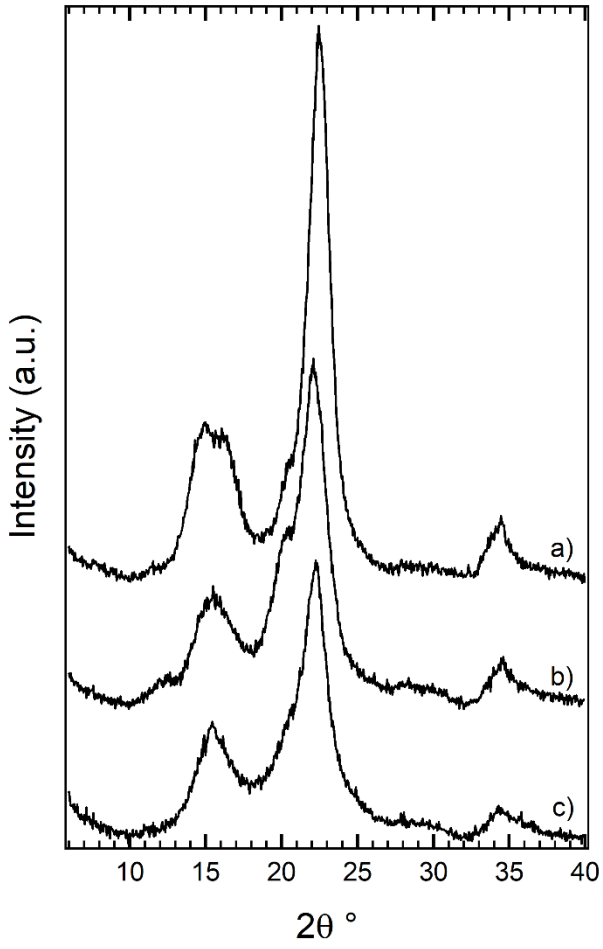

Figure C54. X-ray diffractograms after ethanolysis of selected cellulose samples: a) MCC, b) MCC-BM50-HLW, and c) MCC-BM50.

Appendix D

Rapid Depolymerization of Decrystallized Cellulose to Soluble Products via Ethanolysis under Mild Conditions

Quantifying Ethanolysis Decomposition Products

Ethanolysis of cellulose produces ethyl-glucopyranoside as a main product. However, ethyl-glucopyranoside can decompose to 5-ethoxytymethylfurfural (5-EMF) and ethyl levulinate as shown is Scheme D1. Analogously, glucose can decompose to 5-hydroxymethyl furfural (5-HMF) and levulinic acid. The degradation of the carbohydrates can limit their selectivity and necessitate additional separation or reduction of reaction severity. To understand the extent to which the carbohydrates resultant from cellulose ethanolysis decompose, we analyzed the solution of cellulose subjected to ethanolysis and quantified the decomposition product. Three main products were observed: 5-EMF, 5-HMF, and furfural. Their yields are plotted as a function of ethanolysis of ball-milled cellulose reaction time in Figure D1.

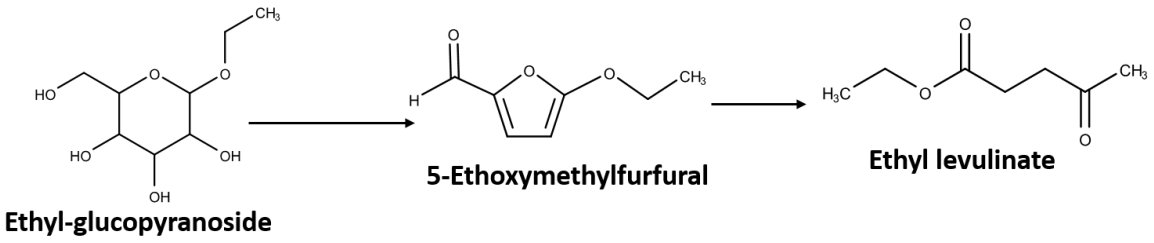

Scheme D16. Decomposition of ethyl-glucopyranoside to 5-ethoxymethylfurfural and ethyl levulinate.

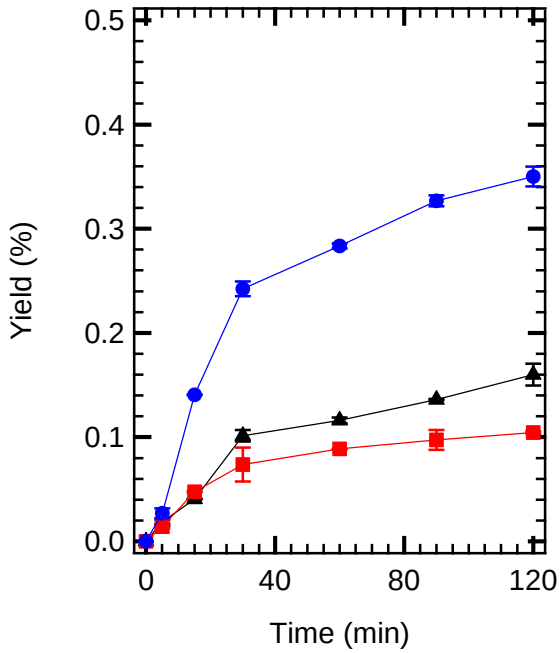

Figure D55. Yields of ethoxymethylfurfural (●), HMF (■), and furfural (▲) products from ethanolysis of ball-milled cellulose.

Detection of Oligomers and their Depolymerization in Ethanolysis Solution

Depolymerization of cellulose can produce soluble oligomeric species in addition to the monomer sugars. The oligomeric species can be further ethanolyzed to monomers. The conversion and monomer yields of ball-milled cellulose during ethanolysis do no converge and monomers and decomposition products account for only 75% of the identified products. This suggests that the remaining 25% can be attributed to oligomers. To detect and understand whether oligomers are formed and remain unreacted during ethanolysis, we analyzed with HPLC the solutions of ball-milled cellulose subjected to ethanolysis for 5 and 15 minutes. The raw chromatograms are presented in Figure D2. In the chromatogram of 5 minutes ethanolyzed sample a intense peak located at 7 minutes of elution time is evident. After another 10 minutes of reaction the peak degenarates and a commensurate increase of the intensity of the ethyl-glucopyranoside peaks is observed. While we cannot unambiguously identify and calibrate for the oligomers as we do not

know they degree of polymerization and such standards are not commercially available, there is strong evidence that the peak located at 7 minutes of elution time is due to oligomeric species. The fact that the peak decreases and the peaks of the monomers exhibit an equivalent increase and that larger cellulosic molecule such as cellobiose elute at an earlier time of 8.2 minutes for this specific HPLC column strongly points to the interpretation of the peak at 7 minutes that it is the results of oligomers. As a result, we interpret that the lack of full mass balance closure as the conversion and yields after ethanolysis do not match is not due to the presence of oligomers, but rather of other unidentified products, likely isomeric monomer species.

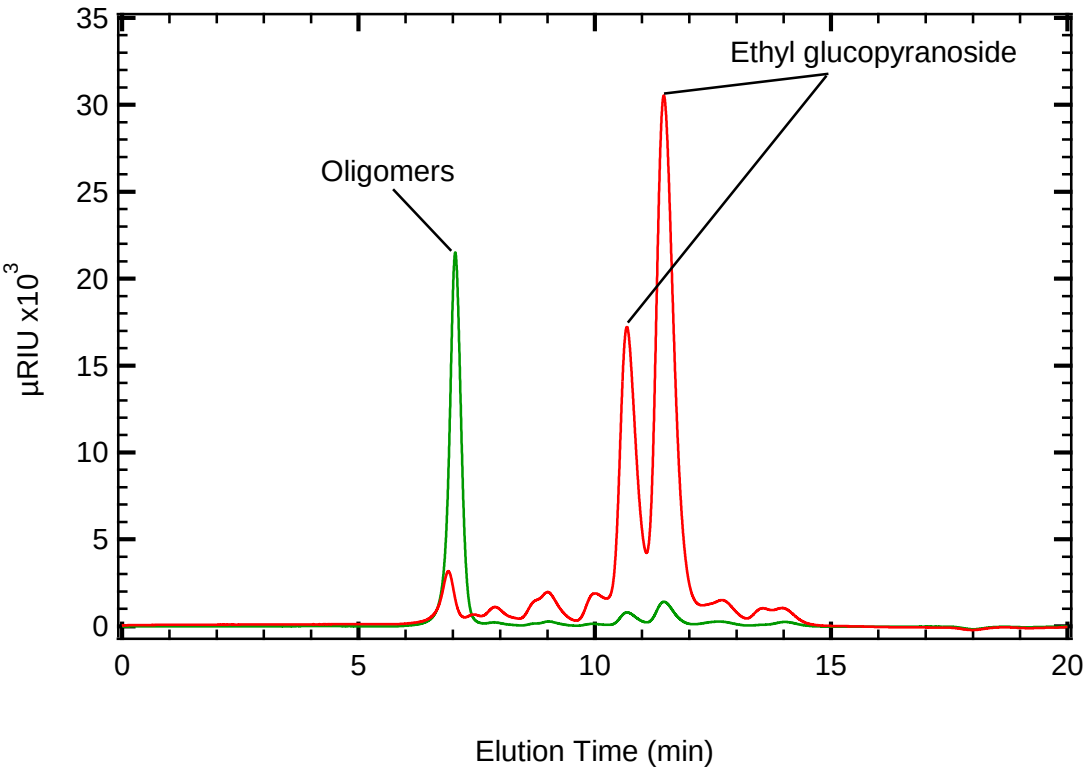

Figure D56. Refractive index chromatograms of the soluble products of cellulose ethanolysis after 5 minutes (green line) and 15 minutes (red line).

Control Study of Cellulose Hydrolysis as a Comparison to Ethanolysis

Ethanolysis of ball-milled cellulose resulted in rapid conversion and product yields; within 30 minutes of ethanolysis reaction 38% of conversion was achieved. To compare the kinetics of hydrolysis as a metric for its potential to produce monomer sugars, ball-milled cellulose was subjected to hydrolysis at the same conditions as the ethnaolysis reaction. The conversion and glucose yields were measured and are plotted in Figure D3.

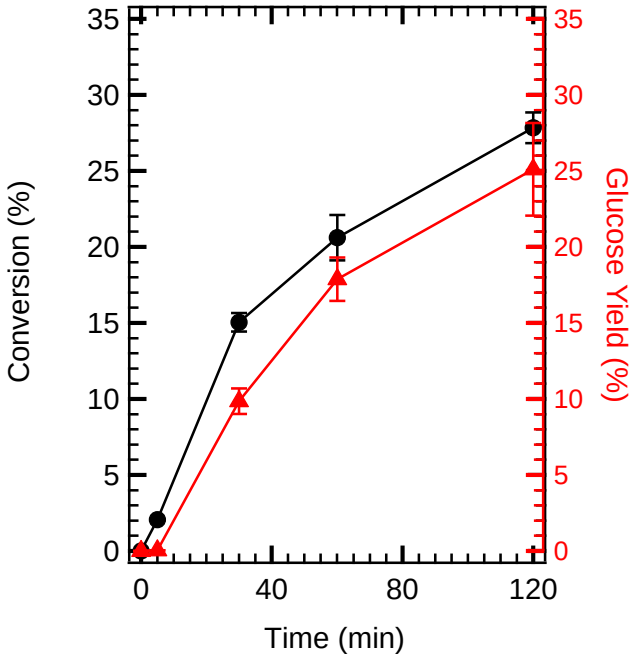

Figure D57. Time study of hydrolysis of ball-milled cellulose. Plotted are conversion (●) and glucose yield (▲). Reaction conditions – 0.1M HCl in water, 410 K.

Detection of Oligomeric Species Extracted from Ethanoylyzed Cellulose by Hot Liquid Water Treatment

The conversion and yields of ball-milled cellulose subjected to ethanolysis leveled off after 30 minutes of reaction time. A second ethanolysis treatment offered additional conversion and yields. This indicated that there could be potential equilibrium of cellulose ethanolysis or solubility limits the prevent further swelling of cellulose and solubilizing depolymerization products. For this

purpose, a ball-milled cellulose substrate subjected to two ethanolysis treatments was treated in hot liquid water as both oligomers and monomers are more soluble in water than ethanol. The liquid was then analyzed with HPLC. The chromatogram of the liquid is presented in Figure D4 and shows an intense peak at 7 minutes and small peaks of ethyl-glucopuranoside. The 7 minute peak is attributed to oligomers. The chromatogram of double-ethanolyzed ball-milled cellulose suggests that oligomers are trapped in the cellulose structure in ethanol environment and are only extractable once a solvent which exhibits greater swelling and solubilitization potential of ethanol is used.

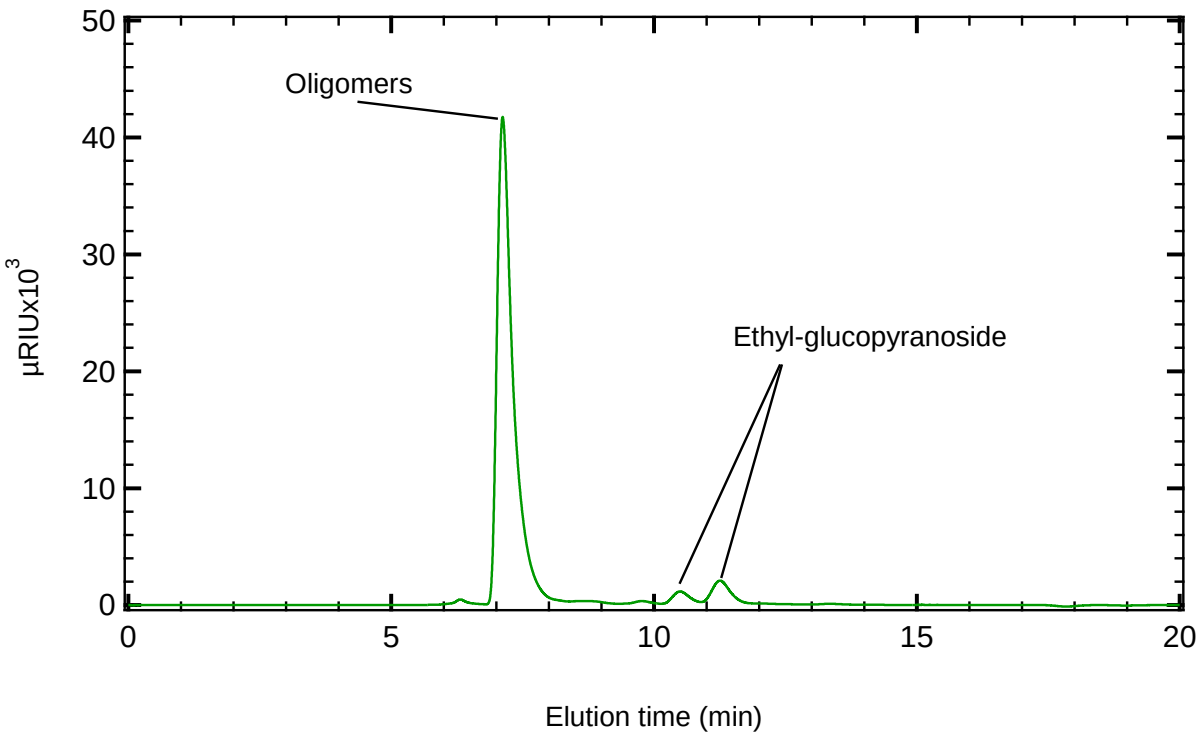

Figure D58. Refractive index chromatogram of the soluble products obtained from MCC-BM50-E90-E90-HLW60.

Determining the Solvent-Induced Recrystallization Potential of Ethanol

Ball-milled cellulose subjected to ethanolysis exhibited an increase of structural order post reaction. This suggested that the amorphous regions were depolymerized and solubilized. However, while ethanol does not promote recrystallization of cellulose at room temperature, no studies were carried out at elevated temperature in the absence of acid. For this purpose and to eliminate attributing the increased crystallinity of ball-milled cellulose after ethanolysis to solvent-induced recrystallization, ball-milled cellulose sample was treated in ethanol at 410 K in the absence of acid and the structure was analyzed with ss-NMR before and after treatment. The NMR spectra are presented in Figure D6. It can be seen that there is little difference between the two spectra, indicating that ethanol does not result in significant solvent induced recrystallization of ball-milled cellulose.

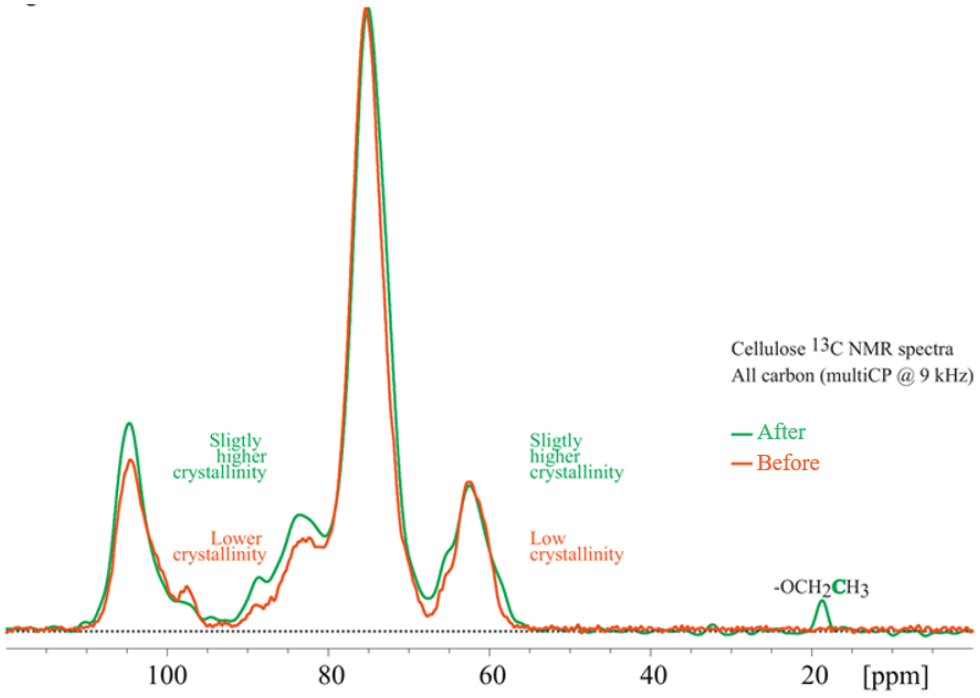

Figure D59. Solid state NMR spectra of MCC-BM50 before and after exposure to ethanol at 410 K for 90 minutes.